Ocean Circulation as a Driver for Changes in Ocean Chemistry in the Middle Ordovician of Argentina

A Dissertation Presented for the
Doctor of Philosophy
Degree
The University of Tennessee, Knoxville

Miles Anthony Henderson
May 2018

Copyright © 2018 by Miles Anthony Henderson
All rights reserved.

Dedication

To the many educators that have shaped my passion for learning and knowledge over these many years.

Especially to my wife, the librarian, for her unending support, encouragement, and allowing me to spend many years in the pursuit of this knowledge.

Acknowledgments

First, I would like to acknowledge my advisor, Dr. Linda Kah, who welcomed me back to Tennessee and has provided endless support, encouragement, and insight throughout these past five years. I'd also like to acknowledge my committee, Drs. Chris Fedo, Jill Mikucki, Colin Sumrall, and Drew Steen, and Ania Szynkiewicz for their support and encouragement at all stages of this dissertation. I would also like to acknowledge my many friends and colleagues in the Department of Earth and Planetary Sciences over the years, especially Ashley Manning-Berg, Kennan Golder, Jason Muhlbauer, Sarah Sheffield, Joseph Panzik, Cameron Hughes, Jen Bauer, Joy Buongiorno, Robert Jacobsen, Latisha Brengman, and Geoffrey Gilleaudeau. Lastly, I'd like to acknowledge my wife, Viktoria, for her encouragement, patience, and support that allowed all of this to be possible.

Abstract

The Ordovician is a critical period of Earth evolution where we observe a dramatic increase in the diversity of marine organisms called the Great Ordovician Biodiversification Event (GOBE). Major pulses in biodiversity of marine phytoplankton are identified in the Middle Ordovician during the GOBE suggesting dramatic changes in nutrient budgets of the shallow oceans. Additionally, carbon isotope evidence suggesting changeover from a greenhouse climate state to an icehouse climate state is also identified in the Middle Ordovician. Disruption of the Early Ordovician stratified ocean with invigorated ocean circulation associated with global cooling through the Middle Ordovician would lead to increased ventilation and upwelling of nutrient rich anoxic deep-waters potentially driving the biodiversity trends observed during the GOBE. Evidence of such a mixing event in the Middle Ordovician may recorded as the globally recognized Middle Darriwilian Isotope Carbon Excursion (MDICE).

In this study, I explore the potential for disruption of ocean stratification driven by global cooling in the Middle Ordovician by investigating the isotopic compositions of carbon, sulfur, strontium, and neodymium from the Precordillera of Argentina, which contains distinct marine facies representing coeval, yet distinct, water depths. In Chapter 1, I evaluate the carbon isotope composition of marine carbonate and organic carbon. Paired C-isotope profiles show decoupling of carbon isotope compositions between shallow- and deep-water environments and confirms the presence of a strong chemocline in the Darriwilian. In Chapter 2, I characterize potential changes in redox conditions in the Precordillera through the sulfur isotope record of carbonate associated sulfate (CAS) and pyrite. Variation in the behavior of marine sulfur between shallow, more oxygenated

surface waters and between deeper-water environments, below the marine chemocline is consistent with increased oxygenation of the deep-ocean in the Middle Ordovician. In Chapter 3, I determined the isotopic compositions of neodymium and strontium to explore the potential for physical stratification of the Middle Ordovician water column. Neodymium and strontium isotope compositions show decoupling between shallow- and deep-water environments suggesting physical stratification of the water column in addition to dynamic stratification indicated in the biogeochemical records of carbon and sulfur.

Table of contents

Introduction 1
1. The Ordovician ocean 1
2. Overview of the present study 3
2.1. Chapter 1 – Examining heterogeneity in the carbon isotope record 4
2.2. Chapter 2 – Evaluating redox conditions with the sulfur isotope record 5
2.3. Chapter 3 – Investigating physical records of paleoceanographic mixing 6
References 9
Chapter 1 Paired isotope records of carbonate and organic matter from the Middle Ordovician of Argentina: Intrabasinal variation and effects of the marine chemocline ... 14
Abstract 15
1. Introduction 16
2. Geologic setting and age 19
2.1. The Argentine Precordillera 19
2.2. Middle Ordovician Strata 20
2.2.1. The Las Chacritas Formation 21
2.2.2. The Las Aguaditas Formation 22
2.3. Biostratigraphic correlation of the Las Chacritas and Las Aguaditas formations 24
3. Analytical methods 27
3.1. Petrographic screening 27
3.2. Isotopic analyses of carbonate phases 27
3.3. Elemental analyses 28
3.4. Isotopic analyses of organic matter 28
4. Results and interpretation 29
4.1. Petrographic characterization 29
4.1.1. Evidence of secondary components 31
4.1.2. Cathodoluminescence petrography 32
4.1.3. Interpretation 33
4.2. Geochemical characterization of carbonate phases 35
4.2.1. Carbon and oxygen isotope compositions 35
4.2.2. Elemental signatures 36
4.2.3. Interpretation 37
4.3. Carbon isotope compositions of organic matter 41
4.3.1. Interpretation 42
4.4. Chemostratigraphic profiles 43
5. Discussion 45
5.1. Summary of observations 45
5.2. Potential for geochemical alteration 47
5.3. Potential for recovery of gradients in ocean chemistry 48
5.4. Implications for the redox structure of the Middle Ordovician oceans 51
5.5. Depositional scenarios 53
6. Conclusions 55
Acknowledgments 56

References 57
Appendix 1 69
Chapter 2 Sulfur cycling in the Darriwilian (Middle Ordovician) of Argentina: Implications for ocean circulation and the redox evolution of the Ordovician ocean 93
Abstract 94
1. Introduction 94
2. Geologic background 96
2.1. Argentine Precordillera 96
2.2. Middle Ordovician strata in the Precordillera 98
2.3. Stratigraphic correlation and age constraints 100
3. Methods 103
3.1. Sample selection and preparation 103
3.2. Major- and trace-element abundances 104
3.3. C- and O-isotope compositions 104
3.4. Sulfur extraction and isotope analysis 105
4. Results 107
4.1. Las Chacritas River Section 108
4.2. Las Aguaditas Creek section 109
4.3. Gualcamayo Formation 109
5. Interpretation and discussion 110
5.1. Assessment of primary geochemical signatures 110
5.2. Sulfur isotope trends in the Precordillera 113
5.2.1. $\delta\,^{34}S_{CAS}$ trends 113
5.2.2. $\delta\,^{34}S_{PY}$ trends 117
5.2.3. $\Delta^{34}S$ trends 119
5.3. Controls on sulfur isotope compositions 120
5.4. Effect of the marine chemocline 121
6. Conclusions 123
Acknowledgements 124
References 125
Appendix 1 133
Chapter 3 Neodymium and strontium isotope stratigraphy of Middle Ordovician carbonate sediments in Argentina: Investigating the link between biogeochemical cycling and physical changes in ocean chemistry 164
Abstract 165
1. Introduction 166
2. Geologic setting and background 169
2.1. Tectonic setting 169
2.2. Middle Ordovician strata 171
2.3. Correlation and age 172
3. Analytical methods 174
3.1. Sample selection and leaching protocols 174
3.2. Analytical chemistry and analysis 176
4. Results and evaluation of potential diagenesis 178

4.1. Isotopic and elemental analysis 178
4.2. REE analysis 179
4.3. Strontium isotopes 179
4.4. Neodymium isotopes 181
5. Discussion 181
5.1. Ordovician paleoceanographic change 181
5.1.1. Isotopic signatures of icehouse-greenhouse ocean states 181
5.1.2. Darriwilian carbon isotope change 182
5.1.3. Darriwilian sulfur isotope change 184
5.2. Strontium isotopes and understanding ocean stratification 185
5.2.1. Strontium isotopes in the Precordillera 188
5.2.2. Neodymium isotopes in the Precordillera 190
6. Conclusions 196
Acknowledgments 197
References 198
Appendix 1 210
Appendix 2 230
Summary 232
Vita 236

List of tables

Table 1.1. Range of isotopic compositions and elemental concentrations recorded in the Las Chacritas Formation 81
Table 1.2. Range of isotopic compositions and elemental concentrations recorded in the Las Aguaditas Formation. 86
Table 1.3. Summary of Darriwilian isotopic and elemental compositions from the Precordillera 92
Table 2.1: Range of isotopic compositions and elemental concentrations recorded in the Las Chacritas River section 146
Table 2.2: Range of isotopic compositions and elemental concentrations recorded in the Las Aguaditas Creek Section 152
Table 2.3: Range of isotopic compositions and elemental concentrations recorded in the Gualcamayo Formation at La Corridita Creek 159
Table 2.4: Summary of Darriwilian isotopic compositions from the Precordillera 163
Table 3.1: Range of isotopic and elemental concentrations of samples from the Las Chacritas River section 217
Table 3.2: Range of isotopic and elemental concentrations of samples from the Las Aguaditas Creek section 218
Table 3.3: REE compositions of the Las Chacritas and Las Aguaditas formations 220
Table 3.4: Measured [Rb], [Sr], and $^{87}Sr/^{86}Sr$ compositions of samples from nitric acid treatment of the Las Chacritas Formation 223
Table 3.5: Measured $^{87}Sr/^{86}Sr$, $^{143}Nd/^{144}Nd$, $^{147}Sm/^{144}Nd$, and ε_{Nd} of the Las Chacritas Formation 225
Table 3.6: Measured $^{87}Sr/^{86}Sr$, $^{143}Nd/^{144}Nd$, $^{147}Sm/^{144}Nd$, and ε_{Nd} of the Las Aguaditas Formation 227

List of figures

Figure 1.1: Paleogeographic reconstruction for the Middle Ordovician (~ 470 Ma) after Cocks and Torsvik (2002). Major landmasses are depicted in white, and Peri-gondwanan terranes are depicted in shades of gray. The Precordilleran terrane is shown in dark gray, in a position close to Gondwana, prior to its final docking..... 69

Figure 1.2: Regional map of the Argentine Precordillera modified from Gomez and Astini (2015). Lower Paleozoic strata crop out in a series of N-S trending thrust sheets and are divided into the Western and Eastern tectofacies. The Western tectofacies consists predominately of metamorphosed and deformed deep-water shale facies. The Eastern tectofacies consists of weakly deformed and unmetamorphosed marine shelf and slope deposits. Coeval measured sections of the Las Chacritas (C) and Las Aguaditas (A) formations were sampled in the Eastern tectofacies to the southwest of San Jose de Jáchal. 70

Figure 1.3: Biostratigraphic chart of Darriwilian strata showing generalized conodont zones for the Argentine Precordillera, specific data from the Las Chacritas and Las Aguaditas formations, and summary of data from Scandinavia, the North Atlantic, and China. Data is compiled from Albanesi and Ortega (2016), Serra et al. (2015), Feltes et al. (2016), Zhang (1998) and Löfgren and Tomacheva (2008), Stouge (1984), and Zhang (1998). Stage slices are after Bergström et al. (2009) and time slices after Webby et al. (2004). Interval of interest is indicated in light gray..... 71

Figure 1.4: Correlation of measured stratigraphic sections of the Las Chacritas and Las Aguaditas formations based on conodont biostratigraphic analysis of Serra et al. (2015) and Feltes et al. (2016). Upper Darriwilian (Dw3) strata in the Precordillera is absent and inferred to have been removed during development of a regional unconformity. Absence of the Upper Darriwilian is identified by the absence of conodonts representing the upper *E. suecicus* Zone and *P. serra* Zone in the Las Chacritas Formation, and the *E. suecicus* and *P. serra* zones in the Las Aguaditas Formation. 72

Figure 1.5: Petrographic microfabrics from the Las Chacritas Formation. A) Fossiliferous packstone with abundant sponge spicules, gastropods, and fragments of bryozoans, trilobites, brachiopods, and echinoderms. B) Intramicrite showing micritic clasts within a micritic- to microsparitic-matrix. Disseminated pyrite (opaque) occurs within the microsparitic matrix. C) Fossiliferous packstone with trilobite fragments, echinoderm fragments, and recrystallized sponge spicules. D) Carbonate mudstone containing predominantly recrystallized sponge spicules. E) CL image of heterogeneous, dully luminescent matrix cut by vein of brightly luminescent calcite with dully luminescent calcite intergrowths. F) CL image of heterogeneously luminescent carbonate matrix with two distinct vein generations: a dully luminescent vein (~ 140 μm diameter) and moderately luminescent vein (> 1 mm diameter)..... 73

Figure 1.6: Petrographic microfabrics from the Las Aguaditas Creek Formation. A) Fossiliferous packstone with abundant fragments of bryozoans, echinoderms, brachiopods, and trilobites, here cut by a large (1 mm diameter) calcite vein and a smaller (~ 15 μm diameter) calcite vein. B) Homogeneous mixture of micritic to

microsparitic carbonate and clay; such fabric characterizes the majority of the Las Aguaditas Formation. C) Homogeneous silty carbonate with disseminated pyrite. D) Laminated carbonate mudstone with a single layer of skeletal fragments within a microsparitic matrix. The white arrow indicates the position of a trilobite fragment. E). CL image showing heterogeneously luminescent micritic matrix composed of dully luminescent micritic clasts within a matrix of micrite (mixed luminescence) and clay (non-luminescent), cut by a coarsely crystalline, moderately luminescent vein. F) CL image of heterogeneous carbonate mudstone with three distinct stages of veins mineralization. 74

Figure 1.7: Cross-plot of carbon and oxygen isotopes from the Las Chacritas (LCF) and Las Aguaditas (LAF) formations. No clear covariant trends occur between C and O for the various carbonate phases (i.e., microsparitic matrix, recrystallized sparry patches within otherwise micritic matrix, and late-stage mineralized veins). Oxygen isotope compositions of micritic carbonate in the Las Chacritas and Las Aguaditas formations are similar, ranging from −4‰ to −6‰ in the Las Chacritas Formation and from −4‰ to −7‰ in the Las Aguaditas Formation. Carbon isotope compositions in both formations range from approximately +1‰ to −2‰. Isotopic compositions of sparry calcite within the carbonate matrix is generally similar to that of matrix micrite, consistent with only minor recrystallization either in the original depositional environment, or within a rock-buffered system. The wide range of $\delta^{18}O$ compositions preserved in vein calcite is consistent with formation by later diagenetic fluids that did not interact substantially with matrix components. 75

Figure 1.8: Isotopic and elemental data for carbonate phases of the Las Chacritas Formation. A) Detail of Figure 7; mineralized veins record a unique trajectory in carbon-oxygen space, indicating little influence of late-stage fluids on matrix components. B) Strontium concentrations of matrix components range from approximately 250 to 2000 ppm, consistent with well-preserved marine limestone. Lower Sr concentrations within sparry matrix is consistent with Sr loss during recrystallization. C) Mn and Fe concentrations are generally elevated, with [Mn] >500 ppm, and [Fe] as high as 8000 ppm. Combined with elevated Sr concentrations that suggest limited recrystallization, elevated Mn and Fe values potentially reflect in-situ incorporation from dysoxic to anoxic marine waters or pore fluids. D) Mn/Sr ratios are generally less than 3, well below the established threshold for little-altered carbonate rocks (Mn/Sr >10; Kaufman et al. 1995). 76

Figure 1.9: Isotopic and elemental data for carbonate phases of the Las Aguaditas Formation. A) Detail of Figure 7; mineralized veins record a unique trajectory in carbon-oxygen space, indicating little influence of late-stage fluids on matrix components. B) Elevated Sr concentrations observed in the Las Aguaditas Formation are consistent with crystallization from seawater or recrystallization in the presence of seawater derived fluids during early diagenesis. C) Evidence for elevated Mn and Fe, in conjunction with elevated Sr concentrations, is consistent with Mn and Fe enrichment in primary and early diagenetic fluids. D) Despite a few Mn/Sr values as high as 6.66, Mn/Sr ratios are generally less than 1, well below the established threshold for little-altered carbonate rocks (Mn/Sr >10; Kaufman et al. 1995). 77

Figure 1.10: C-isotope records from the Las Chacritas and Las Aguaditas formations. Chemostratigraphic profiles show $\delta^{13}C_{carb}$ compositions are consistently near −1‰ through the pre-MDICE *Y. crassus* conodont zone. In the Las Chacritas Formation, $\delta^{13}C_{carb}$ values increase from approximately −1.0‰ in the lower *E. pseudoplanus* Zone to greater than +1.0‰ in the *E. suecicus* Zone. This nearly 2‰ positive shift in $\delta^{13}C_{carb}$ values is consistent with the initiation of the MDICE. In time-equivalent strata of the Las Aguaditas Formation, however, $\delta^{13}C_{carb}$ values abruptly decline to approximately −1.5‰. Three-point moving averages are fit to $\delta^{13}C_{carb}$ profiles..... 78
Figure 1.11: C-isotope records from the Las Chacritas and Las Aguaditas formations. Organic C-isotopes record substantial variation between −25‰ and −30‰, although most values are near −28‰. C-isotope values within the deeper-water Las Aguaditas Formation are similarly volatile, yet show an abrupt transition to values near −30‰ at the transition between the Las Aguaditas Formation and the underlying San Juan Formation. Differences in isotopic composition between the two sections potentially reflect local control on the isotopic composition of DIC. Three-point moving averages are fit to $\delta^{13}C_{org}$ profiles..... 79
Figure 1.12: Interpretation of the marine shelf of the Las Chacritas and Las Aguaditas formations. Sedimentological data suggests that the Las Chacritas Formation (C) represents depositional environments between fair-weather and storm wave base, whereas sedimentary features of the Las Aguaditas Formation (A) suggest deposition at or near storm wave base. We suggest that the presence of a persistent marine chemocline (cf. Thompson and Kah, 2012) can best explain $\delta^{13}C_{carb}$ and $\delta^{13}C_{org}$ profiles of Figure 10. When carbonate formation occurs above the marine chemocline, marine carbonate reflects the isotopic composition of DIC within well-mixed oxygenated waters. By contrast, deposition below the marine chemocline may contain a mix of allochthonous and autochthonous components (C') and (A'). Carbon isotopes of autochthonous carbonate reflect a mixture of marine DIC and DIC from the remineralization of organic matter. Similarly, carbon isotopes of autochthonous organic matter potentially reflect a combination of photosynthetic and heterotrophic metabolisms, resulting in isotopically depleted signatures..... 80
Figure 2.1: Carbon and sulfur isotope profiles from Argentina and western Newfoundland (Fig. 11 of Kah et al, 2016). The mid-Dapingian negative carbon isotope excursion (thin dotted line) correlates to a positive trend in the isotopic composition of sedimentary pyrite and is interpreted to reflect enhanced euxinic conditions. The abrupt shift in the isotopic composition of marine sulfate ($\delta^{34}S_{CAS}$) in the early Darriwilian (heavy dotted line) corresponds with much slower change in isotopic composition of marine sulfide ($\delta^{34}S_{PY}$). Kah et al. (2016) interpret the isotopic enrichment of sedimentary sulfide to reflect deposition of HS^-, as pyrite, within an anoxic marine reservoir, ultimately leading to the formation of "superheavy pyrite" (grey band). 133
Figure 2.2: Location map of the Argentine Precordillera modified after Gomez and Astini (2015). Lower Paleozoic strata crop out along a series of N-S trending thrust sheets and are divided into the western and eastern Tectofacies (Astini et al., 1995). The western tectofacies consists primarily of deformed and metamorphosed deep-water

facies. Moderately to weakly deformed and unmetamorphosed marine shelf and slope deposits are exposed in the eastern tectofacies. The Gualcamayo (1) Formation was sampled to the southwest of Guandacol at the La Corridita Creek section. Samples of the Las Aguaditas (2) and Las Chacritas (3) formations were collected from measured sections southwest of San Jose de Jáchal. Radiometric age dates of K-bentonite deposits in the San Juan Formation at Cerro La Chilca (4) and Talacasto (5) suggest Dapingian ages (ca. 470 Ma; Thompson et al., 2012); however, these ages do not discretely define the age of the San Juan throughout the Precordillera (see text for discussion). 134
Figure 2.3: Time-correlation of Ordovician strata of the eastern tectofacies in the Argentine Precordillera adapted from Astini et al. (1995) and Thompson and Kah (2012). This southwest to northeast directed section illustrates the diachronous nature of the uppermost San Juan Formation across the Precordillera. Tectonic convergence of the Precordillera terrane with the Gondwanan margin resulted the formation of a foreland basin and deposition of deep-water facies to the north. Forebulge migration in the Middle Ordovician resulted in removal of shallower water facies and development of the Talacasto-Tambolar unconformity across the carbonate platform of the Precordillera. P = Pachaco section, T = Talacasto section, S = Las Silla section, C = Las Chacritas section, A = Las Aguaditas section, and Ch = La Chilca section. ... 135
Figure 2.4: Correlation of measured stratigraphic sections of the Las Chacritas, Las Aguaditas, and Gualcamayo formations based on the biostratigraphy of Serra et al. (2015), Feltes et al. (2016), and stratigraphic correlations and biostratigraphy of Astini et al. (1994), Albanesi et al. (1999), and Ortega and Albanesi (2000). Upper Darriwilian (Dw3) strata across the Precordillera were removed during development of the regional Talacasto-Tambolar unconformity (Astini et al., 1995). The absence of upper Darriwilian strata is identified by the absence of conodonts representing the upper *Eoplacognathus suecicus* and *Pygodus serra* conodont zones in the Las Chacritas Formation and the entirety of the *E. suecicus* and *P. serra* conodont zones in the Las Aguaditas Formation. In the Gualcamayo Formation, conodont biostratigraphy indicates the presence of the *Pygodus anitae* subzone of the upper *E. suecicus* Zone of stage slice Dw2, which is truncated by late Darriwilian clastic deposits of the Las Vacas/Las Plantas formations. Note the change in scale for the Gualcamayo Formation stratigraphic column. 136
Figure 2.5: Carbon and sulfur isotopic records of the Las Chacritas Formation. $\delta^{13}C_{carb}$ data from Henderson et al. (2018) show the globally recognized positive 2‰ shift of the MDICE in the *E. pseudoplanus* conodont Zone. $\delta^{34}S_{CAS}$ data are somewhat variable through the *E. pseudoplanus* Zone with isotopic compositions averaging around +25‰. $\delta^{34}S_{CAS}$ variability slightly decreases in the uppermost *E. pseudoplanus* and *E. suecicus* conodont zones with values remaining around −25‰. $\delta^{34}S_{PY}$ data are highly variable throughout the section reflecting pyrite formation in sedimentary pore fluids. A shift in $\delta^{34}S_{PY}$ values is noted in the uppermost *E. pseudoplanus* Zone and may be associated with increased organic carbon burial during the MDICE. $\Delta^{34}S$ ($\delta^{34}S_{CAS} - \delta^{34}S_{PY}$) values are generally heavy around 20-30‰ through the section but

drop in the uppermost *E. pseudoplanus* Zone as $\delta^{34}S_{PY}$ values get heavier. Conodont biostratigraphy from Serra et al. (2015)..... 138
Figure 2.6: Carbon and sulfur isotope records of the lower member of the Las Aguaditas Formation. $\delta^{13}C_{carb}$ data show a trend to more negative values around –1.5 through the MDICE interval and are interpreted to reflect incorporation of ^{13}C depleted dissolved inorganic carbon below the chemocline (cf. Henderson et al. 2018). Variability of $\delta^{34}S_{CAS}$ is interpreted to reflect small-scale shifts in the position of the chemocline, potentially between the sediment and the water column. $\delta^{34}S_{PY}$ is highly variable throughout the section with values decreasing from around +12‰ in *Y. crassus* Zone of the uppermost San Juan Formation to < 0‰ in the upper *Y. crassus* Zone of the Las Aguaditas Formation. $\delta^{34}S_{PY}$ values then increase through the MDICE interval in the *E. pseudoplanus/D. tablepointensis* Zone. Variability in $\delta^{34}S_{PY}$ reflects utilization of available H_2S in sedimentary pore fluids during pyrite formation. $\Delta^{34}S$ ($\delta^{34}S_{CAS} - \delta^{34}S_{PY}$) is highly variable between around 0‰ and 40‰ reflecting variability in both $\delta^{34}S_{PY}$ and $\delta^{34}S_{CAS}$ at or near the chemocline. Conodont biostratigraphy from Feltes et al. (2016). 140
Figure 2.7: Sulfur isotope records of the Gualcamayo Formation at La Corridita Creek. $\delta^{34}S_{CAS}$ shows a similar, but less pronounced change from values around 0‰ in the lower Darriwilian (Dw1) to values between +5‰ and +10‰ in the Middle to Late Darriwilian (Dw2-Dw3). $\delta^{34}S_{PY}$ values in the lower Darriwilian around –10‰ increase to values around +5‰ in the *U. dentatus* graptolite zone and gradually increase to around +10‰ in the Middle Darriwilian (Dw2) *H. lentus* graptolite Zone. $\Delta^{34}S$ ($\delta^{34}S_{CAS} - \delta^{34}S_{PY}$) values in the Gualcamayo Formation decline from around +10‰ in the *U. dentatus* graptolite Zone to values generally < 0‰ suggesting increased oxidation and disproportionation of sulfide to sulfate and intermediates within a deep-water H_2S reservoir. Graptolite biostratigraphy from Castro et al. (2003) correlated to conodont biostratigraphy of Ortega and Albanesi (2000) from Cerro Potrerillo. 142
Figure 2.8: Cross-plots of isotopic data for the Las Chacritas, Las Aguaditas, and Gualcamayo formations for evaluation of diagenetic alteration or pyrite oxidation during CAS extractions. A) CAS (ppm) vs. $\delta^{18}O_{carb}$, B) $\delta^{34}S_{CAS}$ vs. $\delta^{18}O_{Carb}$, C) $\delta^{34}S_{CAS}$ vs. S_{PY} (ppm), D) $\delta^{34}S_{CAS}$ vs. $\delta^{34}S_{PY}$. See text for discussion. 143
Figure 2.9: Dual reservoir model proposed for marine S-cycling initially proposed by Thompson and Kah (2012) after Rothman et al. (2003) and defined in Kah et al. (2016). Marine sulfur is divided into two chemically reactive reservoirs: a shallow water SO_4^{2-} reservoir and a reduced sulfur HS^-, which includes all phases of reduced sulfur species. This model has an input flux from crustal weathering (F_W, δ_W) as well as output fluxes as sedimentary sulfur as gypsum (F_{GYP}, δ_{GYP}), carbonate-associated sulfate (F_{CAS}, δ_{CAS}), or pyrite (F_{PY}, δ_{PY}) and allows for fluxes between reservoirs via microbial sulfate reduction (MSR; F_{MSR}, δ_{MSR}) and either biotic (F_{OX1}, δ_{OX1}) or abiotic sulfide oxidation (F_{OX2}, δ_{OX2})..... 144
Figure 2.10: Interpretation of the marine shelf of the Precordillera during deposition of the Las Chacritas, Las Aguaditas, and Gualcamayo formations in the Darriwilian.

Sedimentological evidence suggests the Las Chacritas Formation was deposited between fair-weather and storm wave-base. Sedimentary and geochemical evidence suggests deposition of the Las Aguaditas below storm wave base and below the marine chemocline through the *E. pseudoplanus/D. tablepointensis* Zone. The Gualcamayo Formation is interpreted to be below the marine chemocline throughout its deposition. We suggest the $\delta^{34}S_{PY}$ and $\delta^{34}S_{CAS}$ data are best explained by the presence of the marine chemocline in the Precordillera (cf. Thompson and Kah, 2012; Henderson et al., 2018). Carbonate formation above the chemocline (Las Chacritas Formation) results in isotopically enriched $\delta^{34}S_{CAS}$ values, whereas carbonate formed below the chemocline (Las Aguaditas and Gualcamayo formations) reflects local SO_4^{2-} with depleted isotopic compositions. Pyrite formation above the chemocline is restricted to sedimentary pore fluids and results in variable enrichment of $\delta^{34}S_{PY}$ depending on the extent of H_2S utilization during pyrite formation. Below the chemocline, pyrite can form syngenetically in the water column from the standing reduced sulfur (H_2S) reservoir as well as from sedimentary pore fluids. 145

Figure 3.1: Strontium isotope curve for the early Paleozoic showing the large drop in $^{87}Sr/^{86}Sr$ values in the Darriwilian-Sandbian interval (Middle Ordovician highlighted in gray). Data plotted in yellow squares and orange circles from Qing et al. (1995) and Saltzman et al. (2014), respectively, from conodont elements. Sr-isotope measurements from fine-grained carbonate mud plotted in blue diamonds and gray triangles from Edwards et al. (2015) and unpublished data from Thompson et al., respectively. Stage slices of the Middle Ordovician interval from Bergström et al. (2009). 210

Figure 3.2: Paleogeographic reconstruction of the Middle Ordovician after Cocks and Torsvik (2002) and Astini et al. (2007). Major landmasses are depicted in white with Perigondwanan terranes in gray. The Precordilleran terrane and the Puna/Famatina Arc are shown in dark gray. Famatina Arc volcanism is the source of Middle Ordovician bentonite deposits identified in late Dapingian/early Darriwilian strata throughout the Precordillera (Fanning et al., 2004). 211

Figure 3.3: Stratigraphic correlation of the Las Chacritas River and Las Aguaditas Creek sections based on conodont biostratigraphic analysis of Serra et al., (2015) and Feltes et al., (2016). Upper Darriwilian strata (Dw3) of the upper *E. suecicus* and *P. serra* conodont Zones in the Las Chacritas Formation and the *E. suecicus* and *P. serra* Zones in the Las Aguaditas Formation have been removed during development of a regional unconformity and are overlain by Sandbian (Sa1) strata of the middle member of the Las Aguaditas Formation. 212

Figure 3.4: Cross-plot of Rb concentration versus Sr-isotope measurement from samples treated with nitric acid and acetic acid from the Las Chacritas Formation. Generally, samples treated with nitric acid have higher Rb concentrations than samples treated with acetic acid, suggesting potential liberation of detrital Rb that adversely affects calculated initial $^{87}Sr/^{86}Sr$ compositions. Therefore, we consider the samples treated with nitric acid to better represent seawater compositions. 213

Figure 3.5: Chemostratigraphic profiles of the Las Chacritas Formation. The $\delta^{13}C_{carb}$ profile from Henderson et al. (2018) shows values around −1‰ through the *Y. crassus*

Zone and the positive ~2‰ expression of the MDICE through the *E. pseudoplanus* and *E. suecicus* zones. Neodymium isotope compositions of the Las Chacritas Formation show an increase in variability from ε_{Nd} values around −6 to −8 to ε_{Nd} values as low as −3. The $^{87}Sr/^{86}Sr$ values of the Las Aguaditas Formation show average compositions declining from around 0.7090 in the Y. crassus Zone to values around 0.7089 in the *E. pseudoplanus* Zone and to values near 0.7088 in the *E. suecicus* Zone. Variability in $^{87}Sr/^{86}Sr$ within individual conodont zones appears strongly correlated with water depth. 214

Figure 3.6: Chemostratigraphic profiles of the Las Aguaditas Formation. The abrupt decline in $\delta^{13}C_{carb}$ values from around −0.5‰ in the Y. crassus Zone to values around −1.5‰ in the *E. pseudoplanus/D. tablepointensis* Zone is interpreted to reflect migration of the Las Aguaditas Formation below the marine chemocline at the onset of the MDICE (Henderson et al., 2018). Neodymium isotope compositions in the *Y. crassus* Zone have ε_{Nd} values between −6 and −8 and no change in ε_{Nd} is observed in the *E. pseudoplanus/D. tablepointensis* Zone. The $^{87}Sr/^{86}Sr$ values of the Las Aguaditas Formation show the general trend for the Middle Ordovician, with values declining from around 0.7090 to values around 0.7088. 215

Figure 3.7: Schematic diagram of the marine shelf of the Precordillera during deposition of the Las Chacritas and Las Aguaditas formations. Geochemical decoupling between shallow- and deep-waters best explains the observed behavior of both ε_{Nd} and $^{87}Sr/^{86}Sr$ compositions. Radiogenic isotope variation can be explained by (1) exchange of Iapetan ocean waters across the Precordillera terrane, (2) volcanic activity and weathering of the Famatina volcanic province, or (3) changes in weathering changes in surface runoff between Gondwanan arc-derived terranes and older cratonic rocks. 216

Figure 3.8: Rare earth element (REE) patterns of the Las Chacritas Formation. REE concentrations were normalized to Post Archean Average Shale (PAAS; Condie, 1993). Samples from the Las Chacritas Formation generally have depleted light REE fraction when compared to the heavy REE fraction. No systematic changes in REE patterns are observed with stratigraphic height. 230

Figure 3.9: Rare earth element (REE) patterns of the Las Aguaditas Formation. REE concentrations were normalized to Post Archean Average Shale (PAAS; Condie, 1993). Samples from the Las Aguaditas Formation generally have depleted light REE fraction when compared to the heavy REE fraction. No systematic changes in REE patterns are observed with stratigraphic height; however, some samples do also show depletion in the HREE fraction, though not as extreme as that observed for the LREE fraction. 231

Introduction

1. The Ordovician ocean

A dramatic increase in the diversity of marine organisms is observed in the Early-Middle Ordovician (Harper, 2006). This event, called the Great Ordovician Biodiversification Event or GOBE, brought the ocean fauna from a primitive state, dominated by trilobites, to an ocean dominated by organisms growing up from the substrate and into the water column (Webby, 2004). Although the biodiversity of marine organisms is well documented (Sepkoski, 1981; Droser and Sheehan, 1997; Droser and Finnegan, 2003), the driver of biological innovation and expansion during this interval remains contentious (cf. Servais et al., 2009). A growing body of evidence suggests changes in nutrient cycling and nutrient availability may have played a key role in the GOBE (Locklair and Lerman, 2005; Saltzman, 2005; Zhang et al., 2010; Servais et al., 2014; Kah et al., 2016). Disruption of stratified oceanic conditions hallmark of early Paleozoic greenhouse environmental conditions (Railsback et al., 1990; Saltzman, 2005) by cooling sea-surface temperatures in the Middle Ordovician (Trotter et al., 2008) would have enhanced delivery of nutrient rich deep-waters to shallow water environments in upwelling zones. Increased nutrient availability in surface oceans could then explain the observed increases in phytoplankton diversity (Servais et al., 2010) and the patterns of the GOBE, where organisms evolve to utilize and compete for these new food sources. However, the transition between greenhouse and icehouse climate states occurs much later in the Late Ordovician (Katian; Saltzman and Young; 2005), which is inconsistent with estimated sea surface temperatures near modern values in the Middle Ordovician (Darriwilian; Trotter et al., 2008). Therefore, the GOBE occurs during the greenhouse

period when cooler sea-surface temperatures should initiate mixing between shallow- and deep-waters of the stratified Early-Middle Ordovician ocean.

Evidence for enhanced mixing, nutrient delivery, and biological production in surface oceans in the Darriwilian is found in the Middle Darriwilian Isotope Carbon Excursion (MDICE) and sulfur isotope evidence suggesting ventilation and increased deep-water oxygenation in the Darriwilian. The increase in $\delta^{13}C$ of carbonate that characterizes the MDICE is recognized globally by a +1‰ shift in China (Schmitz et al., 2010; Kah et al., 2016), +1.5‰ in Estonia (Ainsaar et al., 2004; Meidla et al., 2004; Ainsaar et al., 2007) and Newfoundland (Thompson and Kah, 2012; Kah et al., 2016), +2‰ in Argentina (Buggisch et al., 2003; Thompson et al., 2012; Albanesi et al., 2013; Henderson et al., 2018), +2.5‰ in Nevada (Young et al., 2016) and Sweden (Calner et al., 2014), and up to +4‰ in Maryland (Leslie et al., 2011). The MDICE is interpreted to reflect changing nutrient fluxes in the surface oceans that resulted in increased organic carbon burial at the time of the GOBE (Zhang et al., 2010), suggesting that oceanographic changes are underway in the Darriwilian. Sulfur isotope compositions are interpreted to reflect increased oxygenation of anoxic deep-waters through the Middle Ordovician (Thompson and Kah, 2012; Young et al., 2016). An abrupt shift in the sulfur isotope composition of carbonate associated sulfate (CAS) from +30‰ to +15‰ in the early Darriwilian of Newfoundland is interpreted to reflect large-scale ventilation and oxygenation of anoxic deep-water in the early Darriwilian of Newfoundland (Thompson and Kah, 2012; Kah et al., 2016). The isotopic composition of sedimentary pyrite, however, shows a protracted response to this ventilation event, suggesting the persistence

of a large anoxic deep-water sulfide reservoir into Middle Darriwilian (Kah et al., 2016). This is consistent with additional evidence for persistent deep-water anoxia (Saltzman et al., 2015) and low sulfate concentrations (~2–5 mM; Thompson and Kah, 2012; Young et al., 2016) in the Ordovician ocean.

In addition to these biogeochemical records, suggesting evidence for enhanced mixing and ocean circulation in the Darriwilian, another remarkable geochemical change is found in the strontium isotope composition of marine carbonate rocks. The $^{87}Sr/^{86}Sr$ record of marine carbonate and biogenic grains dramatically falls from radiogenic values near 0.7090 to less-radiogenic values near 0.7078 through the Darriwilian-Sandbian interval (Veizer and Compston, 1974; Burke et al., 1982; Denison et al., 1998; Shields et al., 2003; Saltzman et al., 2014; Edwards et al., 2015). The drop in Sr-isotope compositions is coincident with evidence for progressive ventilation and mixing of deep-ocean water body suggested by the biogeochemical records, suggesting the possibility that each of these systems is reflecting global-scale paleoceanographic change in the Darriwilian.

2. Overview of the present study

This study examines the carbon, sulfur, strontium, and neodymium isotope records from carbonate rocks of the Las Chacritas River and the Las Aguaditas Creek sections and the carbonaceous black shales of the Gualcamayo Formation at the La Corridita Creek section in the Precordillera of northwestern Argentina. These strata represent distinct, yet coeval, shallow- to deep-water facies deposited along a deepening marine shelf as the Precordillera terrane approached Gondwana in the Middle

Ordovician. This study provides additional data for the expression of geochemical gradients among facies in the Middle Ordovician ocean. This dissertation is divided into three chapters as outlined below.

2.1. Chapter 1 – Examining heterogeneity in the carbon isotope record

In Chapter 1, I investigate the expression of the Middle Darriwilian Carbon Isotope Excursion (MDICE) across marine shelf environments in the Argentine Precordillera. Previous work on the MDICE in Argentina identified a positive 2‰ shift in the $\delta^{13}C$ compositions but did not recognize the MDICE in time-equivalent strata of the deeper-water Las Aguaditas Formation (Albanesi et al., 2013). Recent high-resolution biostratigraphic investigations of these units suggests that the MDICE interval, or at least the initiation of the MDICE, should be preserved in both of the Las Chacritas and Las Aguaditas formations (Feltes et al., 2016; Feltes, 2017; Serra et al., 2017). Recent studies have identified heterogeneity in the C-isotope record of carbonate among depositional environments and water depths (Panchuk et al., 2006; Gilleaudeau and Kah, 2013; Edwards and Saltzman, 2016; Saltzman and Edwards, 2017). In this study, I present paired carbon isotope data of carbonate and organic carbon from the Las Chacritas and Las Aguaditas formations. Carbonate of the Las Chacritas Formation preserves the positive 2‰ shift in $\delta^{13}C_{carb}$ values characteristic of the MDICE; however, in equivalent strata of the Las Aguaditas Formation, $\delta^{13}C_{carb}$ values abruptly fall to < -1‰. This negative shift in $\delta^{13}C_{carb}$ values represents the first known divergence from the globally recognized pattern of the MDICE. There are also small, but distinct, changes in the organic carbon isotope records of these formations. $\delta^{13}C_{org}$ values in the Las Chacritas

Formation do not change through the MDICE interval; however, an abrupt shift in $\delta^{13}C_{org}$ values is observed prior to the recognized MDICE interval in the Las Aguaditas Formation. The divergent C-isotope trends of carbonate and organic carbon suggest deposition, or early diagenetic stabilization, in different parts of the water column – above and below the marine chemocline, respectively – during the MDICE interval. This is consistent with elevated concentrations of Mn and Fe in well-preserved carbonate phases (Thompson and Kah, 2012; Gilleaudeau and Kah, 2013; Henderson et al., 2018) and a growing consensus for regionally anoxic conditions for the Middle Ordovician ocean (Thompson and Kah, 2012; Marenco et al., 2013; Saltzman et al., 2015; Algeo et al., 2016; Kah et al., 2016; Young et al., 2016).

2.2. Chapter 2 – Evaluating redox conditions with the sulfur isotope record

In Chapter 2, I evaluate local redox conditions preserved in Middle Ordovician sedimentary rocks deposited in different water depths. Previous work on the Middle Ordovician sulfur cycle suggests dramatic changes to the marine sulfur cycle in the Darriwilian (Thompson and Kah, 2012; Kah et al., 2016), that are best explained by a dual reservoir model for S-cycling in which marine waters are depicted as having two distinct, reactive marine reservoirs for sulfur (Kah et al., 2016). Changes in the sulfur isotope composition of the Middle Ordovician suggest reduction of stratified ocean conditions and ventilation of anoxic deep-waters, potentially driven by cooler sea-surface temperatures (Trotter et al., 2008), resulting in invigorated ocean circulation, and subsequent delivery of cooler, more oxygenated water to deeper portions of the water column. Previous S-isotope work in the Ordovician, however, has focused mainly on

shallow water carbonate successions (Thompson and Kah, 2012; Kah et al., 2016; Young et al., 2016). Here, I expand our understanding of sulfur cycling in the Middle Ordovician ocean with high-resolution $\delta^{34}S_{CAS}$ and $\delta^{34}S_{PY}$ records from three formations in the Argentine Precordillera—the Las Chacritas, Las Aguaditas, and Gualcamayo formations—that represent distinct, yet coeval depositional environments that span from well-mixed and oxygenated waters to waters beneath the marine chemocline. Sulfur isotope data from these formations record facies dependent $\delta^{34}S$ compositions that are related to the position of a persistent marine chemocline during the Middle Ordovician. These new S-isotope data are used to further constrain the behavior of marine sulfur and evaluate the utility of a dual-reservoir model for sulfur cycling in the Early Paleozoic.

2.3. Chapter 3 – Investigating physical records of paleoceanographic mixing

In Chapter 3, I investigate the potential for physiochemical stratification of the Ordovician ocean with neodymium and strontium isotope compositions. Stratified ocean conditions of the Early Ordovician are suggested by biogeochemical records of carbon and sulfur; however, it is unclear whether such stratification was dynamically maintained by redox conditions of the water column (Küspert, 1982) or by physical separation of distinct water masses (Railsback et al., 1990). Dramatic changes in the biogeochemical cycles of carbon and sulfur have been recognized in the Ordovician. Specifically, initiation of the Middle Darriwilian Isotope Carbon Excursion (MDICE; Ainsaar et al., 2004) corresponds to a sharp change in the isotopic composition of both carbonate-associated sulfate (CAS) and pyrite and extends through an interval marked by deposition of "superheavy" pyrite (i.e. where S-isotope values of pyrite are heavier than associated

values for marine sulfate; Thompson and Kah, 2012; Marenco et al., 2013; Kah et al., 2016). These geochemical changes have been attributed to changes in marine circulation that result in deep-water ventilation and shifting nutrient fluxes associated with redox stratification of the Ordovician oceans (Thompson and Kah, 2012; Henderson et al., 2018). Interestingly, these biogeochemical changes are coincident with a globally recognized shift in the $^{87}Sr/^{86}Sr$ value of seawater (Veizer and Compston, 1974; Burke et al., 1982; Richter et al., 1992; McArthur, 1994; Shields et al., 2003), which decreases from ~0.7090 in the Middle Darriwilian (ca. 462 Ma) to ~0.7078 by the Early Sandbian (ca. 458 Ma). Traditionally, the isotopic composition of marine strontium is thought to be homogeneous in the ocean because of its long residence time in seawater (Taylor and McLennan, 1985; Banner, 2004). However, during times of persistent ocean stratification, as observed for the Early-Middle Ordovician, marine strontium may have behaved differently, potentially resulting in the development of a strontium isotope gradient between shallow and deep-water (cf. Banner, 2004).

Here, I present new strontium and neodymium isotope data from the Middle Darriwilian Las Chacritas and Las Aguaditas formations of the Argentine Precordillera, which represent coeval shallower- and deeper-water depositional environments. These formations occur just prior to the start of the large shift in Sr-isotope compositions observed worldwide (Qing et al., 1998; Shields et al., 2003; Saltzman et al., 2014; Edwards et al., 2015). $^{87}Sr/^{86}Sr$ data from these formations fit within the global framework for Sr-isotope change with values ranging from above 0.7090 to approximately 0.7088. To test whether distinct oceanographic reservoirs of Sr, or a

persistent gradient in marine $^{87}Sr/^{86}Sr$ compositions, may play a role in the observed $^{87}Sr/^{86}Sr$ change of Middle Ordovician oceans, I examine the relative behavior of strontium and the behavior of neodymium—which has a much shorter residence time than Sr and has been used to distinguish discrete oceanic water masses—in these successions. Environmental differences in the isotopic composition of both strontium and neodymium in the units suggests geochemical decoupling between shallow and deep waters, confirming the presence of physical stratification in Middle Darriwilian ocean waters in the Precordillera.

References

Ainsaar, L., Meidla, T., and Tinn, O., Middle and Upper Ordovician stable isotope stratigraphy across the facies belts in the East Baltic, *in* Proceedings 8th Meeting on the Working Group on the Ordovician Geology of Baltoscandia, Tallinn and Tartu, Estonia, 2004, Tartu University Press, p. 11-12.

Ainsaar, L., Meidla, T., Tinn, O., Martma, T., and Dronov, A., 2007, Darriwilian (Middle Ordovician) carbon isotope stratigraphy in Baltoscandia: Acta Paleontologica Sinica, v. 46, p. 1-8.

Albanesi, G. L., Bergström, S. M., Schmitz, B., Serra, F., Feltes, N. A., Voldman, G. G., and Ortega, G., 2013, Darriwilian (Middle Ordovician) $\delta^{13}C_{carb}$ chemostratigraphy in the Precordillera of Argentina: Documentation of the Middle Darriwilian Isotope Carbon Excursion (MDICE) and its use for intercontinental correlation: Palaeogeography, Palaeoclimatology, Palaeoecology, v. 389, p. 48-63. http://dx.doi.org/10.1016/j.palaeo.2013.02.028

Algeo, T. J., Marenco, P. J., and Saltzman, M. R., 2016, Co-evolution of oceans, climate, and the biosphere during the 'Ordovician Revolution': A review: Palaeogeography, Palaeoclimatology, Palaeoecology, v. 458, p. 1-11. https://doi.org/10.1016/j.palaeo.2016.05.015

Banner, J. L., 2004, Radiogenic isotopes: systematics and applications to earth surface processes and chemical stratigraphy: Earth-Science Reviews, v. 65, p. 141-194. http://dx.doi.org/10.1016/S0012-8252(03)00086-2

Buggisch, W., Keller, M., and Lehnert, O., 2003, Carbon isotope record of Late Cambrian to Early Ordovician carbonates of the Argentine Precordillera: Palaeogeography, Palaeoclimatology, Palaeoecology, v. 195, p. 357-373. http://dx.doi.org/10.1016/S0031-0182(03)00365-1

Burke, W. H., Denison, R. E., Hetherington, E. A., Koepnick, R. B., Nelson, H. F., and Otto, J. B., 1982, Variation of seawater $^{87}Sr/^{86}Sr$ throughout Phanerozoic time: Geology, v. 10, p. 516-519. 10.1130/0091-7613(1982)10<516:vosstp>2.0.co;2

Calner, M., Lehnert, O., Wu, R., Dahlqvist, P., and Joachimski, M. M., 2014, $\delta^{13}C$ chemostratigraphy in the Lower–Middle Ordovician succession of Öland (Sweden) and the global significance of the MDICE: GFF, v. 136, p. 48-54. http://dx.doi.org/10.1080/11035897.2014.901409

Denison, R. E., Koepnick, R. B., Burke, W. H., and Hetherington, E. A., 1998, Construction of the Cambrian and Ordovician seawater $^{87}Sr/^{86}Sr$ curve: Chemical Geology, v. 152, p. 325-340. http://dx.doi.org/10.1016/S0009-2541(98)00119-3

Droser, M. L., and Finnegan, S., 2003, The Ordovician Radiation: A Follow-up to the Cambrian Explosion?1: Integrative and Comparative Biology, v. 43, p. 178-184. 10.1093/icb/43.1.178

Droser, M. L., and Sheehan, P. M., 1997, Palaeoecology of the Ordovicianradiation; Resolution of Large-Scale Patterns with Individual Clade Histories,

Palaeogeography and Environments: Geobios, v. 30, Supplement 1, p. 221-229. http://dx.doi.org/10.1016/S0016-6995(97)80027-7

Edwards, C. T., and Saltzman, M. R., 2016, Paired carbon isotopic analysis of Ordovician bulk carbonate ($\delta^{13}C_{carb}$) and organic matter ($\delta^{13}C_{org}$) spanning the Great Ordovician Biodiversification Event: Palaeogeography, Palaeoclimatology, Palaeoecology, v. 458, p. 102-117. http://dx.doi.org/10.1016/j.palaeo.2015.08.005

Edwards, C. T., Saltzman, M. R., Leslie, S. A., Bergström, S. M., Sedlacek, A. R. C., Howard, A., Bauer, J. A., Sweet, W. C., and Young, S. A., 2015, Strontium isotope ($^{87}Sr/^{86}Sr$) stratigraphy of Ordovician bulk carbonate: Implications for preservation of primary seawater values: GSA Bulletin, v. 127, p. 1275-1289. 10.1130/b31149.1

Feltes, N., Albanesi, G. L., and Bergstrom, S. M., 2016, Conodont biostratigraphy and global correlation of the middle Darriwilian-lower Sandbian (Ordovician) Las Aguaditas Formation, Precordillera of San Juan, Argentina: Andean Geology, v. 43, p. 60-85. http://dx.doi.org/10.5027/andgeoV43n1-a04

Feltes, N. A., 2017, Fauna de conodontes y graptolitos de la Formación Las Aguaditas (Ordovícico) en el cordón de Los Blanquitos, Precordillera Central de San Juan, Argentina [Ph.D.: Universidad Nacional de Córdoba, 453 p.

Gilleaudeau, G. J., and Kah, L. C., 2013, Carbon isotope records in a Mesoproterozoic epicratonic sea: Carbon cycling in a low-oxygen world: Precambrian Research, v. 228, p. 85-101. http://dx.doi.org/10.1016/j.precamres.2013.01.006

Harper, D. A. T., 2006, The Ordovician biodiversification: Setting an agenda for marine life: Palaeogeography, Palaeoclimatology, Palaeoecology, v. 232, p. 148-166. http://dx.doi.org/10.1016/j.palaeo.2005.07.010

Henderson, M. A., Serra, F., Feltes, N. A., Albanesi, G. L., and Kah, L. C., 2018, Paired isotope records of carbonate and organic matter from the Middle Ordovician of Argentina: Intrabasinal variation and effects of the marine chemocline: Palaeogeography, Palaeoclimatology, Palaeoecology, v. 490, p. 107-130. https://doi.org/10.1016/j.palaeo.2017.10.018

Kah, L. C., Thompson, C. K., Henderson, M. A., and Zhan, R., 2016, Behavior of marine sulfur in the Ordovician: Palaeogeography, Palaeoclimatology, Palaeoecology, v. 458, p. 133-153. http://dx.doi.org/10.1016/j.palaeo.2015.12.028

Küspert, W., 1982, Environmental Changes During Oil Shale Deposition as Deduced from Stable Isotope Ratios, *in* Einsele, G., and Seilacher, A., eds., Cyclic and Event Stratification: Berlin, Heidelberg, Springer Berlin Heidelberg, p. 482-501. 10.1007/978-3-642-75829-4_36

Leslie, S. A., Saltzman, M. R., Bergström, S. M., Repetski, J. E., Howard, A., and Seward, A. M., Conodont biostratigraphy and stable isotope stratigraphy across the Ordovician Knox/Beekmantown unconformity in the central Appalachians, *in*

Proceedings Ordovician of the World 2011, Volume Serie, Cuadernos del Museo Geomin-Minero, Publicaciones del Instituto Geológico y Minero de España.

Locklair, R. E., and Lerman, A., 2005, A model of Phanerozoic cycles of carbon and calcium in the global ocean: Evaluation and constraints on ocean chemistry and input fluxes: Chemical Geology, v. 217, p. 113-126. http://dx.doi.org/10.1016/j.chemgeo.2004.12.010

Marenco, P. J., Marenco, K. N., Lubitz, R. L., and Niu, D., 2013, Contrasting long-term global and short-term local redox proxies during the Great Ordovician Biodiversification Event: A case study from Fossil Mountain, Utah, USA: Palaeogeography, Palaeoclimatology, Palaeoecology, v. 377, p. 45-51. http://dx.doi.org/10.1016/j.palaeo.2013.03.007

McArthur, J. M., 1994, Recent trends in strontium isotope stratigraphy: Terra Nova, v. 6, p. 331-358. 10.1111/j.1365-3121.1994.tb00507.x

Meidla, T., Backman, L., Dronov, A., Holmer, L., and Sturesson, U., Middle-Upper Ordovician carbon isotope record from Västergötland (Sweden) and East Baltic, *in* Proceedings 8th Meeting on the Working Group on the Ordovician Geology of Baltoscandia, Tallinn and Tartu, Estonia, 2004, Tartu University Press, p. 67-68.

Panchuk, K. M., Holmden, C. E., and Leslie, S. A., 2006, Local controls on carbon cycling in the Ordovician midcontinent region of North America, with implications for carbon isotope secular curves: Journal of Sedimentary Research, v. 76, p. 200-211. http://dx.doi.org/10.2110/jsr.2006.017

Qing, H., Barnes, C. R., Buhl, D., and Veizer, J., 1998, The strontium isotopic composition of Ordovician and Silurian brachiopods and conodonts: relationships to geological events and implications for coeval seawater: Geochimica et Cosmochimica Acta, v. 62, p. 1721-1733. http://dx.doi.org/10.1016/S0016-7037(98)00104-5

Railsback, L. B., Ackerly, S. C., Anderson, T. F., and Cisneti, J. L., 1990, Palaeontological and isotope evidence for warm saline deep waters in Ordovician oceans: Nature, v. 343, p. 156-159. http://dx.doi.org/10.1038/343156a0

Richter, F. M., Rowley, D. B., and DePaolo, D. J., 1992, Sr isotope evolution of seawater: the role of tectonics: Earth and Planetary Science Letters, v. 109, p. 11-23. http://dx.doi.org/10.1016/0012-821X(92)90070-C

Saltzman, M. R., 2005, Phosphorus, nitrogen, and the redox evolution of the Paleozoic oceans: Geology, v. 33, p. 573-576. http://dx.doi.org/10.1130/g21535.1

Saltzman, M. R., and Edwards, C. T., 2017, Gradients in the carbon isotopic composition of Ordovician shallow water carbonates: A potential pitfall in estimates of ancient CO_2 and O_2: Earth and Planetary Science Letters, v. 464, p. 46-54. http://dx.doi.org/10.1016/j.epsl.2017.02.011

Saltzman, M. R., Edwards, C. T., Adrain, J. M., and Westrop, S. R., 2015, Persistent oceanic anoxia and elevated extinction rates separate the Cambrian and Ordovician radiations: Geology, v. 43, p. 807-810. 10.1130/g36814.1

Saltzman, M. R., Edwards, C. T., Leslie, S. A., Dwyer, G. S., Bauer, J. A., Repetski, J. E., Harris, A. G., and Bergström, S. M., 2014, Calibration of a conodont apatite-based Ordovician $^{87}Sr/^{86}Sr$ curve to biostratigraphy and geochronology: Implications for stratigraphic resolution: Geological Society of America Bulletin. 10.1130/b31038.1

Saltzman, M. R., and Young, S. A., 2005, Long-lived glaciation in the Late Ordovician? Isotopic and sequence-stratigraphic evidence from western Laurentia: Geology, v. 33, p. 109-112. http://dx.doi.org/10.1130/g21219.1

Schmitz, B., Bergström, S. M., and Xiaofeng, W., 2010, The middle Darriwilian (Ordovician) $\delta^{13}C$ excursion (MDICE) discovered in the Yangtze Platform succession in China: implications of its first recorded occurrences outside Baltoscandia: Journal of the Geological Society, v. 167, p. 249-259. http://dx.doi.org/10.1144/0016-76492009-080

Sepkoski, J. J., Jr., 1981, A Factor Analytic Description of the Phanerozoic Marine Fossil Record: Paleobiology, v. 7, p. 36-53. 10.2307/2400639

Serra, F., Feltes, N. A., Ortega, G., and Albanesi, G. L., 2017, Lower middle Darriwilian (Ordovician) graptolites and index conodonts from the Central Precordillera of San Juan Province, Argentina: Geological Journal, p. n/a-n/a. 10.1002/gj.3043

Servais, T., Danelian, T., Harper, D. A. T., and Munnecke, A., 2014, Possible oceanic circulation patterns, surface water currents and upwelling zones in the Early Palaeozoic: Gff, v. 136, p. 229-233. http://dx.doi.org/10.1080/11035897.2013.876659

Servais, T., Owen, A. W., Harper, D. A. T., Kröger, B., and Munnecke, A., 2010, The Great Ordovician Biodiversification Event (GOBE): The palaeoecological dimension: Palaeogeography, Palaeoclimatology, Palaeoecology, v. 294, p. 99-119. http://dx.doi.org/10.1016/j.palaeo.2010.05.031

Servais, T. H., D.AT., Li, J., Munnecke, A., Owen, A.W., Sheehan, P.M.,, 2009, Understanding the Great Ordovician Biodiversification Event (GOBE): Influences from paleogeography, paleoclimate, or paleoecology?: GSA Today, v. 19, p. 4-10.

Shields, G. A., Carden, G. A. F., Veizer, J., Meidla, T., Rong, J.-Y., and Li, R.-Y., 2003, Sr, C, and O isotope geochemistry of Ordovician brachiopods: a major isotopic event around the Middle-Late Ordovician transition: Geochimica et Cosmochimica Acta, v. 67, p. 2005-2025. http://dx.doi.org/10.1016/S0016-7037(02)01116-X

Taylor, S. R., and McLennan, S. M., 1985, The Continental Crust: Its Composition and Evolution, Oxford, Blackwell, pp.

Thompson, C. K., and Kah, L. C., 2012, Sulfur isotope evidence for widespread euxinia and a fluctuating oxycline in Early to Middle Ordovician greenhouse oceans: Palaeogeography, Palaeoclimatology, Palaeoecology, v. 313-314, p. 189-214. http://dx.doi.org/10.1016/j.palaeo.2011.10.020

Thompson, C. K., Kah, L. C., Astini, R., Bowring, S. A., and Buchwaldt, R., 2012, Bentonite geochronology, marine geochemistry, and the Great Ordovician Biodiversification Event (GOBE): Palaeogeography, Palaeoclimatology, Palaeoecology, v. 321–322, p. 88-101. http://dx.doi.org/10.1016/j.palaeo.2012.01.022

Trotter, J. A., Williams, I. S., Barnes, C. R., Lécuyer, C., and Nicoll, R. S., 2008, Did Cooling Oceans Trigger Ordovician Biodiversification? Evidence from Conodont Thermometry: Science, v. 321, p. 550-554. http://dx.doi.org/10.1126/science.1155814

Veizer, J., and Compston, W., 1974, $^{87}Sr/^{86}Sr$ composition of seawater during the Phanerozoic: Geochimica et Cosmochimica Acta, v. 38, p. 1461-1484. http://dx.doi.org/10.1016/0016-7037(74)90099-4

Webby, B. D., Droser, M.L., Paris, F., and Percival, I., 2004, The Great Ordovician Biodiversification Event, *in* Webby, B. D., Droser, M.L., Paris, F., and Percival, I., ed., The Great Ordovician Biodviersification Event: New York, Columbia University Press, p. 484. http://dx.doi.org/10.1017/S0016756805220782

Young, S. A., Gill, B. C., Edwards, C. T., Saltzman, M. R., and Leslie, S. A., 2016, Middle–Late Ordovician (Darriwilian–Sandbian) decoupling of global sulfur and carbon cycles: Isotopic evidence from eastern and southern Laurentia: Palaeogeography, Palaeoclimatology, Palaeoecology, v. 458, p. 118-132. http://dx.doi.org/10.1016/j.palaeo.2015.09.040

Young, S. A., Saltzman, M. R., Foland, K. A., Linder, J. S., and Kump, L. R., 2009, A major drop in seawater $^{87}Sr/^{86}Sr$ during the Middle Ordovician (Darriwilian): Links to volcanism and climate?: Geology, v. 37, p. 951-954. 10.1130/g30152a.1

Zhang, T., Shen, Y., and Algeo, T. J., 2010, High-resolution carbon isotopic records from the Ordovician of South China: Links to climatic cooling and the Great Ordovician Biodiversification Event (GOBE): Palaeogeography, Palaeoclimatology, Palaeoecology, v. 289, p. 102-112. http://dx.doi.org/10.1016/j.palaeo.2010.02.020

Chapter 1
Paired isotope records of carbonate and organic matter from the Middle Ordovician of Argentina: Intrabasinal variation and effects of the marine chemocline

This chapter was originally published in Palaeogeography, Palaeoclimatology, Palaeoecology in January 2018 by Miles A. Henderson, Fernanda Serra, Nicolás A. Feltes, Guillermo L. Albanesi, and Linda C. Kah:

Miles A. Henderson, Fernanda Serra, Nicolás A. Feltes, Guillermo L. Albanesi, and Linda C. Kah. "Paired isotope records of carbonate and organic matter from the Middle Ordovician of Argentina: Intrabasinal variation and the effects of the marine chemocline." Palaeogeography, Palaeoclimatology, Palaeoecology 490 (2018): 107-130.

Miles A. Henderson collected the data and drafted the manuscript and figures. Dr. Linda C. Kah provided advice on the science and edited the manuscript and figures. Drs. Guillermo L. Albanesi, Nicolás A. Feltes, and Fernanda Serra aided with fieldwork and biostratigraphic correlation.

Abstract

We investigate the expression of the Middle Darriwilian isotope carbon excursion (MDICE) across marine shelf environments in the Argentine Precordillera. Previous work identified the MDICE in the Las Chacritas Formation in Argentina, but did not recognize the expression of the MDICE in time-equivalent strata of the deeper-water Las Aguaditas Formation (Albanesi et al., 2013; Palaeogeography, Palaeoclimatology, Palaeoecology, v. 398, p. 48–66). Recent biostratigraphic investigations of these units have, for the first time, provided the opportunity for high-resolution correlation, which suggest that the MDICE, or at least the initiation of the MDICE, should be observed in

both the Las Chacritas and Las Aguaditas formations. Here we present new paired carbon isotope data of carbonate and organic carbon from the Las Chacritas and Las Aguaditas formations. We identify a 2‰ positive shift in the isotopic composition of marine carbonate in the Las Chacritas Formation, whereas values abruptly fall to < −1‰ in equivalent strata of the Las Aguaditas Formation. This is the first record of divergence from the globally recognized MDICE event. There are also small, yet distinct differences in the isotopic composition of marine organic matter between these two sections. We suggest that the divergent C-isotope trends of carbonate in the Las Chacritas and Las Aguaditas formations represent deposition in fundamentally different parts of the water column — above and below the marine chemocline, respectively — during the MDICE interval. This interpretation is consistent with data from the Las Aguaditas Formation that shows elevated Mn and Fe concentrations in carbonate phases with little evidence for recrystallization, and with a growing consensus for regionally anoxic conditions for the Middle Ordovician. Our data indicate that redox gradients can play a critical role in the behavior of marine carbon isotope excursions.

1. Introduction

The carbon isotope record of marine carbonate minerals has become a widely used geochemical tool for correlating stratigraphic sections (cf. Berger and Vincent, 1981; Saltzman and Thomas, 2012; Kah et al., 2012; Azmy et al., 2014). Because dissolved inorganic carbon (DIC) in surface oceans has a relatively short residence time relative to oceanic mixing, high resolution stratigraphic signatures may be resolved. Globally recognized excursions in the carbon isotope composition of marine carbonate

minerals thus allow for chemostratigraphic correlation among geographically disparate sections, even in the absence of biostratigraphic control (Halverson et al., 2005).

Marine carbonate rocks of the Ordovician are bracketed by large (+5‰ to +7‰) perturbations in the isotopic composition of marine DIC including the late Cambrian Steptoean positive carbon isotope excursion (SPICE; Saltzman et al., 1998) and the late Ordovician Katian (Saltzman and Young, 2005) and Hirnantian carbon isotope excursions (HICE; Brenchley et al., 1994; Finney et al., 1999). These large-scale perturbations have been associated with episodes of climatic cooling, enhanced ocean circulation, and elevated organic productivity (Saltzman, 2005). Between these periods of isotopic volatility, stability in marine carbon isotopes is hypothesized to result from generally sluggish circulation and reduced organic productivity driven by greenhouse climates. Such periods of enhanced stability are recognized by only small-magnitude isotope excursions (to approximately +2‰), such as the Middle Darriwilian isotope carbon excursion (MDICE).

The MDICE was first recognized in Baltoscandia (Ainsaar et al., 2004; Meidla et al., 2004; Martma, 2005; Ainsaar et al., 2007; Kaljo et al., 2007; Calner et al., 2014), and later recognized in equivalent-aged strata in China (Schmitz et al., 2010; Zhang et al., 2010; Kah et al., 2016), North America (Leslie et al., 2011; Thompson et al., 2012; Young et al., 2016), and in the Precordillera of Argentina (Thompson et al., 2012; Albanesi et al., 2013), making it one of the most widely recognized Ordovician excursions. The MDICE is characterized by a near monotonic rise of carbon isotope compositions from approximately −2‰ during the Dapingian to values > +1‰ during the

Middle Darriwilian. Although relatively small in magnitude, the MDICE event appears to coincide with an inferred decrease in ocean temperatures prior to the Hirnantian glaciation (Trotter et al., 2008) and potential deep-water ventilation (Thompson et al., 2012; Marenco et al., 2013; Kah et al., 2016), both of which are consistent with a potentially fundamental shift in the behavior of the oceans that may have participated in the Great Ordovician Biodiversification Event (GOBE; Webby et al., 2004; Harper et al., 2006; Servais et al., 2010; Rasmussen et al., 2016). The behavior of the MDICE across a variety of environments may therefore provide an additional constraint on the physical and chemical behavior of marine systems at this time.

Recent revisions to the biostratigraphy of Darriwilian carbonate successions in the Argentine Precordillera (Serra et al., 2015; Feltes et al., 2016) suggest that the MDICE, or at least its initiation, should occur in the upper *Eoplacognathus pseudoplanus* and lower *Eoplacognathus suecicus* conodont biozones of the Las Chacritas and Las Aguaditas formations, whose facies represent distinct environments on a deepening marine shelf. Here we use recent biostratigraphic correlations to explore the relationships between C-isotope records of carbonate and organic matter during the middle Darriwilian within time-equivalent, yet distinct, depositional environments. This is the first study to use paired C-isotopes record of carbonate and organic carbon to evaluate the expression of the MDICE across time correlative units and distinct depositional environments, and will further our understanding of potential marine conditions at this critical interval in Earth history.

2. Geologic setting and age

2.1. The Argentine Precordillera

The Precordillera is the remnant of an independent microcontinent terrane that rifted from the southeast margin of Laurentia in the early Cambrian (ca. 530–539 Ma; Thomas et al., 2001), and was transported across the Iapetus ocean before docking with Gondwana during the Late Ordovician (Ramos et al., 1986; Astini et al., 1995; Thomas and Astini, 1996; Astini and Thomas, 1999; Thomas et al., 2002; Thomas, 2011). Although the paleogeographic location of the Precordillera through this interval is not well constrained (Fig. 1; Cocks and Torsvik, 2002); transfer across the Iapetus Ocean is inferred from a decrease in fauna with Laurentian affinity through the Tremadocian and increasing biotic exchange with Baltica and Gondwana during the Darriwilian and Sandbian (Harper et al., 1996; Benedetto, 2004; Benedetto et al., 2009). Proximity of the Precordillera terrane to the Gondwanan margin by the Dapingian (Thompson et al., 2012) is confirmed by the presence of bentonite deposits that are associated with volcanism in the Famatina arc province (Astini et al., 1995; Huff et al., 1995; Huff et al., 1997; Huff et al., 1998; Pankhurst et al., 2000; Fanning et al., 2004).

Within the Precordillera, more than 2500 m of Cambrian to Ordovician strata are exposed in a series of North–South trending thrust sheets that comprise the Andean foothills between 28˚ and 33˚ S (Fig. 2; Ramos et al., 1986; Astini et al., 1995; Keller, 1999). The region is subdivided into the eastern and western tectofacies, which record carbonate, evaporite, and siliciclastic deposition in marine shelf and slope environments (Astini et al., 1995). Little deformed and unmetamorphosed strata of the eastern tectofacies record a transition from passive margin carbonate deposition to siliciclastic

deposition associated with the development of a foreland basin inboard of the Precordillera terrane (Astini et al., 1995). Deeper-water facies of the western tectofacies are more strongly deformed, and were subjected to low-grade metamorphism during regional shortening (Allmendinger et al., 1990; Zapata and Allmendinger, 1996; Alvarez-Marron et al., 2006; Allmendinger and Judge, 2014).

2.2. Middle Ordovician Strata

Relatively undeformed Early and Middle Ordovician strata are exposed in the eastern tectofacies within the Niquivil thrust sheet in San Juan Province, Argentina (von Gosen, 1997). Strata include the Tremadocian La Silla Formation, the Floian–Darriwilian San Juan Formation, and the Darriwilian–Sandbian Las Chacritas, Las Aguaditas, and Gualcamayo formations. The transition to Middle Ordovician (Dapingian) strata occurs in the San Juan Formation, which records the transition from shallow subtidal carbonate deposition to storm-dominated subtidal deposits (Canas, 2003). The contact between the San Juan Formation and overlying strata of the Las Chacritas, Las Aguaditas, and Gualcamayo formations is marked by a transition to deeper-water, siliciclastic-rich to siliciclastic-dominated facies (Astini, 1995b; Carrera and Astini, 1998). This transition is time-transgressive (Astini, 1995a), reflecting differential subsidence as the Precordilleran terrane converged upon Gondwana. In some places (e.g., Talacasto and Pachaco sections, Thompson et al., 2012), the San Juan Formation is terminated by an unconformity and overlain by Silurian strata. This unconformity is associated with the formation of the Talacasto-Tambolar Arch and migration of the forebulge during the Late Ordovician, and

resulted in the removal of late Darriwilian through early Silurian strata across much of the Precordillera (Astini et al., 1995).

Precise chronologic ages are best determined for the San Juan Formation, which contains abundant bentonites (Huff et al., 1995). The most recent determination of dates from the San Juan Formation range from 473.45 ± 0.70 Ma to 469.53 ± 0.62 Ma (U-Pb_{zircon}; Thompson et al., 2012), which is consistent with earlier analyses that yielded dates of 470 ± 3.3 Ma to 469 ± 3.2 Ma (Fanning et al., 2004). As noted previously, the upper contact of the San Juan Formation is diachronous, and at the Talacasto section, the San Juan Formation is truncated by an unconformity. These Dapingian ages therefore do not distinctly define the age of the uppermost San Juan Formation. There are no current geochronological dates to precisely constrain the age of overlying Las Chacritas, Las Aguaditas, and Gualcamayo formations.

2.2.1. The Las Chacritas Formation

For this study, the Las Chacritas Formation was investigated in the northern La Trampa Range along the Las Chacritas River, approximately 37 km south of San Jose de Jáchal, San Juan Province, Argentina (30°33'39.06" S, 68°51'49.62" W; Fig. 2). Sedimentologic and biostratigraphic relationships at the Las Chacritas River section have been previously reported (Peralta and Baldis, 1995; Carrera and Astini, 1998; Peralta et al., 1999; Heredia et al., 2005; Albanesi et al., 2013; Serra et al., 2015; Serra et al., 2017). The following is a summary of both previous investigations and current observations of the Las Chacritas River section. The Las Chacritas Formation is an approximately 60-m-thick succession of interbedded carbonate and black shale that conformably, and

transitionally, overlies fossiliferous packstone, wackestone, and mudstone lithologies of the San Juan Formation (Keller, 1999). Strata of San Juan Formation thin from ~1 m to 5–10 cm in thickness toward the top of the unit. The contact between the San Juan Formation and the overlying Las Chacritas Formation is marked by a hardground surface and the occurrence of a thin bentonite horizon.

The Las Chacritas Formation is divided into two members; a lower member of fossiliferous mudstone, wackestone, and packstone and an upper member of mudstone, spiculitic mudstone, and a thin interval of bioclastic grainstone (Peralta et al., 1999). At the locality sampled for this study, the Las Chacritas Formation is approximately 65 m thick based on field measurement combined with conodont biostratigraphy (Serra et al., 2015). The formation consists of 2–10 cm thick beds of fossiliferous mudstone, wackestone, and packstone interbedded with < 2 cm thick partings of black shale. Higher in the section, fossiliferous wackestone and spiculitic mudstone beds are thinner (2–5 cm thick) with thicker (> 2 cm thick) interbeds of black shale. Carrera (1997) identified sponges in the Las Chacritas Formation belonging to the *Archaeoscyphia* Biofacies which is associated with deposition below fair-weather wave base, but above storm wave base. The top of the Las Chacritas Formation is marked by a regional unconformity overlain by Sandbian calcareous and siliciclastic deposits of the deeper-water, middle member of the Las Aguaditas Formation (Peralta et al., 1999).

2.2.2. The Las Aguaditas Formation

The Las Aguaditas Formation was investigated at its type section along Las Aguaditas Creek in the Los Blanquitos Range, approximately 10 km to the southwest of

San Jose de Jáchal, San Juan Province, Argentina (30°18'16.38" S, 68°49'13.40" W; Fig. 2). The following is a summary of previous (Keller et al., 1993; Astini, 1995b; Keller, 1999; Albanesi et al., 2013; Feltes et al., 2016) and current observations of the Las Aguaditas Formation. At Las Aguaditas Creek, the Las Aguaditas Formation conformably, and gradationally, overlies fossiliferous, nodular packstone, wackestone, and mudstone lithologies of the San Juan Formation (Keller et al., 1993). Transitional strata of the upper San Juan Formation are dominated by 5–10-cm thick mudstone beds, although a 20-cm-thick packstone interval was observed just below the contact with calcareous mudstone of the overlying Las Aguaditas Formation.

The Las Aguaditas Formation is approximately 300 m thick, and spans Darriwilian through the early Sandbian time (Keller et al., 1993; Astini, 1995b; Feltes, 2017). Darriwilian-age strata occur in the 43-meter-thick lower member, which is composed of thinly bedded (1–5 cm) carbonate mudstone and wackestone, interbedded with prominent intervals (< 10 cm thick) of calcareous black shale. Limestone of the Las Aguaditas Formation contains abundant sponge spicules and trilobite fragments, yet lacks evidence of bioturbation. Nodular wackestone intervals exhibit differential cementation and dissolution associated with bioturbation on the seafloor (Keller et al., 1993). The interpreted depositional setting for the lower member of the Las Aguaditas Formation is in relatively deep water, at or below storm wave base. The top of the lower member of the Las Aguaditas Formation is marked by a disconformity identified by the abrupt appearance of Sandbian conodonts (Albanesi et al., 2013; Feltes et al., 2016).

2.3. Biostratigraphic correlation of the Las Chacritas and Las Aguaditas formations

A general chronologic framework of Ordovician strata in the Precordillera, based on conodont and graptolite biostratigraphy, is well established (Albanesi and Ortega, 2016). High-resolution conodont and graptolite biostratigraphic investigations are consistent with a primarily Darriwilian age for the Las Chacritas and Las Aguaditas formations, and have provided a more detailed correlation between these two units (Figs. 3 and 4; Albanesi et al., 2013; Serra et al., 2015; Feltes et al., 2016; Serra et al., 2017). Conodont elements are abundant in the upper San Juan and Las Chacritas formations (Serra et al., 2015). In deeper water facies of the lower member of the Las Aguaditas Formation, relatively few conodont elements were recovered (Feltes et al., 2016). Conodont fauna are dominated by tropical, generally shallow-water (< 200 m) assemblages in the Early Ordovician, though an increasing number of temperate water taxa are identified by the Middle Ordovician (Albanesi and Ortega, 2016).

Conodont elements recovered from limestone of the Las Chacritas and Las Aguaditas formations record the presence of *Yangtzeplacognathus crassus*, *E. pseudoplanus*, *E. suecicus*, and *Pygodus anserinus* Zones, with the *Lenodus variabilis* and *Y. crassus* Zones occurring in the uppermost San Juan Formation (Fig. 3). Using the chronostratigraphic correlations of Bergström et al. (2009) and Webby et al. (2004), lower Darriwilian conodont Zones (stage slice (SS) Dw1 of Bergström et al., 2009, and time slice (TS) 4a of Webby et al., 2004) are identified in the *L. variabilis* Zone and correlate to the *L. variabilis* Zone identified in Scandinavia and China, and the *Histiodella sinuosa* Zone in North America (Albanesi and Ortega, 2016). In the sections investigated for this study, the top of the *L. variabilis* Zone was identified in the San Juan

Formation, 3.75 m below the base of the Las Chacritas Formation and 24 m below the base of the Las Aguaditas Formation.

The *Y. crassus* Zone, which marks the transition to the Middle Darriwilian (SS Dw2, TS 4b) is approximately 40 m thick in the Las Chacritas Formation and 36 m thick in the Las Aguaditas Formation. The lower boundary of the *Y. crassus* Zone is marked by the presence of the *Paroistodus horridus* subzone in the Precordillera (Albanesi and Barnes, 2000). The upper boundary of the *Y. crassus* Zone is marked by the presence of *Dzikodus tablepointensis* in the Las Aguaditas Formation and the first appearance of *Eoplacognathus pseudoplanus* in the Las Chacritas Formation (Albanesi and Barnes, 2000; Albanesi et al., 2013; Serra et al., 2015; Feltes et al., 2016). The *Y. crassus* Zone correlates to strata in south China, Scandinavia, Baltica, and the North Atlantic (Fig. 3; cf. Serra et al., 2015).

The base of the *E. pseudoplanus* Zone (SS Dw2) is identified 36 m above the base of the Las Chacritas Formation and extends to 58 m above the base of the unit (Serra et al., 2015). In the Las Aguaditas Formation, the *E. pseudoplanus* Zone is 24 m thick and characterized by the co-occurrence of *D. tablepointensis*. The *E. pseudoplanus* Zone is identified in shallow water environments in Baltoscandia, whereas *D. tablepointensis* is characteristic of deeper-water water environments found in China and Newfoundland (Feltes et al., 2016). The upper *E. pseudoplanus* Zone in the Precordillera is marked by the occurrence of *Microzarkodina hagetiana* and *M. ozarkodella* (Serra et al., 2015; Feltes et al., 2016). The *E. pseudoplanus* Zone is equivalent to the *E. pseudoplanus* Zone in Baltoscandia. Identification of the *Histiodella holodenta* subzone in the top of the *E.*

pseudoplanus Zone allows for correlation to China (Zhang, 1998), Baltoscandia (Viira, 2011), and the uppermost Table Point Formation in the Table Head Group of Newfoundland (Stouge, 1984). In the Las Chacritas River section, the top of the *E. pseudoplanus* Zone is marked by the occurrence of *Histiodella kristinae* which typifies the lower subzone of the *E. suecicus* Zone and defines the rest of SS Dw2 in the Precordillera (Serra et al., 2015). The *E. suecicus* zone correlates to the *E. suecicus* Zone of Baltoscandia and with the *H. kristinae* Zone and the *Periodon zgierzensis* Zone of the Table Point Group of Western Newfoundland (Stouge, 2012; Serra et al., 2015).

A disconformity is identified at the top of both the Las Chacritas and Las Aguaditas formations by the occurrence of the Sandbian conodont elements of *Pygodus anserinus* (SS Sa1; Albanesi et al., 2013; Serra et al., 2015; Feltes et al., 2016). In the Las Chacritas Formation, the top of the *E. suecicus* (SS Dw2, TS 4b) and the *P. serra* (SS Dw3, TS 4C) conodont zones are missing. In the deeper water Las Aguaditas Formation, the top of the *E. pseudoplanus*, the *E. suecicus,* the *P. serra,* and lower subzone of the *P. anserinus* zones have been removed. More extensive removal of deeper water strata from the Las Aguaditas Formation cannot readily be explained by sea level fall, and has thus been attributed to forebulge migration. Emplacement of a tectonic load on a rigid lithosphere typically results in migration of the forebulge away from the tectonic load, resulting in preferential uplift and erosion of shallower water environments (Beaumont, 1981). Patterns of missing time in the Precordillera are attributed to forebulge migration associated with oblique convergence of the northward-deepening carbonate platform with

the Gondwanan margin that resulted in flexural uplift and differential erosion of initially deeper water environments (cf. Catuneanu, 2004).

3. Analytical methods

3.1. Petrographic screening

Carbonate samples were cut into mirror-image billets used, respectively, for thin sections and polished thick sections. Thin and thick sections were analyzed using conventional petrographic and cathodoluminescence (CL) analysis to assess the range of carbonate fabrics and identify phases that show evidence of post-depositional recrystallization. Discrete carbonate phases were drilled from polished thick sections with 0.3 or 0.5 mm drill bits using a Servo tabletop drill press. Splits of resulting powders were used for isotopic and elemental analyses.

3.2. Isotopic analyses of carbonate phases

For isotopic analysis of carbonate phases, approximately 0.25 mg of carbonate powder was loaded into a glass vial with a septum cap, flushed with ultra-high purity helium gas for 5 minutes, then acidified with 100 µl of phosphoric acid at 72˚C for at least 1 hour. The resulting CO_2 gas was sampled using a Thermo-Finnegan GasBench II and transferred into a Thermo-Finnegan DeltaPlus XL mass spectrometer for isotope ratio measurement at the University of Tennessee. Isotope ratios of carbon and oxygen are reported in delta notation as per mil (‰) relative to the Vienna Pee Dee Belemnite (VPDB) standard. Precision and calibration of data were monitored through routine analysis of internal laboratory and the IAEA LSVEC ($\delta^{13}C = -46.6‰$; $\delta^{18}O = -26.41‰$) and NBS 19 ($\delta^{13}C = +1.95‰$; $\delta^{18}O = -2.2‰$) international standards. Analyses were

reproducible to better than ± 0.1‰ for carbon and ± 0.2‰ for oxygen, based on analysis of replicates and internal laboratory standards.

3.3. Elemental analyses

Drilled carbonate powders were analyzed for major (Ca, Mg) and trace (Sr, Mn, Fe) element concentrations with a Perkin-Elmer Optima 2100 DV inductively coupled plasma-optical emission spectrometer (ICP-OES) at the University of Tennessee. Approximately 1 mg of carbonate powder was acidified with trace metal grade 2% HNO_3, and agitated for > 1 hour to assure complete dissolution of carbonate. Solutions were centrifuged and decanted into a clean sample tubes to remove any insoluble materials prior to analysis. Spectra were calibrated using a series of gravimetric standards, with reproducibility for all elements better than ± 5% based on replicate measurements of sample and standard solutions.

3.4. Isotopic analyses of organic matter

For isotope determination of organic carbon phases, approximately 100 mg of bulk sample powder was acidified with 10 ml of 3M HCl until all reaction was complete. Residual powders were rinsed three times with Milli-Q water and dried at 50˚C. Approximately 3.5 mg of insoluble residue was weighed into tin cups for combustion in a Costech ECS 4010 elemental analyzer. The resulting CO_2 gas was transferred into a Thermo-Finnegan DeltaPlus XL mass spectrometer via a Thermo-Finnegan Conflo III interface at the University of Tennessee. Precision and calibration of data were monitored through routine analysis of internal laboratory and the USGS40 and USGS41 ($\delta^{13}C$ equal to −26.39‰ and +37.63‰, respectively) international standards. Isotope ratios are

reported in delta notation as per mil (‰) relative to the Vienna Pee Dee Belemnite (VPDB) standard. Analyses were reproducible to better than ± 0.12‰ based on analysis of replicates and internal laboratory standards.

4. Results and interpretation

4.1. Petrographic characterization

Petrographic analysis of Darriwilian carbonate rocks from the San Juan and overlying Las Chacritas and Las Aguaditas formations are consistent with field observations that strata are composed of primarily carbonate mudstone, wackestone, and packstone. Petrographic observations, however, provide additional detail that highlights the similarities and differences between the formations. Strata of the upper San Juan Formation in both the Las Chacritas River and Las Aguaditas Creek sections are composed of fossiliferous wackestone and packstone (Figs. 5A and 6A), dominated by a matrix of either micrite or finely crystalline microspar (< 5 μm). Dolomitization is rare in all formations and, when present, is found in sections that have also experienced fabric destructive recrystallization of micrite to sparry calcite cement. Stylolitization is common in the upper San Juan Formation and the Las Chacritas Formation, but is not easily defined in the shale-rich deposits of the Las Aguaditas Formation. Skeletal grains are common in the San Juan Formation and consist of bryozoans, gastropods, echinoderms, brachiopods, and sponge spicules. Skeletal grains in the San Juan Formation are typically 0.02 to 1.6 mm in size, with measurements representing the longest diameter of a circumscribed ellipse; most skeletal fragments represent disarticulated elements, yet with few broken elements. Preservation of skeletal microfabrics is variable, with most

echinoderm, brachiopod, and trilobite elements retaining their primary microstructures; by contrast, gastropods and sponges are more commonly represented by molds filled with fine calcite spar.

Deepening in the Precordillera is reflected in the transition from subtidal packstone of the upper San Juan Formation to predominantly wackestone and carbonate mudstone in the Las Chacritas and Las Aguaditas formations. The Las Chacritas Formation is composed largely of carbonate mudstone (Fig. 5B) and wackestone, with intermittent packstone intervals (Fig. 5C) in the *E. pseudoplanus* Zone. Carbonate mudstone in the Las Chacritas Formation is typically poorly laminated, and contains continuous to discontinuous clay laminations, which occur primarily as drapes along bedding planes. In some sections, micrite has been recrystallized to finely crystalline (< 5 μm) microspar. Allochems in the Las Chacritas Formation consist of micritic intraclasts (Fig. 5B), brachiopod and trilobite fragments, and sponge spicules. Skeletal microfabrics are variably preserved, with brachiopod and sponge spicules largely recrystallized and the prismatic microstructure of trilobite fragments nearly always preserved. Fewer skeletal grains are observed toward the top of the Las Chacritas Formation, where only rare trilobite fragments and recrystallized sponge spicules are identified. Recrystallization of matrix components to a coarse calcite spar is observed, although recrystallization is not abundant and is concentrated within rare, more fossiliferous horizons. Disseminated pyrite is also identified throughout the Las Chacritas Formation (Figs. 5B–D) and does not appear to be associated with any specific depositional texture.

The Las Aguaditas Formation is composed primarily of carbonate mudstone and wackestone with intermittent clay and silt laminations. Clay minerals are interlaminated with micrite and occur as flocculated aggregates dispersed throughout micritic laminations (Fig. 6B). Silty carbonate (Fig. 6C) is identified in one sample of the Las Aguaditas Formation. Allochems in the Las Aguaditas Formation are restricted to trilobite fragments, except in rare beds that contain fragments of brachiopods, trilobites, bryozoans, and sponge spicules (Fig. 6D). Recrystallization of micrite to fine-grained microspar generally occurs along bedding planes and within rare packstone beds. Disseminated pyrite is identified in the Las Aguaditas Formation, and occurs predominantly along bedding planes.

4.1.1. Evidence of secondary components

At least three generations of calcite veins are distinguished by cross-cutting relationships in the strata of the upper San Juan, Las Chacritas, and Las Aguaditas formations within the field area, and are likely associated with Andean orogenesis that resulted in uplift and exposure of these successions (Astini et al., 1995; Allmendinger and Judge, 2014). A small network of thin (~50 μm) dark-colored (in hand sample) veins represent the first stage of vein formation. These veins are cut by thin (< 1 mm) white veins (cf. Fig. 6A), which are, in turn, cross-cut by a third generation of thick (1-7 mm) white veins. All vein stages have sharp contacts with surrounding rock. In thin section the first stage of veins is characterized by fine-grained equant calcite spar. The larger thin white veins and the final generation of veins are both characterized by coarse, calcite spar

exhibiting competitive growth into the center of the veins (i.e. syntaxial growth; Scholle and Ulmer-Scholle, 2003).

4.1.2. Cathodoluminescence petrography

Cathodoluminescence (CL) analysis of carbonate lithologies from the upper San Juan, Las Chacritas, and Las Aguaditas formations show a variety of luminescence characteristics. Overall, CL analyses revealed dully luminescent, fine-grained limestone with variably luminescent, spar filled fractures and voids. The upper San Juan Formation is characterized by a dark orange dully luminescent matrix with brightly luminescent to moderately luminescent skeletal grains. Luminescence of later stage veins in the San Juan Formation is variable, from brightly luminescent to non-luminescent, and shows the sharp contrast between the host limestone and vein-filling cement. Large veins are generally compositionally zoned, with highly luminescent calcite spar evolving to dully luminescent calcite spar as the vein was filled.

In the Las Chacritas Formation, micrite and fine-grained microspar exhibit dark orange luminescence, with only small fossil fragments showing brighter luminescence (Fig. 5E). The heterogeneous, yet uniform, luminescence within matrix components is attributed to presence of disseminated siliciclastic and clay rich grains, which are non-luminescent. Skeletal grains in the Las Chacritas Formation generally exhibit dull luminescence, similar to matrix components; however, spar-filled sponge spicule molds and rare echinoderm fragments are brightly luminescent (Fig. 5E). Later stage veins in the Las Chacritas Formation appear similar to those observed in the underlying San Juan Formation, with predominantly brightly luminescent calcite spar in large veins (Figs. 5E

and 5F), although non-luminescent calcite spar is observed in small veins (< 0.5 mm) and in the center of some of the larger veins.

Limestone of the Las Aguaditas Formation exhibits a uniform dark to moderate orange luminescence. As with the Las Chacritas Formation, micritic and microsparitic matrix phases of the Las Aguaditas Formation are uniformly heterogeneous (Fig. 6E), although the luminescence is slightly darker, which may reflect an increase in the proportion of non-luminescent clay minerals. Skeletal grains in the Las Aguaditas Formation generally are less luminescent than the surrounding matrix, except for molds of sponge spicules, which are filled with brightly luminescent cement (Fig. 6F). Luminescence of later stage calcite veins in the Las Aguaditas Formation is variable with both brightly luminescent large veins (Fig. 6E) and dull to moderately luminescent smaller veins (Fig. 6F). Luminescence characteristics of veins are distinct from that of adjacent carbonate phases.

4.1.3. Interpretation

Limestone of the San Juan, Las Chacritas, and Las Aguaditas formations consist largely of micritic and microsparitic, carbonate mudstone and wackestone. Petrographic fabrics observed in these successions are consistent with deposition in subtidal marine environments. The poorly laminated micrite of the Las Chacritas Formation with intermittent clay drapes on bedding planes suggests deposition in relatively quiet water, below fair-weather wave base, with wackestone and packstone intervals likely representing reworking of shallower-water facies during storm events. Increased clay content and lamination within mudstone facies combined with a paucity of grain-rich

intervals in the Las Aguaditas Formation suggests deposition predominantly below storm wave base.

The primary depositional phase of these limestones is micrite and finely crystalline microspar. The absence of more coarsely crystalline phases suggests that these phases have undergone only minimal diagenetic recrystallization, because the process of dissolution and reprecipitation typically results in significant grain coarsening. Coarse grained calcite cements occur only within grain-rich lithologies, or as vein-filling components. Fossil components in both formations are well preserved; however, distinct differences in the abundance and diversity of fossils is observed between the units. Fauna in the lower Las Chacritas Formation is like that of the underlying San Juan Formation; however, fauna in the upper Las Chacritas Formation are restricted to trilobite fragments and recrystallized sponge spicules. In the Las Aguaditas Formation, only trilobite fragments and sponge spicules are observed. This restriction in faunal diversity is consistent with deposition of the Las Chacritas and Las Aguaditas formations along a deepening slope away from a remnant carbonate platform.

Dull orange luminescence observed for the matrix of both the Las Chacritas and Las Aguaditas formations is consistent with minimal recrystallization. Variation in the luminescence of matrix material appears to be largely restricted to discrete fossil grains and silty regions. Although the veins identified provide evidence for multiple later-diagenetic episodes of fluid flow, CL analysis shows no clear evidence that fluids participated in the alteration of matrix components. Furthermore, generally dull luminescence of micritic and microsparitic matrix suggests recrystallization occurred

during early seafloor diagenesis. Early diagenetic recrystallization of the matrix material on the seafloor would have been buffered by interstitial fluids, with compositions near that of the original seawater. Previous studies have considered these fine-grained components to be most likely to record "near primary" seawater geochemical compositions (Kaufman et al., 1991; Kah et al., 1999; Bartley et al., 2007).

4.2. Geochemical characterization of carbonate phases

4.2.1. Carbon and oxygen isotope compositions

Geochemical results from the Las Chacritas River and Las Aguaditas Creek sections are reported in Tables 1 and 2 and summarized in Table 3. Overall carbon isotope compositions, range from −2.25 to +1.41‰ (Tables 1-3; Figs. 7, 8A, and 9A). $\delta^{13}C$ values of petrographically well-preserved micritic and microsparitic phases in the Las Chacritas River section range from −1.48 to +1.41‰ (Table 1). Secondary carbonate phases, represented by spar within coarse-grained lithologies in the Las Chacritas Formation, have $\delta^{13}C$ values that range from −1.10 to +0.44‰. $\delta^{13}C$ compositions of vein-filling cements in the Las Chacritas formation range from −1.45 to +0.69‰. Similarly, $\delta^{13}C$ values for micritic phases in the Las Aguaditas Formation range from −2.25 to +0.56‰ (Table 2). Secondary carbonate in the Las Aguaditas Formation ranges from −0.58 to +1.0‰. Carbon isotope compositions of vein-filling cements in the Las Aguaditas Formation range from −1.37 to +0.52‰.

The O-isotopic compositions of micritic phases in the Las Chacritas Formation range from −7.23 to −3.14‰ (Table 1). $\delta^{18}O$ compositions for secondary carbonate (spar) range from −6.94 to −3.02‰. Vein-filling cements have $\delta^{18}O$ compositions ranging from

−8.80 to −4.53‰. In the Las Aguaditas Formation, $\delta^{18}O$ compositions for micritic phases range from −5.81 to −4.06‰ (Table 2). Oxygen isotope compositions of sparry calcite in the Las Aguaditas Formation range from −5.44 to −3.22‰. Vein-filling cements in the Las Aguaditas Formation have oxygen isotope compositions ranging from −10.76 to −2.88‰.

4.2.2. Elemental signatures

Major- and trace-element chemistry of microdrilled carbonate phases were analyzed for Ca, Mg, Sr, Fe, and Mn concentrations (Tables 1 and 2, Figs. 8 and 9). All carbonate phases from the Las Chacritas and Las Aguaditas formations have Mg/Ca ratios of less than 0.07, consistent with stoichiometric calcite. Strontium concentrations of matrix components in the Las Chacritas Formation range from 174 to 1330 ppm with an average concentration of 530 ± 252 ppm (n = 94; Table 1). Secondary carbonate spar has Sr concentrations from 190 to 585 ppm with an average of 363 ± 99 ppm (n = 20). Vein filling cements have Sr concentrations from 204 to 1383 ppm with an average concentration of 587 ± 278 ppm (n = 23). Manganese and iron concentrations in the Las Chacritas Formation range from 98 to 1553 ppm and 421 to 11,496 ppm with average values of 476 ± 196 and 2546 ± 1898 ppm (n = 94), respectively. Secondary calcite spar in the Las Chacritas Formation has concentrations ranging from 213 to 773 ppm and 492 to 3854 ppm with average values of 521 ± 156 and 1398 ± 772 ppm (n = 20) respectively for Mn and Fe.

Similarly, petrographically well-preserved micrite in the Las Aguaditas Formation has Sr concentrations ranging from 283 to 2166 ppm with an average of 788 ± 402 ppm

(n = 80; Table 2). Strontium concentrations from secondary calcite phases, spar- and vein-filling cements, in the Las Aguaditas Formation range from 207 to 994 ppm and 278 to 1434 ppm with average concentrations of 467 ± 198 ppm (n = 28) and 781 ± 333 ppm (n = 23), respectively. Manganese and Fe concentrations of micritic carbonate in the Las Aguaditas Formation range from 163 to 3274 ppm and 525 to 6715 ppm with average concentrations of 642 ± 618 ppm and 6815 ± 2668 ppm (n = 80), respectively. Secondary carbonate (spar) from the Las Aguaditas Formation has Mn and Fe concentrations ranging from 206 to 2318 ppm and 278 to 6644 ppm with average concentrations of 549 ± 519 and 2264 ± 1688 ppm (n = 28), respectively. Later vein-filling cements in the Las Aguaditas Formation have Mn and Fe concentrations ranging from 156 to 1512 ppm and 278 to 6992 ppm with average concentrations of 561 ± 349 ppm and 3877 ± 1711 ppm (n = 23), respectively.

4.2.3. Interpretation

Carbonate minerals are chemically reactive and therefore susceptible to dissolution and recrystallization both syndepositionally, in the presence of seawater or modified pore fluids, and during later diagenesis in the presence of non-native fluids. Cross-plots of isotopic ($\delta^{13}C$ and $\delta^{18}O$) and elemental (Ca, Mg, Sr, Mn, and Fe) data provide a useful tool for assessing systematic variation associated with diagenetic alteration, because the degree of chemical alteration resulting from water-rock interaction has predictable behaviors (cf. Banner and Hanson, 1990). Potential end-member fluid compositions can further be inferred by comparing the geochemical composition of fine-

grained depositional phases, such as micrite and microspar, and secondary carbonate phases, such as coarsely crystalline, vein-filling cement.

Carbon and oxygen compositions of depositional and diagenetic carbonate phases are shown in Figure 7. Carbon isotope compositions of depositional phases within both the Las Chacritas and Las Aguaditas formations fall broadly between −1.5‰ and +1.5‰, which is consistent with Darriwilian-aged carbonates worldwide (Ainsaar et al., 2004; Saltzman and Young, 2005; Kaljo et al., 2007; Schmitz et al., 2010; Zhang et al., 2010; Thompson et al., 2012; Albanesi et al., 2013; Edwards and Saltzman, 2016). Oxygen isotope compositions, similarly, fall largely between −4.5‰ and −6‰, which is consistent with well-preserved marine carbonate rocks of the lower Paleozoic (Carpenter and Lohmann, 1997; Veizer et al., 1999; Jaffrés et al., 2007). There are no discrete trends indicative of isotopic resetting resulting from interaction of carbonate minerals with meteoric waters, which are often characterized by depletion in both ^{13}C and ^{18}O (Marshall, 1992). There is, however, a noted difference in composition between micrite-dominated matrix phases and more grain-rich matrix phases, which contain a greater amount of intergranular sparry cement. Micrite-dominated phases in both the Las Chacritas and Las Aguaditas formations have lower carbon and oxygen isotope compositions, by ~ 1‰ and 0.5‰ respectively. Although this difference in isotopic composition is small, its correspondence to lithologies that are inferred to represent shallower (grain-rich) and deeper (micrite-dominated) depositional environments suggest different diagenetic pathways. Possibilities include: (1) the presence of primary differences in the composition of shallower and deeper water bodies, (2) differences in

primary porosity leading to early diagenetic stabilization by isotopically different fluids (i.e., seawater for grain-rich phases, and modified substrate pore fluids for micritic phases; cf. Schrag et al., 2013), or (3) preferential alteration of specific phases in the presence of late diagenetic fluids.

Examination of the Las Chacritas and Las Aguaditas formations separately (Figs. 8A and 9A) reveals that there is no consistent pattern between the composition of primary phases and that of secondary calcite phases, which is consistent with only minimal isotope exchange between carbonate minerals and later diagenetic fluids. This observation is consistent with an interpretation in which the isotopic variation between micrite and grain-rich lithologies reflects a primary difference in the composition of early diagenetic fluids.

Trace elements incorporated into carbonate phases can provide additional insight into the depositional and diagenetic history of these samples. Strontium concentrations of carbonate rocks, in particular, are easily altered during diagenetic recrystallization (Brand and Veizer, 1980; Banner and Hanson, 1990). In both the Las Chacritas and Las Aguaditas formations (Figs. 8B and 9B), there is no clear relationship between the Sr concentration of depositional phases and that of vein mineralization, which supports an interpretation of only minimal isotopic exchange during late-stage diagenesis. Strontium concentrations in both formations are consistently lower in grain-rich lithologies, suggesting potential for a greater degree of early diagenetic recrystallization. In both formations, however, grain-rich lithologies average 313 ± 60 ppm Sr, which is similar to that expected from calcite precipitated from open marine waters (Veizer, 1983). More

elevated Sr concentrations (> 1000 ppm) within micritic lithologies, along with $\delta^{18}O$ compositions typical of well-preserved marine carbonate, suggests minimal recrystallization of primary carbonate phases. Secondary carbonate phases with Sr concentrations similar to those of primary phases further suggest the limestone of the Las Chacritas and Las Aguaditas formations have not undergone significant diagenetic recrystallization, because Sr is commonly excluded from the crystal lattice with recrystallization, even at low water-rock ratios. Combined, the fabric retentive nature of carbonate phases in the Las Chacritas and Las Aguaditas formations, combined with these observations suggest that recrystallization of matrix phases likely occurred in penecontemporaneous marine or modified marine fluids.

Elevated concentrations of redox-sensitive trace elements, such as Mn and Fe, can be used as evidence for recrystallization of carbonate phases in reducing fluids associated with deep-burial (Veizer, 1983). Low concentrations of Mn and Fe, however, are expected for carbonate phases derived from oxygenated marine waters, and higher concentrations may reflect deposition or early diagenetic stabilization in sub-oxic to anoxic fluids. Manganese concentrations of depositional carbonate phases in the Las Chacritas and Las Aguaditas formations are typically < 500 ppm, although concentrations reach as high as 1553 ppm in the Las Chacritas Formation and 3274 ppm in the Las Aguaditas Formation. Iron concentrations are even more variable (Figs. 8C and 9C). Elevated Mn and Fe concentrations co-occur with Sr concentrations that indicate limited alteration of marine carbonate phases. Combined with interpretations of deposition during flooding of the San Juan platform, suggesting that elevated Mn and Fe

concentrations may record incorporation of these elements during precipitation of early diagenetic stabilization of carbonate in anoxic marine fluids or pore waters (cf. Thompson and Kah, 2012; Gilleaudeau and Kah, 2013a).

Combined, these observations suggest deposition and early diagenetic stabilization of carbonate lithologies of the Las Chacritas and Las Aguaditas formations in sub-oxic to anoxic marine fluids or marine pore waters. These samples likely preserve carbon isotope values that reflect their environments of deposition and early diagenetic stabilization; resetting of carbon isotope values typically requires extensive water-rock interaction not supported by the preserved isotopic and elemental compositions (Banner and Hanson, 1990). Even under the assumption that elevated Mn concentrations reflect recrystallization during later diagenesis, Mn/Sr ratios as high as 10 have been shown to retain near primary marine carbon isotope compositions (Kaufman and Knoll, 1995). Depositional carbonate phases in the Las Chacritas and Las Aguaditas formations (Figs. 8D and 9D) generally have Mn/Sr < 1. Samples with Mn/Sr > 1 occur in the uppermost strata of the San Juan Formation in both sections, suggesting a possible stratigraphic control on Sr and Mn concentrations. There is no petrographic evidence of differential diagenesis in these samples; however, these carbonates were deposited during marine transgression, which is consistent with elevated Mn concentrations potentially associated with transgression of deeper, anoxic marine fluids across the shelf.

4.3. Carbon isotope compositions of organic matter

Sedimentary organic matter ranges from 0.04 to 0.53 wt. % in the Las Chacritas Formation and from 0.03 to 0.36 wt. % in the Las Aguaditas Formation. The carbon

isotope composition of organic matter is similar in both units, ranging between −30.45 to −24.16‰ in the Las Chacritas Formation and −30.84 to −22.76‰ in the Las Aguaditas Formation.

4.3.1. Interpretation

Photosynthetic production of organic matter from the marine DIC pool results in organic matter depleted in ^{13}C by approximately 22–30‰ (Hayes et al., 1999), which is consistent with isotopic compositions observed within the Las Chacritas and Las Aguaditas formations. Carbon isotope compositions of marine organic matter, however, can also be affected by diagenetic alteration, terrestrial organic input, and heterotrophic reworking within the depositional environment. The isotopic composition of sedimentary organic carbon may be affected by thermal maturation and post-depositional fluid flow that results in isotopically heavier $\delta^{13}C_{org}$ compositions (Hayes et al., 1999; Derry, 2010). Approximate burial temperatures for the Las Chacritas and Las Aguaditas formations are provided by conodont elements, which have conodont alteration indices of 2.5–3 (Serra et al., 2015; Feltes et al., 2016), corresponding to burial temperatures of 90–190˚C (Epstein et al., 1977). Differences in thermal histories for the Las Chacritas and Las Aguaditas formations may explain some of the $\delta^{13}C_{org}$ variation between these formations; however, it does not explain stratigraphic changes in $\delta^{13}C_{org}$ in a single outcrop where a uniform thermal history is expected.

Although purported terrestrially derived organic carbon has been identified in Darriwilian strata (cf. Strother et al., 1996), the isotopic composition of this organic carbon (~ −29‰; Jahren et al., 2003) is unlikely to be easily differentiated from marine

organic carbon and is not further considered. Remineralization of organic carbon by heterotrophic metabolic activities in the substrate can result in either isotopic enrichment, through aerobic oxidation of organic matter under well-mixed and oxygenated conditions, or isotopic depletion, via secondary input of isotopically light organic carbon via chemoautotrophic microbial metabolisms (cf. Hayes et al. 1999; further discussed in Section 5).

4.4. Chemostratigraphic profiles

Petrographic, isotopic, and elemental data suggest that the Las Chacritas and Las Aguaditas formations likely retain near-primary marine geochemical signatures, associated with deposition and early diagenetic stabilization at or near the sediment-water interface. Chemostratigraphic profiles for the Las Chacritas and Las Aguaditas formations are shown in Figure 10. In the Las Chacritas section, $\delta^{13}C_{carb}$ increases from around −1‰ to around 0‰ at the top of the *L. variabilis* Zone within the San Juan Formation. In the *Y. crassus* Zone, $\delta^{13}C_{carb}$ is relatively stable around −1‰, with values of −0.73 ± 0.26‰ in the lower *Y. crassus* Zone, and −0.90 ± 0.29‰ in the upper *Y. crassus* zone (Fig. 10). $\delta^{13}C_{carb}$ compositions then steadily increase from around −1‰ to +0.5‰ through the *E. pseudoplanus* Zone before reaching a high of +1.4‰ in the basal *E. suecicus* Zone. $\delta^{13}C_{carb}$ values return to near 0‰ in the *P. anserinus* Zone.

At the Las Aguaditas Creek section, $\delta^{13}C_{carb}$ values in the *Y. crassus* Zone (here representing the uppermost San Juan Formation and lowermost Las Aguaditas Formation) are similar to values recorded in the Las Chacritas creek section, with values of −0.31 ± 0.20‰ in the lower *Y. crassus* Zone, and −0.61 ± 0.25‰ in the upper *Y.*

crassus Zone. By contrast, $\delta^{13}C_{carb}$ compositions in the *E. pseudoplanus/D. tablepointensis* Zone of the Las Aguaditas Formation, rather than rising to positive values, abruptly fall to values of −1.15 ± 0.52‰. An abrupt transition to $\delta^{13}C_{carb}$ values near 0.25‰ marks the *P. anserinus* Zone.

The $\delta^{13}C_{org}$ record is more variable. In the uppermost strata of the San Juan Formation, $\delta^{13}C_{org}$ values are relatively stable ~ −29‰ and increase in the Las Chacritas Formation to values near −28‰ through the *Y. crassus* Zone and the lower *E. pseudoplanus* Zone (Fig. 11). Variability in $\delta^{13}C_{org}$ increases in the transition from the *Y. crassus* to the *E. pseudoplanus* zones, with values ranging between −24.16 and −29.79‰. $\delta^{13}C_{org}$ then records an abrupt decrease to values near −30‰ through remainder of the *E. pseudoplanus* Zone and within the *E. suecicus* Zone. Values remain near −30‰ in the *P. anserinus* Zone.

The $\delta^{13}C_{org}$ record of the Las Aguaditas Formation is more variable than the shallower water Las Chacritas Formation. At the Las Aguaditas Creek Section, $\delta^{13}C_{org}$ values from the lower *Y. crassus* Zone in the San Juan Formation are variable around −26‰, before abruptly falling to values that remain near −30‰ in the upper *Y. crassus* Zone. $\delta^{13}C_{org}$ values, although more variable, remain near −30‰ in the *E. pseudoplanus/D. tablepointensis* Zone. Above the unconformity at the top of the lower member of the Las Aguaditas Formation values increase to around −26‰ before falling to around −31‰.

5. Discussion

5.1. Summary of observations

Combined petrographic and geochemical data suggest early diagenetic stabilization at or near the seafloor, in the presence of marine, or potentially modified marine, porewaters with little evidence for alteration of chemical compositions by late diagenetic fluids. The Las Chacritas and Las Aguaditas formations reflect deposition during the *Y. crassus* and *E. pseudoplanus* conodont biozones (Darriwilian, Dw2) and the lowermost *E. suecicus* Zone (Darriwilian, Dw3), which include the timeframe of the globally recognized MDICE (Meidla et al., 2004; Ainsaar et al., 2007; Schmitz et al., 2010; Zhang et al., 2010; Thompson et al., 2012; Albanesi et al., 2013; Edwards and Saltzman, 2014; Kah et al., 2016; Young et al., 2016). Within this framework, we explore the origin of distinct isotopic patterns between coeval shallower-water facies of the Las Chacritas Formation and deeper-water facies of the Las Aguaditas Formation through the MDICE interval.

The isotopic composition of marine carbonate recorded in the Las Chacritas and Las Aguaditas formations show a similar stable trend through the *Y. crassus* Zone, although $\delta^{13}C_{carb}$ values are heavier in the Las Aguaditas Formation by approximately 0.4‰ (Fig. 10). During the MDICE interval, which occurs within the *E. pseudoplanus* and *E. suecicus* Zones, the Las Chacritas Formation records $\delta^{13}C_{carb}$ values increasing from around −1.0‰ to around +1.0‰. Whereas Albanesi et al. (2013) measured bulk $\delta^{13}C_{carb}$ values of marine carbonate, which can result in the mixing of early and late diagenetic phases, our microsampling of discrete carbonate phases yields data suggesting the expression of the MDICE is stronger in the Precordillera than previously recognized.

The ~ 2.0‰ positive shift in $\delta^{13}C_{carb}$ values recorded in the Las Chacritas Formation is comparable to the global expression of the MDICE, which ranges from ~ 1‰ in China (Schmitz et al., 2010; Kah et al., 2016), to ~ 1.5‰ in Estonia (Meidla et al., 2004; Ainsaar et al., 2007; Kaljo et al., 2007) and Newfoundland (Thompson and Kah, 2012), to ~ 2.5‰ in Nevada, USA (Young et al., 2016) and Sweden (Calner et al., 2014), and to up to ~ 4‰ in Maryland, USA (Leslie et al., 2011), despite the erosional removal of the upper *E. suecicus* Zone.

By contrast, the MDICE interval in time equivalent strata of the Las Aguaditas Formation is characterized by an abrupt shift to values near −1.5‰. To our knowledge, the Las Aguaditas Formation provides the first clear divergence from the globally observed positive isotopic shift. Previous work in the Las Aguaditas Formation recognized carbon isotope composition near −1‰ through the MDICE interval (Albanesi et al., 2013), but attributed the lack of a clear MDICE signal to removal of strata associated with the top of the *E. pseudoplanus* and *E. suecicus* conodont zones. Recent biostratigraphic analysis, however, identified the *Histiodella kristinae* Subzone in the uppermost strata of the Lower Member of the Las Aguaditas Formation, which is commonly associated with the *E. suecicus* zone, although the *E. suecicus* Zone is not formally recognized in the Las Aguaditas Formation (Serra et al., 2015; Feltes et al., 2016). Therefore, the MDICE, or at least the initiation of the MDICE interval, should be present in both formations.

The presence of stratigraphically younger conodonts in the *E. suecicus* Zone in the Las Chacritas Formation (*Histiodella bellburnensis*; Serra et al., 2015) and the lack of

this zone in the Las Aguaditas Formation suggests that the regional disconformity identified at the top of each section represents less time in shallower-water depositional environments. This is consistent with oblique convergence of the Precordillera terrane and associated uplift and erosion of strata associated with migration of the peripheral bulge (cf. Catuneanu, 2004).

5.2. Potential for geochemical alteration

The presence of a regional disconformity suggests the possibility that geochemical signatures preserved in the Las Chacritas and Las Aguaditas formations may be affected by diagenetic overprinting from isotopically depleted waters during subaerial exposure. C-isotope compositions that are depleted in ^{13}C have been identified beneath subaerial exposure surfaces identified in Neoproterozoic to Cenozoic carbonate successions (Beeunas and Knauth, 1985; Andrews, 1991; Sarkar et al., 1998; Railsback et al., 2003; Banerjee et al., 2006). Such isotopic depletions can be as large as 4–6‰ at the exposure surface and become smaller at depth (Allan and Matthews, 1982). Subaerial exposure also commonly leads to covariant trends in $\delta^{13}C_{carb}$ and $\delta^{18}O$ (Knauth and Kennedy, 2009), because meteoric fluids are commonly depleted in both ^{13}C (Derry, 2010) and ^{18}O (Bowen and Wilkinson, 2002). Interaction of carbonate minerals with meteoric fluids during subaerial exposure also typically yield a decrease in Sr concentrations, reflecting both the propensity for Sr to be rejected from the carbonate lattice during recrystallization (Brand and Veizer, 1980) and the relatively low Sr concentration of terrestrial fluids (Banner, 1995).

In the Las Aguaditas Formation, petrographic and geochemical data suggest little interaction with late diagenetic fluids. Carbonate mudstone and wackestone within this interval is petrographically well preserved and lacks both petrographic or cathodoluminescent evidence of grain coarsening associated with dissolution and reprecipitation reactions. Strontium concentrations in this interval are some of the highest in the formation (averaging 1175 ± 400 ppm, n = 20), which is inconsistent with extensive diagenetic alteration by meteoric or other post-depositional fluids (Fig. 9B; Table 2). Furthermore, the strata beneath the unconformity contain elevated concentrations of both Mn (378 ± 90 ppm; n = 12; Fig. 9C) and Fe (378 ± 90 ppm and 2373 ± 1459 ppm; n = 12), which is inconsistent with alteration by well oxygenated surface fluids (Lohmann, 1988).

5.3. Potential for recovery of gradients in ocean chemistry

A number of high-resolution geochemical studies have explored the potential for spatial heterogeneity of the marine carbon isotope record (Gilleaudeau and Kah, 2013; Edwards and Saltzman, 2016; Saltzman and Edwards, 2017), especially within epicratonic seas, where carbonate rocks have been shown to exhibit a systematic reduction in $\delta^{13}C_{carb}$ compositions, when compared to coeval pericratonic and offshore marine environments (Holmden et al., 1998; Panchuk et al., 2006). Aerobic activity in surface waters would lead to enhanced organic matter oxidation by heterotrophic microorganisms and increased redox stratification of the water column in the Early-Middle Ordovician (cf. Kah et al., 2016). Under low oxygen conditions, Mn and Fe are readily reduced through microbial processes either within the water column or within

substrate pore fluids (Thamdrup et al., 2000), where they can then be incorporated into carbonate minerals. Carbonate minerals with elevated Mn and Fe concentrations and little petrographic evidence of post-depositional recrystallization have been used to argue for deposition under low oxygen conditions (Kah et al., 2012; Thompson and Kah, 2012; Gilleaudeau and Kah, 2013; Guo et al., 2013). Such a scenario is consistent with elevated concentrations of Mn and Fe, combined with elevated Sr and an absence of petrographic evidence for substantial post-depositional recrystallization, in the Las Chacritas and Las Aguaditas formations suggesting deposition of both of these units near a marine chemocline.

Combined, petrographic and geochemical data suggest little post-depositional alteration of micritic carbonate phases from the Las Chacritas and Las Aguaditas formations and thus, likely reflect early diagenetic stabilization in seawater or seawater modified by microbial activity within the shallow substrate. In this case, an abrupt divergence between the Las Chacritas and Las Aguaditas formations suggest that facies may be sampling geochemically distinct parts of the marine water column. Here we suggest that an abrupt shift in the carbon isotopic composition of the Las Aguaditas at the initiation of the MDICE may reflect variation in the composition of marine DIC in carbonate deposited at or near a marine chemocline.

Relative isotopic stasis in the $\delta^{13}C_{carb}$ record of both the Las Chacritas and Las Aguaditas formations prior to the MDICE interval (Fig. 10) is consistent with deposition in a well-mixed water column (cf. Fig. 12). In a well-mixed oxygenated water column, isotopically depleted photosynthetic organic matter produced in surface waters ($\delta^{13}C_{org}$ ~

−25 to −30‰; Freeman et al., 2001) and removed as sedimentary organic carbon. Organic carbon burial results in ^{13}C enrichment of DIC, which is incorporated into marine carbonate minerals with minimal isotopic fractionation (Spero et al., 1997), driving the positive excursion in $\delta^{13}C_{carb}$ compositions of the Las Chacritas Formation. Remineralization of organic carbon in well-oxygenated waters and within the shallow substrate by aerobic marine heterotrophs, typically results in a small positive shift (~ 1.5‰; Hayes et al., 1989) in $\delta^{13}C_{org}$ compositions and the formation of isotopically light CO_2 (Hayes et al., 1989). More extensive remineralization of sedimentary organic carbon in substrate underlying oxygenated waters can result in both a shift toward isotopically light organic carbon (up to several ‰; cf. Guo et al., 2013) and incorporation of isotopically light CO_2 into carbonate minerals (cf. Schrag et al., 2013). This may explain the observed ~ 0.5‰ offset in $\delta^{13}C_{carb}$ compositions between the Las Chacritas and the Las Aguaditas formations prior to the MDICE. The Las Chacritas Formation does not record evidence for either substantial microbial remineralization (Fig. 11) nor incorporation of isotopically light DIC (Fig. 10) through either the *Y. crassus* or *E. pseudoplanus* zones which is consistent with deposition above the oxycline.

By contrast, the Las Aguaditas Formation records an abrupt shift in $\delta^{13}C_{org}$ compositions to more negative values prior to the onset of the MDICE (Fig. 11). The shift to isotopically light $\delta^{13}C_{org}$ compositions in the Las Aguaditas Formation is also associated with greater volatility in $\delta^{13}C_{carb}$ values in the uppermost *Y. crassus* Zone, and with an abrupt shift in $\delta^{13}C_{carb}$ compositions in the *E. pseudoplanus* Zone at the start of the MDICE (Fig. 10). This shift is associated with an increase in deeper-water facies and

suggests the presence of active microbial remineralization of organic matter either within the water column, or within the shallow substrate and is interpreted to reflect strengthening of the oxycline and deposition of the Las Aguaditas Formation below oxycline. When the Las Aguaditas Formation falls below the oxycline, $\delta^{13}C_{carb}$ is offset by ~2‰ from coeval shallow water carbonate record of the Las Chacritas Formation, reflecting the input of isotopically depleted DIC resulting from microbial metabolisms in anoxic water. A similar shift is observed in the Las Chacritas section in the *E. suecicus* Zone and the *P. anserinus* Zone, which records deposition of deeper-water facies of the Las Chacritas and Las Aguaditas formations (Figs. 10 and 11). Correspondence between isotopic shifts in both organic carbon and marine carbonate in the Las Aguaditas Formation support an interpretation that isotopic differences between the Las Chacritas and Las Aguaditas sections reflect the presence of an oxycline and the local production of isotopically light DIC pool. Early diagenetic stabilization of carbonate phases above or below the marine chemocline is consistent with minimal grain coarsening of micrite and enrichment of Mn and Fe consistent with incorporation of trace elements from anoxic fluids.

5.4. Implications for the redox structure of the Middle Ordovician oceans

A scenario of deposition at or near a marine chemocline is consistent with growing model for Ordovician ocean behavior, wherein persistent greenhouse conditions from the early Cambrian through the Middle Ordovician (Saltzman, 2005) combined with low-latitude continental positions (Cocks and Torsvik, 2002) and high global sea level (Haq and Schutter, 2008) would have shifted the location of bottom water formation to

low-latitude epeiric seas resulting in the formation of warm-saline deep water (Railsback et al., 1990). Formation of saline deep-water in low- to mid-latitude evaporative seas, rather than in polar regions like in the modern ocean (Foster and Carmack, 1976; England, 1992), would result in a reduction in both thermal and density gradients of the ocean, effectively reducing the rate of ocean mixing between well-mixed surface and deep-water bodies (Railsback et al., 1990).

Because the isotopic composition of marine DIC reflects a balance of continental runoff, surface gas exchange with the atmosphere, and remineralization of organic carbon the water column and sediment pore fluids (Zhang et al., 1995), differences in the C-isotope composition of DIC between surface waters and deeper water in the ocean are dependent on the degree and rate of mixing between deeper water and well-mixed surface water (Patterson and Walter, 1994). Under conditions marked by reduced mixing, biogeochemical cycling would then result in pronounced geochemical gradients. Additionally, reduction of oxygen solubility during greenhouse periods would have further reduced oxygen concentrations at depth, potentially leading to redox stratification of the water column (Küspert, 1982; Railsback et al., 1990).

Development of a marine chemocline, with well-mixed oxygenated surface waters and oxygen depleted to anoxic deep waters, has been previously linked to excursions in the isotopic compositions of marine carbon in the Paleozoic (Knoll et al., 1996; Saltzman, 2005; Thompson and Kah, 2012; Marenco et al., 2013; Kah et al., 2016). Specifically, stasis in $\delta^{13}C$ compositions during the early Paleozoic greenhouse has been attributed to nitrogen limitation, which promotes denitrification and subsequent development of

anoxic conditions in the water column (Saltzman, 2005). Under anoxic conditions, phosphorus is more easily remobilized from sediments to the water column leading to increased productivity, burial of organic carbon, and subsequent positive $\delta^{13}C$ excursions (Saltzman, 2005). Positive $\delta^{13}C$ excursions (e.g., SPICE, MDICE, and HICE) are then associated with upwelling of nutrient-rich deep waters into shallow water environments (Van Cappellen and Ingall, 1994; Pope and Steffen, 2003; Servais et al., 2014), resulting in enhanced organic productivity of surface waters.

5.5. Depositional scenarios

The carbon isotope record of carbonate and organic matter from the Las Chacritas and Las Aguaditas formations suggest deposition near the position of the oxycline. Relatively stable $\delta^{13}C_{carb}$ values and $\delta^{13}C_{org}$ values of −26 to −28‰ in the lower *Y. crassus* Zone of both sections suggests deposition of strata above the oxycline (Fig. 12). An abrupt shift to lower $\delta^{13}C_{org}$ values (near −30‰) at the onset of the Las Aguaditas Formation suggests a shift to deposition at or below the oxycline. Continuation of distinctly lower $\delta^{13}C_{org}$ values in the Las Aguaditas Formation, and increased volatility of $\delta^{13}C_{org}$ values in the Las Chacritas Formation in the *E. pseudoplanus* Zone suggests that the marine chemocline may, at this time, be affecting both sections, although preservation of the MDICE suggests that the Las Chacritas River section remained above the oxycline at this time. Finally, an abrupt shift to lower $\delta^{13}C_{org}$ values (near −30‰) in the *E. suecicus* Zone of the Las Chacritas River section suggests that by the late Darriwilian, deposition in both the Las Chacritas River and Las Aguaditas Creek sections occurred beneath the

marine chemocline as carbonate production was unable to keep up with sea level rise (Fig. 12).

Through each of these transitions, a change in the relative position of the oxycline is required to drive the observed isotopic change. Three such mechanisms are possible. In the first scenario, enhanced nutrient delivery resulting from continental weathering may have driven enhanced productivity in surface waters, resulting in expansion of marine anoxia in deeper waters at the onset of deposition of the Las Aguaditas Formation. Although this model is consistent with the observed $\delta^{13}C_{carb}$ and $\delta^{13}C_{org}$ compositions for the Las Chacritas and Las Aguaditas formations, it is inconsistent with sedimentological evidence for abrupt deepening at the onset of Las Aguaditas deposition. It is also unlikely that marine anoxia would be able to persist in environments, such as those inferred for the uppermost San Juan Formation and Las Chacritas Formation, that contain evidence for storm mixing. Furthermore, this scenario is inconsistent with sulfur isotope evidence from the middle Darriwilian (Kah et al., 2016). Rapid fluctuations in the $\delta^{34}S$ composition of marine sulfate, differential rates of change in the isotopic composition of marine sulfate and sulfide, and the occurrence of "superheavy" pyrite have been used to argue for increased ventilation of a persistent anoxic water body in the middle Darriwilian (Thompson and Kah, 2012; Marenco et al., 2013; Kah et al., 2016).
In a second scenario, relative sea level rise through the middle Darriwilian results in a shift in the position of the Las Aguaditas Formation to below the marine chemocline (Fig. 12). This scenario is consistent with sedimentological evidence from the Las Chacritas River and Las Aguaditas Creek sections, and may be explained either by an inferred

global sea level rise in the middle Darriwilian (~ 464 Ma, Haq et al., 2008), or preferential subsidence of the Precordilleran margin associated with the initial docking of the Precordilleran terrane to Gondwana (Astini et al., 1995; Astini and Thomas, 1999; Thomas et al., 2002).

In a final scenario, in addition to a relative change in sea level, global cooling through the Early to Middle Ordovician (Trotter et al., 2008) could have invigorated thermohaline circulation, potentially leading to ventilation of anoxic deep-water. Prior to this hypothesized ventilation event, ocean stratification would result in the formation of isotopically light DIC in deep water. Subsequent intrusion of deeper water into shallow water environments in the middle Ordovician, via upwelling or ventilation, would reintroduce this isotopically light carbon into the shallow-water DIC pool along with bio-essential nutrients. Increased productivity in surface waters would then trigger increased productivity and organic carbon burial, ultimately resulting in the MDICE. Upwelling of ^{13}C depleted DIC from deep water may impart a localized signal on the isotopic compositions closest to the zone of upwelling (Patterson and Walter, 1994). Isotopic depletion during upwelling is expected to be greatest along the upwelling front, where upwelling water first comes into contact with surface water (Panchuk et al., 2006), resulting in isotopic depletion in the area closest to the chemocline (Kolata et al., 2001), which may, here, be reflected in increased isotopic volatility in the MDICE interval.

6. Conclusions

Recent revisions to the biostratigraphy of the Middle Darriwilian Las Chacritas and Las Aguaditas formations in the Argentine Precordillera indicate that both formations

should record the presence of the MDICE interval, or at least its initiation. We investigated the expression of the MDICE across depositional environments within a single basin. We identify the MDICE as a positive 2‰ shift in carbonate in the *E. pseudoplanus* and *E. suecicus* zones in the Las Chacritas Formation, while equivalent strata in the deeper water Las Aguaditas Formation record an abrupt decrease in the isotopic composition of marine carbonate. To our knowledge, this is the first recording of isotopic compositions during the MDICE interval that diverge from the global positive isotopic excursion. Paired carbon isotope from marine carbonate and organic carbon suggest that divergent behavior of the MDICE interval results from deposition above and below a marine chemocline. Sedimentological differences between the Las Chacritas and Las Aguaditas formations suggest the presence of a persistent oxycline just below storm wave base, with differences in the isotopic behavior of the two sections related to their position relative to this marine chemocline.

Acknowledgments

Funding for this projected was provided by the New Directions grant from the American Chemical Society Petroleum Research Fund (to Kah), along with student grants from Sigma Xi, the Geological Society of America, and SEPM (to Henderson). We thank R. Bales (University of Tennessee), and M. Mango (University of Cordoba) for assistance with fieldwork; A. Faiia and A. Szynkiewicz (University of Tennessee) for help with isotopic analyses; and the University of Tennessee Department of Chemistry for access to the ICP-OES.

References

Ainsaar, L., Meidla, T., Tinn, O., 2004. Middle and Upper Ordovician stable isotope stratigraphy across the facies belts in the East Baltic, in: Hints, O., Ainsaar, L. (Eds.), 8th Meeting on the Working Group on the Ordovician Geology of Baltoscandia. Tartu University Press, Tallinn and Tartu, Estonia, pp. 11-12.

Ainsaar, L., Meidla, T., Tinn, O., Martma, T., Dronov, A., 2007. Darriwilian (Middle Ordovician) carbon isotope stratigraphy in Baltoscandia. Acta Paleontologica Sinica 46, 1-8.

Albanesi, G.L., Barnes, C.R., 2000. Subspeciation within a Punctuated Equilibrium Evolutionary Event: Phylogenetic History of the Lower-Middle Ordovician *Paroistodus originalis-P. horridus* Complex (Conodonta). Journal of Paleontology 74, 492-502. https://doi.org/10.1666/0022-3360(2000)074%3C0492:SWAPEE%3E2.0.CO;2

Albanesi, G.L., Bergström, S.M., Schmitz, B., Serra, F., Feltes, N.A., Voldman, G.G., Ortega, G., 2013. Darriwilian (Middle Ordovician) $\delta^{13}C_{carb}$ chemostratigraphy in the Precordillera of Argentina: Documentation of the middle Darriwilian Isotope Carbon Excursion (MDICE) and its use for intercontinental correlation. Palaeogeography, Palaeoclimatology, Palaeoecology 389, 48-63. http://dx.doi.org/10.1016/j.palaeo.2013.02.028

Albanesi, G.L., Ortega, G., 2016. Conodont and Graptolite Biostratigraphy of the Ordovician System of Argentina, in: Michael, M. (Ed.), Stratigraphy & Timescales. Academic Press, pp. 61-121. http://dx.doi.org/10.1016/bs.sats.2016.10.002

Allan, J.R., Matthews, R.K., 1982. Isotope signatures associated with early meteoric diagenesis. Sedimentology 29, 797-817. http://dx.doi.org/10.1111/j.1365-3091.1982.tb00085.x

Allmendinger, R.W., Figueroa, D., Snyder, D., Beer, J., Mpodozis, C., Isacks, B.L., 1990. Foreland shortening and crustal balancing in the Andes at 30˚- S latitude. Tectonics 9, 789-809. http://dx.doi.org/10.1029/TC009i004p00789

Allmendinger, R.W., Judge, P.A., 2014. The Argentine Precordillera: A foreland thrust belt proximal to the subducted plate. Geosphere 10, 1203-1218. http://dx.doi.org/10.1130/ges01062.1

Alvarez-Marron, J., Rodriguez-Fernandez, R., Heredia, N., Busquets, P., Colombo, F., Brown, D., 2006. Neogene structures overprinting Palaeozoic thrust systems in the Andean Precordillera at 30°S latitude. Journal of the Geological Society 163, 949-964. http://dx.doi.org/10.1144/0016-76492005-142

Andrews, J.E., 1991. Geochemical indicators of depositional and early diagenetic facies in Holocene carbonate muds, and their preservation potential during stabilisation. Chemical Geology 93, 267-289. http://dx.doi.org/10.1016/0009-2541(91)90118-B

Astini, R.A., 1995a. Geologic meaning of Arenig-Llanvirn diachronous black shales (Gualcamayo Alloformation) in the Argentine Precordillera, tectonic or eustatic? SEPM Fieldtrip Guidebook 77, 217-220.

Astini, R.A., 1995b. Sedimentologia de la Formacion Las Aguaditas (talud carbonatico) y evolucion de la cuenca precordillera durante el Ordovicico medio. Revista de la Asociacion Geologica Argentina 50, 143-164.

Astini, R.A., Benedetto, J.L., Vaccari, N.E., 1995. The early Paleozoic evolution of the Argentine Precordillera as a Laurentian rifted, drifted, and collided terrane: A geodynamic model. Geological Society of America Bulletin 107, 253-273. https://doi.org/10.1130/0016-7606(1995)107%3C0253:TEPEOT%3E2.3.CO;2

Astini, R.A., Thomas, W.A., 1999. Origin and evolution of the Precordillera terrane of western Argentina; a drifted Laurentian orphan. Special Paper - Geological Society of America 336, 1-20. https://dx.doi.org/10.1130/0-8137-2336-1.1

Azmy, K., Stouge, S., Brand, U., Bagnoli, G., Ripperdan, R., 2014. High-resolution chemostratigraphy of the Cambrian–Ordovician GSSP: Enhanced global correlation tool. Palaeogeography, Palaeoclimatology, Palaeoecology 409, 135-144. http://dx.doi.org/10.1016/j.palaeo.2014.05.010

Banerjee, S., Bhattacharya, S.K., Sarkar, S., 2006. Carbon and oxygen isotope compositions of the carbonate facies in the Vindhyan Supergroup, central India. Journal of Earth System Science 115, 113-134. http://dx.doi.org/10.1007/bf02703029

Banner, J.L., 1995. Application of the trace element and isotope geochemistry of strontium to studies of carbonate diagenesis. Sedimentology 42, 805-824. http://dx.doi.org/10.1111/j.1365-3091.1995.tb00410.x

Banner, J.L., Hanson, G.N., 1990. Calculation of simultaneous isotopic and trace-element variations during water-rock interaction with applications to carbonate diagenesis. Geochimica Et Cosmochimica Acta 54, 3123-3137. http://dx.doi.org/10.1016/0016-7037(90)90128-8

Bartley, J.K., Kah, L.C., McWilliams, J.L., Stagner, A.F., 2007. Carbon isotope chemostratigraphy of the Middle Riphean type section (Avzyan Formation, Southern Urals, Russia): Signal recovery in a fold-and-thrust belt. Chemical Geology 237, 211-232. http://dx.doi.org/10.1016/j.chemgeo.2006.06.018

Beaumont, C., 1981. Foreland basins. Geophysical Journal of the Royal Astronomical Society 65, 291-329. http://dx.doi.org/10.1111/j.1365-246X.1981.tb02715.x

Beeunas, M.A., Knauth, L.P., 1985. Preserved stable isotopic signature of subaerial diagenesis in the 1.2-b.y. Mescal Limestone, central Arizona: Implications for the timing and development of a terrestrial plant cover. Geological Society of America Bulletin 96, 737-745. http://dx.doi.org/10.1130/0016-7606(1985)96<737:psisos>2.0.co;2

Benedetto, J.L., 2004. The allochthony of the Argentine Precordillera ten years later (1993-2003): A new paleobiogeographic test of the microcontinental model. Gondwana Research 7, 1027-1039. http://dx.doi.org/10.1016/s1342-937x(05)71082-0

Benedetto, J.L., Vaccari, N.E., Waisfeld, B.G., Sanchez, T.M., Foglia, R.D., 2009. Cambrian and Ordovician biogeography of the South American margin of Gondwana and accreted terranes. Early Palaeozoic Peri-Gondwana Terranes: New Insights from Tectonics and Biogeography 325, 201-232. http://dx.doi.org/10.1144/sp325.11

Berger, W.H., Vincent, E., 1981. Chemostratigrapy and biostratigraphic correlation: Exercises in systematic stratigraphy, Proceedings 26th International Geological Congress, Geology of oceans symposium. Oceanologica Acta, Paris, France, pp. 115-127.

Bergström, S.M., Chen, X.U., Gutiérrez-Marco, J.C., Dronov, A., 2009. The new chronostratigraphic classification of the Ordovician System and its relations to major regional series and stages and to $\delta^{13}C$ chemostratigraphy. Lethaia 42, 97-107. http://dx.doi.org/10.1111/j.1502-3931.2008.00136.x

Bowen, G.J., Wilkinson, B., 2002. Spatial distribution of $\delta^{18}O$ in meteoric precipitation. Geology 30, 315-318. http://dx.doi.org/10.1130/0091-7613(2002)030<0315:SDOOIM>2.0.CO;2

Brand, U., Veizer, J., 1980. Chemical diagenesis of a multicomponent carbonate system; 1, Trace elements. Journal of Sedimentary Research 50, 1219-1236. http://dx.doi.org/10.1306/212F7BB7-2B24-11D7-8648000102C1865D

Brenchley, P.J., Marshall, J.D., Carden, G.A.F., Robertson, D.B.R., Long, D.G.F., Meidla, T., Hints, L., Anderson, T.F., 1994. Bathymetric and isotopic evidence for a short-lived Late Ordovician glaciation in a greenhouse period. Geology 22, 295-298. http://dx.doi.org/10.1130/0091-7613(1994)022<0295:baiefa>2.3.co;2

Calner, M., Lehnert, O., Wu, R., Dahlqvist, P., Joachimski, M.M., 2014. $\delta^{13}C$ chemostratigraphy in the Lower–Middle Ordovician succession of Öland (Sweden) and the global significance of the MDICE. GFF 136, 48-54. http://dx.doi.org/10.1080/11035897.2014.901409

Canas, F.L., 2003. Selected sections of Lower to Middle Ordovician carbonate sedimentation of the Argentine Precordillera: The La Silla and San Juan formations at Cerros La Silla and Niquivil. INSUEGO, Miscelanea 8.

Carpenter, S.J., Lohmann, K.C., 1997. Carbon isotope ratios of Phanerozoic marine cements: Re-evaluating the global carbon and sulfur systems. Geochimica et Cosmochimica Acta 61, 4831-4846. http://dx.doi.org/10.1016/S0016-7037(97)00361-X

Carrera, M.G., 1997. Análisis paleoecológico de la fauna de poríferos del Llanvirniano tardío de la Precordillera Argentina. Ameghiniana 34, 309-316.

Carrera, M.G., Astini, R.A., 1998. Valoracion de las restriciones ambientales durante la transicion Argenigiano-Llanvirniano, Ordovicico de la Precordillera Argentina. Revista de la Asociacion Geologica Argentina 53, 41-56.

Catuneanu, O., 2004. Retroarc foreland systems—evolution through time. Journal of African Earth Sciences 38, 225-242. http://dx.doi.org/10.1016/j.jafrearsci.2004.01.004

Cocks, L.R.M., Torsvik, T.H., 2002. Earth geography from 500 to 400 million years ago; a faunal and palaeomagnetic review. Journal of the Geological Society of London 159, Part 6, 631-644. http://dx.doi.org/10.1144/0016-764901-118

Derry, L.A., 2010. A burial diagenesis origin for the Ediacaran Shuram–Wonoka carbon isotope anomaly. Earth and Planetary Science Letters 294, 152-162. http://dx.doi.org/10.1016/j.epsl.2010.03.022

Edwards, C.T., Saltzman, M.R., 2014. Carbon isotope ($\delta^{13}C_{carb}$) stratigraphy of the Lower–Middle Ordovician (Tremadocian–Darriwilian) in the Great Basin, western United States: Implications for global correlation. Palaeogeography, Palaeoclimatology, Palaeoecology 399, 1-20. http://dx.doi.org/10.1016/j.palaeo.2014.02.005

Edwards, C.T., Saltzman, M.R., 2016. Paired carbon isotopic analysis of Ordovician bulk carbonate ($\delta^{13}C_{carb}$) and organic matter ($\delta^{13}C_{org}$) spanning the Great Ordovician Biodiversification Event. Palaeogeography, Palaeoclimatology, Palaeoecology 458, 102-117. http://dx.doi.org/10.1016/j.palaeo.2015.08.005

England, M.H., 1992. On the Formation of Antarctic Intermediate and Bottom Water in Ocean General Circulation Models. Journal of Physical Oceanography 22, 918-926. http://dx.doi.org/10.1175/1520-0485(1992)022<0918:otfoai>2.0.co;2

Epstein, A.G., Epstein, J.B., Harris, L.D., Geological, S., 1977. Conodont color alteration — an index to organic metamorphism : experimental and field studies showing the application of conodont color alteration to geothermometry, metamorphism, and structural geology and for assessing hydrocarbon potential. U.S. Govt. Print. Off., Washington.

Fanning, C.M., Pankhurst, R.J., Rapela, C.W., Baldo, E.G., Casquet, C., Galindo, C., 2004. K-bentonites in the Argentine Precordillera contemporaneous with rhyolite volcanism in the Famatinian Arc. Journal of the Geological Society 161, 747-756. http://dx.doi.org/10.1144/0016-764903-130

Feltes, N., Albanesi, G.L., Bergstrom, S.M., 2016. Conodont biostratigraphy and global correlation of the middle Darriwilian-lower Sandbian (Ordovician) Las Aguaditas Formation, Precordillera of San Juan, Argentina. Andean Geology 43, 60-85. http://dx.doi.org/10.5027/andgeoV43n1-a04

Feltes, N.A., 2017. Fauna de conodontes y graptolitos de la Formación Las Aguaditas (Ordovícico) en el cordón de Los Blanquitos, Precordillera Central de San Juan, Argentina Universidad Nacional de Córdoba, Unpublished, p. 453.

Finney, S.C., Berry, W.B.N., Cooper, J.D., Ripperdan, R.L., Sweet, W.C., Jacobson, S.R., Soufiane, A., Achab, A., Noble, P.J., 1999. Late Ordovician mass extinction: A new perspective from stratigraphic sections in central Nevada. Geology 27, 215-218. http://dx.doi.org/10.1130/0091-7613(1999)027<0215:lomean>2.3.co;2

Foster, T.D., Carmack, E.C., 1976. Frontal zone mixing and Antarctic Bottom water formation in the southern Weddell Sea. Deep Sea Research and Oceanographic Abstracts 23, 301-317. http://dx.doi.org/10.1016/0011-7471(76)90872-X

Freeman, K.H., 2001. Isotopic Biogeochemistry of Marine Organic Carbon. Reviews in Mineralogy and Geochemistry 43, 579-605. http://dx.doi.org/10.2138/gsrmg.43.1.579

Gilleaudeau, G.J., Kah, L.C., 2013. Carbon isotope records in a Mesoproterozoic epicratonic sea: Carbon cycling in a low-oxygen world. Precambrian Research 228, 85-101. http://dx.doi.org/10.1016/j.precamres.2013.01.006

Guo, H., Du, Y., Kah, L.C., Huang, J., Hu, C., Huang, H., Yu, W., 2013. Isotopic composition of organic and inorganic carbon from the Mesoproterozoic Jixian Group, North China: Implications for biological and oceanic evolution. Precambrian Research 224, 169-183. https://doi.org/10.1016/j.precamres.2012.09.023

Halverson, G.P., Hoffman, P.F., Schrag, D.P., Maloof, A.C., Rice, A.H.N., 2005. Toward a Neoproterozoic composite carbon-isotope record. Geological Society of America Bulletin 117, 1181-1207. http://dx.doi.org/10.1130/b25630.1

Haq, B.U., Schutter, S.R., 2008. A chronology of Paleozoic sea-level changes. Science 322, 64-68. http://dx.doi.org/10.1126/science.1161648

Harper, D.A.T., 2006. The Ordovician biodiversification: Setting an agenda for marine life. Palaeogeography, Palaeoclimatology, Palaeoecology 232, 148-166. http://dx.doi.org/10.1016/j.palaeo.2005.07.010

Harper, D.A.T., Mac Niocaill, C., Williams, S.H., 1996. The palaeogeography of early Ordovician Iapetus terranes: an integration of faunal and palaeomagnetic constraints. Palaeogeography, Palaeoclimatology, Palaeoecology 121, 297-312. http://dx.doi.org/10.1016/0031-0182(95)00079-8

Hayes, J.M., Popp, B.N., Takigiku, R., Johnson, M.W., 1989. An isotopic study of biogeochemical relationships between carbonates and organic carbon in the Greenhorn Formation. Geochimica et Cosmochimica Acta 53, 2961-2972. http://dx.doi.org/10.1016/0016-7037(89)90172-5

Hayes, J.M., Strauss, H., Kaufman, A.J., 1999. The abundance of ^{13}C in marine organic matter and isotopic fractionation in the global biogeochemical cycle of carbon during the past 800 Ma. Chemical Geology 161, 103-125. http://dx.doi.org/10.1016/S0009-2541(99)00083-2

Heredia, S., Beresi, M., Peralta, S., 2005. Darriwilian conodont biostratigraphy of the Las Chacritas Formation, Central Precordillera (San Juan Province, Argentina). Geologica Acta 3, 385-394.

Holmden, C., Creaser, R.A., Muehlenbachs, K., Leslie, S.A., Bergström, S.M., 1998. Isotopic evidence for geochemical decoupling between ancient epeiric seas and bordering oceans: Implications for secular curves. Geology 26, 567-570. http://dx.doi.org/10.1130/0091-7613(1998)026<0567:iefgdb>2.3.co;2

Huff, W., Davis, D., Bergstrom, S., Krekeler, M., Kolata, D., Cingolani, C., 1997. A biostratigraphically well-constrained K-bentonite U-Pb zircon age of the lowermost Darriwilian Stage (Middle Ordovician) from the Argentine Precordillera. Episodes 20, 29-33. https://doi.org/10.1144/0016-764903-130

Huff, W.D., Bergstrom, S.M., Kolata, D.R., Cingolani, C., Davis, D.W., 1995. Middle Ordovician K-bentonites discovered in the Precordillera of Argentina: Geochemical and paleogeographical implications, in: Cooper, J.D., Droser, M.L., Finney, S.C. (Eds.), Ordovician oddesy: short papers for the seventh international symposium on the Ordovician system. SEPM, Las Vegas, Nevada.

Huff, W.D., Bergström, S.M., Kolata, D.R., Cingolani, C.A., Astini, R.A., 1998. Ordovician K-bentonites in the Argentine Precordillera: relations to Gondwana margin evolution. Geological Society, London, Special Publications 142, 107-126. 10.1144/gsl.sp.1998.142.01.06

Jaffrés, J.B.D., Shields, G.A., Wallmann, K., 2007. The oxygen isotope evolution of seawater: A critical review of a long-standing controversy and an improved geological water cycle model for the past 3.4 billion years. Earth-Science Reviews 83, 83-122. http://dx.doi.org/10.1016/j.earscirev.2007.04.002

Jahren, A.H., Porter, S., Kuglitsch, J.J., 2003. Lichen metabolism identified in Early Devonian terrestrial organisms. Geology 31, 99-102. 10.1130/0091-7613(2003)031<0099:lmiied>2.0.co;2

Kah, L.C., Bartley, J.K., Teal, D.A., 2012. Chemostratigraphy of the Late Mesoproterozoic Atar Group, Taoudeni Basin, Mauritania: Muted isotopic variability, facies correlation, and global isotopic trends. Precambrian Research 200–203, 82-103. http://dx.doi.org/10.1016/j.precamres.2012.01.011

Kah, L.C., Sherman, A.G., Narbonne, G.M., Knoll, A.H., Kaufman, A.J., 1999. $\delta^{13}C$ stratigraphy of the Proterozoic Bylot Supergroup, Baffin Island, Canada: implications for regional lithostratigraphic correlations. Canadian Journal of Earth Sciences 36, 313-332. http://dx.doi.org/10.1139/e98-100

Kah, L.C., Thompson, C.K., Henderson, M.A., Zhan, R., 2016. Behavior of marine sulfur in the Ordovician. Palaeogeography, Palaeoclimatology, Palaeoecology 458, 133-153. http://dx.doi.org/10.1016/j.palaeo.2015.12.028

Kaljo, D., Martma, T., Saadre, T., 2007. Post-Hunnebergian Ordovician carbon isotope trend in Baltoscandia, its environmental implications and some similarities with that of Nevada. Palaeogeography, Palaeoclimatology, Palaeoecology 245, 138-155. http://dx.doi.org/10.1016/j.palaeo.2006.02.020

Kaufman, A.J., Hayes, J.M., Knoll, A.H., Germs, G.J.B., 1991. Isotopic compositions of carbonates and organic carbon from upper Proterozoic successions in Namibia: stratigraphic variation and the effects of diagenesis and metamorphism. Precambrian Research 49, 301-327. http://dx.doi.org/10.1016/0301-9268(91)90039-D

Kaufman, A.J., Knoll, A.H., 1995. Neoproterozoic variations in the C-isotopic composition of seawater: stratigraphic and biogeochemical implications. Precambrian Research 73, 27-49. http://dx.doi.org/10.1016/0301-9268(94)00070-8

Keller, M., 1999. Argentine Precordillera: Sedimentary and plate tectonic history of a Laurentian crustal fragment in South America. Geological Society of America Special Paper 341. https://dx.doi.org/10.1130/0-8137-2341-8.1

Keller, M., Eberlein, S., Lehnert, O., 1993. Sedimentology of middle ordovician carbonates in the Argentine precordillera: evidence of regional relative sea-level changes. Geol Rundsch 82, 362-377. http://dx.doi.org/10.1007/BF00191838

Knauth, L.P., Kennedy, M.J., 2009. The late Precambrian greening of the Earth. Nature 460, 728-732. http://dx.doi.org/doi:10.1038/nature08213

Knoll, A.H., Bambach, R.K., Canfield, D.E., Grotzinger, J.P., 1996. Comparative Earth History and Late Permian Mass Extinction. Science 273, 452-457. 10.1126/science.273.5274.452

Kolata, D.R., Huff, W.D., Bergström, S.M., 2001. The Ordovician Sebree Trough: An oceanic passage to the Midcontinent United States. GSA Bulletin 113, 1067-1078. http://dx.doi.org/10.1130/0016-7606(2001)113<1067:TOSTAO>2.0.CO;2

Küspert, W., 1982. Environmental Changes During Oil Shale Deposition as Deduced from Stable Isotope Ratios, in: Einsele, G., Seilacher, A. (Eds.), Cyclic and Event Stratification. Springer Berlin Heidelberg, Berlin, Heidelberg, pp. 482-501. 10.1007/978-3-642-75829-4_36

Leslie, S.A., Saltzman, M.R., Bergström, S.M., Repetski, J.E., Howard, A., Seward, A.M., 2011. Conodont biostratigraphy and stable isotope stratigraphy across the Ordovician Knox/Beekmantown unconformity in the central Appalachians, in: Gutierrez-Alonso, G., Diego, G.B. (Eds.), Ordovician of the World. Publicaciones del Instituto Geológico y Minero de España.

Lohmann, K.C., 1988. Geochemical Patterns of Meteoric Diagenetic Systems and Their Application to Studies of Paleokarst, in: James, N.P., Choquette, P.W. (Eds.), Paleokarst. Springer New York, New York, NY, pp. 58-80. http://dx.doi.org/10.1007/978-1-4612-3748-8_3

Marenco, P.J., Marenco, K.N., Lubitz, R.L., Niu, D., 2013. Contrasting long-term global and short-term local redox proxies during the Great Ordovician Biodiversification Event: A case study from Fossil Mountain, Utah, USA. Palaeogeography, Palaeoclimatology, Palaeoecology 377, 45-51. http://dx.doi.org/10.1016/j.palaeo.2013.03.007

Marshall, J.D., 1992. Climatic and oceanographic isotopic signals from the carbonate rock record and their preservation. Geological Magazine 129, 143-160. https://doi.org/10.1017/S0016756800008244

Martma, T., 2005. Ordovician carbon isotopes, in: Põldvere, A. (Ed.), Mehikoorma (421) Drill Core: Estonian Geological Sections. Estonian Geological Survey Bulletin, pp. 25-27.

Meidla, T., Backman, L., Dronov, A., Holmer, L., Sturesson, U., 2004. Middle-Upper Ordovician carbon isotope record from Västergötland (Sweden) and East Baltic, in: Hints, O., Ainsaar, L. (Eds.), 8th Meeting on the Working Group on the Ordovician Geology of Baltoscandia. Tartu University Press, Tallinn and Tartu, Estonia, pp. 67-68.

Panchuk, K.M., Holmden, C.E., Leslie, S.A., 2006. Local controls on carbon cycling in the Ordovician midcontinent region of North America, with implications for carbon isotope secular curves. Journal of Sedimentary Research 76, 200-211. http://dx.doi.org/10.2110/jsr.2006.017

Pankhurst, R.J., Rapela, C.W., Fanning, C.M., 2000. Age and origin of coeval TTG, I- and S-type granites in the Famatinian belt of NW Argentina. Geological Society of America Special Papers 350, 151-168. http://dx.doi.org/10.1130/0-8137-2350-7.151

Patterson, W.P., Walter, L.M., 1994. Depletion of ^{13}C in seawater $\Sigma C0_2$ on modern carbonate platforms: Significance for the carbon isotopic record of carbonates. Geology 22, 885-888. http://dx.doi.org/10.1130/0091-7613(1994)022<0885:docisc>2.3.co;2

Peralta, G.L., Baldis, B.A.J., 1995. Graptolites y trilobites del Ordovícico tardío en el perfil del río de Las Chacritas, Precordillera Central de San Juan, Argentina. V Congreso Argentino Paleontología y Bioestratigrafía, Trelew (1994), Actas, 201-205.

Peralta, S.H., Heredia, S., Beresi, M.S., 1999. Upper Arenigian-lower Llanvirnian sequence of the Las Chacritas river, Central Precordillera, San Juan Province, Argentina. Acta Universitatis Carolinae Geologica 43, 123-126.

Pope, M.C., Steffen, J.B., 2003. Widespread, prolonged late Middle to Late Ordovician upwelling in North America: A proxy record of glaciation? Geology 31, 63-66. http://dx.doi.org/10.1130/0091-7613(2003)031<0063:wplmtl>2.0.co;2

Railsback, L.B., Ackerly, S.C., Anderson, T.F., Cisneti, J.L., 1990. Palaeontological and isotope evidence for warm saline deep waters in Ordovician oceans. Nature 343, 156-159. http://dx.doi.org/10.1038/343156a0

Railsback, L.B., Holland, S.M., Hunter, D.M., Jordan, E.M., Díaz, J.R., Crowe, D.E., 2003. Controls on Geochemical Expression of Subaerial Exposure in Ordovician Limestones from the Nashville Dome, Tennessee, U.S.A. Journal of Sedimentary Research 73, 790-805. http://dx.doi.org/10.1306/020503730790

Ramos, V.A., Jordan, T.E., Allmendinger, R.W., Mpodozis, C., Kay, S.M., Cortes, J.M., Palma, M., 1986. Paleozoic terranes of the Central Argentine-Chilean Andes. Tectonics 5, 855-880. http://dx.doi.org/10.1029/TC005i006p00855

Rasmussen, C.M.Ø., Ullmann, C.V., Jakobsen, K.G., Lindskog, A., Hansen, J., Hansen, T., Eriksson, M.E., Dronov, A., Frei, R., Korte, C., Nielsen, A.T., Harper, D.A.T., 2016. Onset of main Phanerozoic marine radiation sparked by emerging Mid Ordovician icehouse. Scientific Reports 6, 18884. http://dx.doi.org/10.1038/srep18884

Saltzman, M.R., 2005. Phosphorus, nitrogen, and the redox evolution of the Paleozoic oceans. Geology 33, 573-576. http://dx.doi.org/10.1130/g21535.1

Saltzman, M.R., Edwards, C.T., 2017. Gradients in the carbon isotopic composition of Ordovician shallow water carbonates: A potential pitfall in estimates of ancient CO_2 and O_2. Earth and Planetary Science Letters 464, 46-54. http://dx.doi.org/10.1016/j.epsl.2017.02.011

Saltzman, M.R., Runnegar, B., Lohmann, K.C., 1998. Carbon isotope stratigraphy of Upper Cambrian (Steptoean Stage) sequences of the eastern Great Basin: Record of a global oceanographic event. Geological Society of America Bulletin 110, 285-297. http://dx.doi.org/10.1130/0016-7606(1998)110<0285:cisouc>2.3.co;2

Saltzman, M.R., Thomas, E., 2012. Carbon isotope stratigraphy, in: Gradstein, F.M., Ogg, J., Schmitz, M.D., Ogg, G. (Eds.), The Geologic Time Scale, 1 ed. Elsevier, pp. 207-232. http://dx.doi.org/10.1016/B978-0-444-59425-9.00011-1

Saltzman, M.R., Young, S.A., 2005. Long-lived glaciation in the Late Ordovician? Isotopic and sequence-stratigraphic evidence from western Laurentia. Geology 33, 109-112. http://dx.doi.org/10.1130/g21219.1

Sarkar, S., Chakraborty, P.P., Bhattacharya, S.K., Banerjee, S., 1998. C12-enrichment along intraformational unconformities within Proterozoic Bhander Limestone, Son valley, India and its implication. Carbonates and Evaporites 13, 108. http://dx.doi.org/10.1007/bf03175440

Schmitz, B., Bergström, S.M., Xiaofeng, W., 2010. The middle Darriwilian (Ordovician) $\delta^{13}C$ excursion (MDICE) discovered in the Yangtze Platform succession in China: implications of its first recorded occurrences outside Baltoscandia. Journal of the Geological Society 167, 249-259. http://dx.doi.org/10.1144/0016-76492009-080

Scholle, P.A., Ulmer-Scholle, D.S., 2003. Color guide to the Petrography of Carbonate Rocks, 2 ed.

Schrag, D.P., Higgins, J.A., Macdonald, F.A., Johnston, D.T., 2013. Authigenic Carbonate and the History of the Global Carbon Cycle. Science 339, 540-543. http://dx.doi.org/10.1126/science.1229578

Serra, F., Albanesi, G.L., Ortega, G., Bergstrom, S.M., 2015. Biostratigraphy and palaeoecology of Middle–Late Ordovician conodont and graptolite faunas of the

Las Chacritas River section, Precordillera of San Juan, Argentina. Geological Magazine 152, 813-829. http://dx.doi.org/10.1017/S0016756814000752

Serra, F., Feltes, N.A., Henderson, M.A., Albanesi, G.L., 2017. Darriwilian (Middle Ordovician) conodont biofacies from the Central Precordillera of Argentina. Marine Micropaleontology 130, 15-28. http://dx.doi.org/10.1016/j.marmicro.2016.12.002

Servais, T., Danelian, T., Harper, D.A.T., Munnecke, A., 2014. Possible oceanic circulation patterns, surface water currents and upwelling zones in the Early Palaeozoic. Gff 136, 229-233. http://dx.doi.org/10.1080/11035897.2013.876659

Servais, T., Owen, A.W., Harper, D.A.T., Kröger, B., Munnecke, A., 2010. The Great Ordovician Biodiversification Event (GOBE): The palaeoecological dimension. Palaeogeography, Palaeoclimatology, Palaeoecology 294, 99-119. http://dx.doi.org/10.1016/j.palaeo.2010.05.031

Spero, H.J., Bijma, J., Lea, D.W., Bemis, B.E., 1997. Effect of seawater carbonate concentration on foraminiferal carbon and oxygen isotopes. Nature 390, 497-500.

Stouge, S., 2012. Middle Ordovician (late Dapingian–Darriwilian) conodonts from the Cow Head Group and Lower Head Formation, western Newfoundland, Canada. Canadian Journal of Earth Sciences 49, 59-90. 10.1139/e11-057

Stouge, S.S., 1984. Conodonts of the Middle Ordovician Table Head Formation, western Newfoundland. Lethaia: Fossils and Strata 16, 1-149.

Strother, P.K., Al-Hajri, S., Traverse, A., 1996. New evidence for land plants from the lower Middle Ordovician of Saudi Arabia. Geology 24, 55-58. 10.1130/0091-7613(1996)024<0055:NEFLPF>2.3.CO;2

Thamdrup, B., Rosselló-Mora, R., Amann, R., 2000. Microbial manganese and sulfate reduction in Black Sea shelf sediments. Applied and Environmental Microbiology 66, 2888-2897. http://dx.doi.org/10.1128/aem.66.7.2888-2897.2000

Thomas, W.A., 2011. The Iapetan rifted margin of southern Laurentia. Geosphere 7, 97-120. http://dx.doi.org/10.1130/ges00574.1

Thomas, W.A., Astini, R.A., 1996. The Argentine Precordillera: A traveler from the Ouachita embayment of North American Laurentia. Science 273, 752-757. http://dx.doi.org/10.1126/science.273.5276.752

Thomas, W.A., Astini, R.A., Bayona, G., 2002. Ordovician collision of the Argentine Precordillera with Gondwana, independent of Laurentian Taconic orogeny. Tectonophysics 345, 131-152. http://dx.doi.org/10.1016/S0040-1951(01)00210-4

Thomas, W.A., Astini, R.A., Denison, R.E., 2001. Strontium isotopes, age, and tectonic setting of Cambrian salinas along the rift and transform margins of the Argentine Precordillera and southern Laurentia. Journal of Geology 109, 231-246. http://dx.doi.org/10.1086/319241

Thompson, C.K., Kah, L.C., 2012. Sulfur isotope evidence for widespread euxinia and a fluctuating oxycline in Early to Middle Ordovician greenhouse oceans. Palaeogeography, Palaeoclimatology, Palaeoecology 313-314, 189-214. http://dx.doi.org/10.1016/j.palaeo.2011.10.020

Thompson, C.K., Kah, L.C., Astini, R., Bowring, S.A., Buchwaldt, R., 2012. Bentonite geochronology, marine geochemistry, and the Great Ordovician Biodiversification Event (GOBE). Palaeogeography, Palaeoclimatology, Palaeoecology 321–322, 88-101. http://dx.doi.org/10.1016/j.palaeo.2012.01.022

Trotter, J.A., Williams, I.S., Barnes, C.R., Lécuyer, C., Nicoll, R.S., 2008. Did Cooling Oceans Trigger Ordovician Biodiversification? Evidence from Conodont Thermometry. Science 321, 550-554. http://dx.doi.org/10.1126/science.1155814

Van Cappellen, P., Ingall, E.D., 1994. Benthic phosphorus regeneration, net primary production, and ocean anoxia: A model of the coupled marine biogeochemical cycles of carbon and phosphorus. Paleoceanography 9, 677-692. http://dx.doi.org/10.1029/94PA01455

Veizer, J., 1983. Chemical diagenesis of carbonates; therory and application of trace element technique, in: Arthur, M.A., Anderson, T.F., Kaplan, I.R., Veizer, J., Land, L.S. (Eds.), Stable isotopes in sedimentary geology. Society of Sedimentary Geology, Tulsa, OK, SEPM Short Course (1983).

Veizer, J., Ala, D., Azmy, K., Bruckschen, P., Buhl, D., Bruhn, F., Carden, G.A.F., Diener, A., Ebneth, S., Godderis, Y., Jasper, T., Korte, C., Pawellek, F., Podlaha, O.G., Strauss, H., 1999. $^{87}Sr/^{86}Sr$, $\delta^{13}C$ and $\delta^{18}O$ evolution of Phanerozoic seawater. Chemical Geology 161, 59-88. http://dx.doi.org/10.1016/S0009-2541(99)00081-9

Viira, V., 2011. Lower and Middle Ordovician conodonts from the subsurface of SE Estonia and adjacent Russia. Estonian Journal of Earth Sciences 60, 1-21. http://dx.doi.org/10.3176/earth.2011.1.01

von Gosen, W., 1997. Early Paleozoic and Andean structural evolution in the Rio Jáchal section of the Argentine Precordillera. Journal of South American Earth Sciences 10, 361-388. http://dx.doi.org/10.1016/S0895-9811(97)00029-1

Webby, B.D., Droser, M.L., Paris, F., and Percival, I., 2004. The Great Ordovician Biodiversification Event, in: Webby, B.D., Droser, M.L., Paris, F., and Percival, I. (Ed.), The Great Ordovician Biodviersification Event. Columbia University Press, New York, p. 484. http://dx.doi.org/10.1017/S0016756805220782

Young, S.A., Gill, B.C., Edwards, C.T., Saltzman, M.R., Leslie, S.A., 2016. Middle–Late Ordovician (Darriwilian–Sandbian) decoupling of global sulfur and carbon cycles: Isotopic evidence from eastern and southern Laurentia. Palaeogeography, Palaeoclimatology, Palaeoecology 458, 118-132. http://dx.doi.org/10.1016/j.palaeo.2015.09.040

Zapata, T.R., Allmendinger, R.W., 1996. Thrust-front zone of the Precordillera, Argentina: A thick-skinned triangle zone. Aapg Bulletin-American Association of Petroleum Geologists 80, 359-381.

Zhang, J., Quay, P.D., Wilbur, D.O., 1995. Carbon isotope fractionation during gas-water exchange and dissolution of CO2. Geochimica et Cosmochimica Acta 59, 107-114. http://dx.doi.org/10.1016/0016-7037(95)91550-D

Zhang, J.H., 1998. Conodonts from the Guniutan Formation (Llanvirnian) in Hubei and Hunan Provinces, south-central China. Almqvist and Wiksell International.

Zhang, T., Shen, Y., Algeo, T.J., 2010. High-resolution carbon isotopic records from the Ordovician of South China: Links to climatic cooling and the Great Ordovician Biodiversification Event (GOBE). Palaeogeography, Palaeoclimatology, Palaeoecology 289, 102-112. http://dx.doi.org/10.1016/j.palaeo.2010.02.020

Appendix 1

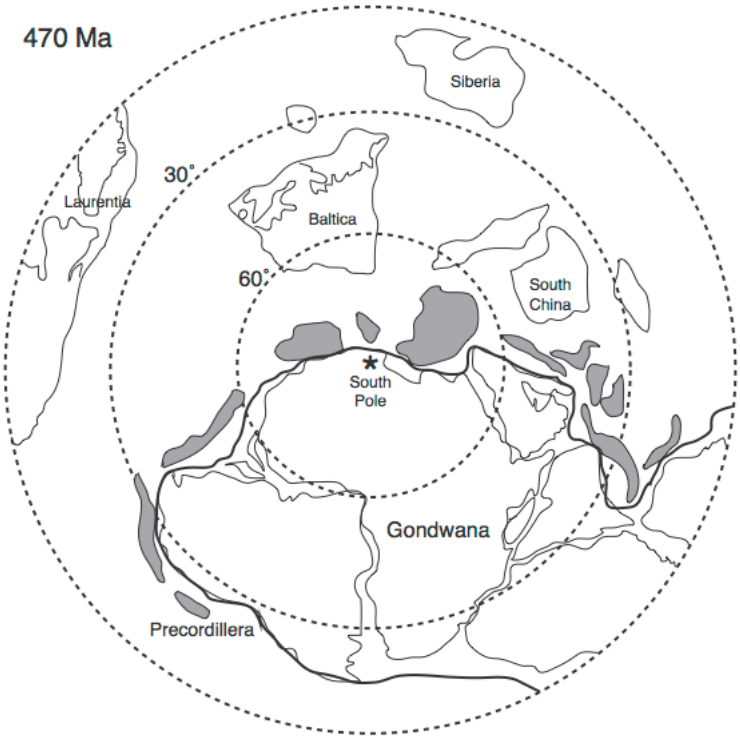

Figure 1.1: Paleogeographic reconstruction for the Middle Ordovician (~ 470 Ma) after Cocks and Torsvik (2002). Major landmasses are depicted in white, and Peri-gondwanan terranes are depicted in shades of gray. The Precordilleran terrane is shown in dark gray, in a position close to Gondwana, prior to its final docking.

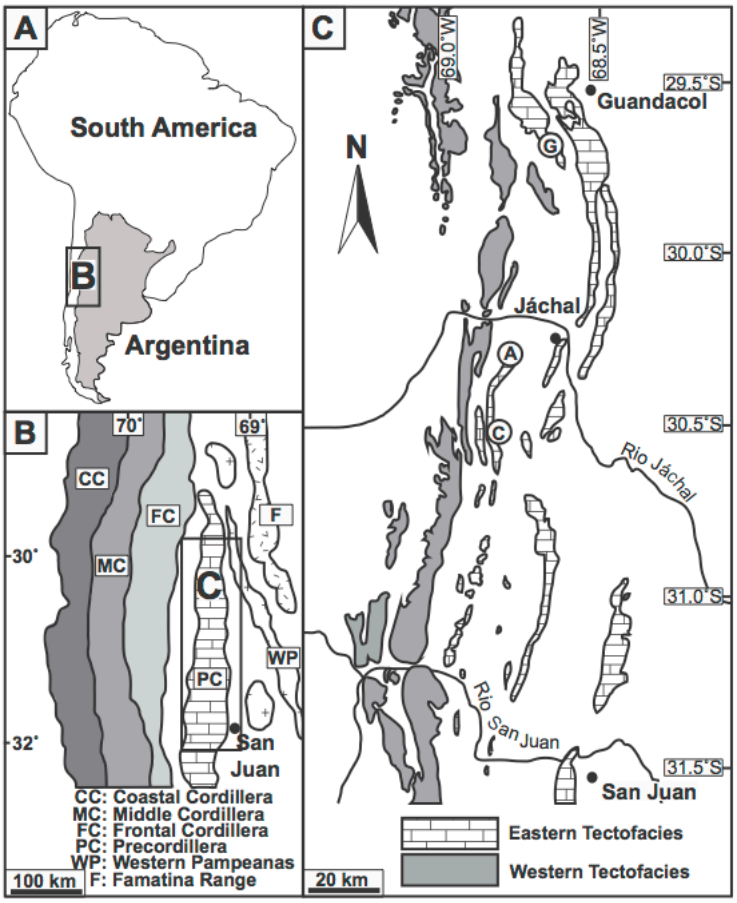

Figure 1.2: Regional map of the Argentine Precordillera modified from Gomez and Astini (2015). Lower Paleozoic strata crop out in a series of N-S trending thrust sheets and are divided into the Western and Eastern tectofacies. The Western tectofacies consists predominately of metamorphosed and deformed deep-water shale facies. The Eastern tectofacies consists of weakly deformed and unmetamorphosed marine shelf and slope deposits. Coeval measured sections of the Las Chacritas (C) and Las Aguaditas (A) formations were sampled in the Eastern tectofacies to the southwest of San Jose de Jáchal.

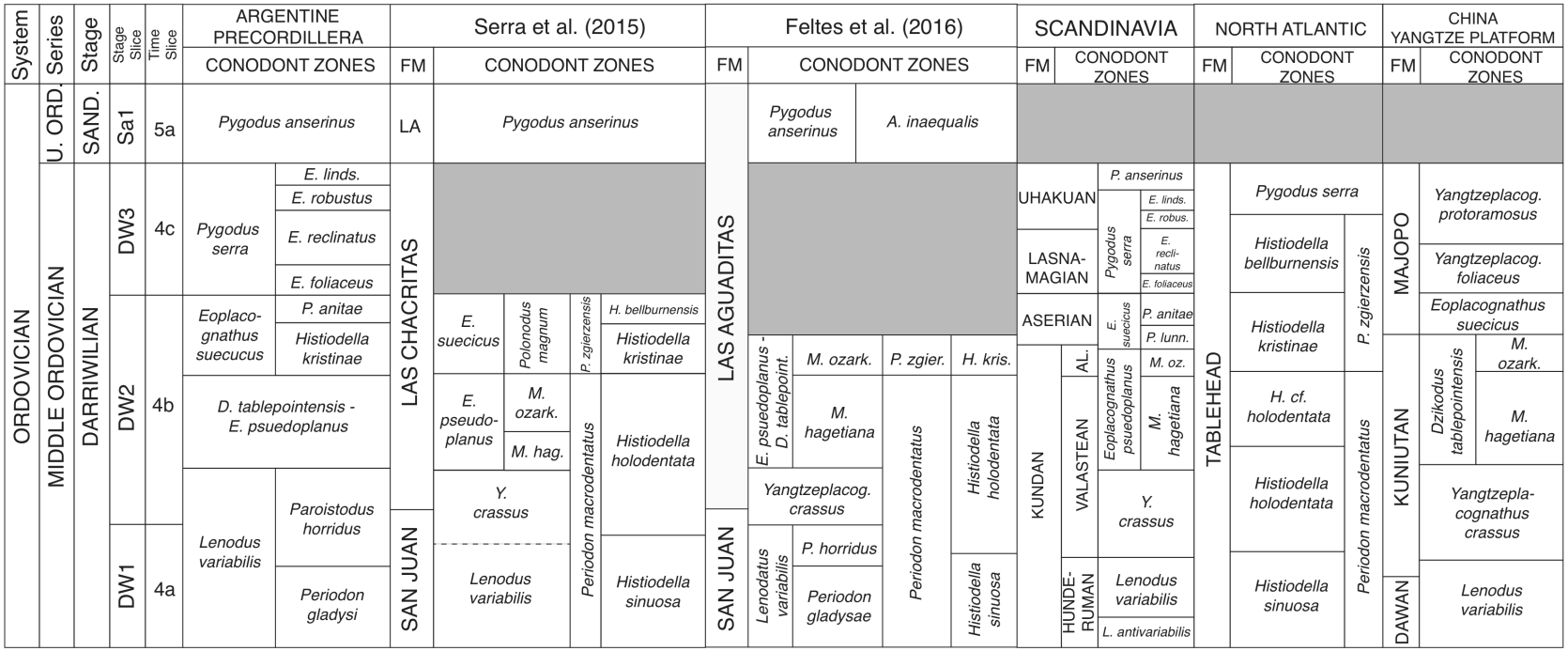

Figure 1.3: Biostratigraphic chart of Darriwilian strata showing generalized conodont zones for the Argentine Precordillera, specific data from the Las Chacritas and Las Aguaditas formations, and summary of data from Scandinavia, the North Atlantic, and China. Data is compiled from Albanesi and Ortega (2016), Serra et al. (2015), Feltes et al. (2016), Zhang (1998) and Löfgren and Tomacheva (2008), Stouge (1984), and Zhang (1998). Stage slices are after Bergström et al. (2009) and time slices after Webby et al. (2004). Interval of interest is indicated in light gray.

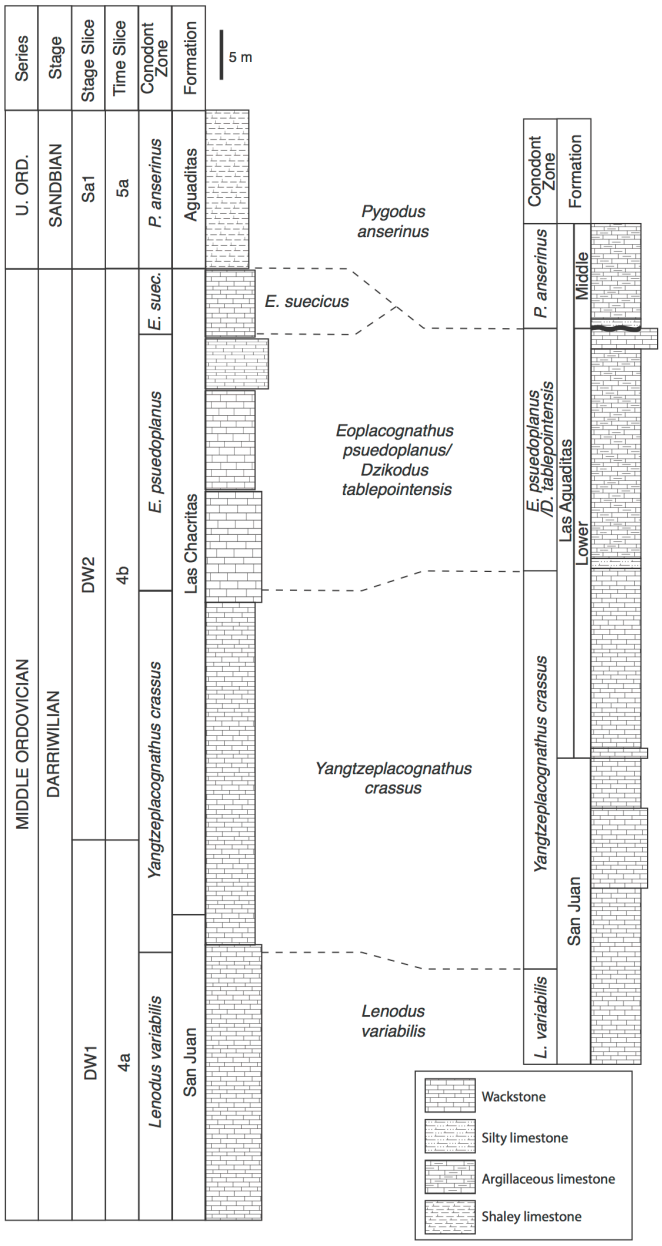

Figure 1.4: Correlation of measured stratigraphic sections of the Las Chacritas and Las Aguaditas formations based on conodont biostratigraphic analysis of Serra et al. (2015) and Feltes et al. (2016). Upper Darriwilian (Dw3) strata in the Precordillera is absent and inferred to have been removed during development of a regional unconformity. Absence of the Upper Darriwilian is identified by the absence of conodonts representing the upper *E. suecicus* Zone and *P. serra* Zone in the Las Chacritas Formation, and the *E. suecicus* and *P. serra* zones in the Las Aguaditas Formation.

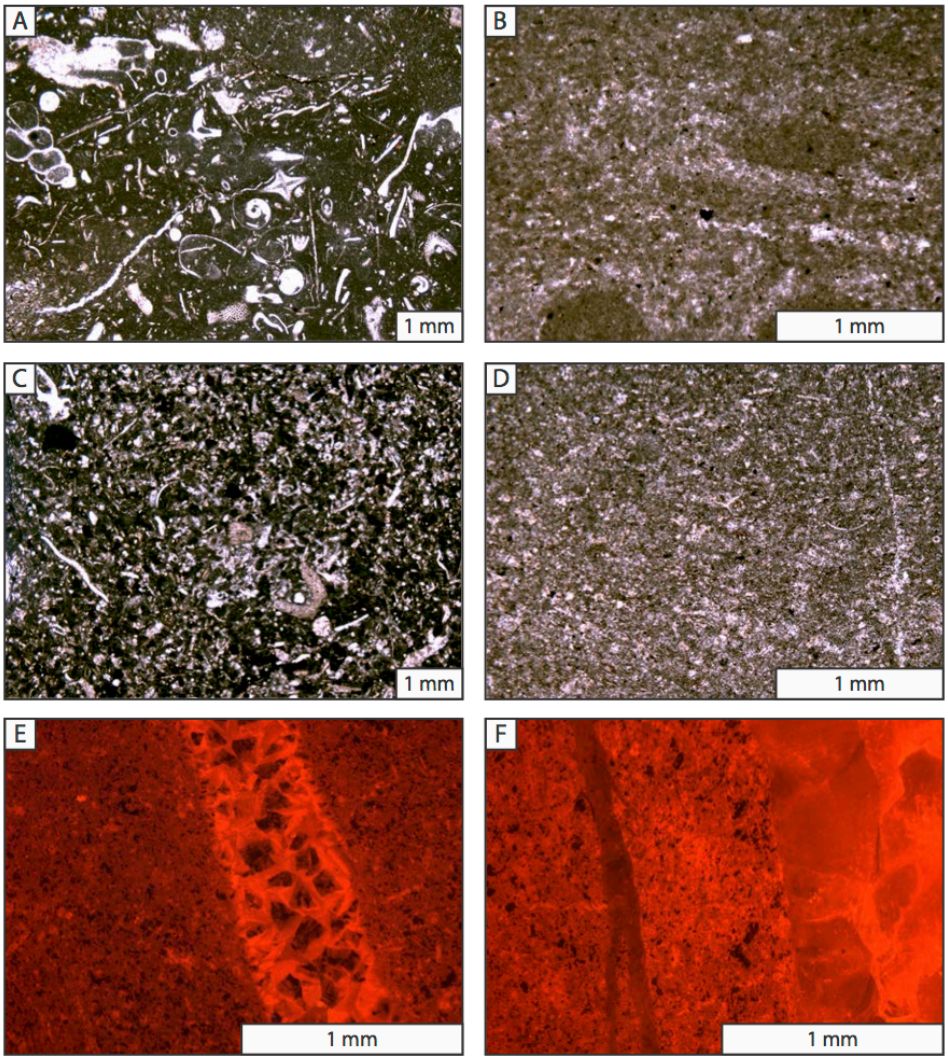

Figure 1.5: Petrographic microfabrics from the Las Chacritas Formation. A) Fossiliferous packstone with abundant sponge spicules, gastropods, and fragments of bryozoans, trilobites, brachiopods, and echinoderms. B) Intramicrite showing micritic clasts within a micritic- to microsparitic-matrix. Disseminated pyrite (opaque) occurs within the microsparitic matrix. C) Fossiliferous packstone with trilobite fragments, echinoderm fragments, and recrystallized sponge spicules. D) Carbonate mudstone containing predominantly recrystallized sponge spicules. E) CL image of heterogeneous, dully luminescent matrix cut by vein of brightly luminescent calcite with dully luminescent calcite intergrowths. F) CL image of heterogeneously luminescent carbonate matrix with two distinct vein generations: a dully luminescent vein (~ 140 μm diameter) and moderately luminescent vein (> 1 mm diameter).

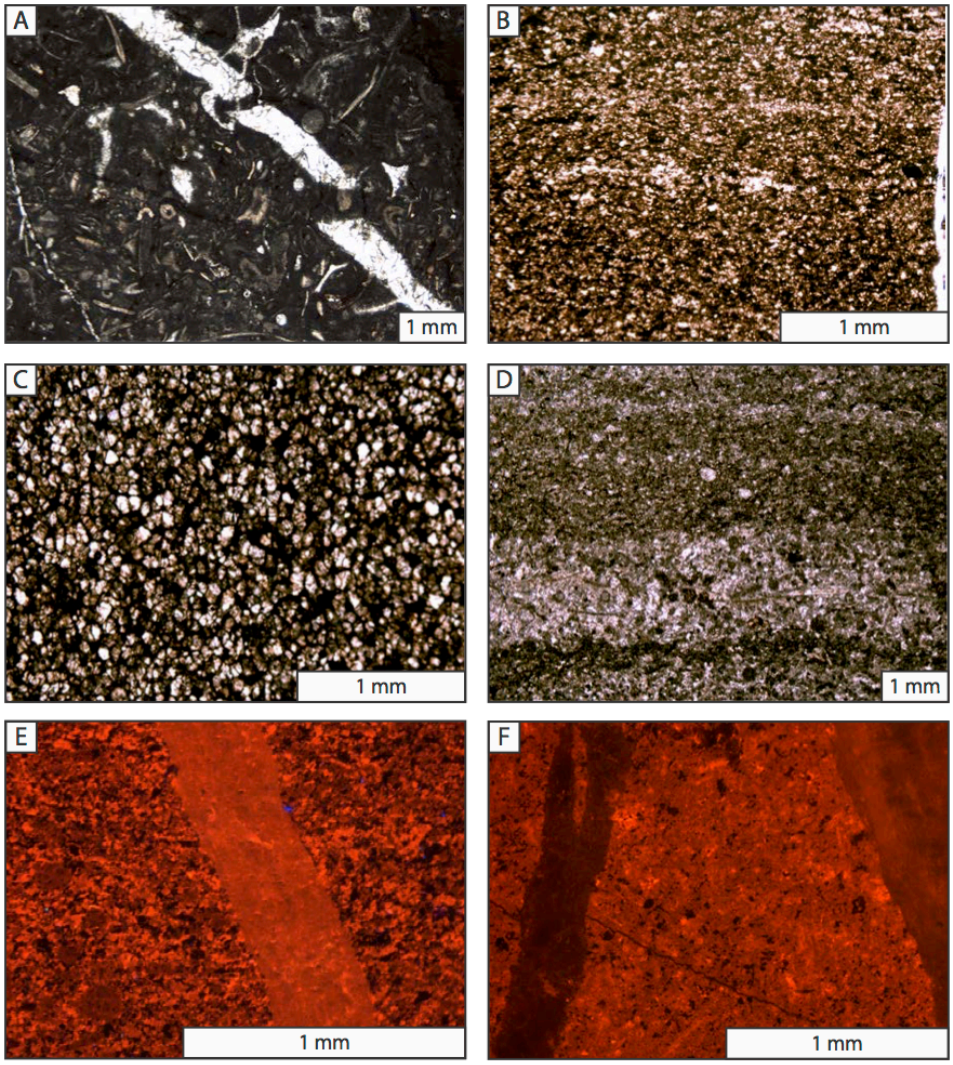

Figure 1.6: Petrographic microfabrics from the Las Aguaditas Creek Formation. A) Fossiliferous packstone with abundant fragments of bryozoans, echinoderms, brachiopods, and trilobites, here cut by a large (1 mm diameter) calcite vein and a smaller (~ 15 μm diameter) calcite vein. B) Homogeneous mixture of micritic to microsparitic carbonate and clay; such fabric characterizes the majority of the Las Aguaditas Formation. C) Homogeneous silty carbonate with disseminated pyrite. D) Laminated carbonate mudstone with a single layer of skeletal fragments within a microsparitic matrix. The white arrow indicates the position of a trilobite fragment. E). CL image showing heterogeneously luminescent micritic matrix composed of dully luminescent micritic clasts within a matrix of micrite (mixed luminescence) and clay (non-luminescent), cut by a coarsely crystalline, moderately luminescent vein. F) CL image of heterogeneous carbonate mudstone with three distinct stages of veins mineralization.

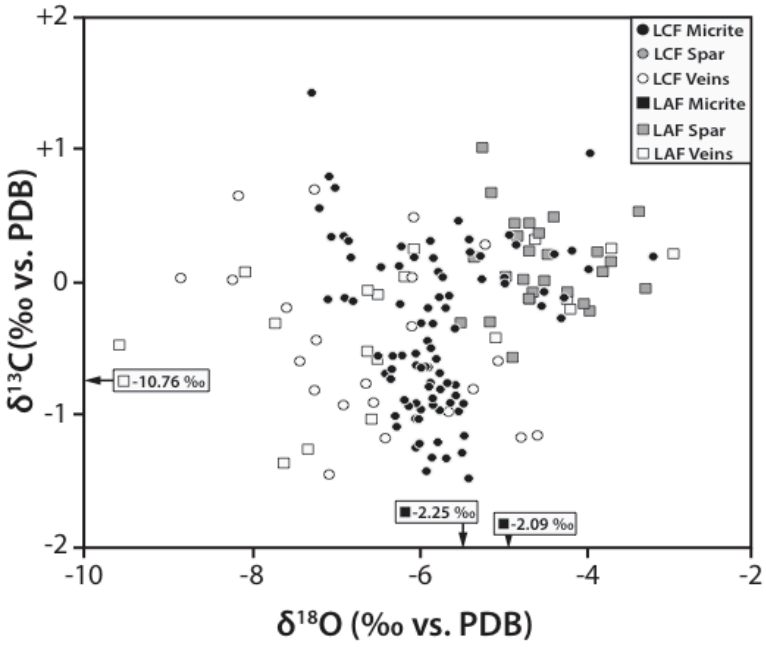

Figure 1.7: Cross-plot of carbon and oxygen isotopes from the Las Chacritas (LCF) and Las Aguaditas (LAF) formations. No clear covariant trends occur between C and O for the various carbonate phases (i.e., microsparitic matrix, recrystallized sparry patches within otherwise micritic matrix, and late-stage mineralized veins). Oxygen isotope compositions of micritic carbonate in the Las Chacritas and Las Aguaditas formations are similar, ranging from −4‰ to −6‰ in the Las Chacritas Formation and from −4‰ to −7‰ in the Las Aguaditas Formation. Carbon isotope compositions in both formations range from approximately +1‰ to −2‰. Isotopic compositions of sparry calcite within the carbonate matrix is generally similar to that of matrix micrite, consistent with only minor recrystallization either in the original depositional environment, or within a rock-buffered system. The wide range of $\delta^{18}O$ compositions preserved in vein calcite is consistent with formation by later diagenetic fluids that did not interact substantially with matrix components.

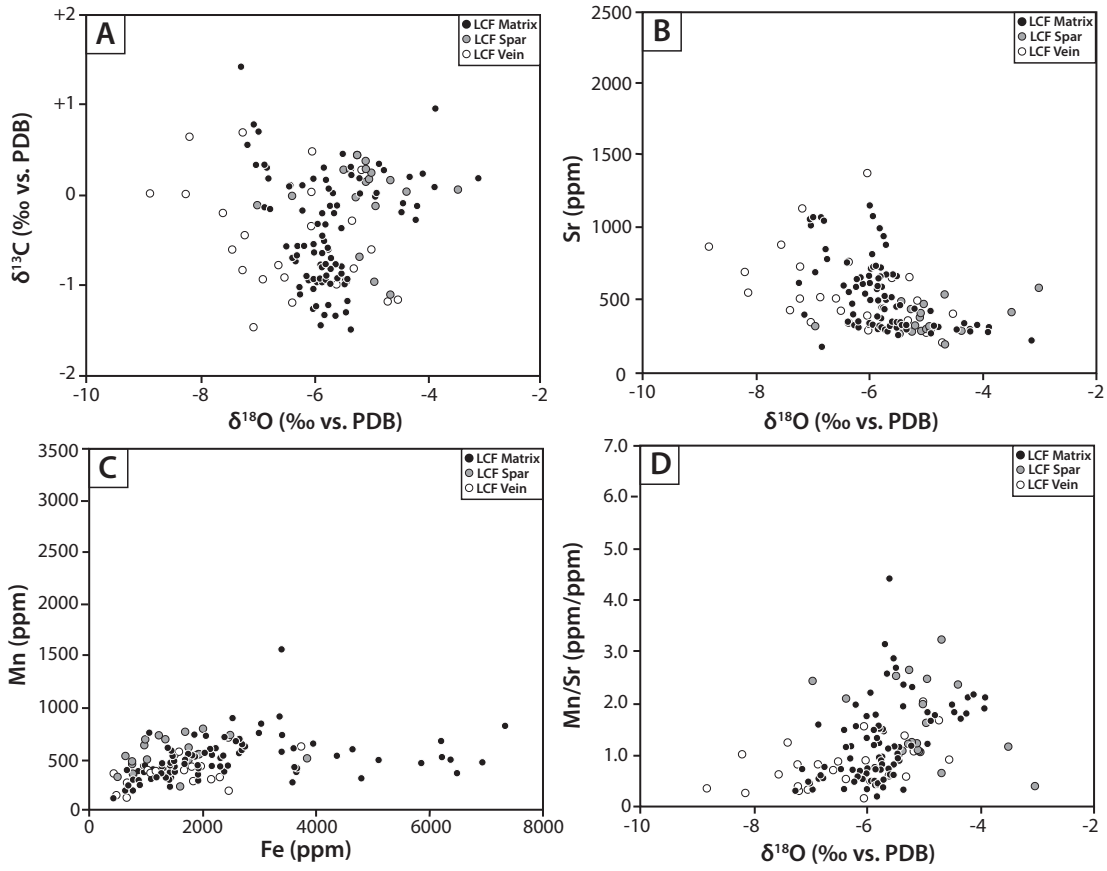

Figure 1.8: Isotopic and elemental data for carbonate phases of the Las Chacritas Formation. A) Detail of Figure 7; mineralized veins record a unique trajectory in carbon-oxygen space, indicating little influence of late-stage fluids on matrix components. B) Strontium concentrations of matrix components range from approximately 250 to 2000 ppm, consistent with well-preserved marine limestone. Lower Sr concentrations within sparry matrix is consistent with Sr loss during recrystallization. C) Mn and Fe concentrations are generally elevated, with [Mn] >500 ppm, and [Fe] as high as 8000 ppm. Combined with elevated Sr concentrations that suggest limited recrystallization, elevated Mn and Fe values potentially reflect in-situ incorporation from dysoxic to anoxic marine waters or pore fluids. D) Mn/Sr ratios are generally less than 3, well below the established threshold for little-altered carbonate rocks (Mn/Sr >10; Kaufman et al. 1995).

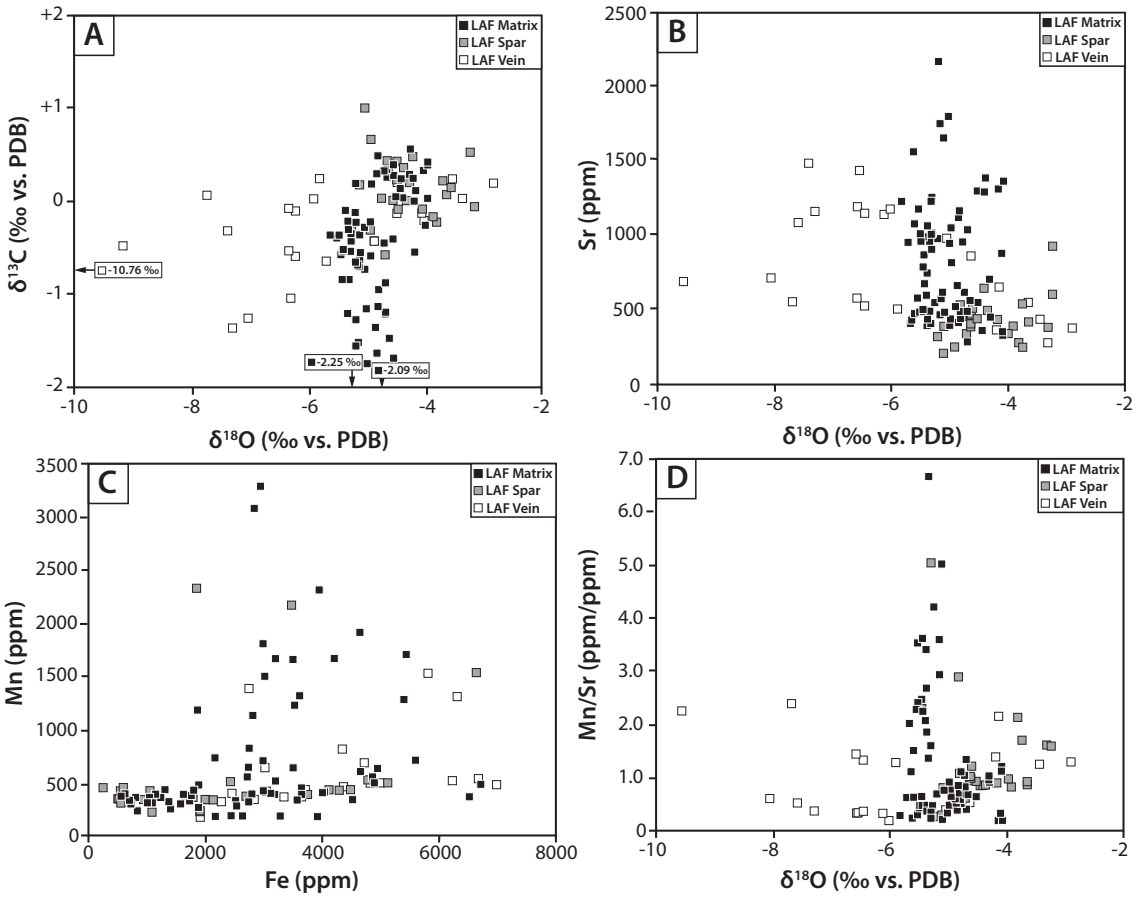

Figure 1.9: Isotopic and elemental data for carbonate phases of the Las Aguaditas Formation. A) Detail of Figure 7; mineralized veins record a unique trajectory in carbon-oxygen space, indicating little influence of late-stage fluids on matrix components. B) Elevated Sr concentrations observed in the Las Aguaditas Formation are consistent with crystallization from seawater or recrystallization in the presence of seawater derived fluids during early diagenesis. C) Evidence for elevated Mn and Fe, in conjunction with elevated Sr concentrations, is consistent with Mn and Fe enrichment in primary and early diagenetic fluids. D) Despite a few Mn/Sr values as high as 6.66, Mn/Sr ratios are generally less than 1, well below the established threshold for little-altered carbonate rocks (Mn/Sr >10; Kaufman et al. 1995).

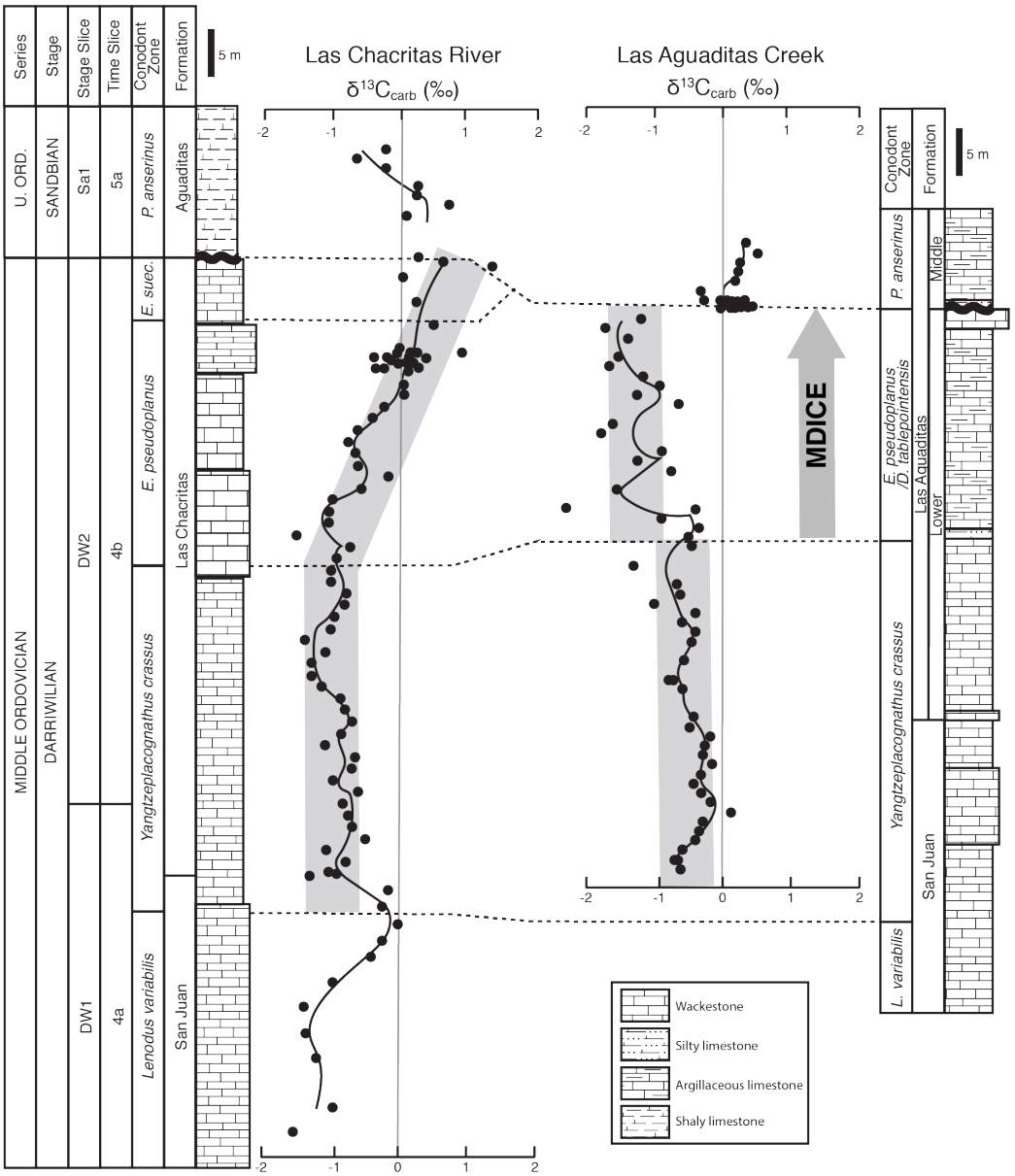

Figure 1.10: C-isotope records from the Las Chacritas and Las Aguaditas formations. Chemostratigraphic profiles show $\delta^{13}C_{carb}$ compositions are consistently near −1‰ through the pre-MDICE *Y. crassus* conodont zone. In the Las Chacritas Formation, $\delta^{13}C_{carb}$ values increase from approximately −1.0‰ in the lower *E. pseudoplanus* Zone to greater than +1.0‰ in the *E. suecicus* Zone. This nearly 2‰ positive shift in $\delta^{13}C_{carb}$ values is consistent with the initiation of the MDICE. In time-equivalent strata of the Las Aguaditas Formation, however, $\delta^{13}C_{carb}$ values abruptly decline to approximately −1.5‰. Three-point moving averages are fit to $\delta^{13}C_{carb}$ profiles.

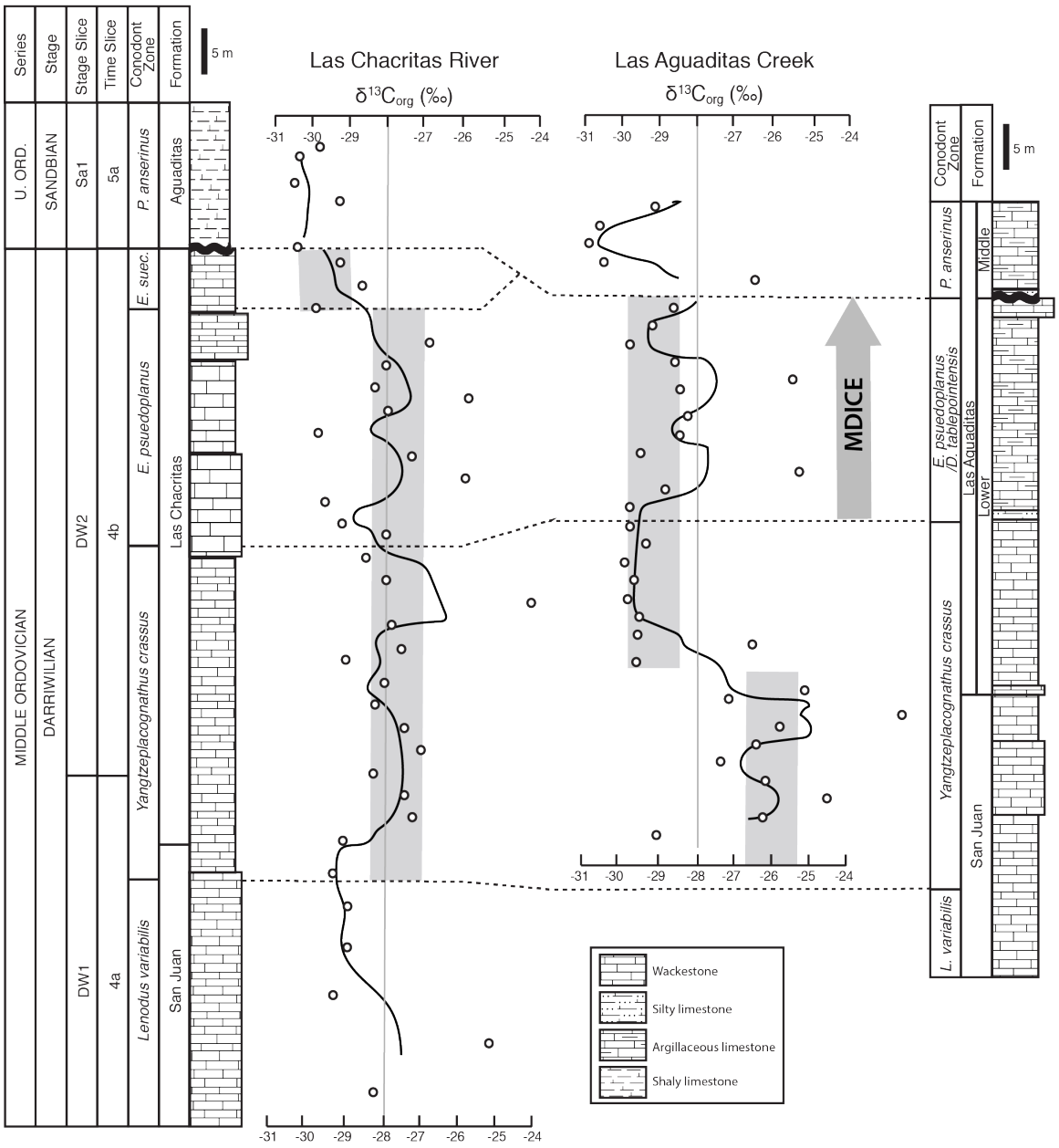

Figure 1.11: C-isotope records from the Las Chacritas and Las Aguaditas formations. Organic C-isotopes record substantial variation between −25‰ and −30‰, although most values are near −28‰. C-isotope values within the deeper-water Las Aguaditas Formation are similarly volatile, yet show an abrupt transition to values near −30‰ at the transition between the Las Aguaditas Formation and the underlying San Juan Formation. Differences in isotopic composition between the two sections potentially reflect local control on the isotopic composition of DIC. Three-point moving averages are fit to $\delta^{13}C_{org}$ profiles.

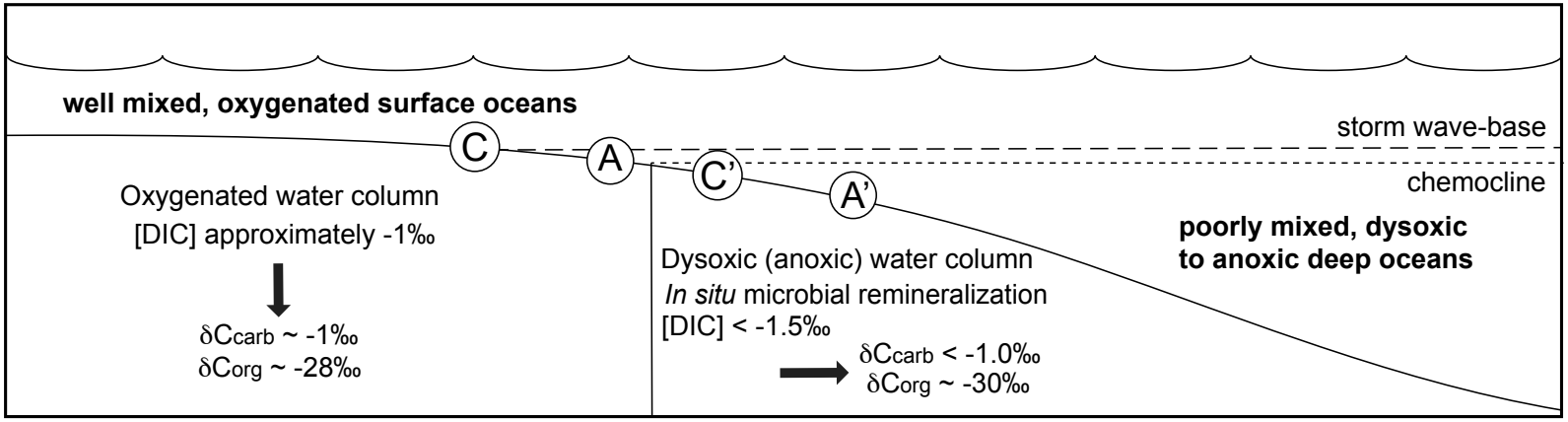

Figure 1.12: Interpretation of the marine shelf of the Las Chacritas and Las Aguaditas formations. Sedimentological data suggests that the Las Chacritas Formation (C) represents depositional environments between fair-weather and storm wave base, whereas sedimentary features of the Las Aguaditas Formation (A) suggest deposition at or near storm wave base. We suggest that the presence of a persistent marine chemocline (cf. Thompson and Kah, 2012) can best explain $\delta^{13}C_{carb}$ and $\delta^{13}C_{org}$ profiles of Figure 10. When carbonate formation occurs above the marine chemocline, marine carbonate reflects the isotopic composition of DIC within well-mixed oxygenated waters. By contrast, deposition below the marine chemocline may contain a mix of allochthonous and autochthonous components (C') and (A'). Carbon isotopes of autochthonous carbonate reflect a mixture of marine DIC and DIC from the remineralization of organic matter. Similarly, carbon isotopes of autochthonous organic matter potentially reflect a combination of photosynthetic and heterotrophic metabolisms, resulting in isotopically depleted signatures.

Table 1.1. Range of isotopic compositions and elemental concentrations recorded in the Las Chacritas Formation

Sample	Height* (m)	Conodont Zone	Phase	$\delta^{13}C_{carb}$ (‰ PDB)	$\delta^{18}O$	$\delta^{13}C_{org}$	$\Delta^{13}C$	Mg/Ca	Sr (ppm)	Mn	Fe
C14-1	-27.6	*L. variabilis*	Micrite	-1.48	-5.34	-28.35	26.87	0.02	332	98	421
C14-1	-27.6	*L. variabilis*	Vein	-1.45	-7.02	--	--	0.01	348	101	659
C14-2	-24.9	*L. variabilis*	Micrite	-0.92	-5.50	--	--	0.02	343	393	1916
C14-4	-19.6	*L. variabilis*	Micrite	-1.16	-5.40	--	--	0.01	310	269	864
C14-5	-17	*L. variabilis*	Micrite	-1.29	-5.43	-29.44	28.15	0.01	338	304	1177
C14-6	-14.3	*L. variabilis*	Micrite	-1.33	-5.61	--	--	0.02	344	380	1122
C14-7	-11.7	*L. variabilis*	Micrite	-0.92	-5.42	-29.02	28.10	0.02	325	364	1495
C14-8	-9	*L. variabilis*	Micrite	-0.36	-5.51	--	--	0.02	311	893	3367
C14-9	-7.2	*L. variabilis*	Micrite	-0.20	-5.63	-29.04	28.84	0.02	319	820	3037
C14-10	-5.4	*L. variabilis*	Micrite	0.02	-5.66	--	--	0.02	280	881	2531
C14-11	-3.6	*Y. crassus*	Micrite	-0.20	-5.83	-29.42	29.22	0.03	300	527	1737
C14-11	-3.6	*Y. crassus*	Vein	-0.20	-7.54	--	--	0.02	885	526	1927
C14-12	-1.8	*Y. crassus*	Micrite	-0.11	-5.59	--	--	0.01	350	1553	3400
C14-13	-0.2	*Y. crassus*	Micrite	-1.25	-5.98	-29.14	27.89	0.07	616	806	7360
C14-14	0	*Y. crassus*	Micrite	-0.88	-5.77	--	--	0.03	592	719	1851
C14-15	1.2	*Y. crassus*	Micrite	-0.97	-5.69	-29.16	28.19	0.01	507	735	1059
C14-16	2.3	*Y. crassus*	Micrite	-0.76	-5.86	--	--	0.02	575	673	2649
C14-17	3.5	*Y. crassus*	Micrite	-1.03	-5.95	-27.34	26.31	0.03	721	502	1838
C14-17	3.5	*Y. crassus*	Vein	-0.60	-7.38	--	--	0.02	429	522	1502
C14-18	4.7	*Y. crassus*	Micrite	-0.45	-5.84	--	--	0.03	496	340	1400
C14-18	4.7	*Y. crassus*	Vein	-0.98	-5.59	--	--	0.02	654	374	1673
C14-19	5.9	*Y. crassus*	Micrite	-0.63	-5.97	-27.53	26.90	0.04	499	357	1438
C14-20	7	*Y. crassus*	Micrite	-0.69	-5.69	--	--	0.01	681	336	1266

Table 1.1 continued

Sample	Height* (m)	Conodont Zone	Phase	$\delta^{13}C_{carb}$ (‰ PDB)	$\delta^{18}O$	$\delta^{13}C_{org}$	$\Delta^{13}C$	Mg/Ca	Sr (ppm)	Mn	Fe
C14-20	7	*Y. crassus*	Vein	-0.81	-5.29	--	--	0.01	656	363	1037
C14-21	8.2	*Y. crassus*	Micrite	-0.78	-5.51	-28.34	27.56	0.02	671	392	2382
C14-22	9.4	*Y. crassus*	Micrite	-0.56	-6.15	--	--	0.02	653	358	2388
C14-23a	11.7	*Y. crassus*	Micrite	-0.92	-5.87	-27.10	26.18	0.00	735	346	6512
C14-23b	11.7	*Y. crassus*	Micrite	-0.91	-5.58	--	--	0.00	672	411	1920
C14-23	11.7	*Y. crassus*	Vein	-0.82	-7.20	--	--	0.00	513	404	1803
C14-24	11.2	*Y. crassus*	Micrite	-0.64	-5.92	--	--	0.03	730	333	1914
C14-25	12.4	*Y. crassus*	Micrite	-0.60	-5.74	-27.54	26.94	0.01	946	653	6233
C14-26	13.6	*Y. crassus*	Micrite	-1.03	-5.99	--	--	0.00	670	403	1487
C14-27	14.9	*Y. crassus*	Micrite	-0.79	-5.83	-28.29	27.50	0.01	651	299	1316
C14-27	14.9	*Y. crassus*	Vein	-1.15	-4.53	--	--	0.00	403	355	839
C14-28	16.1	*Y. crassus*	Micrite	-0.64	-5.84	--	--	0.01	595	221	675
C14-29	17.4	*Y. crassus*	Micrite	-0.76	-5.80	-28.05	27.29	0.00	662	248	3596
C14-30	18.6	*Y. crassus*	Micrite	-0.81	-5.70	--	--	0.00	885	298	1438
C14-30	18.6	*Y. crassus*	Spar	-0.85	-3.02	--	--	0.00	585	213	1602
C14-31	19.8	*Y. crassus*	Micrite	-1.09	-6.21	-29.06	27.97	0.01	648	292	4805
C14-33	21.1	*Y. crassus*	Micrite	-1.22	-5.94	-27.61	26.39	0.00	819	357	960
C14-34	22.3	*Y. crassus*	Micrite	-1.21	-5.72	--	--	0.01	526	416	972
C14-35	23.6	*Y. crassus*	Micrite	-1.01	-6.23	-27.87	26.86	0.01	592	403	3629
C14-36	24.8	*Y. crassus*	Micrite	-1.32	-5.79	--	--	0.00	724	297	767
C14-36	24.8	*Y. crassus*	Vein	-1.17	-4.71	--	--	0.00	204	338	427
C14-37	26	*Y. crassus*	Micrite	-0.94	-6.06	-24.16	23.22	0.00	544	272	766
C14-38	27.3	*Y. crassus*	Micrite	-0.89	-6.11	--	--	0.00	612	408	2304
C14-38	27.3	*Y. crassus*	Spar	-1.10	-4.67	--	--	0.00	542	332	772

Table 1.1 continued

Sample	Height* (m)	Conodont Zone	Phase	$\delta^{13}C_{carb}$ (‰ PDB)	$\delta^{18}O$	$\delta^{13}C_{org}$	$\Delta^{13}C$	Mg/Ca	Sr (ppm)	Mn	Fe
C14-39	28.5	*Y. crassus*	Micrite	-0.76	-5.60	-28.00	27.24	0.00	517	363	856
C14-39	28.5	*Y. crassus*	Spar	-0.94	-5.43	--	--	0.00	489	474	1757
C14-39	28.5	*Y. crassus*	Vein	-0.77	-6.58	--	--	0.00	510	344	1083
C14-40	29.8	*Y. crassus*	Micrite	-0.73	-6.29	--	--	0.00	474	414	1272
C14-40	29.8	*Y. crassus*	Vein	-1.18	-6.35	--	--	0.00	767	383	1424
C14-41	31	*Y. crassus*	Micrite	-0.95	-5.85	-28.54	27.59	0.01	597	435	1679
C14-42	32.3	*Y. crassus*	Micrite	-0.93	-5.78	--	--	0.00	451	412	937
C14-43	33.5	*Y. crassus*	Micrite	-0.86	-5.51	-28.03	27.17	0.00	452	359	1512
C14-43	33.5	*Y. crassus*	Spar	-0.68	-5.19	--	--	0.00	324	396	1182
C14-43	33.5	*Y. crassus*	Vein	-0.93	-6.85	--	--	0.01	519	409	1967
C14-44	34.7	*Y. crassus*	Micrite	-0.66	-6.28	-29.15	28.49	0.01	402	363	1026
C14-44	34.7	*Y. crassus*	Vein	-0.91	-6.49	--	--	0.01	427	359	1399
C14-45	37.2	*Y. crassus*	Micrite	-0.98	-5.45	-29.61	28.63	0.01	466	466	1479
C14-46	38.5	*Y. crassus*	Micrite	-0.96	-5.93	--	--	0.02	1086	500	6236
C14-47	39.7	*Y. crassus*	Micrite	-0.92	-5.98	-25.93	25.01	0.01	1157	356	3664
C14-48	40.9	*Y. crassus*	Micrite	-0.50	-5.81	--	--	0.01	324	423	1414
C14-49	42.2	*Y. crassus*	Micrite	-0.12	-5.70	-27.31	27.19	0.01	293	434	1280
C14-50	43.4	*Y. crassus*	Micrite	-0.54	-5.99	--	--	0.01	341	591	1369
C14-51	44.7	*E. pseudoplanus*	Micrite	-0.58	-5.74	-29.79	29.21	0.01	450	391	3678
C14-51	44.7	*E. pseudoplanus*	Spar	-0.95	-4.94	--	--	0.00	318	509	632
C14-52	45.9	*E. pseudoplanus*	Micrite	-0.69	-6.35	--	--	0.01	556	631	3956
C14-52	45.9	*E. pseudoplanus*	Vein	-0.44	-7.17	--	--	0.02	1139	304	2301
C14-53	47.1	*E. pseudoplanus*	Micrite	-0.56	-6.26	-27.96	27.40	0.02	327	374	659
C14-54	48.4	*E. pseudoplanus*	Micrite	-0.32	-5.78	-25.83	25.51	0.01	371	573	2125

Table 1.1 continued

Sample	Height* (m)	Conodont Zone	Phase	$\delta^{13}C_{carb}$ (‰ PDB)	$\delta^{18}O$	$\delta^{13}C_{org}$	$\Delta^{13}C$	Mg/Ca	Sr (ppm)	Mn	Fe
C14-55	49.6	*E. pseudoplanus*	Micrite	-0.17	-6.18	-28.30	28.13	0.01	352	539	2035
C14-55	49.6	*E. pseudoplanus*	Vein	-0.34	-6.03	--	--	0.01	394	603	3744
C14-56	50.9	*E. pseudoplanus*	Micrite	0.11	-6.18	--	--	0.01	310	608	2735
C14-56	50.9	*E. pseudoplanus*	Spar	-0.01	-6.35	--	--	0.01	342	710	2497
C14-57	52.1	*E. pseudoplanus*	Micrite	0.11	-6.38	-28.01	28.12	0.01	352	517	1810
C14-58	53.3	*E. pseudoplanus*	Micrite	0.17	-5.77	--	--	0.01	310	463	1687
C14-78	53.7	*E. pseudoplanus*	Vein	0.27	-5.16	--	--	0.00	496	518	1888
C14-80	53.7	*E. pseudoplanus*	Spar	0.29	-5.11	--	--	0.00	379	457	751
C14-82	53.7	*E. pseudoplanus*	Spar	0.04	-4.38	--	--	0.00	287	673	1335
C14-85	54.1	*E. pseudoplanus*	Spar	0.16	-4.67	--	--	0.00	190	615	969
C14-86	54.1	*E. pseudoplanus*	Spar	0.17	-5.05	--	--	0.00	475	489	3854
C14-58	54.6	*E. pseudoplanus*	Vein	0.03	-6.03	--	--	0.03	1383	172	2459
C14-59	54.6	*E. pseudoplanus*	Micrite	0.18	-5.99	-26.83	27.01	0.01	337	439	1428
C14-59	54.6	*E. pseudoplanus*	Spar	0.29	-5.36	--	--	0.01	319	335	757
C14-90	54.5	*E. pseudoplanus*	Spar	0.07	-3.50	--	--	0.00	416	473	1011
C14-91	54.5	*E. pseudoplanus*	Vein	-0.29	-5.32	--	--	0.00	358	484	1734
C14-92	54.5	*E. pseudoplanus*	Spar	0.15	-5.09	--	--	0.00	409	433	746
C14-94	54.5	*E. pseudoplanus*	Spar	0.25	-5.00	--	--	0.00	298	588	1752
C14-95	54.5	*E. pseudoplanus*	Spar	-0.03	-5.26	--	--	0.00	438	524	1950
C14-96	54.9	*E. pseudoplanus*	Spar	-0.11	-6.94	--	--	0.00	320	773	2008
C14-97	54.9	*E. pseudoplanus*	Spar	0.28	-5.46	--	--	0.00	268	674	988
C14-96	54.9	*E. pseudoplanus*	Vein	-0.60	-4.99	--	--	0.00	272	548	1577
C14-99	54.9	*E. pseudoplanus*	Spar	0.44	-5.24	--	--	0.00	282	743	1687
C14-99	55.3	*E. pseudoplanus*	Vein	0.01	-8.18	--	--	0.00	696	687	2458

Table 1.1 continued

Sample	Height* (m)	Conodont Zone	Phase	$\delta^{13}C_{carb}$ (‰ PDB)	$\delta^{18}O$	$\delta^{13}C_{org}$	$\Delta^{13}C$	Mg/Ca	Sr (ppm)	Mn	Fe
C14-100	54.9	*E. pseudoplanus*	Spar	-0.12	-4.92	--	--	0.00	289	713	1215
C14-60	55.8	*E. pseudoplanus*	Micrite	0.07	-5.72	--	--	0.01	436	410	2158
C14-60	55.8	*E. pseudoplanus*	Spar	0.38	-5.09	--	--	0.01	285	306	492
C14-62	58.3	*E. pseudoplanus*	Micrite	0.55	-7.13	-29.87	30.42	0.01	400	278	1405
C14-62	58.3	*E. pseudoplanus*	Vein	0.48	-6.01	--	--	0.01	289	253	658
C14-64	60.8	*E. suecicus*	Micrite	0.30	-5.81	-28.65	28.95	0.01	1000	171	626
C14-65	62	*E. suecicus*	Micrite	--	--	--	--	0.01	1330	286	1081
C14-66	63.3	*E. suecicus*	Micrite	0.10	-6.39	-29.23	29.33	0.01	762	233	889
C14-66	63.3	*E. suecicus*	Vein	0.02	-8.80	--	--	0.01	872	282	2152
C14-67	64.5	*E. suecicus*	Micrite	1.41	-7.23	--	--	0.01	621	169	767
C14-67	64.5	*E. suecicus*	Vein	0.64	-8.12	--	--	0.01	553	123	464
C14-68	65	*E. suecicus*	Micrite	0.70	-6.94	-30.32	31.02	0.01	695	203	1421
C14-68	65	*E. suecicus*	Vein	0.69	-7.20	--	--	0.01	733	262	1832
C14-69	65.5	*E. suecicus*	Micrite	0.33	-6.84	--	--	0.01	1075	534	8362
C14-70	70	*E. suecicus*	Micrite	0.18	-6.76	-29.22	29.40	0.02	854	446	6954
C14-71	71	*E. suecicus*	Micrite	0.78	-7.01	--	--	0.01	1021	472	5115
C14-72	72	*P. anserinus*	Micrite	0.30	-6.79	-30.45	30.75	0.03	1053	602	11496
C14-73	73	*P. anserinus*	Micrite	0.33	-6.98	--	--	0.01	1078	438	5876
C14-74	74	*P. anserinus*	Micrite	-0.14	-7.03	-30.31	30.17	0.01	1066	470	6394
C14-76	76	*P. anserinus*	Micrite	-0.56	-6.44	-29.74	29.18	0.01	603	420	2448
C14-77	77	*P. anserinus*	Micrite	-0.15	-6.73	--	--	0.01	785	584	3617

*Height relative to the contact between the San Juan and Las Aguaditas Formations

Table 1.2. Range of isotopic compositions and elemental concentrations recorded in the Las Aguaditas Formation.

Sample	Height* (m)	Conodont Zone	Phase	$\delta^{13}C_{carb}$ (‰ PDB)	$\delta^{18}O$	$\delta^{13}C_{org}$	$\Delta^{13}C$	Mg/Ca	Sr (ppm)	Mn	Fe
A14-1	-16	*Y. crassus*	Micrite	-0.58	-5.62	-29.12	28.54	0.01	431	456	1909
A14-2	-15	*Y. crassus*	Micrite	-0.61	-5.29	--	--	0.01	405	627	2764
A14-2	-15	*Y. crassus*	Micrite	-0.66	-5.36	--	--	0.01	396	716	2194
A14-2	-15	*Y. crassus*	Vein	-0.64	-5.88	--	--	0.02	503	621	3039
A14-3	-14	*Y. crassus*	Micrite	-0.54	-5.58	-26.37	25.83	0.01	474	690	3005
A14-3	-14	*Y. crassus*	Vein	-0.59	-6.44	--	--	0.02	524	671	4736
A14-4	-13	*Y. crassus*	Micrite	-0.36	-5.65	--	--	0.02	409	807	2781
A14-4	-13	*Y. crassus*	Vein	-0.53	-6.56	--	--	0.01	577	804	4362
A14-5	-12	*Y. crassus*	Micrite	-0.29	-5.49	-24.70	24.41	0.02	488	1119	2832
A14-6	-11	*Y. crassus*	Micrite	-0.23	-5.38	--	--	0.01	599	1213	3547
A14-7	-10	*Y. crassus*	Micrite	0.19	-5.36	-26.30	26.49	0.02	443	1170	1890
A14-7	-10	*Y. crassus*	Vein	-0.32	-7.67	--	--	0.02	551	1294	6319
A14-8	-9	*Y. crassus*	Micrite	-0.12	-5.43	--	--	0.01	501	1795	3009
A14-9	-8	*Y. crassus*	Micrite	-0.26	-5.14	-27.46	27.20	0.01	466	1658	4227
A14-10	-7	*Y. crassus*	Micrite	-0.37	-5.41	--	--	0.03	675	1490	3034
A14-10	-7	*Y. crassus*	Vein	-0.21	-4.13	--	--	0.02	651	1369	2770
A14-11	-6	*Y. crassus*	Micrite	-0.28	-5.23	-26.54	26.26	0.01	550	2297	3964
A14-12	-5	*Y. crassus*	Micrite	-0.10	-5.54	--	--	0.03	578	1300	3632
A14-12	-5	*Y. crassus*	Vein	-0.48	-9.54	--	--	0.01	686	1512	5821
A14-13	-4	*Y. crassus*	Micrite	-0.25	-5.13	-25.90	25.65	0.03	572	1654	3225
A14-14	-3	*Y. crassus*	Micrite	-0.22	-5.10	--	--	0.02	614	3065	2865
A14-15	-2	*Y. crassus*	Micrite	-0.13	-5.37	-22.76	22.63	0.01	487	1644	3521
A14-16	-1	*Y. crassus*	Micrite	-0.43	-5.44	-27.25	26.82	0.01	783	1897	4662

Table 1.2 continued

Sample	Height* (m)	Conodont Zone	Phase	$\delta^{13}C_{carb}$ (‰ PDB)	$\delta^{18}O$	$\delta^{13}C_{org}$	$\Delta^{13}C$	Mg/Ca	Sr (ppm)	Mn	Fe
A14-16	-1	*Y. crassus*	Spar	-0.31	-5.44	--	--	0.02	956	2156	3498
A14-17	0	*Y. crassus*	Micrite	-0.37	-5.32	-25.27	24.90	0.01	492	3274	2963
A14-17	0	*Y. crassus*	Spar	0.18	-5.28	--		0.02	462	2318	1874
A14-20	3	*Y. crassus*	Micrite	-0.55	-4.30	-29.61	29.06	0.05	705	693	5606
A14-21	4	*Y. crassus*	Micrite	-0.69	-5.32	--	--	0.03	963	1265	5403
A14-21	4	*Y. crassus*	Micrite	-0.73	-5.19	--	--	0.04	975	615	4959
A14-22	5	*Y. crassus*	Micrite	--	--	-26.63	--	--	--	--	--
A14-23	6	*Y. crassus*	Micrite	-0.52	-5.58	-29.58	29.06	0.03	1075	622	3523
A14-25	8	*Y. crassus*	Micrite	-0.41	-4.69	-29.55	29.14	0.02	857	379	3081
A14-26	9	*Y. crassus*	Micrite	-0.36	-5.28	--	--	0.01	1010	380	3135
A14-26	9	*Y. crassus*	Vein	-0.43	-5.03	--	--	0.02	979	326	2857
A14-27	10	*Y. crassus*	Micrite	-0.54	-5.44	-29.86	29.32	0.03	991	587	4670
A14-28	11	*Y. crassus*	Micrite	-0.36	-5.28	--	--	0.01	906	378	2814
A14-29	12	*Y. crassus*	Micrite	-0.95	-4.95	-29.71	28.76	0.04	815	484	4902
A14-30	13	*Y. crassus*	Micrite	-0.57	-5.27	--	--	0.03	1016	396	4069
A14-31	14	*Y. crassus*	Micrite	-0.63	-5.28	-29.92	29.29	0.03	1250	317	1764
A14-33	16	*Y. crassus*	Micrite	-1.28	-5.36	-29.38	28.10	0.03	1060	427	3670
A14-35	18	*Y. crassus*	Micrite	-0.40	-5.69	-29.79	29.39	0.00	951	540	4880
A14-36	19	*E. pseudoplanus/ D. tablepointensis*	Micrite	-0.45	-4.85	--	--	0.02	663	302	2767
A14-37	20	*E. pseudoplanus/ D. tablepointensis*	Micrite	-0.29	-5.48	-29.79	29.50	0.02	959	413	1826
A14-38	21	*E. pseudoplanus/ D. tablepointensis*	Micrite	-0.84	-5.48	--	--	0.01	1011	391	4022

Table 1.2 continued

Sample	Height* (m)	Conodont Zone	Phase	$\delta^{13}C_{carb}$ (‰ PDB)	$\delta^{18}O$	$\delta^{13}C_{org}$	$\Delta^{13}C$	Mg/Ca	Sr (ppm)	Mn	Fe
A14-39	22	*E. pseudoplanus/ D. tablepointensis*	Micrite	-0.36	-5.81	-28.89	28.53	0.01	1229	267	1069
A14-39	22	*E. pseudoplanus/ D. tablepointensis*	Spar	1.00	-5.19	--	--	0.01	994	206	1115
A14-40	23	*E. pseudoplanus/ D. tablepointensis*	Micrite	-2.25	-5.42	--	--	0.01	866	369	1643
A14-40	23	*E. pseudoplanus/ D. tablepointensis*	Vein	-1.04	-6.52	--	--	0.01	1434	402	3056
A14-41	24	*E. pseudoplanus/ D. tablepointensis*	Micrite	-1.52	-5.32	-25.41	23.89	--	--	--	--
A14-43	26	*E. pseudoplanus/ D. tablepointensis*	Micrite	-0.71	-5.29	-29.52	28.81	0.02	1233	215	873
A14-44	27	*E. pseudoplanus/ D. tablepointensis*	Micrite	-1.21	-5.51	--	--	0.02	1175	282	1046
A14-45	28	*E. pseudoplanus/ D. tablepointensis*	Micrite	-0.84	-5.60	-28.51	27.67	0.01	1560	280	1609
A14-47	30	*E. pseudoplanus/ D. tablepointensis*	Micrite	-1.75	-5.15	-28.31	26.56	0.06	1748	321	3593
A14-48	31	*E. pseudoplanus/ D. tablepointensis*	Micrite	-1.56	-5.36	--	--	0.01	743	233	1429
A14-50	33	*E. pseudoplanus/ D. tablepointensis*	Micrite	-0.59	-5.08	-28.49	27.90	0.04	1652	263	2564
A14-51	34	*E. pseudoplanus/ D. tablepointensis*	Micrite	-1.20	-4.83	-25.58	24.38	0.02	1120	538	2740

Table 1.2 continued

Sample	Height* (m)	Conodont Zone	Phase	$\delta^{13}C_{carb}$ (‰ PDB)	$\delta^{18}O$	$\delta^{13}C_{org}$	$\Delta^{13}C$	Mg/Ca	Sr (ppm)	Mn	Fe
A14-52	35	*E. pseudoplanus/ D. tablepointensis*	Micrite	-0.88	-4.82	--	--	0.02	1156	368	1802
A14-53	36	*E. pseudoplanus/ D. tablepointensis*	Micrite	-1.14	-4.96	-28.63	27.49	0.01	1048	372	1172
A14-54	37	*E. pseudoplanus/ D. tablepointensis*	Micrite	-1.64	-4.98	--	--	0.02	944	408	1080
A14-55	38	*E. pseudoplanus/ D. tablepointensis*	Micrite	-1.48	-4.76	-29.79	28.31	0.02	955	417	1340
A14-57	40	*E. pseudoplanus/ D. tablepointensis*	Micrite	-1.36	-5.00	-29.21	27.85	0.02	1795	495	3226
A14-57	40	*E. pseudoplanus/ D. tablepointensis*	Vein	-1.37	-7.57	--	--	0.02	1086	500	6236
A14-58	41	*E. pseudoplanus/ D. tablepointensis*	Micrite	-1.69	-4.68	--	--	0.02	1037	357	1792
A14-58	41	*E. pseudoplanus/ D. tablepointensis*	Vein	-1.26	-7.28	--	--	0.01	1157	356	3664
A14-59	42	*E. pseudoplanus/ D. tablepointensis*	Micrite	-1.16	-5.17	--	--	0.03	2166	475	6715
A14-59	42	*E. pseudoplanus/ D. tablepointensis*	Micrite	-2.09	-4.88	-28.68	26.59	0.02	518	290	1021
A14-65	43.2	*P. anserinus*	Micrite	0.42	-4.07	--	--	0.01	352	378	625
A14-66	44.2	*P. anserinus*	Spar	-0.06	-3.22	--	--	0.01	319	492	2452
A14-77	43.2	*P. anserinus*	Spar	0.48	-4.33	--	--	0.00	600	482	5132
A14-77	43.2	*P. anserinus*	Vein	-0.13	-4.62	--	--	0.00	859	411	3728

Table 1.2 continued

Sample	Height* (m)	Conodont Zone	Phase	$\delta^{13}C_{carb}$ (‰ PDB)	$\delta^{18}O$	$\delta^{13}C_{org}$	$\Delta^{13}C$	Mg/Ca	Sr (ppm)	Mn	Fe
A14-82	43.2	*P. anserinus*	Spar	-0.31	-5.09	--	--	0.00	924	212	1942
A14-87	43.2	*P. anserinus*	Spar	0.03	-4.90	--	--	0.00	493	320	2165
A14-87	43.2	*P. anserinus*	Vein	0.07	-8.04	--	--	0.00	713	384	2482
A14-92	43.2	*P. anserinus*	Spar	0.22	-3.80	--	--	0.00	207	432	628
A14-64	43.4	*P. anserinus*	Microspar	0.03	-4.07	--	--	0.02	327	374	659
A14-64	43.4	*P. anserinus*	Spar	0.07	-3.73	--	--	0.01	247	408	578
A14-64	43.4	*P. anserinus*	Vein	0.52	-3.30	--	--	0.01	278	436	278
A14-78	43.4	*P. anserinus*	Spar	0.36	-4.50	--	--	0.00	380	332	528
A14-78	43.4	*P. anserinus*	Vein	-0.13	-4.18	--	--	0.00	362	482	4831
A14-83	43.4	*P. anserinus*	Spar	-0.23	-3.90	--	--	0.00	535	414	4308
A14-83	43.4	*P. anserinus*	Vein	0.03	-3.43	--	--	0.00	434	519	6681
A14-88	43.4	*P. anserinus*	Spar	-0.09	-4.59	--	--	0.00	439	510	4802
A14-88	43.4	*P. anserinus*	Vein	-0.10	-6.44	--	--	0.00	1144	346	3367
A14-93	43.4	*P. anserinus*	Spar	0.66	-5.08	--	--	0.00	388	291	591
A14-93	43.4	*P. anserinus*	Vein	0.20	-4.60	--	--	0.00	468	444	4381
A14-65	44.4	*P. anserinus*	Spar	0.07	-3.73	--	--	0.01	247	408	578
A14-79	43.6	*P. anserinus*	Spar	0.15	-3.64	--	--	0.00	512	417	4125
A14-84	43.6	*P. anserinus*	Spar	-0.09	-4.16	--	--	0.00	387	326	969
A14-89	43.6	*P. anserinus*	Spar	0.34	-4.77	--	--	0.00	419	321	2035
A14-89	43.6	*P. anserinus*	Vein	0.25	-3.63	--	--	0.00	548	478	5014
A14-62	43.8	*P. anserinus*	Micrite	0.25	-4.80	--	--	0.01	496	298	1125
A14-62	43.8	*P. anserinus*	Vein	0.03	-6.11	--	--	0.02	1139	304	2301
A14-80	43.8	*P. anserinus*	Spar	0.20	-4.39	--	--	0.00	431	342	1824
A14-85	43.8	*P. anserinus*	Spar	-0.17	-3.97	--	--	0.00	453	418	4499

Table 1.2 continued

Sample	Height* (m)	Conodont Zone	Phase	$\delta^{13}C_{carb}$ (‰ PDB)	$\delta^{18}O$	$\delta^{13}C_{org}$	$\Delta^{13}C$	Mg/Ca	Sr (ppm)	Mn	Fe
A14-90	43.8	*P. anserinus*	Spar	0.01	-4.69	--	--	0.00	640	356	2711
A14-90	43.8	*P. anserinus*	Vein	-0.07	-6.56	--	--	0.00	1189	318	2026
A14-61	44	*P. anserinus*	Micrite	0.11	-4.28	--	--	0.01	450	391	3678
A14-61	44	*P. anserinus*	Spar	0.43	-4.62	--	--	0.01	337	325	548
A14-81	44	*P. anserinus*	Spar	0.23	-4.62	--	--	0.00	388	348	1700
A14-81	44	*P. anserinus*	Vein	0.20	-2.88	--	--	0.00	376	465	6992
A14-86	44	*P. anserinus*	Spar	0.01	-4.45	--	--	0.00	461	369	3778
A14-91	44	*P. anserinus*	Spar	-0.58	-4.82	--	--	0.00	530	1519	6644
A14-66	45	*P. anserinus*	Micrite	-0.26	-4.10	-26.57	26.31	0.03	880	244	1908
A14-67	46	*P. anserinus*	Micrite	0.24	-4.51	--	--	0.01	1295	164	3938
A14-68	47	*P. anserinus*	Micrite	0.29	-4.39	-30.47	30.76	0.01	1288	164	3300
A14-68	47	*P. anserinus*	Vein	0.24	-6.00	--	--	0.01	1173	156	1933
A14-69	48	*P. anserinus*	Micrite	0.33	-4.15	--	--	0.01	1309	163	2197
A14-70	49	*P. anserinus*	Micrite	0.56	-4.37	-30.84	31.40	0.03	1383	172	2459
A14-71	50	*P. anserinus*	Micrite	0.39	-4.06	--	--	0.03	1365	171	2659
A14-72	51	*P. anserinus*	Micrite	--	--	-30.59	--	--	--	--	--
A14-74	53	*P. anserinus*	Micrite	--	--	-29.14	--	--	--	--	--
A14-76	55	*P. anserinus*	Micrite	--	--	-26.64	--	--	--	--	--

*Height relative to the contact between the San Juan and Las Aguaditas Formations

Table 1.3. Summary of Darriwilian isotopic and elemental compositions from the Precordillera

		$\delta^{13}C_{carb}$ (‰ PDB)	$\delta^{18}O$	$\delta^{13}C_{org}$	Sr (ppm)	Mn	Fe
Las Chacritas River Section							
Matrix	Average	-0.39	-5.74	-28.32	530	476	2546
	St. Dev.	0.59	0.74	1.37	252	196	1898
Spar	Average	-0.11	-5.03	--	363	521	1398
	St. Dev.	0.48	0.81	--	99	156	772
Veins	Average	-0.46	-6.46	--	587	379	1609
	St. Dev.	0.60	1.14	--	278	145	752
L. variabilis	Average	-0.85	-5.50	-28.23	322	489	1770
	St. Dev.	0.51	0.11	1.50	19	278	957
Y. crassus	Average	-0.82	-5.86	-27.96	600	455	2250
	St. Dev.	0.29	0.20	1.23	191	219	1692
E. pseudoplanus	Average	0.04	-5.26	-28.08	333	537	2456
	St. Dev.	0.34	0.94	1.35	72	117	875
E. suecicus	Average	0.54	-6.71	-29.35	920	314	3152
	St. Dev.	0.43	0.44	0.61	218	138	2956
P. anserinus	Average	-0.04	-6.79	-30.16	917	503	5966
	St. Dev.	0.33	0.21	0.31	191	76	3120
Las Aguaditas Creek Section							
Matrix	Average	-0.38	-4.98	-28.17	788	642	2668
	St. Dev.	0.65	0.47	1.91	402	618	1495
Spar	Average	0.14	-4.39	--	467	549	2264
	St. Dev.	0.33	0.62	--	198	519	1688
Veins	Average	0.52	-2.88	--	1434	1512	6992
	St. Dev.	0.48	1.92	--	333	349	1711
L. variabilis	--	--	--	--	--	--	--
Y. crassus	Average	-0.44	-5.31	-27.67	708	1095	3500
	St. Dev.	0.27	0.27	2.08	248	763	1008
E. pseudoplanus	Average	-1.19	-5.16	-28.40	1179	353	1179
	St. Dev.	0.54	0.31	1.39	404	86	404
E. suecicus	--	--	--	--	--	--	--
P. anserinus	Average	0.22	-4.53	-29.04	605	356	2124
	St. Dev.	0.18	0.35	1.81	348	263	1601

Chapter 2
Sulfur cycling in the Darriwilian (Middle Ordovician) of Argentina: Implications for ocean circulation and the redox evolution of the Ordovician ocean

Abstract

Dramatic changes to the marine sulfur cycle in the Darriwilian are suggested by the sulfur isotope record from Argentina, Newfoundland, and China, derived from carbonate-associated sulfate (CAS) and pyrite (Kah et al., 2016). These changes are explained by a dual reservoir model for S-cycling in which marine waters are depicted as having two distinct, reactive marine reservoirs for sulfur. In this scenario, changes in sulfur cycling record the diminishment of ocean stratification and oxidation of deep-water, potentially associated with changes in ocean circulation and delivery of cool, oxygenated water to deeper portions of the water column. Previous S-isotope work in the Ordovician, however, has focused mainly on shallow water carbonate successions. Here, we expand our understanding of the S-isotope record of the Middle Ordovician with additional high-resolution $\delta^{34}S_{CAS}$ and $\delta^{34}S_{PY}$ values from three formations in the Argentine Precordillera—the Las Chacritas, Las Aguaditas, and Gualcamayo formations—that represent distinct, yet coeval depositional environments that span from well-mixed and oxygenated waters to waters beneath the marine chemocline. Sulfur isotope data from these formations record facies dependent $\delta^{34}S$ values that are related to the position of a persistent marine chemocline during the Middle Ordovician. These new S-isotope data are used to further constrain the behavior of marine sulfur and test the utility of a dual-reservoir model for sulfur cycling in the Early Paleozoic.

1. Introduction

Greenhouse conditions of the Early-Middle Ordovician are associated with a combination of high sea level and extensive epeiric seas (Haq and Schutter, 2008), low-latitude continental positions (Torsvik and Cocks, 2013), and elevated sea surface

temperatures (Trotter et al., 2008). Under these conditions, origination of warm saline deep-water in low-latitude evaporative seas would result in sluggish ocean circulation, and stratified ocean conditions (Railsback et al., 1990). Invigorated ocean circulation and mixing between shallow and deep-water environments associated with global cooling (Trotter et al., 2008; Quinton et al., 2015) in the earliest Middle Ordovician has been invoked to explain changes in the isotopic composition of marine sulfur recorded as carbonate associated sulfate (CAS) and pyrite from carbonates from Newfoundland and Argentina (Thompson and Kah, 2012). This includes an abrupt 15‰ shift in the isotopic composition of carbonate associated sulfate ($\delta^{34}S_{CAS}$) observed in lower Darriwilian strata (Fig. 1), which is interpreted to reflect rapid ventilation of anoxic deep water, and a protracted change in the isotopic composition of coeval sulfide ($\delta^{34}S_{PY}$), which is interpreted to reflect a decrease in the size of an anoxic deep-water sulfide reservoir (Kah et al., 2016). These isotopic signatures are furthermore inferred to reflect existence of a persistent euxinic (anoxic and sulfidic) deep-water reservoir, at least locally in the early-Middle Ordovician (Thompson and Kah, 2012; Kah et al., 2016).

Enhanced rates of ocean mixing, and disruption of Early Ordovician greenhouse stratified ocean conditions associated with global cooling in the Middle-Late Ordovician (Trotter et al., 2008) would have led to upwelling of nutrient-rich deep water and changing nutrient budgets in the shallow ocean (Saltzman, 2005). However, the transition from greenhouse to icehouse climate conditions, defined by carbon isotope values, is not identified until the Katian–Hirnantian (Ainsaar et al., 2010; Lefebvre et al., 2010; Dronov, 2013; Quinton and MacLeod, 2014; Zhou et al., 2015). Within the Darriwilian,

evidence for enhanced productivity and organic carbon burial in surface waters may be reflected as a +2‰ to +4‰ shift in the carbon isotope values of marine carbonate identified worldwide as the Middle Darriwilian carbon isotope excursion, or MDICE (Ainsaar et al., 2004; Meidla et al., 2004; Ainsaar et al., 2007; Kaljo et al., 2007; Schmitz et al., 2010; Zhang et al., 2010; Albanesi et al., 2013; Calner et al., 2014; Young et al., 2016; Henderson et al., 2018).

Enhanced mixing and increased ocean ventilation during the MDICE has also been suggested to be associated with growth in the size of the marine sulfate reservoir (up to 5 mM; cf. Thompson and Kah, 2012; Kah et al., 2016; Young et al. 2016). Here we note that the consequences of such mixing between shallow- and deep-water that drives ventilation of deep-water environments should be reflected as a stepwise change in the sulfur isotope composition of coeval sulfate and pyrite between deeper and shallower water environments. Here we evaluate the geochemical consequences of Middle Ordovician ocean ventilation in the aftermath of the large Early Darriwilian event with paired sulfur isotope data from carbonates from the Las Chacritas and Las Aguaditas formations and carbonaceous black shales of the Gualcamayo Formation to reconstruct potential vertical changes in the redox structure of the Middle Ordovician ocean.

2. Geologic background

2.1. Argentine Precordillera

The Precordillera preserves a thick succession (> 2500 m) of Cambrian to Ordovician sedimentary strata that crop out along a series of North-South trending thrust sheets in northwestern Argentina between 28˚ and 33˚ S (Fig. 2; Ramos et al., 1986;

Astini et al., 1995; Keller 1999). These strata represent the remnants of an independent microcontinent terrane that rifted from the southeast margin of Laurentia in the early Cambrian (530-539 Ma; Thomas et al., 2001) and migrated across the Iapetus Ocean before approaching Gondwanan margin in the Early-Middle Ordovician (Ramos et al., 1986; Astini et al., 1995; Thomas and Astini, 1996; Astini and Thomas, 1999; Thomas and Astini, 1999; Thomas et al., 2002). Although the paleogeographic history of the Precordillera is not well constrained, proximity to the Gondwanan margin by the Middle Ordovician is inferred from faunal changes (Harper et al., 1996; Benedetto, 2004; Benedetto et al., 2009) and widespread bentonite deposits sourced from the Famatina Arc in Dapingian and Darriwilian-aged strata (Astini et al., 1995; Huff et al., 1997; Huff et al., 1998; Pankhurst et al., 1998; Fanning et al., 2004; Thompson et al., 2012).

The Precordillera is subdivided into the eastern and western tectofacies (Fig. 2; Astini et al., 1995), which preserve a combination of intertidal, marine shelf, and distal ramp to basin deposits (Keller, 1999; Cañas, 2003). The western tectofacies consists primarily of strongly deformed and metamorphosed distal ramp and basin environments (Astini et al., 1995; Voldman et al., 2009). By contrast, the eastern tectofacies consists of minimally deformed and unmetamorphosed strata that preserve passive margin carbonate deposition and siliciclastic deposition associated with development of a foreland basin inboard of the Precordillera terrane (Astini et al., 1995). Middle Ordovician strata of the eastern tectofacies are represented by platform carbonates of the San Juan Formation, transitional carbonate-siliciclastic strata of the Las Chacritas and Las Aguaditas

formations, and dominantly siliciclastic deposits of the Las Azules and Gualcamayo formations (Fig. 2; Keller, 1999; Serra et al., 2017).

2.2. Middle Ordovician strata in the Precordillera

Darriwilian-aged strata first occur within the San Juan Formation (Albanesi and Ortega, 2016). The San Juan Formation consists of boundstones, oncolitic packstone, wackestone, nodular wackestone, and fossiliferous mudstone (Thompson and Kah, 2012), and record the transition from subtidal shelf deposition to deeper-water, storm dominated deposition (Cañas, 2003). The top of the San Juan Formation is time-transgressive, reflecting differential subsidence as the Precordillera terrane approached Gondwana (Fig. 3; Astini, 1995). In the southwest, at the Pachaco and Talacasto sections, the top of the San Juan Formation has been removed and the San Juan is overlain by Silurian strata (Talacasto-Tambolar unconformity; Thompson et al., 2012). In the northeast, the San Juan Formation is overlain by transitional carbonate-siliciclastic strata of the Darriwilian-Sandbian Las Chacritas and Las Aguaditas formations and black shale of the Darriwilian-Sandbian Los Azules and Gualcamayo formations (Keller, 1999).

The Las Chacritas and Las Aguaditas formations conformably overlie the San Juan Formation to the southwest of San Jose de Jáchal (Fig. 2). For this study, the Las Chacritas Formation was sampled along the Las Chacritas River in the northern La Trampa Range (30˚33’39.06” S, 68˚51’49.62” W), where the formation is approximately 65 m thick and is subdivided into two members: a lower member of fossiliferous mudstone, wackestone, and packstone and an upper member dominated by carbonate mudstone and spiculitic mudstone (Peralta et al., 1999; Henderson et al., 2018). Thin

partings of calcareous black shale (< 2 cm) are interbedded with carbonate strata of the Las Chacritas Formation and become progressively thicker toward the top of the section. Faunal assemblages support sedimentological interpretations suggesting deposition of the Las Chacritas Formation predominantly between normal and storm wave base (Carrera, 1997; Henderson et al., 2018), with only the uppermost strata deposited below storm wavebase.

The Las Aguaditas Formation was sampled along Las Aguaditas Creek in the Los Blanquitos Range (30˚18’16.38” S, 68˚49’13.40” W). The Las Aguaditas Formation is approximately 300 m thick (Keller et al., 1993). Darriwilian strata occur in the 43-m-thick lower member, which consists of thinly bedded carbonate mudstone and wackestone interbedded with prominent intervals of calcareous black shale that are overlain by late Ordovician (Sandbian) strata (Feltes et al., 2016). Carbonate strata of the Las Aguaditas Formation contain abundant sponge spicules and trilobite fragments and lack evidence of bioturbation suggesting deposition in relatively deep water, at or below storm wave base (Henderson et al., 2018).

More basinal facies are preserved in the Las Azules and Gualcamayo formations (Fig. 3; Astini et al., 1995). For this study, the Gualcamayo Formation was sampled along La Corridita Creek, which feeds into the Gualcamayo River, approximately 26 km to the southwest of Guandacol, La Rioja Province, Argentina (29°45'17.00" S, 68°39'22.10" W). At La Corridita Creek, the Gualcamayo Formation is approximately 275 m thick and consists of thinly bedded, carbonaceous black shale that conformably overlies the San Juan Formation (Albanesi et al., 1999). At this locality, the Gualcamayo Formation is

divided into two members, a lower member that contains interbedded carbonate and shale facies, and a middle member of carbonaceous black shale representing deep carbonate ramp to restricted basin deposits (Astini, 1994; Albanesi, 1999). The upper member of the Gualcamayo Formation at this locality has been removed by thrust faulting, which juxtaposes fine-gray sandstone of the Sandbian–Katian Trapiche Formation over the middle member of the Gualcamayo Formation (Astini, 1994; Máspero Castro et al., 2003).

2.3. Stratigraphic correlation and age constraints

Stratigraphic correlation of Middle Ordovician strata in the Precordillera is complicated by diachronous age of the uppermost San Juan Formation and by the potential of cryptic unconformities between sections (Fig. 3; Astini, 1995; Thompson and Kah, 2012; Heredia et al., 2017); however, Middle Ordovician ages are suggested by radiometric age dates from K-bentonite deposits (Huff et al., 1997; Fanning et al., 2004; Thompson et al., 2012) and by detailed biostratigraphic studies (Albanesi and Ortega, 2016). Precise radiometric ages have been determined for the San Juan Formation, which contains abundant bentonite deposits (Huff et al., 1995). High resolution U-Pb_{zircon} analyses for K-bentonites at the top of the San Juan Formation at Talacasto and Cerro La Chilca yield dates of 473 ± 0.70 Ma and 469.53 ± 0.62 Ma (Thompson et al., 2012) and are consistent with earlier analyses with ages of 470 ± 3.3 Ma to 469 ± 3.2 Ma (Fanning et al., 2004). However, because of the diachronous age of the uppermost strata of the San Juan Formation throughout the Precordillera, these Dapingian ages do not discretely define the age of the uppermost San Juan Formation. Absolute age constraints from

bentonite deposits within the Las Chacritas, Las Aguaditas, and Gualcamayo formations have not yet been determined; however, the general chronologic framework for the Precordillera has been established from conodont and graptolite biostratigraphy (Albanesi and Ortega, 2016).

Recent high-resolution conodont biostratigraphic investigations of carbonate strata from the Las Chacritas River (Serra et al., 2015) and Las Aguaditas Creek (Feltes et al., 2016) sections confirm a Darriwilian age for these units and provide a basis for stratigraphic correlation for these sections (Fig. 4). Conodonts recovered from the Las Chacritas River and Las Aguaditas Creek sections identify the presence of the *Lenodus variabilis*, *Yangtzeplacognathus crassus*, *Eoplacognathus pseudoplanus*, *Dzikodus tablepointensis*, *Eoplacognathus suecicus*, and *Pygodus anserinus* conodont zones (Albanesi et al., 2013; Serra et al., 2015; Feltes et al., 2016). In both these sections, exposed strata of the San Juan Formation contain conodonts belonging to the *L. variabilis* and *Y. crassus* zones indicating an Early Darriwilian age (stage slice Dw1 of Bergström et al., 2009). In these sections, the transition from the *L. variabilis* to *Y. crassus* zones in the San Juan Formation occurs approximately 3.5 m below the base of the Las Chacritas Formation (Serra et al., 2015) and approximately 24 m below the base of the Las Aguaditas Formation (Feltes et al., 2016). In the Precordillera, the transition between Early (Dw1) and Middle Darriwilian (Dw2) strata occurs in the *Y. crassus* Zone (Albanesi and Ortega, 2016).

Middle Darriwilian (Dw2) strata of the Las Chacritas and Las Aguaditas formations are represented by the *Y. crassus*, the *E. pseudoplanus,* and the *E. suecicus*

zones (Serra et al., 2015; Feltes et al., 2016). The *Y. crassus* Zone is approximately 40 m thick in the Las Chacritas Formation (Serra et al., 2015) and 36 m thick in the Las Aguaditas Formation (Feltes et al., 2016). The *E. pseudoplanus* Zone is identified 36 m above the base of the Las Chacritas Formation and extends to 58 m above the base of the unit (Serra et al., 2015). The *E. pseudoplanus* Zone in the Las Aguaditas Formation is 24 m thick and is characterized by the co-occurrence of *D. tablepointensis* (Feltes et al., 2016). The upper *E. pseudoplanus* Zone in the Precordillera is marked by the occurrence of *Microzarkodina hagetiana* and *M. ozarkodella* in the Las Chacritas and Las Aguaditas formations (Serra et al., 2015; Feltes et al., 2016; Serra et al., 2017). In the Las Chacritas Formation, the *E. suecicus* zone is identified by the occurrence of *Histiodella kristinae* (Serra et al., 2015). Although the *E. suecicus* Zone is not formally recognized in the Las Aguaditas Formation, *H. kristinae* was identified at the top of the lower member (Feltes et al., 2016). Conodonts of the Sandbian upper *P. anserinus* Zone are identified above the *E. suecicus* Zone in the Las Chacritas Formation and the *E. pseudoplanus/D. tablepointensis* zones in the Las Aguaditas Formation and identify a disconformity that has removed the upper *E. suecicus* and *P. serra* conodont zones (Serra et al., 2015; Feltes et al., 2016).

High-resolution biostratigraphic work has not been completed for the Gualcamayo Formation; therefore, we rely on available graptolite biostratigraphy of the La Corridita Creek Section (Máspero Castro et al., 2003) and correlation of outcrop exposures in the Guandacol-Gualcamayo River area (Astini, 1994) with the regional conodont biostratigraphy (Fig. 4; Albanesi, 1999; Ortega and Albanesi, 2000). In the La

Corridita Creek section, the transition from Dw1 to Dw2 is marked by the top of the *Undulograptus dentatus* graptolite Zone approximately 143 m above the base of the Gualcamayo Formation (Fig. 4; Máspero Castro et al., 2013). The *U. dentatus* zone is correlated to the *P. horridus* subzone of the *L. variabilis* subzone in the Precordillera (Albanesi and Barnes, 2000; Albanesi and Ortega, 2016). The transition to Middle Darriwilian strata is marked by 23-m-thick *H. lentatus* graptolite Zone (Máspero Castro et al., 2003), which correlates to the Middle Darriwilian *Y. crassus* conodont Zone (Albanesi and Barnes, 2000). The transition to Upper Darriwilian strata (Dw3) in the Gualcamayo Formation is marked by the appearance of the *Pterograptus elgans* graptolite Zone approximately 191 m above the base of the Gualcamayo Formation (Máspero Castro et al., 2003). Therefore, we infer the lower and middle members of the Gualcamayo Formation correlate with the Las Chacritas Formation and the lower member of the Las Aguaditas Formation as identified in this study (Albanesi, 1999; Albanesi et al., 2006).

3. Methods

3.1. Sample selection and preparation

Samples of the Las Chacritas, Las Aguaditas, and Gualcamayo formations collected in the field were returned to the laboratory and washed to remove surface contaminants. Fresh rock surfaces were obtained by removing weathered surfaces with a water-cooled diamond blade saw. A fraction of each carbonate sample and representative shale was slabbed and cut into mirror-image billets for thin- and thick-sections for conventional petrographic and cathodoluminescence (CL) analysis. The remaining

fraction was further cut to remove secondary carbonate veins. Fine-grained carbonate (micrite or finely crystalline microspar), which is generally considered to preserve marine geochemical and isotopic compositions, was preferentially targeted for analysis when available. Carbonaceous black shales were collected approximately 0.5 m into the outcrop in an attempt to avoid surface weathering products and were cut to remove any visually altered (oxidized) material along parting surfaces. All samples were then crushed and homogenized with a SPEX CertiPrep 800M ceramic ball mill or a SPEX CertiPrep 8530 shatterbox.

3.2. Major- and trace-element abundances

Microdrilled carbonate powders of the Las Chacritas and Las Aguaditas formations were prepared and analyzed for major- (Ca and Mg) and trace- (Sr, Mn, Fe) element concentrations with a Perkin-Elmer Optima 2100 DV inductively coupled plasma-optical emission spectrometer (ICP-OES) at the University of Tennessee (see Henderson et al., 2018 for discussion of elemental trends of carbonate phases). Major- and trace-element concentrations from the Gualcamayo Formation were determined via IE3 Aqua Regia ICP analysis by Activation Laboratories, Ltd., Ontario, Canada.

3.3. C- and O-isotope compositions

Carbon and oxygen isotope compositions of micritic to microsparitic carbonate phases from the Las Chacritas and Las Aguaditas formations were determined with a Thermo-Finnegan GasBench II and transferred into a Thermo-Finnegan DeltaPlus XL mass spectrometer at the University of Tennessee. In this manuscript, carbon and oxygen

isotope compositions—discussed in detail in Henderson et al. (2018)—are used as a framework within which to examine sulfur isotope compositions.

3.4. Sulfur extraction and isotope analysis

Sulfur isotope compositions were determined for both carbonate associated sulfate (CAS) and sedimentary pyrite. For CAS extractions of the Las Chacritas and Las Aguaditas formations, approximately 50 g of powdered rock was soaked for 12 hours in 300 ml of 5.65–6% laboratory grade sodium hypochlorite (NaOCl) solution and rinsed 4 times with 18Ω deionized water to remove soluble iron sulfides and organically bound sulfur (Burdett et al., 1989; Gill et al., 2007). Carbonate samples were acidified slowly with 3N HCl to maintain a pH > 3, to minimize potential pyrite oxidation. Acidified solutions were filtered to remove insoluble and undissolved residue and sample residues were set aside for pyrite extractions. Samples were brought to a pH of 9 with NaOH pellets to precipitate any dissolved iron oxide and filtered. Samples were then acidified to pH 3 before addition of a saturated $BaCl_2$ solution (250 mg/l) to precipitate CAS as $BaSO_4$. Samples were left at room temperature overnight (> 12 hours) to ensure complete precipitation. Barium sulfate was then filtered using 0.45 μm filters, dried at 30˚C, and weighed. Sulfate concentrations were estimated from weight measurements of $BaSO_4$ precipitate from the extractions. For pyrite sulfur, approximately 5 g of insoluble residue from CAS extractions was reacted with a mixture of ~40 ml 12N HCl and ~40 ml 1.0 M chromium chloride solution in an extraction flask purged with nitrogen gas (N_2; Canfield et al., 1986). H_2S gas evolved during the FeS_2 extraction was carried by N_2 gas through a buffer solution (0.1 M citric buffer solution at pH 4) into a 0.1 M $AgNO_3$ solution where

it precipitated as Ag_2S. The Ag_2S was then filtered, rinsed, and dried on a baked 0.22 μm quartz-fiber filter and stored for isotopic analysis.

Gualcamayo Formation samples were put through a three-step sequential sulfur extraction method after Mayer and Krouse (2004) to isolate and extract sulfur phases. Elemental sulfur (S^0) was extracted from approximately 5 g of crushed rock with dichloromethane in Sohxlet extraction thimbles, adsorbed to copper pellets, and extracted with 30 ml of 6 N HCl in a nitrogen purged extraction flask to evolve H_2S gas. The H_2S gas was passed through a citric acid buffer solution into 0.1 M $AgNO_3$ solution to precipitate Ag_2S and filtered, rinsed, and dried onto a baked 0.22 μm quartz-fiber filter and stored for isotopic analysis. Acid-volatile sulfur (monosulfide; S^-) and acid soluble sulfur (S^{6+}) were then extracted from the same sediment sample with 6 N HCl in N_2 purged extraction flasks. Evolved H_2S gas was passed through the citric acid buffer solution into 0.1 M $AgNO_3$ solution to precipitate as Ag_2S, which was filtered, rinsed, and dried onto quartz fiber filters. The contents of the reaction flask were then transferred into 50 ml centrifuge tubes and centrifuged to isolate insoluble residue. Insoluble residues were rinsed and centrifuged 3 times to ensure removal of acid soluble sulfur. The resulting solution was brought to pH of 9 with NaOH pellets to precipitate iron hydroxides. Solutions were then filtered to remove iron hydroxides, acidified to pH 3 and saturated $BaCl_2$ solution was added to precipitate $BaSO_4$. In the final extraction step, insoluble residues were transferred into extraction flasks and purged with N_2 for extraction of pyrite sulfur (S^{2-}). Approximately 20 ml of chromium chloride solution and 20 ml of 12 N HCl was reduced with zinc and added to the solution for sulfide

extractions. Evolved H_2S gas was passed through a citric buffer into a $AgNO_3$ solution to precipitate Ag_2S. The samples were then filtered onto a 0.22 μm quartz-fiber filter and stored for isotopic analysis.

Approximately 0.5 mg of $BaSO_4$ or Ag_2S was loaded into tin capsules with excess V_2O_5 for measurement sulfur isotope compositions ($\delta^{34}S$). Samples were combusted in a Costech ECS 4010 elemental analyzer and resulting SO_2 gas was transferred with a Thermo-Finnegan Conflo III interface into a Thermo-Finnegan DeltaPlus XL mass spectrometer at the University of Tennessee. Precision and calibration of data was monitored through routine analysis of internal laboratory standards and the NBS-127 ($\delta^{34}S$ = +21.12‰) and IAEA-SO-6 ($\delta^{34}S$ = −34.05‰) international standards. Analyses were reproducible to better than ± 0.2‰ based on replicates and internal laboratory standards.

4. Results

Geochemical results are presented in Figures 5, 6, and 7, and Tables 1 through 3, and summarized in Table 4. Although S-isotope compositions of both CAS and pyrite are quite heterogeneous, we recognize three stratigraphic intervals that contain distinct geochemical patterns. In the shallower water successions of the Las Chacritas River and Las Aguaditas Creek sections, these include a San Juan interval, which starts in the *L. variablis* Zone of the upper San Juan Formation and continues into the *Y. crassus* Zone; a pre-MDICE interval, which starts in the *Y. crassus* Zone; and a MDICE interval, which starts at the *E. pseudoplanus* conodont Zone and ends at the unconformity represented by the presence of the Sandbian *P. anserinus* Zone. In the deepest water deposits of the

Gualcamayo Formation, these intervals are defined by their $\Delta^{34}S_{(CAS\text{-}PY)}$ values and include the transitional facies just above the San Juan Formation, the lower part of the middle member of the Gualcamayo Formation, and the upper part of the middle member of the Gualcamayo Formation, which coincides with the start of the *U. dentatus* Zone.

4.1. Las Chacritas River Section

Sulfur isotope compositions of carbonate associated sulfate (CAS) and pyrite measured from the Las Chacritas River section range between −13.64‰ and +36.47‰ (Fig. 5; Table 1). The Las Chacritas River section is divided into three parts: A San Juan interval, a pre-MDICE interval, and a MDICE interval (Table 4). In the San Juan interval, $\delta^{34}S_{CAS}$ values range from +17.94‰ to + 33.89‰ with values averaging +26.17 ± 5.64‰ (n=7). $\delta^{34}S_{PY}$ values range from −12.33‰ to + 11.35‰ and average −2.88 ± 9.09‰ (n = 7), and $\Delta^{34}S_{(CAS\text{-}PY)}$ values range from +12.32‰ to +46.21‰ with an average value of +29.06 ± 11.61‰ (n=7). In the Pre-MDICE *Y. crassus* Zone, $\delta^{34}S_{CAS}$ values range from +14.15‰ to +36.47‰, with an average value of +24.35 ± 6.45‰ (n = 15) and $\delta^{34}S_{PY}$ values range from −13.64‰ to +5.51‰, with an average value of −3.98 ± 5.99‰ (n = 15). $\Delta^{34}S$ values in this interval range from +18.60‰ to +46.21‰ and average +28.33 ± 9.35‰ (n=15). Through the MDICE interval, $\delta^{34}S_{CAS}$ values range from +22.66‰ to +32.99‰ and average +26.10 ± 2.78‰ (n = 12), and $\delta^{34}S_{PY}$ values range from −13.17‰ to +17.40‰ with an average value of +1.82 ± 10.27‰ (n = 12). The increase in $\delta^{34}S_{PY}$ values results in a decline in $\Delta^{34}S$ values through the MDICE interval, where $\Delta^{34}S$ values range from +12.91‰ to +36.07 and average +24.43 ± 8.55‰ (n = 12).

4.2. Las Aguaditas Creek section

Sulfur isotope compositions from the Las Aguaditas Creek section range from −6.56‰ to +41.56‰ (Fig. 6; Table 2). Like the Las Chacritas River section, we divide the Las Aguaditas Creek section into three stratigraphic intervals: A San Juan, a Pre-MDICE, and an MDICE interval (Table 4). In the San Juan interval, $\delta^{34}S_{CAS}$ values range from +21.50‰ to +35.34‰ and average +26.86 ± 3.31‰ (n = 10); $\delta^{34}S_{PY}$ values range from +3.40‰ to +25.77‰ and average +13.19 ± 7.40‰ (n = 10). $\Delta^{34}S$ values in the San Juan interval range from +0.73‰ to +26.57‰ with an average value of +17.63 ± 7.78‰ (n = 10). In the pre-MDICE interval, $\delta^{34}S_{CAS}$ values are more variable, ranging from +11.02‰ to +32.43‰ and averaging +21.46 ± 8.93‰ (n = 8). $\delta^{34}S_{PY}$ values range from −6.56‰ to +16.07‰ and average +3.26 ± 8.88‰ (n = 8). $\Delta^{34}S$ in the pre-MDICE interval in the Las Aguaditas Formation range from +1.61‰ to +35.58‰ and average +16.31 ± 11.17‰ (n = 8). Through the MDICE interval of the Las Aguaditas Formation $\delta^{34}S_{CAS}$ values range from +11.88‰ to +41.56‰, with an average +26.33 ± 9.74‰ (n = 12) and $\delta^{34}S_{PY}$ values range from −6.56‰ to +16.07‰, with an average value of +10.43 ± 7.49‰ (n = 12). These values result in increasing $\Delta^{34}S$ values from around −2.91‰ to values near +42.90‰ through the MDICE interval of the Las Aguaditas Formation (average Δ34 = +15.48 ± 13.76‰; n = 12).

4.3. Gualcamayo Formation

$\delta^{34}S$ values of the Gualcamayo Formation sampled at La Corridita Creek (Fig. 7; Table 3) range from −21.52‰ to +15.62‰ (excluding a single value of +34.56‰, just below the unconformity identified at the top of the section). Like the shallower water

formations discussed above, the $\delta^{34}S$ data from the Gualcamayo Formation is divided into three intervals based on their average $\Delta^{34}S$ compositions (Fig. 7; Table 4). Here the transitional facies of the lower member of the Gualcamayo Formation has $\delta^{34}S_{CAS}$ values of −1.80‰ and −2.76‰, $\delta^{34}S_{PY}$ values of −1.88‰ and −2.33‰, and $\Delta^{34}S$ values of −4.64‰ and +0.53‰. In the lower part of the middle member of the Gualcamayo Formation $\delta^{34}S_{CAS}$ values range from −4.90‰ to +5.79‰, with an average of +0.83 ± 3.87‰ (n = 9) and $\delta^{34}S_{PY}$ values range from −21.52‰ to +1.88‰, with an average value of −11.83 ± 5.56‰ (n=9). $\Delta^{34}S$ values in the lower strata of the middle member range from +9.54‰ to +21.74‰, with an average of +12.67 ± 3.97‰ (n = 9). $\delta^{34}S$ values of CAS and pyrite are similar through the rest of the middle member of the Gualcamayo Formation, with $\delta^{34}S_{CAS}$ ranging from −3.48‰ to +13.73‰ (average +4.87 ±3.87‰; n = 29) and $\delta^{34}S_{PY}$ ranging from −2.57‰ and +15.62‰ (average +7.71 ± 4.22‰; n = 31). $\Delta^{34}S$ compositions of the upper middle member of the Gualcamayo Formation range from −13.9‰ to +9.60‰, with an average of −3.29 ± 5.56‰ (n = 31).

5. Interpretation and discussion

5.1. Assessment of primary geochemical signatures

The reactive nature of carbonate rocks results in distinct geochemical and textural changes that can be used to assess the extent to which geochemical and isotopic signatures may potentially be altered (Banner and Hanson, 1990; Kaufman et al., 1991). Cross-plots of geochemical data allow for assessment of systematic variation and are often used to evaluate the degree of water-rock interaction and diagenetic alteration of carbonate minerals (Banner and Hanson, 1990). Diagenetic alteration of marine

carbonates by meteoric fluids frequently results in decreased strontium concentrations (Brand and Veizer, 1980) and decreases in both $\delta^{13}C$ (Derry, 2010) and $\delta^{18}O$ (Bowen and Wilkinson, 2002) values. Increases in Mn and Fe concentrations of marine carbonates can also result from interaction with reducing fluids during burial diagenesis (Veizer, 1983). Although diagenetic effects on carbonate geochemistry are well understood (Bartley et al., 2007; Swart, 2015), fewer studies have investigated the potential for post-depositional alteration of $\delta^{34}S$ values. Significant reduction in CAS concentrations have been documented during meteoric diagenesis; however, $\delta^{34}S$ values appear rock-buffered between primary and diagenetic carbonate phases, and therefore retain their primary isotopic compositions (Gill et al., 2008). Pyrite oxidation during sample processing has also been shown to result in lower $\delta^{34}S_{CAS}$ values if pyrite oxidation occurs during the extraction process (Marenco et al., 2008).

Carbonate rocks of the Las Chacritas and Las Aguaditas formations are generally micritic to microspartitic, and show little petrographic evidence for recrystallization of primary depositional phases (cf. Henderson et al., 2018). Late state diagenetic features, such as vein and void filling cements, have distinct boundaries in terms of both their petrography and geochemical composition, which suggests minimal interaction between primary and later diagenetic phases (Henderson et al., 2018). There are also no clear relationships between Sr, Mn, or Fe concentrations of petrographically well-preserved carbonate phases and later diagenetic calcite in the Las Chacritas and Las Aguaditas Formations (Henderson et al., 2018); elevated concentrations of Fe and Mn observed in the Las Chacritas and Las Aguaditas formations are attributed to precipitation or early

diagenetic stabilization of carbonate in anoxic marine fluids or pore fluids (Thompson and Kah, 2012; Gilleaudeau and Kah, 2013; Henderson et al., 2018) rather than burial diagenesis (Kaufman et al., 1991). There are also no clear patterns observed between $\delta^{13}C$ and $\delta^{18}O$ values of primary depositional phases and late diagenetic phases (Henderson et al., 2018), which is consistent with minimal isotopic exchange between carbonate minerals and later diagenetic fluids (Banner and Hanson, 1990; Marshall, 1992). Combined, these data suggest that primary depositional phases in the Las Chacritas and Las Aguaditas formations have undergone minimal post-depositional exchange with diagenetic fluids.

Alteration of carbonate phases and pyrite oxidation during diagenesis and weathering can significantly affect preserved geochemical and isotopic signatures. The lack of any covariant trends between CAS concentrations and $\delta^{18}O_{carb}$ values (Fig. 8A; R^2 values < 0.06) and between $\delta^{34}S_{CAS}$ values and $\delta^{18}O_{carb}$ values (Fig. 8B; R^2 values < 0.07) for the Las Chacritas and Las Aguaditas formations is consistent with petrographic and geochemical evidence for little interaction with diagenetic fluids and the likelihood for preservation of marine $\delta^{34}S_{CAS}$ values (Gill et al., 2008). There are also no significant correlations observed between $\delta^{34}S_{CAS}$ values and S_{PY} concentrations (Fig. 8C; $R^2 < 0.02$) or between $\delta^{34}S_{CAS}$ values and $\delta^{34}S_{PY}$ values (Fig. 8D; $R^2 < 0.24$) for the Las Chacritas, Las Aguaditas, or Gualcamayo formations, suggesting no obvious influence of contaminant CAS resulting from pyrite oxidation during the extraction process (cf. Marenco et al., 2008).

5.2. Sulfur isotope trends in the Precordillera

Previous sulfur isotope work on Ordovician carbonate strata from the Precordillera of Argentina and elsewhere suggest a dramatic change in the sulfur isotope composition of both CAS and pyrite beginning in the early Darriwilian (Fig. 1; Thompson and Kah, 2012). These changes in isotopic composition have been interpreted to reflect a deep-ocean ventilation event that continued through at least the Middle Darriwilian (Dw2; Kah et al., 2016; Young et al., 2016), associated with more vigorous ocean circulation and the potential reorganization of ocean circulation patterns driven by cooler sea-surface temperatures (Trotter et al., 2008). The coeval isotopic compositions of the Gualcamayo, Las Aguaditas, and Las Chacritas formations in this study provide further constraints on this model by providing a detailed look at the sulfur isotope composition of paired carbonate associated sulfate and pyrite within distinct shallow- to deep-water environments.

5.2.1. $\delta^{34}S_{CAS}$ trends

Comparison of Middle Ordovician strata in the Argentine Precordillera show substantial heterogeneity in sulfur isotope compositions of sulfate among facies. Such heterogeneity between coeval sections is consistent with previous S-isotope work from the Early-Middle Ordovician (Thompson and Kah, 2012) that suggests a combination of a small marine sulfate reservoirs and the regional effects of episodic, small scale exchange between distinct oxidized and reduced sulfur reservoirs.

Middle Ordovician strata from Newfoundland also record a dramatic drop in the S-isotopic composition of marine sulfate from ~30‰ to ~15‰, which is interpreted as a major ventilation event of anoxic deep-water that delivered isotopically light sulfur to the

surface oceans in the Early Darriwilian (Dw1; Thompson and Kah, 2012; Kah et al., 2016). In the Precordillera, Early Darriwilian (Dw1) strata are identified in the San Juan Formation (*L. variabilis* and lower *Y. crassus* conodont Zones; Albanesi and Ortega, 2016) at the Las Chacritas River and Las Aguaditas Creek sections (Serra et al., 2015; Feltes et al., 2016), which were deposited between fairweather and storm wave-base. In this study, these deposits represent our shallowest water facies, and preserve $\delta^{34}S_{CAS}$ values of around +25‰. $\delta^{34}S_{CAS}$ values around +25‰ for these early Darriwilian (Dw1) strata are consistent with previous values for the isotopic composition of marine SO_4^{2-} from low-resolution chemostratigraphic work in these sections (~ +20‰; Kah et al., 2016) and from coeval shallow-water carbonate strata from Newfoundland, Canada (~20‰; Thompson and Kah, 2012; Kah et al., 2016), Maryland, USA (~ +30‰; Young et al., 2016) and Oklahoma, USA (~ +30‰; Young et al., 2016). Additional variability in $\delta^{34}S_{CAS}$ values of the San Juan Formation in the present study may result from higher resolution stratigraphic sampling (~3 m) that more effectively captures the heterogeneity of the S-isotope record. Alternatively, the grainier texture of the packstone-wackestone assemblage of the San Juan Formation could result in mixing of skeletal and micritic components, which have been shown to record variable $\delta^{34}S_{CAS}$ values (Present et al., 2015). However, consistency between $\delta^{34}S_{CAS}$ values from shallow-water carbonates from the Precordillera of Argentina and across Laurentia suggests an isotopic composition for seawater sulfate in well-mixed surface waters in the Darriwilian of around +25‰.

In the overlying Las Chacritas Formation, which represents middle to deep-shelf facies deposited above storm wave-base, $\delta^{34}S_{CAS}$ values are similar to those of the lower Darriwilian deposits in the San Juan Formation (Fig. 5). $\delta^{34}S_{CAS}$ compositions in the Pre-MDICE interval of the Las Chacritas Formation (Dw1 to Dw2) are slightly lighter (~ +20‰) than in the underlying San Juan Formation (~ +25‰), which may potentially be associated with a deepening of facies at the transition from packstone/wackestone in the San Juan Formation to the wackestone/mudstone assemblage of the Las Chacritas Formation and a greater degree of exchange with an underlying reduced sulfur reservoir.

Finally, in the Las Chacritas Formation, the +2‰ shift in $\delta^{13}C$ values identified as the MDICE corresponds to the *E. pseudoplanus*/*E. suecicus* Zones (Dw2; Albanesi et al., 2013; Henderson et al. 2018). During this period of enhanced organic carbon production and burial, $\delta^{34}S_{CAS}$ values are less variable and remain around +25‰, which matches the isotopic composition of seawater sulfate for the Middle Darriwilian observed globally (Thompson and Kah, 2012; Kah et al., 2016; Young et al., 2016). Reduction of variability recorded in the Las Chacritas Formation may reflect the predominance of shallower-water facies at this time, which may have experienced less influence from a more distal reduced sulfur reservoir.

In deeper-water deposits of the Las Aguaditas Formation, $\delta^{34}S_{CAS}$ compositions are generally around 10‰ lighter than $\delta^{34}S_{CAS}$ from the underlying strata of the San Juan Formation (Fig. 6). The decline in $\delta^{34}S_{CAS}$ values is consistent with the decline in $\delta^{34}S_{CAS}$ observed with the transition from the San Juan to the Las Chacritas, and interpreted to reflect proximity of this facies to the marine chemocline (cf. Henderson et al., 2018). In

this scenario, both the decline in overall isotopic composition and the increased variability in $\delta^{34}S_{CAS}$ values would reflect fluctuations in the position of the chemocline that would result in delivery of isotopically light sulfur across the chemocline. In the Las Aguaditas Formation, the transition to the *E. pseudoplanus/D. tablepointensis* Zone is associated with a deepening of facies and a negative excursion in $\delta^{13}C$ values. These strata are equivalent to the *E. pseudoplanus* Zone of the Las Chacritas Formation, where the positive expression of the MDICE is identified. Henderson et al., (2018) demonstrate that this shift to isotopically lighter $\delta^{13}C$ values are most likely associated with carbonate precipitation, or early diagenetic stabilization, below the chemocline, as identified by a sharp change in $\delta^{13}C_{org}$ values. Near the chemocline, SO_4^{2-} incorporated into carbonate minerals during early-diagenetic stabilization in seawater derived pore fluids is expected to be enriched in ^{34}S during microbial sulfate reduction (MSR) under low sulfate conditions (cf. Gomes and Hurtgen, 2013, 2015). Such microbial derived enrichments may explain the some of the extreme variability observed for the Pre-MDICE and MDICE intervals in the Las Aguaditas Formation. Additionally, increased mixing between shallow and deep-water would drive fluctuations in the position of the chemocline would deliver isotopically light SO_4^{2-} across the chemocline from beneath the chemocline.

The deepest water facies in this study is represented by carbonaceous black shale of the Gualcamayo Formation. $\delta^{34}S_{CAS}$ values from the Gualcamayo Formation exhibit relatively little isotopic change throughout the section (Fig. 7), which is consistent with continuous deposition below the chemocline. Below the chemocline, $\delta^{34}S_{CAS}$

compositions around 0‰ may reflect the oxidative flux of SO_4^{2-} derived from anoxic deep-waters prevalent in the Early-Middle Ordovician stratified oceans (Thompson and Kah, 2012; Saltzman et al., 2015; Kah et al., 2016; Young et al., 2016; Edwards et al., 2018; Henderson et al., 2018). Oxidation of a deep-water sulfide reservoir (see Thompson and Kah, 2012; Kah et al., 2016) with depleted ^{34}S values and authigenic carbonate formation would result in the low $\delta^{34}S_{CAS}$ values of the deeper water facies in the Precordillera.

5.2.2. $\delta^{34}S_{PY}$ trends

Like $\delta^{34}S_{CAS}$ trends in the Precordillera, the $\delta^{34}S_{PY}$ values also show heterogeneity between both individual samples and between sections. In the shallowest water facies of the San Juan Formation, $\delta^{34}S_{PY}$ values are extremely variable at both the Las Chacritas River and Las Aguaditas Creek sections (Table 4). At the Las Chacritas River locality $\delta^{34}S_{PY}$ values fall between around −12‰ and +11‰. These compositions are lighter than those observed in the San Juan Formation at Las Aguaditas Creek, where $\delta^{34}S_{PY}$ values range from +3‰ to +26‰. In this shallow-water environment with evidence for mixing with oxygenated surface waters, elevated $\delta^{34}S_{PY}$ values suggest pyrite formation in sedimentary pore fluids, where SO_4^{2-} limitation results in elevated $\delta^{34}S_{PY}$ values as the local SO_4^{2-} reservoir (pore-fluid) available for microbial sulfate reduction (MSR) is utilized (Gomes and Hurtgen, 2013, 2015). Elevated $\delta^{34}S_{PY}$ values in the San Juan interval in the Las Aguaditas Creek section suggests more utilization of sulfate in pore fluids during MSR than in the San Juan interval of Las Chacritas River section. During MSR, $^{32}SO_4^{2-}$ is preferentially utilized as an electron donor and as the size of the local

SO_4^{2-} reservoir gets smaller sulfate reducing microbes will utilize a larger proportion available sulfate resulting in the formation of H_2S with heavy $\delta^{34}S$ compositions (Gomes and Hurtgen, 2015).

The transition between the San Juan and Las Chacritas Formation is associated with a slight decline in $\delta^{34}S_{PY}$ values (Fig. 5). A similar shift to lower $\delta^{34}S_{PY}$ values is observed with the transition to the Las Aguaditas Formation (Fig. 6). In both cases, the shift to lower $\delta^{34}S_{PY}$ values is associated with a deepening of facies and potential decrease in mixing with oxygenated surface water or potential increase in exchange with a deep-water reduced sulfur reservoir. Here, heterogeneity in $\delta^{34}S_{PY}$ compositions observed in the Pre-MDICE interval of both the Las Chacritas and Las Aguaditas formations would reflect a larger influence of an isotopically light deep-water sulfide reservoir and mixing across near the chemocline. An increase in $\delta^{34}S_{PY}$ values from values around −13‰ to values near +15‰ is observed in through the MDICE interval of the Las Chacritas Formation (Fig. 5). A similar shift is observed through the MDICE interval of the deeper water the Las Aguaditas Formation; however, this shift is more abrupt with values increasing from around +8‰ to >15‰. We interpret this shift to reflect an increase in SO_4^{2-} reduction under reduced oxygen conditions, either in the water column or in pore-fluids below the chemocline. Below the chemocline increased rates of MSR would utilize a greater proportion of available sulfate resulting in elevated $\delta^{34}S_{PY}$ compositions (Gomes and Hurtgen, 2013). Such a scenario is consistent with C-isotope evidence for migration of the Las Aguaditas below the below the chemocline at the onset of the MDICE (Henderson et al., 2018). The different behavior of the change to

heavier $\delta^{34}S_{PY}$ compositions between these facies suggests differences in MSR rates and SO_4^{2-} above and below the chemocline. Sulfate limitation in sedimentary pore fluids generally results in heavier and isotopically variable sedimentary pyrite like that observed for the Las Aguaditas and Las Chacritas formations (Lyons et al., 2009). When MSR is not limited by sulfate availability, fractionation reflects progressive depletion of sulfate in pore waters (Habicht et al., 2002) and enrichment in coeval $\delta^{34}S_{PY}$ values (Gomes and Hurtgen, 2015).

$\delta^{34}S_{PY}$ values around −12‰ characterize the lower member of the Gualcamayo Formation (Fig. 7). At the start of the *U. dentatus* Zone (Dw1), values abruptly increase to around +7‰, where they remain through the rest of the Darriwilian in the Gualcamayo Formation at La Corridita Creek. The abrupt transition in $\delta^{34}S_{PY}$ values in the deep-water Gualcamayo Formation coincides with the abrupt change in $\delta^{34}S_{CAS}$ compositions identified in Early Darriwilian (Dw1) shallower water deposits the Early Darriwilian of Newfoundland (Fig. 1; Kah et al., 2016). Such a shift in $\delta^{34}S_{PY}$ compositions suggests a dramatic reduction in the size of a deep-water sulfide reservoir, but persistent deep-water anoxia through the Darriwilian.

5.2.3. $\Delta^{34}S$ trends

Variability in the $\Delta^{34}S$ records ($\Delta^{34}S = \delta^{34}S_{CAS} - \delta^{34}S_{PY}$) of the San Juan, Las Chacritas, Las Aguaditas, and Gualcamayo formations reflects variability in the parent SO_4^{2-} reservoir, as seen in the $\Delta^{34}S$ trends between these formations. The greatest variability in $\Delta^{34}S$ is observed in the Las Aguaditas Formation, which was deposited at or near the position of the chemocline in the Precordillera. Less variability is observed in

$\Delta^{34}S$ values of the shallow water deposits of the San Juan and Las Chacritas formations and in the deepest water deposits of the Gualcamayo Formation, which were deposited below and above the marine chemocline, respectively. Here, stasis in $\Delta^{34}S$ values in the Gualcamayo formation suggests formation of sedimentary sulfide minerals within the water column. Increased volatility in the $\Delta^{34}S$ record of the Las Aguaditas Formation, which was deposited at or near the position of the chemocline in the Precordillera, suggests local changes in the redox state during sediment deposition and pyrite formation, potentially in sedimentary pore-fluids.

5.3. Controls on sulfur isotope compositions

Under the dual-reservoir model for S-cycling (Fig. 9), a decline in the size of the HS^- reservoir, either via either microbial or chemical oxidation to sulfate, or other sulfur intermediates, would result in isotopically light sulfide being delivered to the sulfate reservoir and a negative shift in the isotopic composition of marine sulfate. Dramatic change is observed in the isotopic composition of marine sulfate in the Early Darriwilian of Newfoundland (Fig. 1; Kah et al., 2016). The rapid shift of $\delta^{34}S_{CAS}$ values from +30‰ to values around +15‰ is interpreted as rapid ventilation of the deep-water H_2S reservoir either through chemical or biological oxidation and reflects the rapid release of isotopically light SO_4^{2+} to the shallow ocean (Thompson and Kah, 2012; Kah et al., 2016). In this case, the size of the sulfate and sulfide reservoirs and the flux of sulfur between reservoirs controls the isotopic composition of sulfur. If the deep-water sulfide reservoir is much larger than the shallow-water sulfate reservoir, oxidation of H_2S and delivery of isotopically light sulfur to the sulfate reservoir would shift $\delta^{34}S_{CAS}$ to lighter

sulfur isotope compositions. However, if the size of the sulfate reservoir is much larger than that of the sulfide reservoir, oxidation of H_2S and delivery to the sulfate reservoir would result in negligible change to $\delta^{34}S_{CAS}$ values. Fluxes between reservoirs greater than the residence time of the smaller reservoir carry dramatically effects on the isotopic composition of the smaller reservoir (Kah et al., 2016). Smaller fluxes will have a protracted response, rather than immediate changes on the isotopic composition of the larger reservoir (Kah et al., 2016). The isotopic composition of sulfate is affected by pyrite burial when the fluxes between these two reservoirs is in equilibrium or with enhanced oxygenation, where H_2S and sulfur intermediates are rapidly reoxidized to SO_4^{2-} (Jørgensen et al., 1990; Elsgaard and Jørgensen, 1992).

5.4. Effect of the marine chemocline

The isotope compositions observed for the Las Chacritas, Las Aguaditas, and Gualcamayo formations represent samples of different water depths in the Precordillera. If we consider the isotopic composition of CAS from the Las Chacritas Formation ($\delta^{34}S_{CAS}$ ~ +25‰) to represent that of the sulfate reservoir and the isotopic composition of pyrite in the Gualcamayo Formation to represent that of the sulfide reservoir ($\delta^{34}S_{PY}$ ~ –10‰), then an approximate value for ε_{SR} (the isotopic difference between SO_4^{2-} and H_2S) can be established (~ 35‰). If pyrite formed just below the oxic-euxinic interface, then $\Delta^{34}S$ values will be similar to the fractionation between SO_4^{2+} and HS^- (ε_{SR}). This behavior results from the fraction of the sulfate reservoir that is consumed by MSR at the oxic-euxinic interface is low and neither the SO_4^{2-} or H_2S reservoirs have evolved to higher isotopic values (cf. Gomes and Hurtgen, 2015). $\Delta^{34}S$ values around 35‰ are

observed in the Pre-MDICE and MDICE intervals of the Las Chacritas Formation and in the Pre-MDICE interval Las Aguaditas Formation consistent with S-cycling near the oxic-anoxic interface. In shallow water environments, above the chemocline, variability in $\delta^{34}S_{CAS}$ values suggests small scale changes and sea-level and influx of isotopically depleted SO_4^{2-} from H_2S oxidation (Thompson and Kah, 2012). With a small SO_4^{2-} reservoir, ~2-5 mM for the Middle Ordovician (Young et al., 2016), slight variations in the extent of MSR (locally) or sulfide oxidation (from the regional H_2S reservoir) can drive large changes in $\delta^{34}S_{CAS}$ values. Above the oxycline in the Precordillera (Fig. 10), $\delta^{34}S_{CAS}$ values become heavier when derived from oxidation of local pore fluid H_2S, which is entirely decoupled from the marine H_2S reservoir. Under an oxygenated water column, pyrite burial at the sediment-water interface, in sedimentary pore-fluids, can result in higher $\delta^{34}S_{PY}$ values (Gomes and Hurtgen, 2015), where $\delta^{34}S_{PY}$ values are not directly sampling the HS^- reservoir but rather HS^- in sedimentary pore fluids, which is dependent on the local availability of SO_4^{2-} for MSR.

Below the chemocline $\delta^{34}S_{CAS}$ changes at a different scale because of cycling at the interface between the oxidized and reduced sulfur reservoirs rather than in sedimentary pore fluids (Fig. 10). Biological oxidation beneath the chemocline, would result in the formation of isotopically light SO_4^{2-} beneath the chemocline that can be incorporated into "authigenic" carbonate minerals in these deep-water carbonaceous shales or as micritic carbonate in the water column beneath the oxic-anoxic interface. In this case, rapid MSR and oxidation at the interface between the oxidized and reduced sulfur reservoirs drives decoupling of the reservoirs and the greatest variability is

observed at the interface nearest to the chemocline, recorded in the Las Aguaditas Formation. In the anoxic portion of the water column, oxidation of HS^- does affect the isotopic composition of residual SO_4^{2+} in the anoxic zone and CAS incorporated into carbonate minerals below the chemocline and $\delta^{34}S_{CAS}$ values reflect the isotopic composition of residual sulfate at the site of carbonate formation (Gomes and Hurtgen, 2013, 2015).

6. Conclusions

Darriwilian strata of the San Juan, Las Chacritas, Las Aguaditas, and Gualcamayo formations in the Precordillera of Argentina preserve variable $\delta^{34}S$ values that are dependent on water depth. The observed S-isotope compositions are consistent with a dual reservoir model for S-cycling (Kah et al., 2016), where $\delta^{34}S_{CAS}$ values around +25‰ reflect the isotopic composition of a shallow-water sulfate reservoir and whereas $\delta^{34}S_{PY}$ values of around −12‰ reflect the isotopic composition of a deep-water sulfide reservoir. Under this model, $\delta^{34}S_{CAS}$ variability in well-mixed surface waters reflects the influence of isotopically light sulfate delivered from mixing across the chemocline and $\delta^{34}S_{PY}$ variability results from sulfate reduction in sedimentary pore fluids. The magnitude of isotopic change observed between formations is consistent with transient oxidation of a deep-water sulfide reservoir, where the greatest extent of oxidation of reduced sulfur occurs closest to the position of the marine chemocline. Beneath the chemocline $\delta^{34}S_{CAS}$ is decoupled from the shallow water reservoir and reflects changes in the rates of MSR and sulfide oxidation. Increasing $\delta^{34}S_{PY}$ values beneath the chemocline reflect

progressive decreases in the size of the deep-water H_2S reservoir associated with cooler temperatures and ventilation of anoxic deep-water through the Darriwilian.

Acknowledgements

Funding for this projected was provided by the American Chemical Society Petroleum Research Fund (54354-ND2 to Kah), along with student grants from Sigma Xi, the Geological Society of America, and SEPM (to Henderson). We thank R. Bales (University of Tennessee) for assistance with fieldwork and A. Faiia (University of Tennessee) for assistance with isotopic analyses.

References

Ainsaar, L., Kaljo, D., Martma, T., Meidla, T., Männik, P., Nõlvak, J., and Tinn, O., 2010, Middle and Upper Ordovician carbon isotope chemostratigraphy in Baltoscandia: A correlation standard and clues to environmental history: Palaeogeography, Palaeoclimatology, Palaeoecology, v. 294, p. 189-201. http://dx.doi.org/10.1016/j.palaeo.2010.01.003

Ainsaar, L., Meidla, T., and Tinn, O., Middle and Upper Ordovician stable isotope stratigraphy across the facies belts in the East Baltic, *in* Proceedings 8th Meeting on the Working Group on the Ordovician Geology of Baltoscandia, Tallinn and Tartu, Estonia, 2004, Tartu University Press, p. 11-12.

Ainsaar, L., Meidla, T., Tinn, O., Martma, T., and Dronov, A., 2007, Darriwilian (Middle Ordovician) carbon isotope stratigraphy in Baltoscandia: Acta Paleontologica Sinica, v. 46, p. 1-8.

Albanesi, G. L., and Barnes, C. R., 2000, Subspeciation within a Punctuated Equilibrium Evolutionary Event: Phylogenetic History of the Lower-Middle Ordovician *Paroistodus originalis-P. horridus* Complex (Conodonta): Journal of Paleontology, v. 74, p. 492-502. https://doi.org/10.1666/0022-3360(2000)074%3C0492:SWAPEE%3E2.0.CO;2

Albanesi, G. L., Bergström, S. M., Schmitz, B., Serra, F., Feltes, N. A., Voldman, G. G., and Ortega, G., 2013, Darriwilian (Middle Ordovician) $\delta^{13}C_{carb}$ chemostratigraphy in the Precordillera of Argentina: Documentation of the middle Darriwilian Isotope Carbon Excursion (MDICE) and its use for intercontinental correlation: Palaeogeography, Palaeoclimatology, Palaeoecology, v. 389, p. 48-63. http://dx.doi.org/10.1016/j.palaeo.2013.02.028

Albanesi, G. L., and Ortega, G., 2016, Conodont and Graptolite Biostratigraphy of the Ordovician System of Argentina, *in* Michael, M., ed., Stratigraphy & Timescales, Volume 1, Academic Press, p. 61-121. http://dx.doi.org/10.1016/bs.sats.2016.10.002

Albanesi, G. L., Ortega, G., Barnes, C. R., and Hunicken, M. A., 1999, Conodont-graptolite biostratigraphy of the Gualcamayo Formation (Middle Ordovician) in the Gualcamayo-Guandacol rivers area, Argentina Precordillera: Acta Universitatis Carolinae - Geologica, v. 43.

Albanesi, G. L., Ortega, G., Barnes, C.R., and Hunicken, M.A. , 1999, Conodont-graptolite biostratigrapohy of the Gualcamayo Formation (Middle Ordovician) in the Gualcamayo-Guandacol rivers area, Argentina Precordillera: Acta Universitatis Carolinae - Geologica, v. 43, p. 45-48.

Astini, R. A., 1994, Analisis sequencial y paleoambientes de las pelitas negras (aloformaction Gualcamayo) que suprayacen a las sucesiones carbonatica eo-Ordovicicas en la Precordillera Argentina: Revista de la Asociacion Geologica Argentina, v. 49, p. 71-84.

Astini, R. A., 1995, Geologic meaning of Arenig-Llanvirn diachronous black shales (Gualcamayo Alloformation) in the Argentine Precordillera, tectonic or eustatic?: SEPM Fieldtrip Guidebook, v. 77, p. 217-220.

Astini, R. A., Benedetto, J. L., and Vaccari, N. E., 1995, The early Paleozoic evolution of the Argentine Precordillera as a Laurentian rifted, drifted, and collided terrane: A geodynamic model: Geological Society of America Bulletin, v. 107, p. 253-273. https://doi.org/10.1130/0016-7606(1995)107%3C0253:TEPEOT%3E2.3.CO;2

Astini, R. A., and Thomas, W. A., 1999, Origin and evolution of the Precordillera terrane of western Argentina; a drifted Laurentian orphan: Special Paper - Geological Society of America, v. 336, p. 1-20. https://dx.doi.org/10.1130/0-8137-2336-1.1

Banner, J. L., and Hanson, G. N., 1990, Calculation of simultaneous isotopic and trace-element variations during water-rock interaction with applications to carbonate diagenesis: Geochimica et Cosmochimica Acta, v. 54, p. 3123-3137. http://dx.doi.org/10.1016/0016-7037(90)90128-8

Bartley, J. K., Kah, L. C., McWilliams, J. L., and Stagner, A. F., 2007, Carbon isotope chemostratigraphy of the Middle Riphean type section (Avzyan Formation, Southern Urals, Russia): Signal recovery in a fold-and-thrust belt: Chemical Geology, v. 237, p. 211-232. http://dx.doi.org/10.1016/j.chemgeo.2006.06.018

Benedetto, J. L., 2004, The allochthony of the Argentine Precordillera ten years later (1993-2003): A new paleobiogeographic test of the microcontinental model: Gondwana Research, v. 7, p. 1027-1039. http://dx.doi.org/10.1016/s1342-937x(05)71082-0

Benedetto, J. L., Vaccari, N. E., Waisfeld, B. G., Sánchez, T. M., and Foglia, R. D., 2009, Cambrian and Ordovician biogeography of the South American margin of Gondwana and accreted terranes: Early Palaeozoic Peri-Gondwana Terranes: New Insights from Tectonics and Biogeography, v. 325, p. 201-232. http://dx.doi.org/10.1144/sp325.11

Bergström, S. M., Chen, X. U., Gutiérrez-Marco, J. C., and Dronov, A., 2009, The new chronostratigraphic classification of the Ordovician System and its relations to major regional series and stages and to $\delta^{13}C$ chemostratigraphy: Lethaia, v. 42, p. 97-107. http://dx.doi.org/10.1111/j.1502-3931.2008.00136.x

Bowen, G. J., and Wilkinson, B., 2002, Spatial distribution of $\delta^{18}O$ in meteoric precipitation: Geology, v. 30, p. 315-318. http://dx.doi.org/10.1130/0091-7613(2002)030<0315:SDOOIM>2.0.CO;2

Brand, U., and Veizer, J., 1980, Chemical diagenesis of a multicomponent carbonate system; 1, Trace elements: Journal of Sedimentary Research, v. 50, p. 1219-1236. http://dx.doi.org/10.1306/212F7BB7-2B24-11D7-8648000102C1865D

Burdett, J. W., Arthur, M. A., and Richardson, M., 1989, A Neogene seawater sulfur isotope age curve from calcareous pelagic microfossils: Earth and Planetary

Science Letters, v. 94, p. 189-198. http://dx.doi.org/10.1016/0012-821X(89)90138-6

Calner, M., Lehnert, O., Wu, R., Dahlqvist, P., and Joachimski, M. M., 2014, $\delta^{13}C$ chemostratigraphy in the Lower–Middle Ordovician succession of Öland (Sweden) and the global significance of the MDICE: GFF, v. 136, p. 48-54. http://dx.doi.org/10.1080/11035897.2014.901409

Cañas, F. L., 2003, Selected sections of Lower to Middle Ordovician carbonate sedimentation of the Argentine Precordillera: The La Silla and San Juan formations at Cerros La Silla and Niquivil: INSUEGO, Miscelanea, v. 8.

Canfield, D. E., Raiswell, R., Westrich, J. T., Reaves, C. M., and Berner, R. A., 1986, The use of chromium reduction in the analysis of reduced inorganic sulfur in sediments and shales: Chemical Geology, v. 54, p. 149-155. http://dx.doi.org/10.1016/0009-2541(86)90078-1

Carrera, M. G., 1997, Análisis paleoecológico de la fauna de poríferos del Llanvirniano tardío de la Precordillera Argentina: Ameghiniana, v. 34, p. 309-316.

Derry, L. A., 2010, A burial diagenesis origin for the Ediacaran Shuram–Wonoka carbon isotope anomaly: Earth and Planetary Science Letters, v. 294, p. 152-162. http://dx.doi.org/10.1016/j.epsl.2010.03.022

Dronov, A., 2013, Late Ordovician cooling event: Evidence from the Siberian Craton: Palaeogeography Palaeoclimatology Palaeoecology, v. 389, p. 87-95. 10.1016/j.palaeo.2013.05.032

Edwards, C. T., Fike, D. A., Saltzman, M. R., Lu, W., and Lu, Z., 2018, Evidence for local and global redox conditions at an Early Ordovician (Tremadocian) mass extinction: Earth and Planetary Science Letters, v. 481, p. 125-135. https://doi.org/10.1016/j.epsl.2017.10.002

Elsgaard, L., and Jørgensen, B. B., 1992, Anoxie transformations of radiolabeled hydrogen sulfide in marine and freshwater sediments: Geochimica et Cosmochimica Acta, v. 56, p. 2425-2435. https://doi.org/10.1016/0016-7037(92)90199-S

Fanning, C. M., Pankhurst, R. J., Rapela, C. W., Baldo, E. G., Casquet, C., and Galindo, C., 2004, K-bentonites in the Argentine Precordillera contemporaneous with rhyolite volcanism in the Famatinian Arc: Journal of the Geological Society, v. 161, p. 747-756. http://dx.doi.org/10.1144/0016-764903-130

Feltes, N., Albanesi, G. L., and Bergstrom, S. M., 2016, Conodont biostratigraphy and global correlation of the middle Darriwilian-lower Sandbian (Ordovician) Las Aguaditas Formation, Precordillera of San Juan, Argentina: Andean Geology, v. 43, p. 60-85. http://dx.doi.org/10.5027/andgeoV43n1-a04

Gill, B. C., Lyons, T. W., and Frank, T. D., 2008, Behavior of carbonate-associated sulfate during meteoric diagenesis and implications for the sulfur isotope

paleoproxy: Geochimica et Cosmochimica Acta, v. 72, p. 4699-4711. http://dx.doi.org/10.1016/j.gca.2008.07.001

Gill, B. C., Lyons, T. W., and Saltzman, M. R., 2007, Parallel, high-resolution carbon and sulfur isotope records of the evolving Paleozoic marine sulfur reservoir: Palaeogeography, Palaeoclimatology, Palaeoecology, v. 256, p. 156-173. http://dx.doi.org/10.1016/j.palaeo.2007.02.030

Gilleaudeau, G. J., and Kah, L. C., 2013, Carbon isotope records in a Mesoproterozoic epicratonic sea: Carbon cycling in a low-oxygen world: Precambrian Research, v. 228, p. 85-101. http://dx.doi.org/10.1016/j.precamres.2013.01.006

Gomes, M. L., and Hurtgen, M. T., 2013, Sulfur isotope systematics of a euxinic, low-sulfate lake: Evaluating the importance of the reservoir effect in modern and ancient oceans: Geology, v. 41, p. 663-666. 10.1130/g34187.1

Gomes, M. L., and Hurtgen, M. T., 2015, Sulfur isotope fractionation in modern euxinic systems: Implications for paleoenvironmental reconstructions of paired sulfate–sulfide isotope records: Geochimica et Cosmochimica Acta, v. 157, p. 39-55. https://doi.org/10.1016/j.gca.2015.02.031

Habicht, K. S., Gade, M., Thamdrup, B., Berg, P., and Canfield, D. E., 2002, Calibration of Sulfate Levels in the Archean Ocean: Science, v. 298, p. 2372-2374. 10.1126/science.1078265

Haq, B. U., and Schutter, S. R., 2008, A chronology of Paleozoic sea-level changes: Science, v. 322, p. 64-68. http://dx.doi.org/10.1126/science.1161648

Harper, D. A. T., Mac Niocaill, C., and Williams, S. H., 1996, The palaeogeography of early Ordovician Iapetus terranes: an integration of faunal and palaeomagnetic constraints: Palaeogeography, Palaeoclimatology, Palaeoecology, v. 121, p. 297-312. http://dx.doi.org/10.1016/0031-0182(95)00079-8

Henderson, M. A., Serra, F., Feltes, N. A., Albanesi, G. L., and Kah, L. C., 2018, Paired isotope records of carbonate and organic matter from the Middle Ordovician of Argentina: Intrabasinal variation and effects of the marine chemocline: Palaeogeography, Palaeoclimatology, Palaeoecology, v. 490, p. 107-130. https://doi.org/10.1016/j.palaeo.2017.10.018

HEREDIA, S., MESTRE, A., SORIA, T., and KAUFMANN, C., 2017, The Ordovician genus *Pygodus* (conodont) in the Cuyania Terrane, Argentina: Geological Magazine, v. 154, p. 1105-1116. 10.1017/s0016756816000728

Huff, W., Davis, D., Bergström, S., Krekeler, M., Kolata, D., and Cingolani, C., 1997, A biostratigraphically well-constrained K-bentonite U-Pb zircon age of the lowermost Darriwilian Stage (Middle Ordovician) from the Argentine Precordillera: Episodes, v. 20, p. 29-33. https://doi.org/10.1144/0016-764903-130

Huff, W. D., Bergström, S. M., Kolata, D. R., Cingolani, C., and Davis, D. W., 1995, Middle Ordovician K-bentonites discovered in the Precordillera of Argentina: Geochemical and paleogeographical implications, *in* Cooper, J. D., Droser, M. L.,

and Finney, S. C., eds., Ordovician oddesy: short papers for the seventh international symposium on the Ordovician system, Volume 77: Las Vegas, Nevada, SEPM, p. 343-349.

Huff, W. D., Bergström, S. M., Kolata, D. R., Cingolani, C. A., and Astini, R. A., 1998, Ordovician K-bentonites in the Argentine Precordillera: relations to Gondwana margin evolution: Geological Society, London, Special Publications, v. 142, p. 107-126. 10.1144/gsl.sp.1998.142.01.06

Jørgensen, B. B., Bang, M., and Blackburn, T. H., 1990, Anaerobic mineralization in marine sediments from the Baltic Sea-North Sea transition: Marine Ecology Progress Series, v. 59, p. 39-54.

Kah, L. C., Thompson, C. K., Henderson, M. A., and Zhan, R., 2016, Behavior of marine sulfur in the Ordovician: Palaeogeography, Palaeoclimatology, Palaeoecology, v. 458, p. 133-153. http://dx.doi.org/10.1016/j.palaeo.2015.12.028

Kaljo, D., Martma, T., and Saadre, T., 2007, Post-Hunnebergian Ordovician carbon isotope trend in Baltoscandia, its environmental implications and some similarities with that of Nevada: Palaeogeography, Palaeoclimatology, Palaeoecology, v. 245, p. 138-155. http://dx.doi.org/10.1016/j.palaeo.2006.02.020

Kaufman, A. J., Hayes, J. M., Knoll, A. H., and Germs, G. J. B., 1991, Isotopic compositions of carbonates and organic carbon from upper Proterozoic successions in Namibia: stratigraphic variation and the effects of diagenesis and metamorphism: Precambrian Research, v. 49, p. 301-327. http://dx.doi.org/10.1016/0301-9268(91)90039-D

Keller, M., 1999, Argentine Precordillera: Sedimentary and plate tectonic history of a Laurentian crustal fragment in South America: Geological Society of America, v. Special Paper 341. https://dx.doi.org/10.1130/0-8137-2341-8.1

Keller, M., Eberlein, S., and Lehnert, O., 1993, Sedimentology of Middle Ordovician carbonates in the Argentine precordillera: Evidence of regional relative sea-level changes: Geologische Rundschau, v. 82, p. 362-377. http://dx.doi.org/10.1007/BF00191838

Lefebvre, V., Servais, T., François, L., and Averbuch, O., 2010, Did a Katian large igneous province trigger the Late Ordovician glaciation?: A hypothesis tested with a carbon cycle model: Palaeogeography, Palaeoclimatology, Palaeoecology, v. 296, p. 310-319. http://dx.doi.org/10.1016/j.palaeo.2010.04.010

Lyons, T. W., Anbar, A. D., Severmann, S., Scott, C., and Gill, B. C., 2009, Tracking Euxinia in the Ancient Ocean: A Multiproxy Perspective and Proterozoic Case Study: Annual Review of Earth and Planetary Sciences, v. 37, p. 507-534. doi:10.1146/annurev.earth.36.031207.124233

Marenco, P. J., Corsetti, F. A., Hammond, D. E., Kaufman, A. J., and Bottjer, D. J., 2008, Oxidation of pyrite during extraction of carbonate associated sulfate: Chemical Geology, v. 247, p. 124-132. http://dx.doi.org/10.1016/j.chemgeo.2007.10.006

Marshall, J. D., 1992, Climatic and oceanographic isotopic signals from the carbonate rock record and their preservation: Geological Magazine, v. 129, p. 143-160. https://doi.org/10.1017/S0016756800008244

Máspero Castro, B., Ortega, G., and Albanesi, G. L., Middle Ordovician graptolite faunas of the Gualcamayo Formation (Middle Member) in the Corridita Creek Section, Northern Precordillera, Argentina, *in* Proceedings Proceedings of the 7th International Graptolite Conference and Field Meeting of the International Subcommission on Silurian Stratigraphy, San Juan, Argentina, 2003, Volume 18, Instituto Superior De Correlación Geológica (INSUGEO).

Mayer, B., and Krouse, H. R., 2004, Procedures for Sulfur Isotope Abundance Studies, *in* de Groot, P. A., ed., Handbook of Stable Isotope Analytical Techniques, Volume 1, Elsevier, p. 563-621. 10.1016/B978-044451114-0/50028-4

Meidla, T., Backman, L., Dronov, A., Holmer, L., and Sturesson, U., Middle-Upper Ordovician carbon isotope record from Västergötland (Sweden) and East Baltic, *in* Proceedings 8th Meeting on the Working Group on the Ordovician Geology of Baltoscandia, Tallinn and Tartu, Estonia, 2004, Tartu University Press, p. 67-68.

Ortega, G. and Albanesi, G. L. , 1999, Graptolite biostratigraphy of the Gualcamayo Formation (Middle Ordovician) at the Los Sapitos Creek Section, Argentina Precordillera: Acata Universitatis Carolinae- Geologica, v. 43, p. 49-52.

Pankhurst, R. J., Rapela, C. W., Saavedra, J., Baldo, E., Dahlquist, J., Pascua, I., and Fanning, C. M., 1998, The Famatinian magmatic arc in the central Sierras Pampeanas: an Early to Mid-Ordovician continental arc on the Gondwana margin: Geological Society, London, Special Publications, v. 142, p. 343-367. 10.1144/gsl.Sp.1998.142.01.17

Peralta, S. H., Heredia, S., and Beresi, M. S., 1999, Upper Arenigian-lower Llanvirnian sequence of the Las Chacritas river, Central Precordillera, San Juan Province, Argentina: Acta Universitatis Carolinae Geologica, v. 43, p. 123-126.

Present, T. M., Paris, G., Burke, A., Fischer, W. W., and Adkins, J. F., 2015, Large Carbonate Associated Sulfate isotopic variability between brachiopods, micrite, and other sedimentary components in Late Ordovician strata: Earth and Planetary Science Letters, v. 432, p. 187-198. http://dx.doi.org/10.1016/j.epsl.2015.10.005

Quinton, P. C., and MacLeod, K. G., 2014, Oxygen isotopes from conodont apatite of the midcontinent, US: Implications for Late Ordovician climate evolution: Palaeogeography Palaeoclimatology Palaeoecology, v. 404, p. 57-66. 10.1016/j.palaeo.2014.03.036

Quinton, P. C., Percival, I. G., Zhen, Y. Y., and MacLeod, K. G., 2015, Factors influencing conodont apatite $\delta^{18}O$ variability in the Ordovician: a case study from New South Wales, Australia: Stratigraphy, v. 12, p. 265-274.

Railsback, L. B., Ackerly, S. C., Anderson, T. F., and Cisneti, J. L., 1990, Palaeontological and isotope evidence for warm saline deep waters in Ordovician oceans: Nature, v. 343, p. 156-159. http://dx.doi.org/10.1038/343156a0

Ramos, V. A., Jordan, T. E., Allmendinger, R. W., Mpodozis, C., Kay, S. M., Cortes, J. M., and Palma, M., 1986, Paleozoic terranes of the Central Argentine-Chilean Andes: Tectonics, v. 5, p. 855-880. http://dx.doi.org/10.1029/TC005i006p00855

Saltzman, M. R., 2005, Phosphorus, nitrogen, and the redox evolution of the Paleozoic oceans: Geology, v. 33, p. 573-576. http://dx.doi.org/10.1130/g21535.1

Saltzman, M. R., Edwards, C. T., Adrain, J. M., and Westrop, S. R., 2015, Persistent oceanic anoxia and elevated extinction rates separate the Cambrian and Ordovician radiations: Geology, v. 43, p. 807-810. 10.1130/g36814.1

Schmitz, B., Bergström, S. M., and Xiaofeng, W., 2010, The middle Darriwilian (Ordovician) $\delta^{13}C$ excursion (MDICE) discovered in the Yangtze Platform succession in China: implications of its first recorded occurrences outside Baltoscandia: Journal of the Geological Society, v. 167, p. 249-259. http://dx.doi.org/10.1144/0016-76492009-080

Serra, F., Albanesi, G. L., Ortega, G., and Bergstrom, S. M., 2015, Biostratigraphy and palaeoecology of Middle–Late Ordovician conodont and graptolite faunas of the Las Chacritas River section, Precordillera of San Juan, Argentina: Geological Magazine, v. 152, p. 813-829. http://dx.doi.org/10.1017/S0016756814000752

Serra, F., Feltes, N. A., Ortega, G., and Albanesi, G. L., 2017, Lower middle Darriwilian (Ordovician) graptolites and index conodonts from the Central Precordillera of San Juan Province, Argentina: Geological Journal, p. n/a-n/a. 10.1002/gj.3043

Swart, P. K., 2015, The geochemistry of carbonate diagenesis: The past, present and future: Sedimentology, v. 62, p. 1233-1304. 10.1111/sed.12205

Thomas, W. A., and Astini, R. A., 1996, The Argentine Precordillera: A traveler from the Ouachita embayment of North American Laurentia: Science, v. 273, p. 752-757. http://dx.doi.org/10.1126/science.273.5276.752

Thomas, W. A., and Astini, R. A., 1999, Simple-shear conjugate rift margins of the Argentine Precordillera and the Ouachita embayment of Laurentia: Geological Society of America Bulletin, v. 111, p. 1069-1079. 10.1130/0016-7606(1999)111<1069:sscrmo>2.3.co;2

Thomas, W. A., Astini, R. A., and Bayona, G., 2002, Ordovician collision of the Argentine Precordillera with Gondwana, independent of Laurentian Taconic orogeny: Tectonophysics, v. 345, p. 131-152. http://dx.doi.org/10.1016/S0040-1951(01)00210-4

Thompson, C. K., and Kah, L. C., 2012, Sulfur isotope evidence for widespread euxinia and a fluctuating oxycline in Early to Middle Ordovician greenhouse oceans: Palaeogeography, Palaeoclimatology, Palaeoecology, v. 313-314, p. 189-214. http://dx.doi.org/10.1016/j.palaeo.2011.10.020

Thompson, C. K., Kah, L. C., Astini, R., Bowring, S. A., and Buchwaldt, R., 2012, Bentonite geochronology, marine geochemistry, and the Great Ordovician Biodiversification Event (GOBE): Palaeogeography, Palaeoclimatology, Palaeoecology, v. 321–322, p. 88-101. http://dx.doi.org/10.1016/j.palaeo.2012.01.022

Torsvik, T. H., and Cocks, L. R. M., 2013, Chapter 2 New global palaeogeographical reconstructions for the Early Palaeozoic and their generation: Geological Society, London, Memoirs, v. 38, p. 5-24. 10.1144/m38.2

Trotter, J. A., Williams, I. S., Barnes, C. R., Lécuyer, C., and Nicoll, R. S., 2008, Did Cooling Oceans Trigger Ordovician Biodiversification? Evidence from Conodont Thermometry: Science, v. 321, p. 550-554. http://dx.doi.org/10.1126/science.1155814

Veizer, J., 1983, Chemical diagenesis of carbonates; therory and application of trace element technique, *in* Arthur, M. A., Anderson, T. F., Kaplan, I. R., Veizer, J., and Land, L. S., eds., Stable isotopes in sedimentary geology, Volume 10: SEPM Short Course (1983), Society of Sedimentary Geology, Tulsa, OK.

Voldman, G. G., Albanesi, G. L., and Ramos, V. A., 2009, Ordovician metamorphic event in the carbonate platform of the Argentine Precordillera: Implications for the geotectonic evolution of the proto-Andean margin of Gondwana: Geology, v. 37, p. 311-314. 10.1130/g25540a.1

Young, S. A., Gill, B. C., Edwards, C. T., Saltzman, M. R., and Leslie, S. A., 2016, Middle–Late Ordovician (Darriwilian–Sandbian) decoupling of global sulfur and carbon cycles: Isotopic evidence from eastern and southern Laurentia: Palaeogeography, Palaeoclimatology, Palaeoecology, v. 458, p. 118-132. http://dx.doi.org/10.1016/j.palaeo.2015.09.040

Zhang, T., Shen, Y., and Algeo, T. J., 2010, High-resolution carbon isotopic records from the Ordovician of South China: Links to climatic cooling and the Great Ordovician Biodiversification Event (GOBE): Palaeogeography, Palaeoclimatology, Palaeoecology, v. 289, p. 102-112. http://dx.doi.org/10.1016/j.palaeo.2010.02.020

Zhou, L., Algeo, T. J., Shen, J., Hu, Z., Gong, H., Xie, S., Huang, J., and Gao, S., 2015, Changes in marine productivity and redox conditions during the Late Ordovician Hirnantian glaciation: Palaeogeography, Palaeoclimatology, Palaeoecology, v. 420, p. 223-234. http://dx.doi.org/10.1016/j.palaeo.2014.12.012

Appendix 1

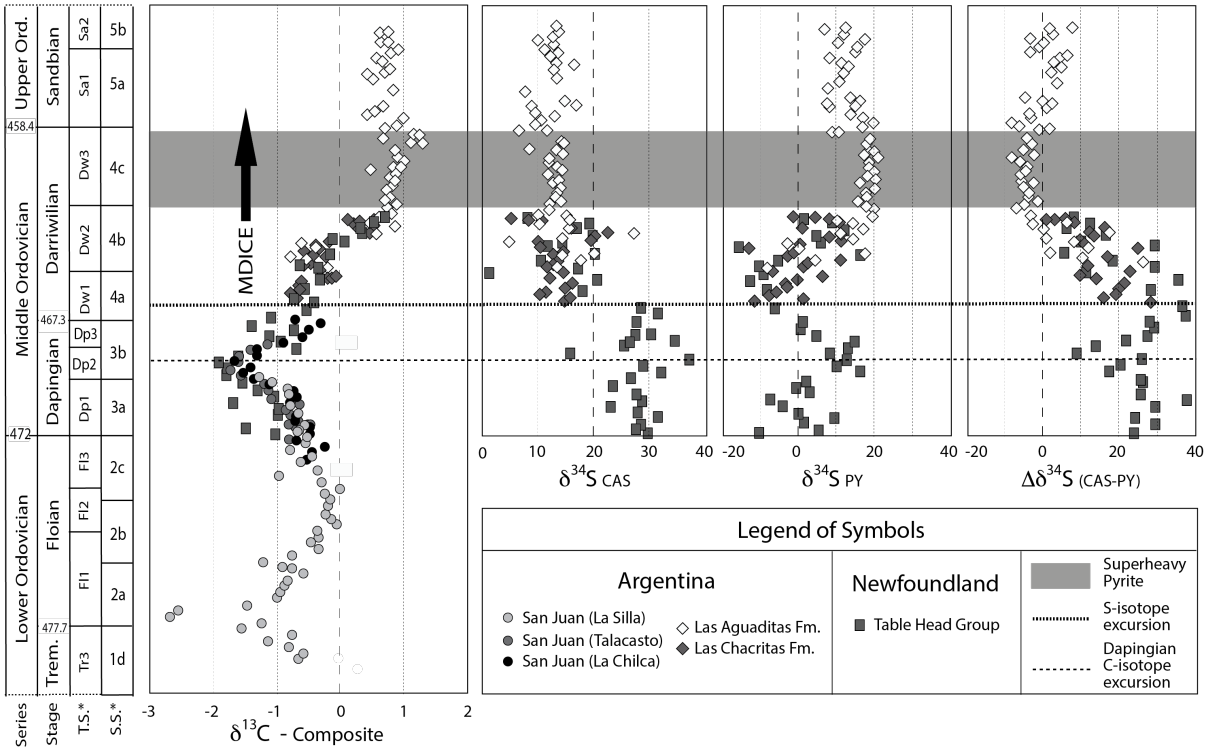

Figure 2.1: Carbon and sulfur isotope profiles from Argentina and western Newfoundland (Fig. 11 of Kah et al, 2016). The mid-Dapingian negative carbon isotope excursion (thin dotted line) correlates to a positive trend in the isotopic composition of sedimentary pyrite and is interpreted to reflect enhanced euxinic conditions. The abrupt shift in the isotopic composition of marine sulfate ($\delta^{34}S_{CAS}$) in the early Darriwilian (heavy dotted line) corresponds with much slower change in isotopic composition of marine sulfide ($\delta^{34}S_{PY}$). Kah et al. (2016) interpret the isotopic enrichment of sedimentary sulfide to reflect deposition of HS^{-}, as pyrite, within an anoxic marine reservoir, ultimately leading to the formation of "superheavy pyrite" (grey band).

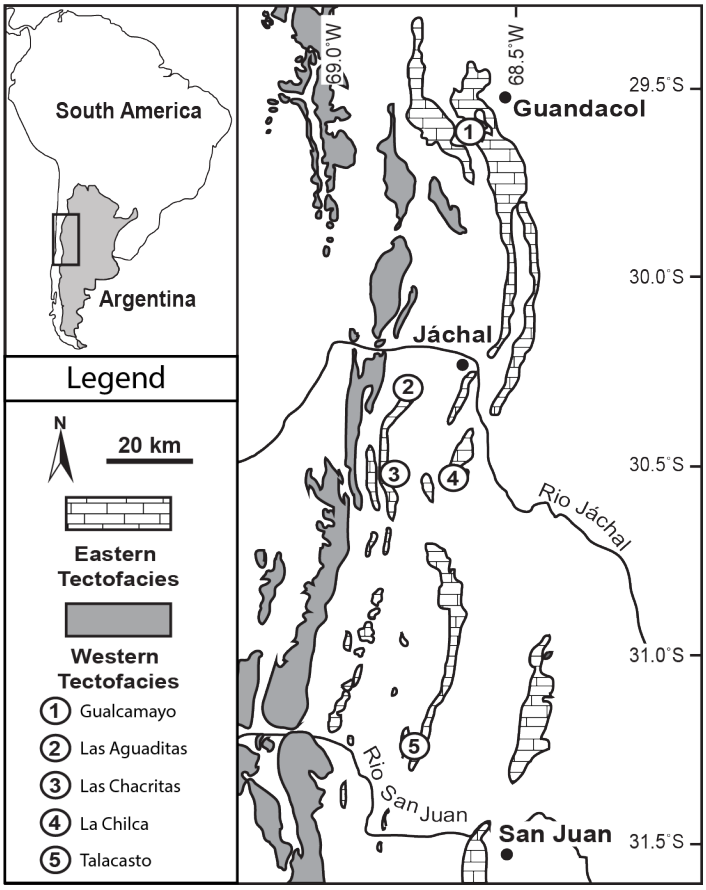

Figure 2.2: Location map of the Argentine Precordillera modified after Gomez and Astini (2015). Lower Paleozoic strata crop out along a series of N-S trending thrust sheets and are divided into the western and eastern Tectofacies (Astini et al., 1995). The western tectofacies consists primarily of deformed and metamorphosed deep-water facies. Moderately to weakly deformed and unmetamorphosed marine shelf and slope deposits are exposed in the eastern tectofacies. The Gualcamayo (1) Formation was sampled to the southwest of Guandacol at the La Corridita Creek section. Samples of the Las Aguaditas (2) and Las Chacritas (3) formations were collected from measured sections southwest of San Jose de Jáchal. Radiometric age dates of K-bentonite deposits in the San Juan Formation at Cerro La Chilca (4) and Talacasto (5) suggest Dapingian ages (ca. 470 Ma; Thompson et al., 2012); however, these ages do not discretely define the age of the San Juan throughout the Precordillera (see text for discussion).

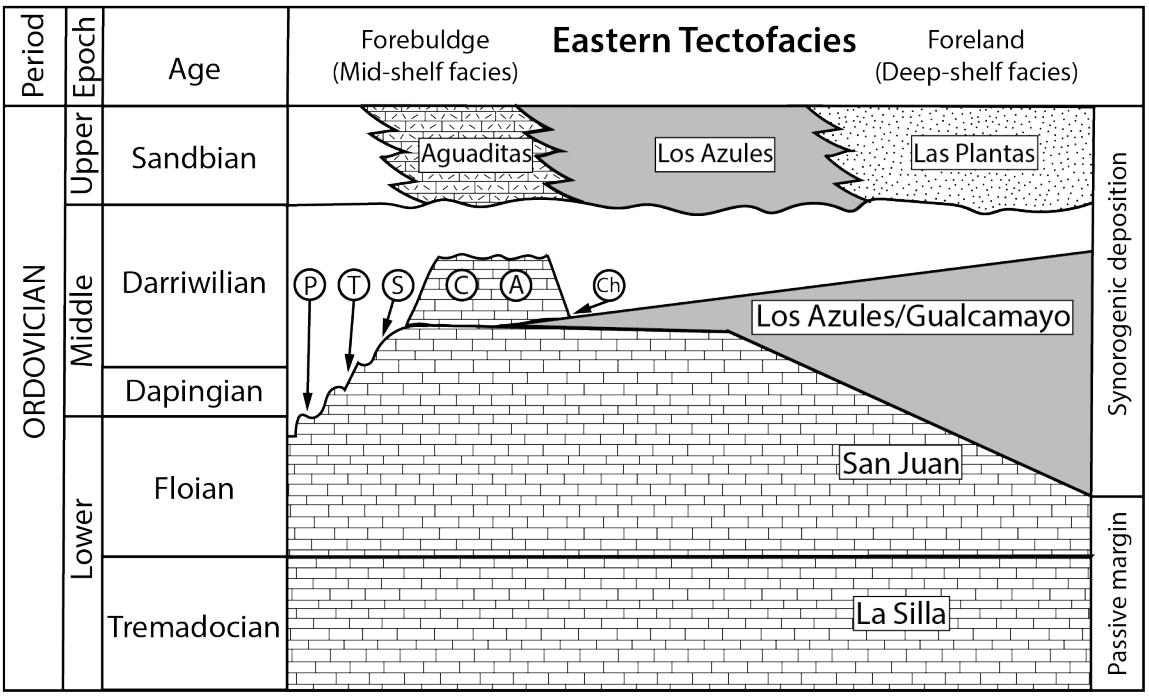

Figure 2.3: Time-correlation of Ordovician strata of the eastern tectofacies in the Argentine Precordillera adapted from Astini et al. (1995) and Thompson and Kah (2012). This southwest to northeast directed section illustrates the diachronous nature of the uppermost San Juan Formation across the Precordillera. Tectonic convergence of the Precordillera terrane with the Gondwanan margin resulted the formation of a foreland basin and deposition of deep-water facies to the north. Forebulge migration in the Middle Ordovician resulted in removal of shallower water facies and development of the Talacasto-Tambolar unconformity across the carbonate platform of the Precordillera. P = Pachaco section, T = Talacasto section, S = Las Silla section, C = Las Chacritas section, A = Las Aguaditas section, and Ch = La Chilca section.

Figure 2.4: Correlation of measured stratigraphic sections of the Las Chacritas, Las Aguaditas, and Gualcamayo formations based on the biostratigraphy of Serra et al. (2015), Feltes et al. (2016), and stratigraphic correlations and biostratigraphy of Astini et al. (1994), Albanesi et al. (1999), and Ortega and Albanesi (2000). Upper Darriwilian (Dw3) strata across the Precordillera were removed during development of the regional Talacasto-Tambolar unconformity (Astini et al., 1995). The absence of upper Darriwilian strata is identified by the absence of conodonts representing the upper *Eoplacognathus suecicus* and *Pygodus serra* conodont zones in the Las Chacritas Formation and the entirety of the *E. suecicus* and *P. serra* conodont zones in the Las Aguaditas Formation. In the Gualcamayo Formation, conodont biostratigraphy indicates the presence of the *Pygodus anitae* subzone of the upper *E. suecicus* Zone of stage slice Dw2, which is truncated by late Darriwilian clastic deposits of the Las Vacas/Las Plantas formations. Note the change in scale for the Gualcamayo Formation stratigraphic column.

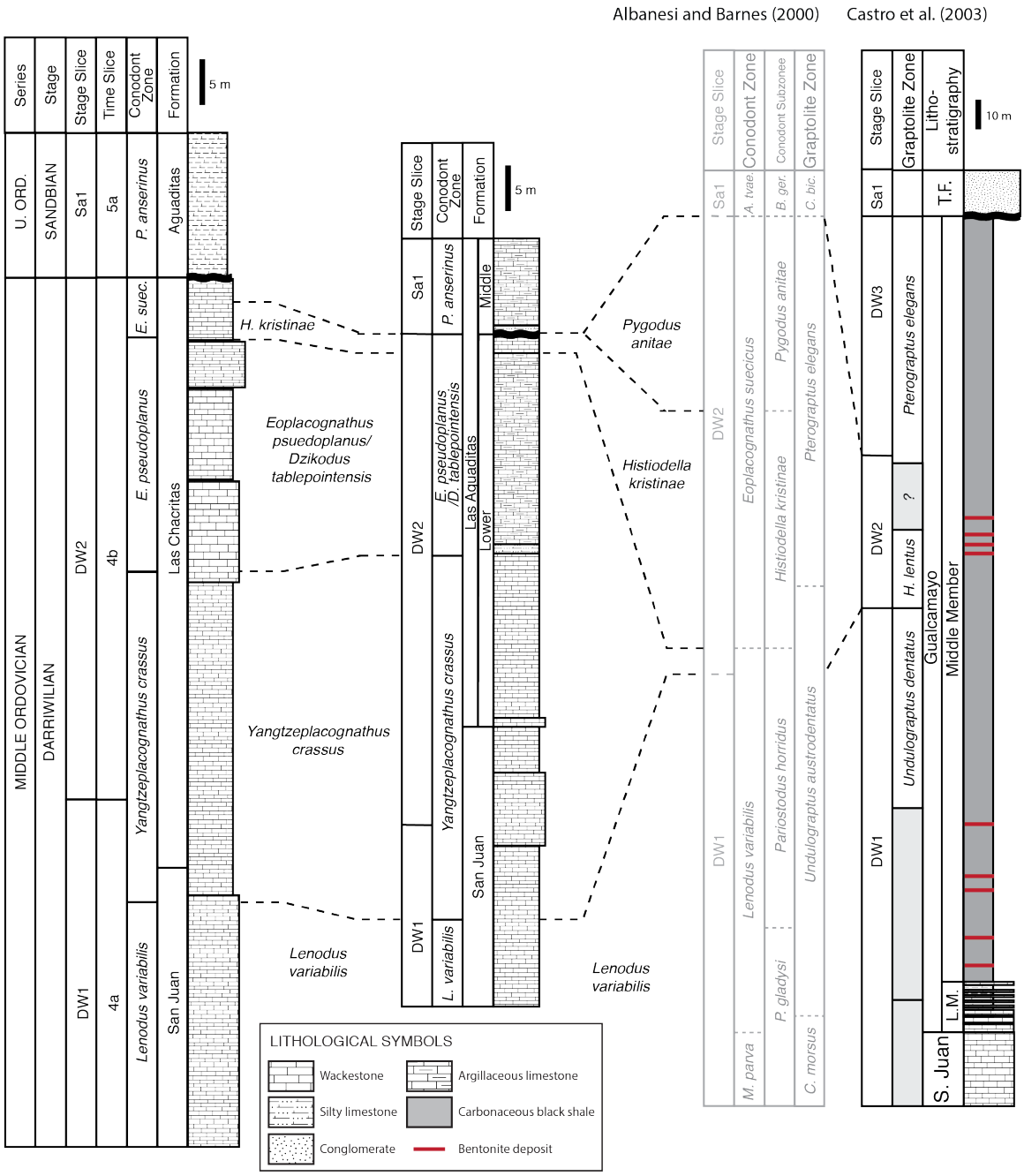
Albanesi and Barnes (2000)
Castro et al. (2003)
Series
Stage
Stage Slice
Time Slice
Conodont Zone
Formation
U. ORD.
SANDBIAN
DARRIWILIAN
MIDDLE ORDOVICIAN
Sa1
5a
4b
4a
DW2
DW1
P. anserinus
E. suec.
E. pseudoplanus
Yangtzeplacognathus crassus
Lenodus variabilis
Aguaditas
Las Chacritas
San Juan
5 m
H. kristinae
Eoplacognathus psuedoplanus/ Dzikodus tablepointensis
Yangtzeplacognathus crassus
Lenodus variabilis
Stage Slice
Conodont Zone
Formation
Sa1
P. anserinus
E. pseudoplanus /D. tablepointensis
L. variabilis
DW2
DW1
Middle
Las Aguaditas
Lower
San Juan
5 m
Pygodus anitae
Histiodella kristinae
Lenodus variabilis
Stage Slice
Conodont Zone
Graptolite Zone
Sa1
DW2
DW1
A. tvae.
Eoplacognathus suecicus
B. ger.
Conodont Subzonee
Pygodus anitae
Histiodella kristinae
C. bic.
Pterograptus elegans
Undulograptus austrodentatus
M. parva
Lenodus variabilis
P. gladysi
Pariostodus horridus
C. morsus
Stage Slice
Graptolite Zone
Litho-stratigraphy
Sa1
DW3
DW2
DW1
Pterograptus elegans
?
H. lentus
Undulograptus dentatus
Gualcamayo
Middle Member
T.F.
L.M.
S. Juan
10 m
LITHOLOGICAL SYMBOLS
Wackestone
Argillaceous limestone
Silty limestone
Carbonaceous black shale
Conglomerate
Bentonite deposit

Figure 2.5: Carbon and sulfur isotopic records of the Las Chacritas Formation. $\delta^{13}C_{carb}$ data from Henderson et al. (2018) show the globally recognized positive 2‰ shift of the MDICE in the *E. pseudoplanus* conodont Zone. $\delta^{34}S_{CAS}$ data are somewhat variable through the *E. pseudoplanus* Zone with isotopic compositions averaging around +25‰. $\delta^{34}S_{CAS}$ variability slightly decreases in the uppermost *E. pseudoplanus* and *E. suecicus* conodont zones with values remaining around −25‰. $\delta^{34}S_{PY}$ data are highly variable throughout the section reflecting pyrite formation in sedimentary pore fluids. A shift in $\delta^{34}S_{PY}$ values is noted in the uppermost *E. pseudoplanus* Zone and may be associated with increased organic carbon burial during the MDICE. $\Delta^{34}S$ ($\delta^{34}S_{CAS} - \delta^{34}S_{PY}$) values are generally heavy around 20-30‰ through the section but drop in the uppermost *E. pseudoplanus* Zone as $\delta^{34}S_{PY}$ values get heavier. Conodont biostratigraphy from Serra et al. (2015).

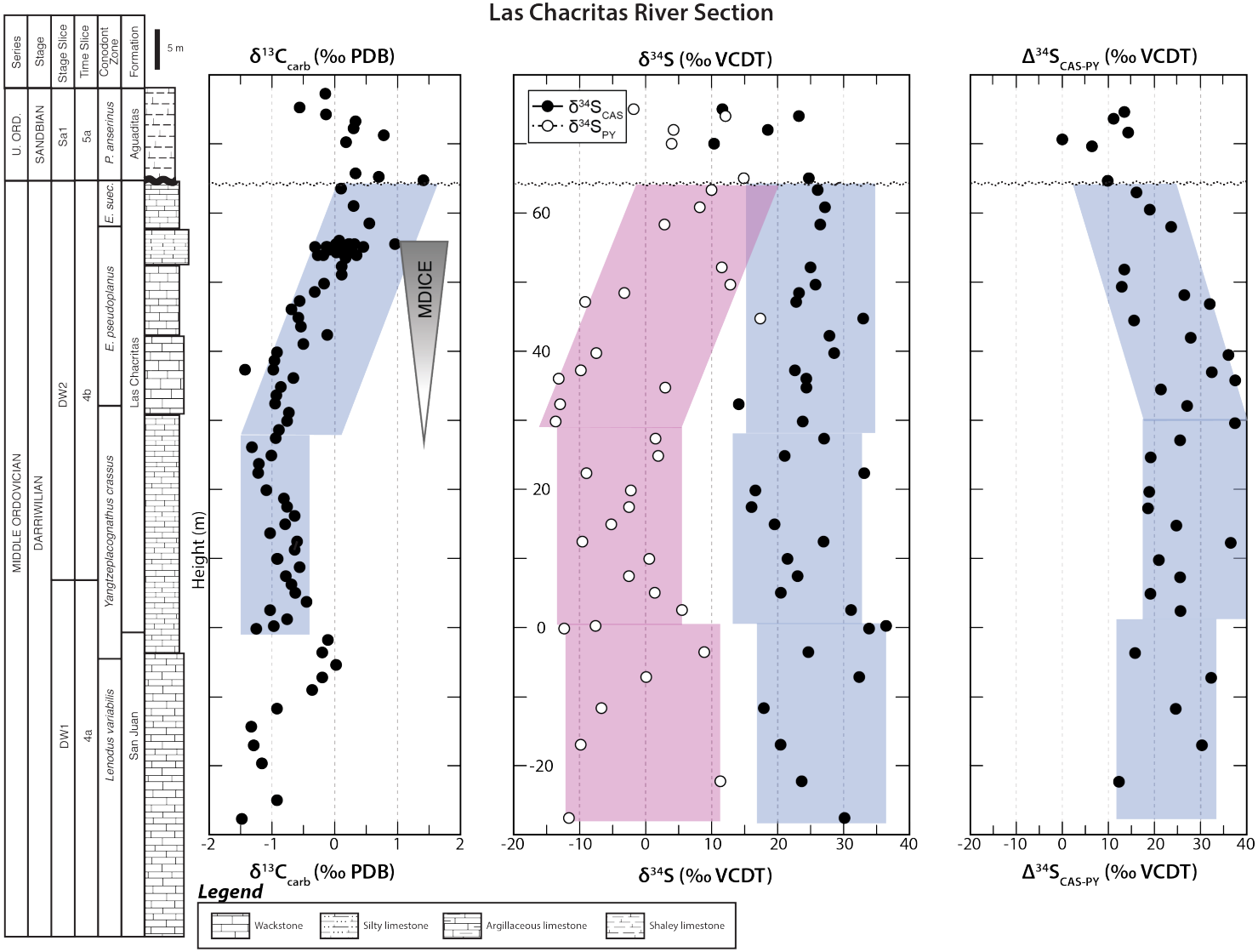
Las Chacritas River Section
Series
Stage
Stage Slice
Time Slice
Conodont Zone
Formation
5 m
U. ORD.
SANDBIAN
Sa1
5a
P. anserinus
Aguaditas
E. suec.
E. pseudoplanus
Las Chacritas
DW2
4b
Yangtzeplacognathus crassus
DARRIWILIAN
DW1
4a
Lenodus variabilis
San Juan
MIDDLE ORDOVICIAN
δ13Ccarb (‰ PDB)
MDICE
Height (m)
δ34S (‰ VCDT)
δ34SCAS
δ34SPY
Δ34SCAS-PY (‰ VCDT)
Legend
Wackstone
Silty limestone
Argillaceous limestone
Shaley limestone

Figure 2.6: Carbon and sulfur isotope records of the lower member of the Las Aguaditas Formation. $\delta^{13}C_{carb}$ data show a trend to more negative values around –1.5 through the MDICE interval and are interpreted to reflect incorporation of ^{13}C depleted dissolved inorganic carbon below the chemocline (cf. Henderson et al. 2018). Variability of $\delta^{34}S_{CAS}$ is interpreted to reflect small-scale shifts in the position of the chemocline, potentially between the sediment and the water column. $\delta^{34}S_{PY}$ is highly variable throughout the section with values decreasing from around +12‰ in *Y. crassus* Zone of the uppermost San Juan Formation to < 0‰ in the upper *Y. crassus* Zone of the Las Aguaditas Formation. $\delta^{34}S_{PY}$ values then increase through the MDICE interval in the *E. pseudoplanus/D. tablepointensis* Zone. Variability in $\delta^{34}S_{PY}$ reflects utilization of available H_2S in sedimentary pore fluids during pyrite formation. $\Delta^{34}S$ ($\delta^{34}S_{CAS} - \delta^{34}S_{PY}$) is highly variable between around 0‰ and 40‰ reflecting variability in both $\delta^{34}S_{PY}$ and $\delta^{34}S_{CAS}$ at or near the chemocline. Conodont biostratigraphy from Feltes et al. (2016).

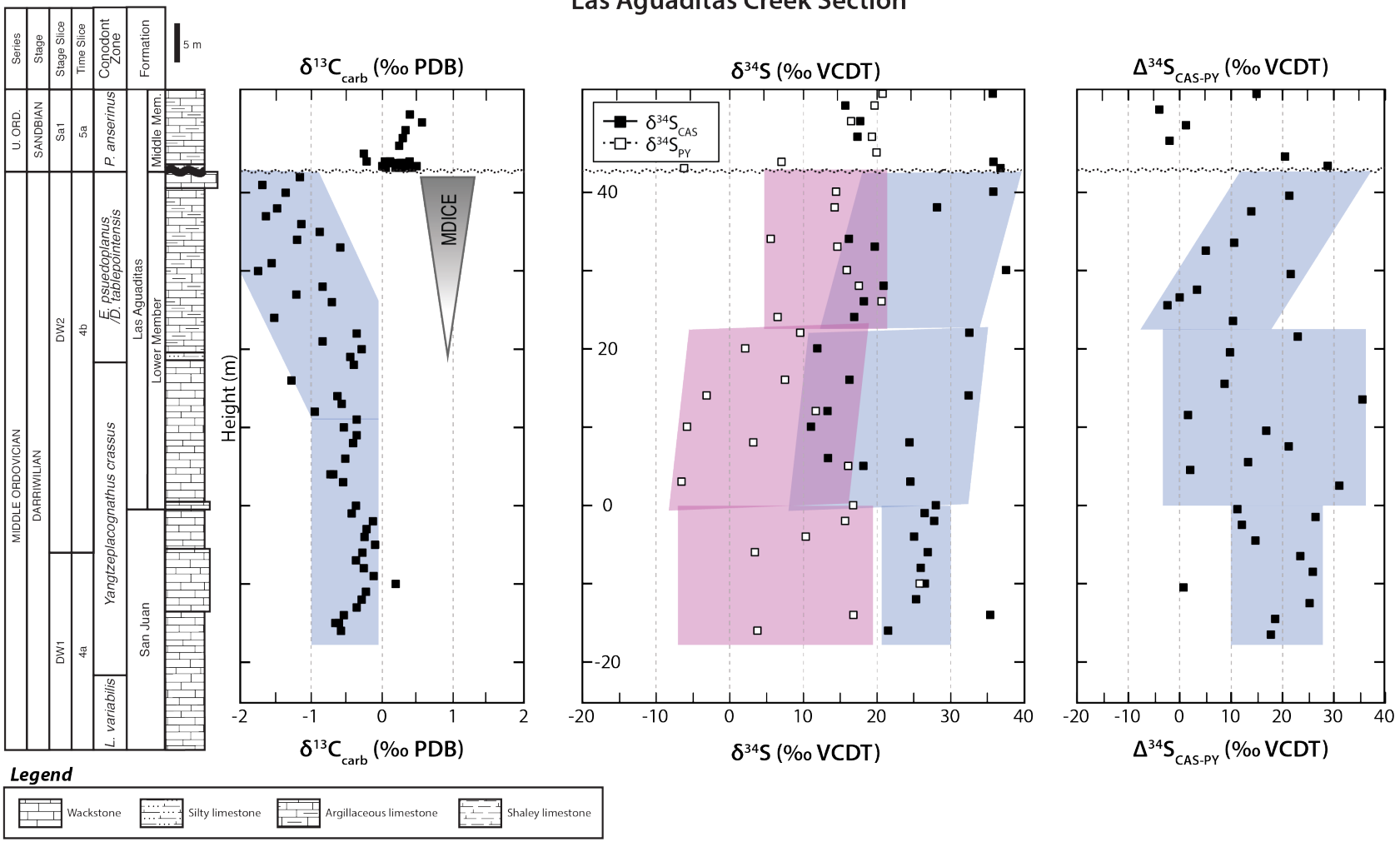
Las Aguaditas Creek Section
Series
Stage
Stage Slice
Time Slice
Conodont Zone
Formation
5 m
U. ORD.
SANDBIAN
DARRIWILIAN
MIDDLE ORDOVICIAN
DW1
DW2
Sa1
4a
4b
5a
P. anserinus
E. psuedoplanus /D. tablepointensis
Yangtzeplacognathus crassus
L. variabilis
Las Aguaditas
Middle Mem.
Lower Member
San Juan
δ13Ccarb (‰ PDB)
MDICE
Height (m)
δ34S (‰ VCDT)
δ34SCAS
δ34SPY
Δ34SCAS-PY (‰ VCDT)
Legend
Wackstone
Silty limestone
Argillaceous limestone
Shaley limestone

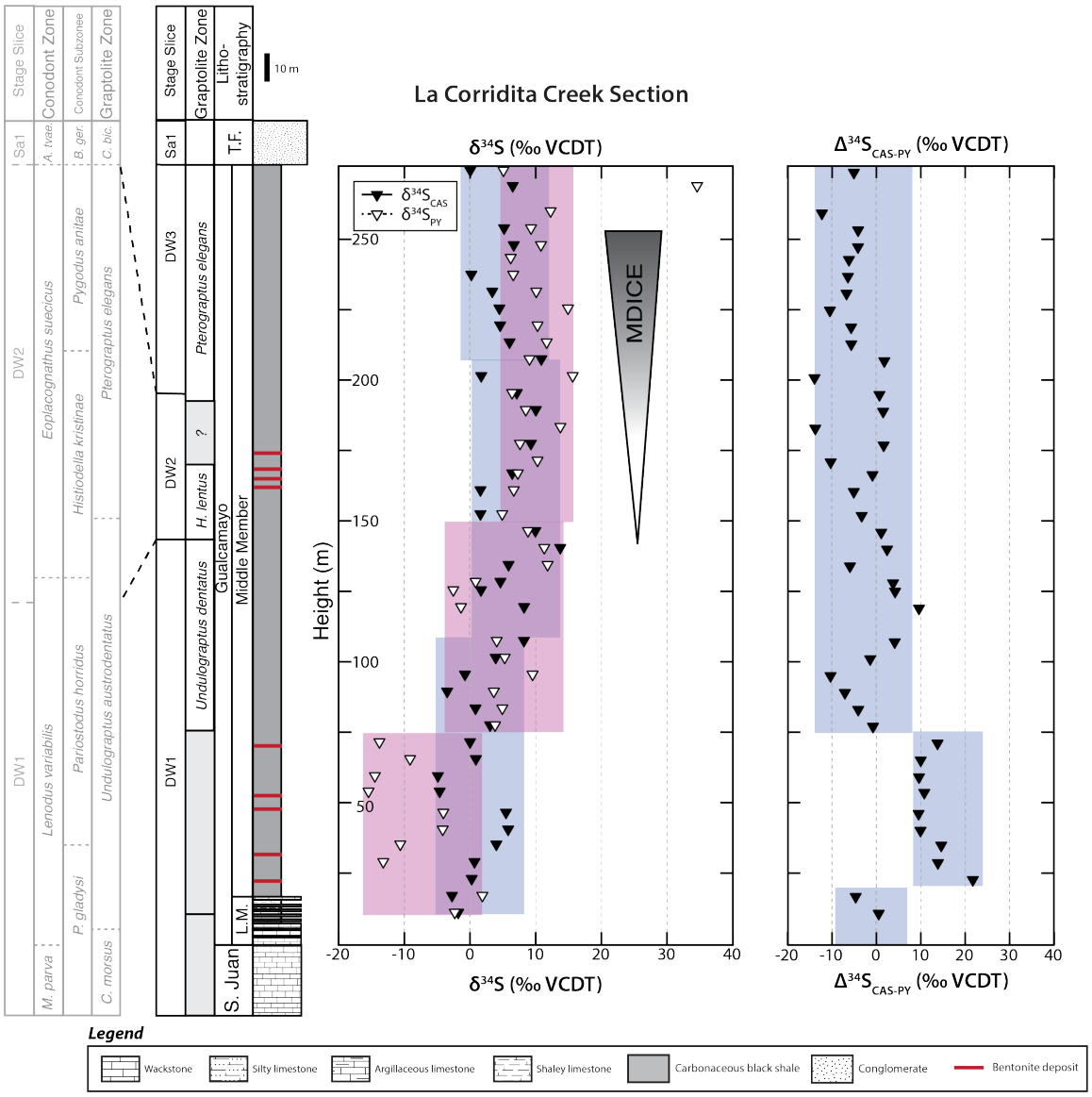

Figure 2.7: Sulfur isotope records of the Gualcamayo Formation at La Corridita Creek. $\delta^{34}S_{CAS}$ shows a similar, but less pronounced change from values around 0‰ in the lower Darriwilian (Dw1) to values between +5‰ and +10‰ in the Middle to Late Darriwilian (Dw2-Dw3). $\delta^{34}S_{PY}$ values in the lower Darriwilian around –10‰ increase to values around +5‰ in the *U. dentatus* graptolite zone and gradually increase to around +10‰ in the Middle Darriwilian (Dw2) *H. lentus* graptolite Zone. $\Delta^{34}S$ ($\delta^{34}S_{CAS} - \delta^{34}S_{PY}$) values in the Gualcamayo Formation decline from around +10‰ in the *U. dentatus* graptolite Zone to values generally < 0‰ suggesting increased oxidation and disproportionation of sulfide to sulfate and intermediates within a deep-water H_2S reservoir. Graptolite biostratigraphy from Castro et al. (2003) correlated to conodont biostratigraphy of Ortega and Albanesi (2000) from Cerro Potrerillo.

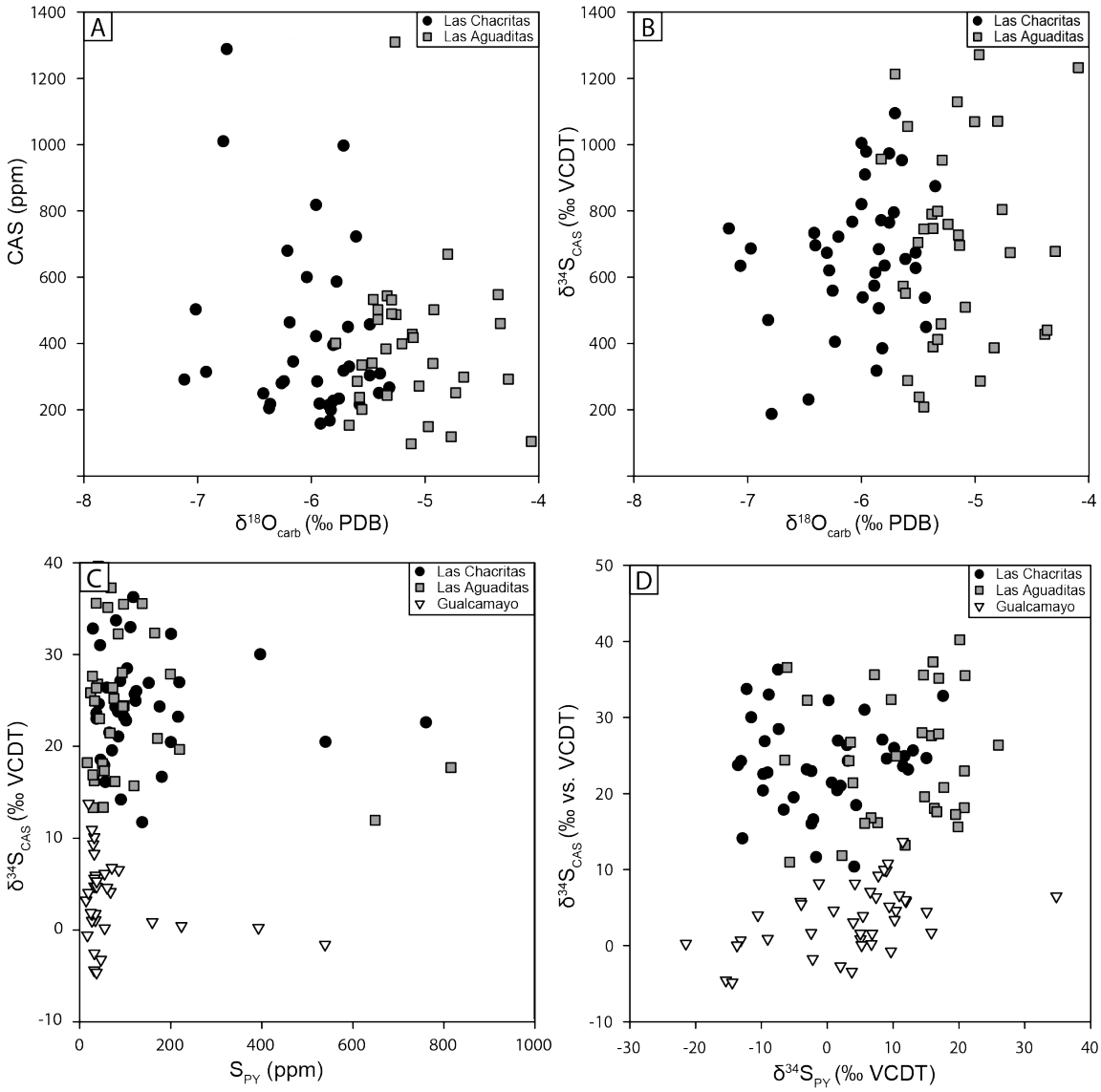

Figure 2.8: Cross-plots of isotopic data for the Las Chacritas, Las Aguaditas, and Gualcamayo formations for evaluation of diagenetic alteration or pyrite oxidation during CAS extractions. A) CAS (ppm) vs. $\delta^{18}O_{carb}$, B) $\delta^{34}S_{CAS}$ vs. $\delta^{18}O_{Carb}$, C) $\delta^{34}S_{CAS}$ vs. S_{PY} (ppm), D) $\delta^{34}S_{CAS}$ vs. $\delta^{34}S_{PY}$. See text for discussion.

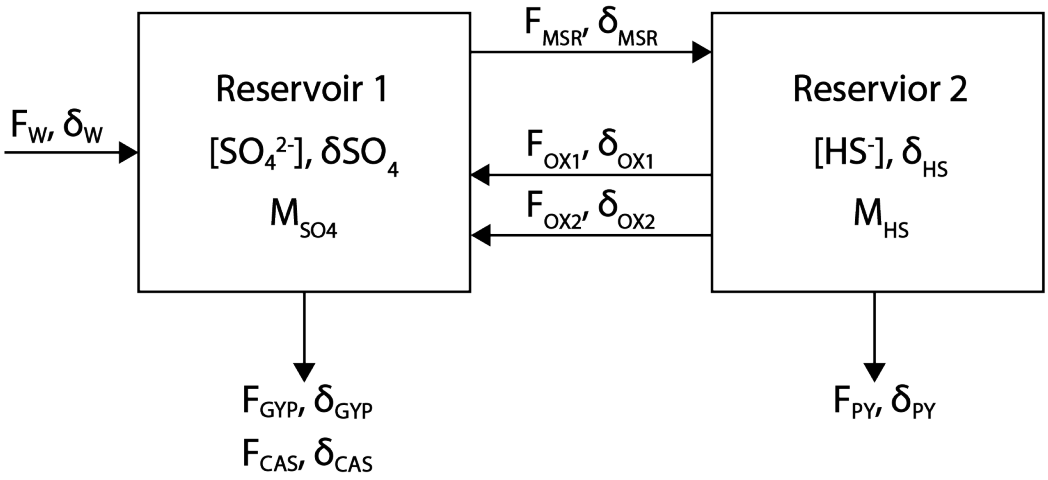

Figure 2.9: Dual reservoir model proposed for marine S-cycling initially proposed by Thompson and Kah (2012) after Rothman et al. (2003) and defined in Kah et al. (2016). Marine sulfur is divided into two chemically reactive reservoirs: a shallow water SO_4^{2-} reservoir and a reduced sulfur HS^-, which includes all phases of reduced sulfur species. This model has an input flux from crustal weathering (F_W, δ_W) as well as output fluxes as sedimentary sulfur as gypsum (F_{GYP}, δ_{GYP}), carbonate-associated sulfate (F_{CAS}, δ_{CAS}), or pyrite (F_{PY}, δ_{PY}) and allows for fluxes between reservoirs via microbial sulfate reduction (MSR; F_{MSR}, δ_{MSR}) and either biotic (F_{OX1}, δ_{OX1}) or abiotic sulfide oxidation (F_{OX2}, δ_{OX2}).

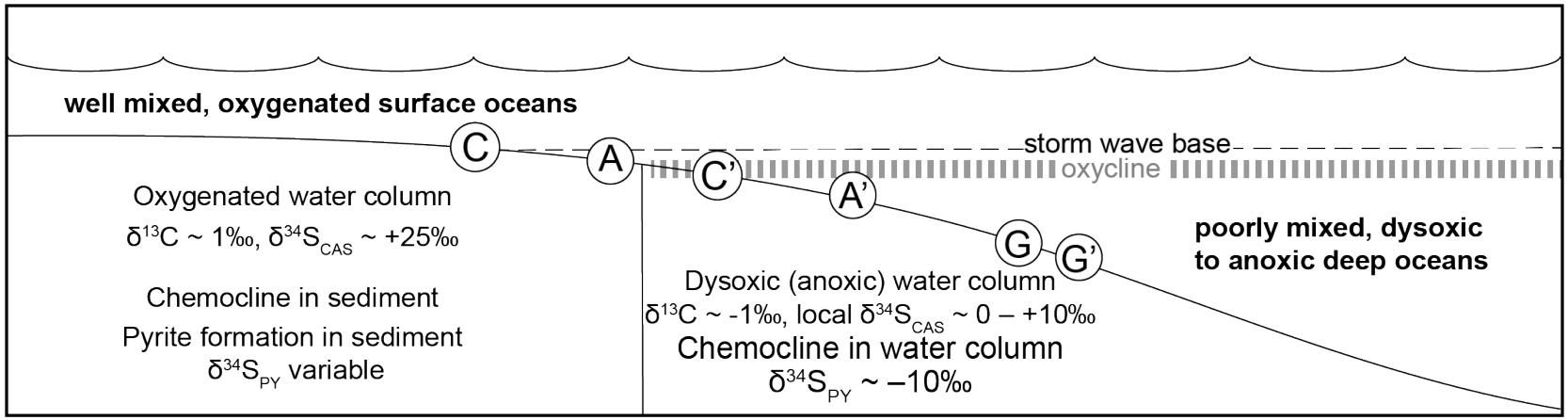

Figure 2.10: Interpretation of the marine shelf of the Precordillera during deposition of the Las Chacritas, Las Aguaditas, and Gualcamayo formations in the Darriwilian. Sedimentological evidence suggests the Las Chacritas Formation was deposited between fair-weather and storm wave-base. Sedimentary and geochemical evidence suggests deposition of the Las Aguaditas below storm wave base and below the marine chemocline through the *E. pseudoplanus/D. tablepointensis* Zone. The Gualcamayo Formation is interpreted to be below the marine chemocline throughout its deposition. We suggest the $\delta^{34}S_{PY}$ and $\delta^{34}S_{CAS}$ data are best explained by the presence of the marine chemocline in the Precordillera (cf. Thompson and Kah, 2012; Henderson et al., 2018). Carbonate formation above the chemocline (Las Chacritas Formation) results in isotopically enriched $\delta^{34}S_{CAS}$ values, whereas carbonate formed below the chemocline (Las Aguaditas and Gualcamayo formations) reflects local SO_4^{2-} with depleted isotopic compositions. Pyrite formation above the chemocline is restricted to sedimentary pore fluids and results in variable enrichment of $\delta^{34}S_{PY}$ depending on the extent of H_2S utilization during pyrite formation. Below the chemocline, pyrite can form syngenetically in the water column from the standing reduced sulfur (H_2S) reservoir as well as from sedimentary pore fluids.

Table 2.1: Range of isotopic compositions and elemental concentrations recorded in the Las Chacritas River section

Sample	Height* (m)	Conodont Zone	$\delta^{13}C_{carb}$ (‰ PDB)	$\delta^{18}O$	$\delta^{34}S_{CAS}$ (‰ VCDT)	$\delta^{34}S_{PY}$	$\Delta^{34}S$	Sr (ppm)	Mn	Fe
C14-1	-27.6	*L. variabilis*	-1.48	-5.34	30.16	-11.63	41.78	332	98	421
C14-2	-24.9	*L. variabilis*	-0.92	-5.50	-	-	-	343	393	1916
C14-3	-22.3	*L. variabilis*	-	-	23.67	11.35	12.32	-	-	-
C14-4	-19.6	*L. variabilis*	-1.16	-5.40	-	-	-	310	269	864
C14-5	-17.0	*L. variabilis*	-1.29	-5.43	20.47	-9.84	30.32	338	304	1177
C14-6	-14.3	*L. variabilis*	-1.33	-5.61	-	-	-	344	380	1122
C14-7	-11.7	*L. variabilis*	-0.92	-5.42	17.94	-6.70	24.64	325	364	1495
C14-8	-9.0	*L. variabilis*	-0.36	-5.51	-	-	-	311	893	3367
C14-9	-7.2	*L. variabilis*	-0.20	-5.63	32.40	0.08	32.32	319	820	3037
C14-10	-5.4	*L. variabilis*	0.02	-5.66	-	-	-	280	881	2531
C14-11	-3.6	*Y. crassus*	-0.20	-5.83	24.69	8.88	15.81	300	527	1737
C14-12	-1.8	*Y. crassus*	-0.11	-5.59	-	-	-	350	1553	3400
C14-13	-0.2	*Y. crassus*	-1.25	-5.98	33.89	-12.33	46.21	616	806	7360
C14-14	0.0	*Y. crassus*	-0.88	-5.77	-	-	-	592	719	1851
C14-15	0.2	*Y. crassus*	-0.97	-5.69	36.47	-7.58	44.06	507	735	1059
C14-16	1.2	*Y. crassus*	-0.76	-5.86	-	-	-	575	673	2649
C14-17	2.5	*Y. crassus*	-1.03	-5.95	31.16	5.51	25.65	721	502	1838
C14-18	3.7	*Y. crassus*	-0.45	-5.84	-	-	-	496	340	1400

Table 2.1. continued.

Sample	Height* (m)	Conodont Zone	$\delta^{13}C_{carb}$ (‰ PDB)	$\delta^{18}O$	$\delta^{34}S_{CAS}$ (‰ VCDT)	$\delta^{34}S_{PY}$	$\Delta^{34}S$	Sr (ppm)	Mn	Fe
C14-19	5.0	*Y. crassus*	-0.63	-5.97	20.51	1.38	19.13	499	357	1438
C14-20	6.2	*Y. crassus*	-0.69	-5.69	-	-	-	681	336	1266
C14-21	7.4	*Y. crassus*	-0.78	-5.51	23.05	-2.53	25.58	671	392	2382
C14-22	8.7	*Y. crassus*	-0.56	-6.15	-	-	-	653	358	2388
C14-23	9.9	*Y. crassus*	-0.92	-5.87	21.52	0.56	20.96	735	346	6512
C14-23	9.9	*Y. crassus*	-0.91	-5.58	-	-	-	672	411	1920
C14-24	11.2	*Y. crassus*	-0.64	-5.92	-	-	-	730	333	1914
C14-25	12.4	*Y. crassus*	-0.60	-5.74	26.99	-9.58	36.57	946	653	6233
C14-26	13.6	*Y. crassus*	-1.03	-5.99	-	-	-	670	403	1487
C14-27	14.9	*Y. crassus*	-0.79	-5.83	19.57	-5.21	24.78	651	299	1316
C14-28	16.1	*Y. crassus*	-0.64	-5.84	-	-	-	595	221	675
C14-29	17.4	*Y. crassus*	-0.76	-5.80	16.09	-2.52	18.60	662	248	3596
C14-30	18.6	*Y. crassus*	-0.81	-5.70	-	-	-	885	298	1438
C14-31	19.8	*Y. crassus*	-1.09	-6.21	16.65	-2.24	18.89	648	292	4805
C14-33	22.3	*Y. crassus*	-1.22	-5.94	33.15	-8.96	42.11	819	357	960
C14-34	23.6	*Y. crassus*	-1.21	-5.72	-	-	-	526	416	972
C14-35	24.8	*Y. crassus*	-1.01	-6.23	21.09	1.90	19.19	592	403	3629
C14-36	26.0	*Y. crassus*	-1.32	-5.79	-	-	-	724	297	767

Table 2.1. continued.

Sample	Height* (m)	Conodont Zone	$\delta^{13}C_{carb}$ (‰ PDB)	$\delta^{18}O$	$\delta^{34}S_{CAS}$ (‰ VCDT)	$\delta^{34}S_{PY}$	$\Delta^{34}S$	Sr (ppm)	Mn	Fe
C14-37	27.3	*Y. crassus*	-0.94	-6.06	27.07	1.49	25.57	544	272	766
C14-38	28.5	*Y. crassus*	-0.89	-6.11	-	-	-	612	408	2304
C14-39	29.8	*Y. crassus*	-0.76	-5.60	23.83	-13.64	37.48	517	363	856
C14-40	31.0	*Y. crassus*	-0.73	-6.29	-	-	-	474	414	1272
C14-41	32.3	*Y. crassus*	-0.95	-5.85	14.15	-12.97	27.11	597	435	1679
C14-42	33.5	*Y. crassus*	-0.93	-5.78	-	-	-	451	412	937
C14-43	34.7	*Y. crassus*	-0.86	-5.51	24.39	2.98	21.41	452	359	1512
C14-44	36.0	*Y. crassus*	-0.66	-6.28	24.36	-13.17	37.53	402	363	1026
C14-45	37.2	*E. pseudoplanus*	-1.43	-5.86	22.66	-9.82	32.47	386	564	1445
C14-45	37.2	*E. pseudoplanus*	-0.98	-5.45	-	-	-	466	466	1479
C14-46	38.5	*E. pseudoplanus*	-0.96	-5.93	-	-	-	1086	500	6236
C14-47	39.7	*E. pseudoplanus*	-0.92	-5.98	28.59	-7.47	36.07	1157	356	3664
C14-48	40.9	*E. pseudoplanus*	-0.50	-5.81	-	-	-	324	423	1414
C14-49	42.2	*E. pseudoplanus*	-0.12	-5.70	27.88	-	27.88	293	434	1280
C14-50	43.4	*E. pseudoplanus*	-0.54	-5.99	-	-	-	341	591	1369
C14-51	44.7	*E. pseudoplanus*	-0.58	-5.74	32.99	17.40	15.59	450	391	3678
C14-52	45.9	*E. pseudoplanus*	-0.69	-6.35	-	-	-	556	631	3956
C14-53	47.1	*E. pseudoplanus*	-0.56	-6.26	22.85	-9.16	32.01	327	374	659

Table 2.1. continued.

Sample	Height* (m)	Conodont Zone	$\delta^{13}C_{carb}$ (‰ PDB)	$\delta^{18}O$	$\delta^{34}S_{CAS}$ (‰ VCDT)	$\delta^{34}S_{PY}$	$\Delta^{34}S$	Sr (ppm)	Mn	Fe
C14-54	48.4	*E. pseudoplanus*	-0.32	-5.78	23.27	-3.23	26.50	371	573	2125
C14-55	49.6	*E. pseudoplanus*	-0.17	-6.18	25.77	12.86	12.91	352	539	2035
C14-56	50.9	*E. pseudoplanus*	0.11	-6.18	-	-	-	310	608	2735
C14-57	52.1	*E. pseudoplanus*	0.11	-6.38	25.02	11.55	13.46	352	517	1810
C14-58	53.3	*E. pseudoplanus*	0.17	-5.77	-	-	-	310	463	1687
C14-79	53.7	*E. pseudoplanus*	0.347	-4.85	-	-	-	322	527	2173
C14-80	53.7	*E. pseudoplanus*	-0.184	-4.47	-	-	-	293	575	4652
C14-82	53.7	*E. pseudoplanus*	-0.271	-4.23	-	-	-	296	529	1754
C14-84	54.1	*E. pseudoplanus*	0.093	-3.91	-	-	-	278	524	1468
C14-85	54.1	*E. pseudoplanus*	0.191	-5.19	-	-	-	442	512	4376
C14-86	54.1	*E. pseudoplanus*	0.025	-4.91	-	-	-	427	510	2369
C14-87	54.1	*E. pseudoplanus*	0.277	-4.78	-	-	-	314	549	3398
C14-90	54.5	*E. pseudoplanus*	0.182	-3.14	-	-	-	221	413	1885
C14-91	54.5	*E. pseudoplanus*	-0.087	-4.44	-	-	-	298	538	2644
C14-92	54.5	*E. pseudoplanus*	-0.018	-4.91	-	-	-	272	495	2318
C14-59	54.6	*E. pseudoplanus*	0.18	-5.99	-	-	-	337	439	1428
C14-93	54.9	*E. pseudoplanus*	0.453	-5.48	-	-	-	258	691	2386
C14-94	54.9	*E. pseudoplanus*	0.202	-4.33	-	-	-	339	569	2701

Table 2.1. continued.

Sample	Height* (m)	Conodont Zone	$\delta^{13}C_{carb}$ (‰ PDB)	$\delta^{18}O$	$\delta^{34}S_{CAS}$ (‰ VCDT)	$\delta^{34}S_{PY}$	$\Delta^{34}S$	Sr (ppm)	Mn	Fe
C14-95	54.9	*E. pseudoplanus*	-0.135	-6.82	-	-	-	174	273	1925
C14-96	54.9	*E. pseudoplanus*	-0.316	-5.92	-	-	-	326	716	3405
C14-97	54.9	*E. pseudoplanus*	-0.122	-4.20	-	-	-	280	587	2219
C14-100	55.3	*E. pseudoplanus*	0.219	-5.33	-	-	-	299	703	2062
C14-101	55.3	*E. pseudoplanus*	0.959	-3.89	-	-	-	311	653	2579
C14-102	55.3	*E. pseudoplanus*	0.019	-5.18	-	-	-	318	733	2998
C14-98	55.3	*E. pseudoplanus*	0.313	-5.34	-	-	-	324	625	2698
C14-99	55.3	*E. pseudoplanus*	0.234	-4.10	-	-	-	327	704	2456
C14-60	55.8	*E. pseudoplanus*	0.07	-5.72	-	-	-	436	410	2158
C14-62	58.3	*E. suecicus*	0.55	-7.13	26.48	2.85	23.63	400	278	1405
C14-64	60.8	*E. suecicus*	0.30	-5.81	27.20	8.22	18.98	1000	171	626
C14-65	62.0	*E. suecicus*	-	-	-	-	-	1330	286	1081
C14-66	63.3	*E. suecicus*	0.10	-6.39	26.09	9.99	16.10	762	233	889
C14-67	64.5	*E. suecicus*	1.41	-7.23	-	-	-	621	169	767
C14-68	65.0	*P. anserinus*	0.70	-6.94	24.75	14.90	9.85	695	203	1421

Table 2.1. continued.

Sample	Height* (m)	Conodont Zone	$\delta^{13}C_{carb}$ (‰ PDB)	$\delta^{18}O$	$\delta^{34}S_{CAS}$ (‰ VCDT)	$\delta^{34}S_{PY}$	$\Delta^{34}S$	Sr (ppm)	Mn	Fe
C14-69	65.5	*P. anserinus*	0.33	-6.84	-	-	-	1075	534	8362
C14-70	70.0	*P. anserinus*	0.18	-6.76	10.40	3.95	6.45	854	446	6954
C14-71	71.0	*P. anserinus*	0.78	-7.01	-	-	-	1021	472	5115
C14-72	72.0	*P. anserinus*	0.30	-6.79	18.54	4.24	14.30	1053	602	11496
C14-73	73.0	*P. anserinus*	0.33	-6.98	-	-	-	1078	438	5876
C14-74	74.0	*P. anserinus*	-0.14	-7.03	23.25	12.12	11.13	1066	470	6394
C14-75	75.0	*P. anserinus*	-0.56	-6.44	11.65	-1.81	13.47	603	420	2448
C14-77	77.0	*P. anserinus*	-0.15	-6.73	-	-	-	785	584	3617

*Stratigraphic height measured relative to the contact between the San Juan and Las Chacritas formations

Table 2.2: Range of isotopic compositions and elemental concentrations recorded in the Las Aguaditas Creek Section

Sample	Height* (m)	Conodont Zone	$\delta^{13}C_{carb}$ (‰ PDB)	$\delta^{18}O$	$\delta^{34}S_{CAS}$ (‰ VCDT)	$\delta^{34}S_{PY}$	$\Delta^{34}S$	Sr (ppm)	Mn	Fe
A14-1	-16.0	*Y. crassus*	-0.58	-5.62	21.50	3.74	17.76	431	456	1909
A14-2	-15.0	*Y. crassus*	-0.61	-5.29	-	-	-	405	627	2764
A14-2	-15.0	*Y. crassus*	-0.66	-5.36	-	-	-	396	716	2194
A14-3	-14.0	*Y. crassus*	-0.54	-5.58	35.34	16.76	18.59	474	690	3005
A14-4	-13.0	*Y. crassus*	-0.36	-5.65	-	-	-	409	807	2781
A14-5	-12.0	*Y. crassus*	-0.29	-5.49	25.28	-	25.28	488	1119	2832
A14-6	-11.0	*Y. crassus*	-0.23	-5.38	-	-	-	599	1213	3547
A14-7	-10.0	*Y. crassus*	0.19	-5.36	26.50	25.77	0.73	443	1170	1890
A14-8	-9.0	*Y. crassus*	-0.12	-5.43	-	-	-	501	1795	3009
A14-9	-8.0	*Y. crassus*	-0.26	-5.14	25.92		25.92	466	1658	4227
A14-10	-7.0	*Y. crassus*	-0.37	-5.41	-	-	-	675	1490	3034
A14-11	-6.0	*Y. crassus*	-0.28	-5.23	26.87	3.40	23.48	550	2297	3964
A14-12	-5.0	*Y. crassus*	-0.10	-5.54	-	-	-	578	1300	3632
A14-13	-4.0	*Y. crassus*	-0.25	-5.13	25.02	10.29	14.73	572	1654	3225
A14-14	-3.0	*Y. crassus*	-0.22	-5.10	-	-	-	614	3065	2865
A14-15	-2.0	*Y. crassus*	-0.13	-5.37	27.74	15.64	12.10	487	1644	3521
A14-16	-1.0	*Y. crassus*	-0.43	-5.44	26.45		26.45	783	1897	4662
A14-17	0.0	*Y. crassus*	-0.37	-5.32	27.98	16.73	11.25	492	3274	2963

Table 2.2. continued.

Sample	Height* (m)	Conodont Zone	$\delta^{13}C_{carb}$ (‰ PDB)	$\delta^{18}O$	$\delta^{34}S_{CAS}$ (‰ VCDT)	$\delta^{34}S_{PY}$	$\Delta^{34}S$	Sr (ppm)	Mn	Fe
A14-20	3.0	*Y. crassus*	-0.55	-4.30	24.51	-6.56	31.07	705	693	5606
A14-21	4.0	*Y. crassus*	-0.69	-5.32	-	-	-	963	1265	5403
A14-21	4.0	*Y. crassus*	-0.73	-5.19	-	-	-	975	615	4959
A14-22	5.0	*Y. crassus*	-	-	18.13	16.07	2.06	-	-	
A14-23	6.0	*Y. crassus*	-0.52	-5.58	13.31		13.31	1075	622	3523
A14-25	8.0	*Y. crassus*	-0.41	-4.69	24.41	3.18	21.23	857	379	3081
A14-26	9.0	*Y. crassus*	-0.36	-5.28	-	-	-	1010	380	3135
A14-27	10.0	*Y. crassus*	-0.54	-5.44	11.02	-5.82	16.83	991	587	4670
A14-28	11.0	*Y. crassus*	-0.36	-5.28	-	-	-	906	378	2814
A14-29	12.0	*Y. crassus*	-0.95	-4.95	13.26	11.65	1.61	815	484	4902
A14-30	13.0	*Y. crassus*	-0.57	-5.27	-	-	-	1016	396	4069
A14-31	14.0	*Y. crassus*	-0.63	-5.28	32.43	-3.16	35.58	1250	317	1764
A14-33	16.0	*Y. crassus*	-1.28	-5.36	16.23	7.49	8.74	1060	427	3670
A14-35	18.0	*Y. crassus*	-0.40	-5.69	-	-	-	951	540	4880
A14-36	19.0	*E. pseudoplanus/ D. tablepointensis*	-0.45	-4.85	-	-	-	663	302	2767

Table 2.2. continued.

Sample	Height* (m)	Conodont Zone	$\delta^{13}C_{carb}$ (‰ PDB)	$\delta^{18}O$	$\delta^{34}S_{CAS}$ (‰ VCDT)	$\delta^{34}S_{PY}$	$\Delta^{34}S$	Sr (ppm)	Mn	Fe
A14-37	20.0	*E. pseudoplanus/ D. tablepointensis*	-0.29	-5.48	11.88	2.08	9.80	959	413	1826
A14-38	21.0	*E. pseudoplanus/ D. tablepointensis*	-0.84	-5.48	-	-	-	1011	391	4022
A14-39	22.0	*E. pseudoplanus/ D. tablepointensis*	-0.36	-5.81	32.52	9.54	22.97	1229	267	1069
A14-40	23.0	*E. pseudoplanus/ D. tablepointensis*	-2.25	-5.42	-	-	-	866	369	1643
A14-41	24.0	*E. pseudoplanus/ D. tablepointensis*	-1.52	-5.32	16.88	6.50	10.38	-	-	-
A14-42	25.0	*E. pseudoplanus/ D. tablepointensis*	-	-	-	-	-	-	-	-
A14-43	26.0	*E. pseudoplanus/ D. tablepointensis*	-0.71	-5.29	18.22	20.60	-2.39	1233	215	873
A14-44	27.0	*E. pseudoplanus/ D. tablepointensis*	-1.21	-5.51	-	-	-	1175	282	1046
A14-45	28.0	*E. pseudoplanus/ D. tablepointensis*	-0.84	-5.60	20.89	17.52	3.37	1560	280	1609

Table 2.2. continued.

Sample	Height* (m)	Conodont Zone	$\delta^{13}C_{carb}$ (‰ PDB)	$\delta^{18}O$	$\delta^{34}S_{CAS}$ (‰ VCDT)	$\delta^{34}S_{PY}$	$\Delta^{34}S$	Sr (ppm)	Mn	Fe
A14-46	29.0	*E. pseudoplanus/ D. tablepointensis*	-	-	-	-	-	-	-	-
A14-47	30.0	*E. pseudoplanus/ D. tablepointensis*	-1.75	-5.15	37.49	15.88	21.61	1748	321	3593
A14-48	31.0	*E. pseudoplanus/ D. tablepointensis*	-1.56	-5.36	-	-	-	743	233	1429
A14-50	33.0	*E. pseudoplanus/ D. tablepointensis*	-0.59	-5.08	19.67	14.59	5.08	1652	263	2564
A14-51	34.0	*E. pseudoplanus/ D. tablepointensis*	-1.20	-4.83	16.15	5.55	10.61	1120	538	2740
A14-52	35.0	*E. pseudoplanus/ D. tablepointensis*	-0.88	-4.82	-	-	-	1156	368	1802
A14-53	36.0	*E. pseudoplanus/ D. tablepointensis*	-1.14	-4.96	41.56		41.56	1048	372	1172
A14-54	37.0	*E. pseudoplanus/ D. tablepointensis*	-1.64	-4.98	-	-	-	944	408	1080
A14-55	38.0	*E. pseudoplanus/ D. tablepointensis*	-1.48	-4.76	28.14	14.22	13.92	955	417	1340

Table 2.2. continued.

Sample	Height* (m)	Conodont Zone	$\delta^{13}C_{carb}$ (‰ PDB)	$\delta^{18}O$	$\delta^{34}S_{CAS}$ (‰ VCDT)	$\delta^{34}S_{PY}$	$\Delta^{34}S$	Sr (ppm)	Mn	Fe
A14-56	39.0	*E. pseudoplanus/ D. tablepointensis*	-	-	-	-	-	-	-	-
A14-57	40.0	*E. pseudoplanus/ D. tablepointensis*	-1.36	-5.00	35.77	14.43	21.34	1795	495	3226
A14-58	41.0	*E. pseudoplanus/ D. tablepointensis*	-1.69	-4.68	-	-	-	1037	357	1792
A14-59	42.0	*E. pseudoplanus/ D. tablepointensis*	-2.09	-4.88	-	-	-	518	290	1021
A14-59	42.0	*E. pseudoplanus/ D. tablepointensis*	-1.16	-5.17	-	-	-	2166	475	6715
A60-1	43.0	*E. pseudoplanus/ D. tablepointensis*	-	-	36.76	-6.20	42.96	-	-	-
A14-65	43.2	*P. anserinus*	0.42	-4.07	-	-	-	352	378	625
A14-65	43.2	*P. anserinus*	0.42	-4.07	-	-	-	352	378	625
A14-77	43.2	*P. anserinus*	0.24	-4.318	-	-	-	446	406	3015
A14-82	43.2	*P. anserinus*	0.052	-4.629	-	-	-	560	349	6525
A14-87	43.2	*P. anserinus*	0.187	-5.067	-	-	-	478	340	1254
A14-92	43.2	*P. anserinus*	0.275	-4.704	-	-	-	343	338	525

Table 2.2. continued.

Sample	Height* (m)	Conodont Zone	$\delta^{13}C_{carb}$ (‰ PDB)	$\delta^{18}O$	$\delta^{34}S_{CAS}$ (‰ VCDT)	$\delta^{34}S_{PY}$	$\Delta^{34}S$	Sr (ppm)	Mn	Fe
A14-64	43.4	*P. anserinus*	0.03	-4.07	-	-	-	327	374	659
A14-64	43.4	*P. anserinus*	0.03	-4.07	-	-	-	327	374	659
A14-78	43.4	*P. anserinus*	0.325	-4.691	-	-	-	475	370	3200
A14-83	43.4	*P. anserinus*	0	-4.311	-	-	-	-	-	-
A14-88	43.4	*P. anserinus*	0.298	-4.979	-	-	-	397	339	836
A14-93	43.4	*P. anserinus*	0.487	-4.964	-	-	-	436	322	712
A14-79	43.6	*P. anserinus*	0.344	-4.733	-	-	-	614	325	4531
A14-84	43.6	*P. anserinus*	0.285	-4.426	-	-	-	361	286	739
A14-89	43.6	*P. anserinus*	0.324	-4.832	-	-	-	413	335	1056
A14-62	43.8	*P. anserinus*	0.25	-4.80	-	-	-	496	298	1125
A14-62	43.8	*P. anserinus*	0.25	-4.8	35.80	7.01	28.79	496	298	1125
A14-80	43.8	*P. anserinus*	0.279	-4.69	-	-	-	490	300	1402
A14-90	43.8	*P. anserinus*	0.339	-4.798	-	-	-	440	293	598
A14-85	43.8	*P. anserinus*	0.133	-4.551	-	-	-	-	-	-
A14-61	44.0	*P. anserinus*	0.11	-4.28	-	-	-	450	391	3678
A14-61	44.0	*P. anserinus*	0.11	-4.28	-	-	-	450	391	3678
A14-81	44.0	*P. anserinus*	0.039	-4.505	-	-	-	548	314	2547

Table 2.2. continued.

Sample	Height* (m)	Conodont Zone	$\delta^{13}C_{carb}$ (‰ PDB)	$\delta^{18}O$	$\delta^{34}S_{CAS}$ (‰ VCDT)	$\delta^{34}S_{PY}$	$\Delta^{34}S$	Sr (ppm)	Mn	Fe
A14-91	44.0	*P. anserinus*	-0.218	-5.504	-	-	-	483	1691	5448
A14-96	44.0	*P. anserinus*	0.385	-4.68	-	-	-	283	363	573
A14-66	45.0	*P. anserinus*	-0.26	-4.10	40.44	19.94	20.50	880	244	1908
A14-67	46.0	*P. anserinus*	0.24	-4.51	-	-	-	1295	164	3938
A14-68	47.0	*P. anserinus*	0.29	-4.39	17.32	19.29	-1.98	1288	164	3300
A14-69	48.0	*P. anserinus*	0.33	-4.15	-	-	-	1309	163	2197
A14-70	49.0	*P. anserinus*	0.56	-4.37	17.68	16.46	1.22	1383	172	2459
A14-71	50.0	*P. anserinus*	0.39	-4.06	-	-	-	1365	171	2659
A14-72	51.0	*P. anserinus*	-	-	15.68	19.66	-3.98	-	-	-
A14-73	52.0	*P. anserinus*	-	-	-	-	-	-	-	-
A14-74	53.0	*P. anserinus*	-	-	35.69	20.75	14.95	-	-	-
A14-75	54.0	*P. anserinus*	-	-	-	-	-	-	-	-
A14-76	55.0	*P. anserinus*	-	-	23.07	20.63	2.44	-	-	-

*Stratigraphic height measured relative to the contact between the San Juan and Las Aguaditas formations

Table 2.3: Range of isotopic compositions and elemental concentrations recorded in the Gualcamayo Formation at La Corridita Creek

Sample	Height* (m)	Conodont Zone	$\delta^{34}S_{CAS}$ (‰ VCDT)	$\delta^{34}S_{PY}$	$\Delta^{34}S$	Sr (ppm)	Mn	Fe	Mo	V
G14- 11	11	*P. gladysi*	-1.80	-2.33	0.53	272	198	7600	1	8
G14- 15	15	*P. gladysi*	-	-	-	158	156	14600	4	12
G14- 17	17	*P. gladysi*	-2.76	1.88	-4.63	268	136	14000	4	13
G14- 23	23	*P. gladysi*	0.24	-21.52	21.75	87	151	10600	5	32
G14- 29	29	*P. gladysi*	0.66	-13.22	13.89	43	87	6500	6	13
G14- 35.2	35.2	*P. gladysi*	4.00	-10.63	14.63	204	950	15900	6	11
G14- 40.5	40.5	*P. gladysi*	5.79	-4.17	9.95	40	145	15100	12	74
G14- 46.5	46.5	*L. variabilis*	5.47	-4.07	9.54	60	45	14500	13	80
G14- 49.5	49.5	*L. variabilis*	-	-	-	56	53	20800	22	55
G14- 54	54	*L. variabilis*	-4.63	-15.46	10.83	57	214	21500	14	49
G14- 59.5	59.5	*L. variabilis*	-4.90	-14.50	9.60	65	119	25200	16	33
G14- 62.5	62.5	*L. variabilis*	-	-	-	98	<5	16600	23	69
G14- 65.5	65.5	*L. variabilis*	0.88	-9.14	10.02	43	110	20100	11	65
G14- 71.5	71.5	*L. variabilis*	0.00	-13.80	13.79	56	252	24400	14	56
G14- 74.5	74.5	*L. variabilis*	-	-	-	31	247	25200	17	51
G14- 77.5	77.5	*L. variabilis*	3.05	3.80	-0.75	50	358	20100	9	76
G14- 83.5	83.5	*L. variabilis*	0.83	4.90	-4.07	49	339	21000	10	57

Table 2.3. continued.

Sample	Height* (m)	Conodont Zone	$\delta^{34}S_{CAS}$ (‰ VCDT)	$\delta^{34}S_{PY}$	$\Delta^{34}S$	Sr (ppm)	Mn	Fe	Mo	V
G14- 89.5	89.5	*L. variabilis*	-3.48	3.60	-7.08	69	37	26900	15	26
G14- 95.5	95.5	*L. variabilis*	-0.79	9.51	-10.30	173	30	25700	20	41
G14- 98.5	98.5	*L. variabilis*	-	-	-	57	34	17200	4	19
G14- 101.5	101.5	*L. variabilis*	3.89	5.26	-1.37	101	355	27600	15	47
G14- 104.5	104.5	*L. variabilis*	-	-	-	34	427	20200	7	59
G14- 107.5	107.5	*L. variabilis*	8.19	4.05	4.14	37	147	21100	9	85
G14- 112	112	*L. variabilis*	-	-	-	103	47	19000	11	93
G14- 115	115	*L. variabilis*	-	-	-	96	45	19100	6	52
G14- 119.5	119.5	*L. variabilis*	8.21	-1.39	9.60	80	73	21400	11	38
G14- 122.5	122.5	*L. variabilis*	-	-	-	41	74	17900	6	44
G14- 125.5	125.5	*L. variabilis*	1.65	-2.57	4.22	49	146	15900	3	36
G14- 128.5	128.5	*L. variabilis*	4.61	0.84	3.77	52	89	15200	8	66
G14- 131.5	131.5	*L. variabilis*	-	-	-	60	156	15300	6	40
G14- 134.5	134.5	*L. variabilis*	5.85	11.78	-5.93	70	72	18100	12	80
G14- 140.5	140.5	*H. kristinae*	13.73	11.28	2.44	123	57	14300	8	84
G14- 143.5	143.5	*H. kristinae*	-	-	-	56	140	19400	17	76
G14- 146.5	146.5	*H. kristinae*	9.93	8.82	1.12	92	44	20500	13	93
G14- 152.5	152.5	*H. kristinae*	1.58	4.89	-3.31	100	36	14800	9	91

Table 2.3. continued.

Sample	Height* (m)	Conodont Zone	$\delta^{34}S_{CAS}$ (‰ VCDT)	$\delta^{34}S_{PY}$	$\Delta^{34}S$	Sr (ppm)	Mn	Fe	Mo	V
G14- 161	161	*H. kristinae*	1.57	6.65	-5.08	148	171	18100	11	117
G14- 167	167	*H. kristinae*	6.40	7.26	-0.86	44	138	15900	7	72
G14- 171.5	171.5	*H. kristinae*	-	10.27	-	67	5	3600	8	26
G14- 177.5	177.5	*H. kristinae*	9.25	7.60	1.65	53	81	22500	2	20
G14- 183.5	183.5	*H. kristinae*	-	13.75	-13.75	181	170	17200	9	28
G14- 189.5	189.5	*H. kristinae*	10.02	8.48	1.54	57	15	5500	2	17
G14- 192.5	192.5	*H. kristinae*	-	-	-	79	24	7800	4	36
G14- 195.5	195.5	*H. kristinae*	7.11	6.39	0.72	63	79	13300	6	45
G14- 201.5	201.5	*H. kristinae*	1.69	15.62	-13.93	40	23	9000	7	55
G14- 207.5	207.5	*H. kristinae*	10.84	9.05	1.79	38	36	11300	6	37
G14- 213.5	213.5	*H. kristinae*	6.01	11.66	-5.65	43	27	8500	9	76
G14- 219.5	219.5	*P. anitae*	4.58	10.26	-5.68	43	6	2500	6	33
G14- 222.5	225.5	*P. anitae*	4.46	14.91	-10.45	82	24	9300	9	51
G14- 227	227	*P. anitae*	-	-	-	52	5	1800	5	43
G14- 231.5	231.5	*P. anitae*	3.38	10.07	-6.69	48	190	21000	4	36
G14- 234.5	234.5	*P. anitae*	-	-	-	140	264	42100	12	67
G14- 237.5	237.5	*P. anitae*	0.18	6.57	-6.38	58	13	15800	8	35
G14- 243.5	243.5	*P. anitae*	-	6.17	-6.17	40	< 5	1200	1	21

Table 2.3. continued.

Sample	Height* (m)	Conodont Zone	$\delta^{34}S_{CAS}$ (‰ VCDT)	$\delta^{34}S_{PY}$	$\Delta^{34}S$	Sr (ppm)	Mn	Fe	Mo	V
G14- 248	248	*P. anitae*	6.64	10.79	-4.14	37	7	4800	12	27
G14- 254	254	*P. anitae*	5.17	9.27	-4.10	57	42	8900	7	17
G14- 260	260	*P. anitae*		12.25	-12.25	41	5	1600	2	28
G14- 263	263	*P. anitae*	-	-	-	45	58	16000	3	34
G14- 269	269	*P. anitae*	6.50	-	-	76	357	31300	13	34
G14- 274.5	274.5	*P. anitae*	0.04	5.08	-5.04	66	212	38900	12	46

*Stratigraphic height measured relative to the contact between the San Juan and Gualcamayo formations

Table 2.4: Summary of Darriwilian isotopic compositions from the Precordillera

	$\delta^{13}C_{carb}$	$\delta^{18}O_{carb}$	$\delta^{34}S_{CAS}$	$\delta^{34}S_{PY}$	$\Delta^{34}S$	Sr	Mn	Fe
Las Chacritas River Section								
San Juan								
Average	-0.78	-5.59	26.17	-2.88	29.06	366	616	2329
St. Dev.	0.51	0.18	5.64	9.09	11.61	103	370	1712
Pre-MDICE								
Average	-0.87	-5.86	24.35	-3.98	28.33	629	415	2232
St. Dev.	0.21	0.20	6.45	5.99	9.35	117	146	1729
MDICE								
Average	-0.07	-5.46	26.10	1.82	24.43	430	493	2266
St. Dev.	0.52	0.91	2.78	10.27	8.55	252	142	1143
Las Aguaditas Creek Section								
San Juan								
Average	-0.31	-5.38	26.86	13.19	17.63	520	1493	3113
St. Dev.	0.20	0.16	3.31	7.40	7.78	100	765	716
Pre-MDICE								
Average	-0.61	-5.20	19.16	3.26	16.31	967	545	4037
St. Dev.	0.25	0.34	7.04	8.88	11.17	174	739	1098
MDICE								
Average	-1.19	-5.16	26.33	10.43	15.48	1179	353	2166
St. Dev	0.54	0.31	9.74	7.49	13.76	404	86	1378
Gualcamayo Formation at La Corridita Creek								
Transitional								
Average	--	--	-2.28	-0.23	-2.05	233	163	12067
St. Dev.	--	--	0.68	2.97	3.65	65	32	3880
Middle Member (lower)								
Average	--	--	0.83	-11.83	12.67	90	206	17100
St. Dev.	--	--	3.87	5.56	3.97	46.83	267	5720
Middle Member (upper)								
Average	--	--	4.87	7.71	-3.29	69	111	16529
St. Dev	--	--	3.87	4.22	5.56	36	114	8956

Chapter 3
Neodymium and strontium isotope stratigraphy of Middle Ordovician carbonate sediments in Argentina: Investigating the link between biogeochemical cycling and physical changes in ocean chemistry

Abstract

Dramatic changes in the biogeochemical cycles of carbon and sulfur have been recognized in the Ordovician. Specifically, initiation of the Middle Darriwilian Isotope Carbon Excursion (MDICE) corresponds to a sharp change in the isotopic composition of both carbonate-associated sulfate (CAS) and pyrite and extends through an interval marked by deposition of "superheavy" pyrite (i.e. where S-isotope values of pyrite are heavier than associated values for marine sulfate). These geochemical changes have been attributed to changes in marine circulation that result in deep-water ventilation and shifting nutrient fluxes associated with redox stratification of the Ordovician oceans. Interestingly, these biogeochemical changes are coincident with a globally recognized shift in the $^{87}Sr/^{86}Sr$ value of seawater, which decreases from ~0.7090 in the Middle Darriwilian (ca. 462 Ma) to ~0.7078 by the early Sandbian (ca. 458). Traditionally, the isotopic composition of marine strontium is thought to be homogeneous in the ocean because of its long residence time in seawater. However, during times of persistent ocean stratification, as observed for the Early-Middle Ordovician, marine strontium may have behaved differently, potentially resulting in the development of a strontium isotope gradient between shallow and deep-water.

Here we present new strontium and neodymium isotope data from the Middle Darriwilian Las Chacritas and Las Aguaditas formations of the Argentine Precordillera, which represent coeval shallower- and deeper-water depositional environments. These formations occur just prior to the start of the large shift in Sr-isotope compositions observed worldwide. $^{87}Sr/^{86}Sr$ data from these formations fit within the global framework for Sr-isotope change with values ranging from above 0.7090 to approximately 0.7088.

To test whether distinct oceanographic reservoirs of Sr, or a persistent gradient in marine Sr-isotope composition, may play a role in the observed $^{87}Sr/^{86}Sr$ change of Middle Ordovician oceans, we examine the relative behavior of strontium and neodymium—which has a much shorter residence time than Sr and has been used to distinguish discrete oceanic water masses—in these successions. Environmental differences in the isotopic composition of both strontium and neodymium in the units suggests geochemical decoupling between shallow and deep waters, confirming the presence of physical stratification in Middle Darriwilian ocean waters in the Precordillera.

1. Introduction

Coincident changes in the isotopic composition of carbon and sulfur are recorded in Darriwilian aged marine sedimentary rocks worldwide. Most notably is the Middle Darriwilian carbon isotope excursion (MDICE), which is represented globally as a positive 2‰ shift in the isotopic composition of marine carbonate (Ainsaar et al., 2004; Meidla et al., 2004; Ainsaar et al., 2007; Kaljo et al., 2007; Schmitz et al., 2010; Zhang et al., 2010; Thompson et al., 2012; Albanesi et al., 2013; Calner et al., 2014; Kah et al., 2016; Young et al., 2016; Henderson et al., 2018). Whereas large-scale changes in the C-isotope composition of marine carbonate in the Paleozoic have been interpreted to reflect vigorous oceanographic circulation and enhanced nutrient availability in icehouse climate states (Saltzman, 2005), more muted C-isotope variability has been attributed to sluggish ocean circulation and nitrogen limitation during greenhouse conditions that reduced productivity and organic carbon burial. A decline in sea-surface temperatures through the early Ordovician to values near modern temperatures (Trotter et al., 2008), would have

initiated a change from greenhouse to icehouse circulation in the Darriwilian. Evidence for enhanced mixing and ultimate ventilation of anoxic deep-water is suggested by both the MDICE excursion and coeval changes in the S-isotope composition of carbonate associated sulfate (CAS) and sedimentary pyrite that are interpreted to reflect ventilation of a deep-ocean anoxic water body (Thompson and Kah, 2012; Kah et al., 2016). Recent geochemical evidence from the Precordillera of Argentina confirms the persistence of a strong chemocline in the Middle Darriwilian and heterogeneous carbon and sulfur isotope signatures between shallow and deep-water during this period of ocean stratification (cf. Henderson et al., 2018; Henderson et al., *in prep*.).

The largest shift in the strontium isotope composition of the Paleozoic (Veizer and Compston, 1974; Burke et al., 1982; McArthur, 1994) coincides with both carbon and sulfur isotope evidence for an ocean ventilation event in the Darriwilian. The strontium isotope composition of the ocean, recorded as the $^{87}Sr/^{86}Sr$ of marine carbonate and biogenic apatite, falls from near 0.7090 in the Early Darriwilian to 0.7078 by the Middle Sandbian (Fig. 1). The nature of this decline has traditionally been explained by changes in the weathering rates of the continental ($^{87}Sr/^{86}Sr >0.7100$) and oceanic ($^{87}Sr/^{86}Sr < 0.7040$) sources (Qing et al., 1998; Shields et al., 2003; Young et al., 2009). Large changes in the isotopic composition of marine Sr through time are inferred to reflect large scale changes in continental weathering linked to orogenesis, in which continental weathering of ancient crust supplies radiogenic strontium to the ocean (Richter et al., 1992; Montañez et al., 1996; Qing et al., 1998) or periods of high volcanic activity and weathering of young volcanic rock (Ronov, 1980; Wright et al., 2002;

Shields et al., 2003; Young et al., 2009), which supplies non-radiogenic strontium to the ocean. Such drastic change in the strontium isotope record of seawater over this time (5–10 x 10^{-5} per m.y.; Saltzman et al., 2014) is, however, difficult to reconcile with the large reservoir size and residence time (~5 million years; Banner, 2004) of strontium in the ocean. Previous modeling efforts to characterize this change would require a 25-fold increase in the continental weathering flux of volcanic arc terranes to maintain the observed rates of Sr-isotope change in the Darriwilian-Sandbian.

During greenhouse periods characterized by sluggish ocean circulation and stratification, like that of the Early-Middle Ordovician, however, there is the potential to develop oceanic reservoirs with distinct Sr-isotope compositions (Banner, 2004). In such a case, the rapid change in the Sr-isotope composition of well-mixed surface waters could reflect changes in ocean circulation that result in the mixing of distinct oceanic reservoirs. Such an oceanic mechanism could drive isotopic change at rates that are potentially inconsistent with traditional models for the behavior of marine $^{87}Sr/^{86}Sr$. In this scenario, radiogenic Sr delivered to the ocean via continental weathering would dominate the Sr-isotopic composition of surface waters, whereas the Sr-isotope composition of deep-water would be influenced by non-radiogenic Sr from alteration of ocean crust. Invigorated ocean circulation in the Darriwilian would have mixed these shallow- and deep-water reservoirs potentially driving, or at least contributing, to the observed $^{87}Sr/^{86}Sr$ shift. To investigate whether changes in ocean circulation and disruption of stratified ocean conditions may have contributed to the dramatic nature of the observed Sr-isotope change, we examined the strontium and neodymium isotope record of marine

carbonates from the Precordillera of Argentina across coeval shallow and deeper water facies. Like strontium, neodymium isotope compositions reflect the composition of their source terrane; however, unlike Sr, which has a long residence time in seawater, Nd has a drastically shorter residence time (~600 years; Banner, 2004), is rapidly scavenged from the water column (Taylor and McLennan, 1985), and commonly records discrete oceanic reservoirs (Holmden et al., 1998; MacLeod et al., 2011; Martin et al., 2012). Because of this behavior, Nd can resolve oceanographic reservoirs with distinct isotopic compositions controlled by the mean age of the weathered crustal material (Piepgras et al., 1979; Piepgras and Wasserburg, 1980). Here we present new Nd- and Sr-isotope data from Darriwilian age strata from the Precordillera of Argentina to evaluate the potential for an oceanographic component, potentially recorded as a shift in Nd-isotope compositions, to the globally recognized drop in $^{87}Sr/^{86}Sr$ of marine carbonate.

2. Geologic setting and background

2.1. Tectonic setting

The Precordillera of Argentina is a remnant microcontinent terrane that rifted from the southeast marine of Laurentia in the early Cambrian (ca. 530-539 Ma; Thomas et al., 2001) and was transferred across the Iapetus ocean before converging with Gondwana in the Late Ordovician (Fig. 2; Ramos et al., 1986; Astini et al., 1995; Thomas and Astini, 1996; Thomas and Astini, 1999; Thomas et al., 2002; Thomas, 2011). Although the paleogeographic location of the Precordillera is not well constrained, proximity to the Laurentian margin in the early Cambrian is supported by detrital zircon ages and Gondwanan faunal assemblages (Astini et al., 1995; Thomas et al., 2001;

Thomas et al., 2015). Transfer across the Iapetus and proximity to the Gondwanan margin by the Ordovician is inferred from a decrease in fauna with Laurentian affinities through the Tremadocian and an increase of Baltic and Gondwanan affinities during the Darriwilian and Sandbian (Astini et al., 1995; Benedetto, 2004; Benedetto et al., 2009). Additionally, abundant bentonite deposits associated accretion of the Famatina volcanic arc with Gondwana (Fig. 2) are identified in Middle Ordovician strata of the Precordillera and indicate proximity of the Precordillera to Gondwana (Astini et al., 1995; Huff et al., 1995; Huff et al., 1997; Huff et al., 1998; Pankhurst et al., 2000; Fanning et al., 2004; Thompson et al., 2012).

A thick section succession (> 2500 m) of Cambrian to Ordovician sedimentary rocks are exposed along North-South trending thrust sheets in the Precordillera of northwestern Argentina between 29˚ and 33˚ S (Ramos et al., 1986) and are subdivided into the western and eastern tectofacies (Astini et al., 1995). Sedimentary deposits of the western tectofacies were subjected to low-grade metamorphism and deformation during regional shortening in the Late Ordovician (Allmendinger et al., 1990; Zapata and Allmendinger, 1996; Allmendinger and Judge, 2014) and are mainly identified as olistoliths within deep-water siliciclastic facies in the Middle-Late Ordovician Los Sombreros Formation (Astini et al., 1995; Keller, 1999). Sedimentary deposits of the eastern tectofacies are weakly deformed and unmetamorphosed and record the transition from the thick Cambrian-Ordovician passive margin carbonate platform succession to synorogenic siliciclastic deposits associated with foreland basin development as the Precordillera terrane approached Gondwana (Astini et al., 1995). Ordovician strata of the

eastern tectofacies are represented by the Early Ordovician La Silla Formation, the Early-Middle Ordovician San Juan Formation, and the Middle-Late Ordovician Las Chacritas, Las Aguaditas, Gualcamayo, and Los Azules formations (Carrera and Astini, 1998).

2.2. Middle Ordovician strata

The transition to Middle Ordovician (Dapingian) strata is located in the San Juan Formation, which consists of intertidal to shallow-subtidal deposits that, by the Darriwilian, transition into storm-dominated subtidal deposits (Keller, 1999; Cañas, 2003). Strata of the San Juan Formation consist of fossiliferous packstone, wackestone, and carbonate mudstone that grade into siliciclastic-rich and siliciclastic-dominated deposits of the Darriwilian-Sandbian Las Chacritas, Las Aguaditas, Los Azules, and Gualcamayo Formations (Keller et al., 1993; Astini, 1994, 1995; Peralta et al., 1999). In this study, we sampled the upper San Juan Formation and the overlying Las Chacritas and Las Aguaditas formations (Fig. 3).

The Las Chacritas Formation was sampled along the Las Chacritas River in the northern La Trampa Range (30°33’39.06” S, 68°51’49.62” W), approximately 37 km south of San Jose de Jáchal. The Las Chacritas Formation consists of a 65-m-thick assemblage of dominantly fossiliferous wackestone and carbonate mudstone with increasing intervals of thinly bedded black shale toward the top of the section (Peralta et al., 1999; Henderson et al., 2018). The Las Chacritas Formation is divided into two members (Peralta et al., 1999); a lower member comprised of 2–10 cm thick beds of fossiliferous mudstone, wackestone, and packstone with < 2 cm thick partings of black shale and an upper member dominated by 2–5-cm-thick fossiliferous wackestone and

spiculitic mudstone beds with thicker (2–5 cm) interbeds of black shale. Based on fossil assemblages (Carrera, 1997) and observed bedding features, the interpreted depositional environment is between fair-weather and storm wave base (Henderson et al., 2018).

The Las Aguaditas Formation was sampled at its type locality along Las Aguaditas Creek in the Los Blanquitos Range (30°18'16.38" S, 68°49'13.40" W), approximately 10 km southwest of San Jose de Jáchal. Here, the Las Aguaditas Formation consists of a 300-m-thick succession of carbonate mudstone, wackestone, and calcareous black shale. Middle-Ordovician strata occur in the 43-m-thick lower member, which is composed of laminated carbonate mudstone and wackestone with interbedded black shale (Feltes et al., 2016; Henderson et al., 2018). Sponge spicules and trilobite fragments dominate the skeletal wackestone of the Las Aguaditas Formation, and laminated mudstone and shale become increasingly common upsection. The section is interpreted as reflecting deposition in relatively deep-water, at or near storm wavebase for the lower portion of the section and deepening to below storm wavebase in the upper part of the measured section.

2.3. Correlation and age

Middle Ordovician strata of the Precordillera are represented by the Dapingian *Baltoniodus triangularis/Tripodus laevis* (Dp1 of Bergström et al., 2009) and *Baltoniodus navis* conodont zones (Dp2), the Dapingian-Darriwilian *Microzarkodina parva* conodont zone (Dp2–Dw1), and the Darriwilian *Lenodus variabilis* (Dw1), *Yangtzeplacognathus crassus* (Dw1–Dw2), *Eoplacognathus pseudoplanus* (Dw2), *Eoplacognathus suecicus* (Dw2*), Pygodus serra* (Dw3), and *Pygodus anserinus* (Dw3–Sa1) conodont zones

(Albanesi and Ortega, 2016). Stratigraphic correlation of Middle Ordovician strata in the fold and thrust belt of the Precordillera is complicated by the diachronous age of the uppermost San Juan Formation, which is younger to the northeast and truncated by unconformities to the southwest (Astini et al., 1995), and by the potential presence of cryptic unconformities in the sections (Heredia et al., 2005; and amended by Heredia and Mestre, 2011; Mestre and Heredia, 2013; Heredia et al., 2017). In this manuscript we use the highest resolution biostratigraphic work currently available for correlation of the Las Chacritas and Las Aguaditas sections (Serra et al., 2015; Feltes et al., 2016; Serra et al., 2017). This work includes identification of several of the conodont subzones identified by Albanesi and Ortega (2016) for the Precordillera. At the localities sampled for this study (Fig. 4), strata of the San Juan Formation span the lower Darriwilian (Dw1) *L. variabilis* and *Y. crassus* zones (Serra et al., 2015; Feltes et al., 2016). Recent conodont and graptolite biostratigraphy indicates the top of the San Juan is younger at the Las Chacritas and Las Aguaditas sections than at Cerro La Chilca (Serra et al., 2017), where bentonite deposits provide an age of 469.53 ± 0.62 Ma ($U\text{-}Pb_{Zircon}$; Thompson et al., 2012).

The transition from Early Darriwilian (Dw1) to Middle Darriwilian (Dw2) strata occurs in the *Y. crassus* Zone, which extends to approximately 36 m above the base of the Las Chacritas Formation and to approximately 19 m above the base of the Las Aguaditas Formation (Fig. 4; Serra et al., 2015; Feltes et al., 2016). The *E. pseudoplanus* Zone of Dw2 is identified from 36 to 58 m above the base of the Las Chacritas Formation (Serra et al., 2015). The top of the *E. pseudoplanus* zone is marked by the occurrence of

Histiodella kristinae, which typifies the lower subzone of the *E. suecicus* Zone, which is approximately 7 m thick in the Las Chacritas Formation. In the Las Aguaditas Formation, the *E. pseudoplanus* Zone is characterized by the co-occurrence of *D. tablepointensis* and extends to the top of the lower member the formation (Feltes et al., 2016; Feltes, 2017). The presence of the *Histiodella holodentata* and *H. kristinae* conodont Zones allow for correlation between the upper Las Chacritas Formation and uppermost strata of the lower member of the Las Aguaditas Formation (cf. Henderson et al., 2018). Finally, the occurrence of the Late Darriwilian to Early Sandbian conodont zone *P. anserinus* above the *E. suecicus* and *E. pseudoplanus/D. tablepointensis* zones, respectively in the Las Chacritas and Las Aguaditas formations (Albanesi et al., 2013; Serra et al., 2015; Feltes et al., 2016), indicates a disconformity marked by the removal of the Late Darriwilian (Dw3) strata in these formations.

3. Analytical methods

3.1. Sample selection and leaching protocols

Biogenic apatite, such as conodont elements, are often utilized for reconstructing the isotopic composition of Nd in seawater (Keto and Jacobsen, 1987; Holmden et al., 1996; Wright et al., 2002; MacLeod et al., 2008; Martin et al., 2012). Conodont elements are generally considered the best record of marine Nd, because of high Nd-concentrations (50–2100 ppm) imparted postmortem at the seawater-sediment interface (Wright et al., 1984; Holmden et al., 1996; Wright et al., 2002). Conodonts from the Las Chacritas and Las Aguaditas sections have conodont alteration indices (CAI; Epstein et al., 1977) of 2.5–3 (Serra et al., 2015; Feltes et al., 2016), which are typically considered to retain their

Nd-isotope signature during diagenesis (Shaw and Wasserburg, 1985). Conodonts picked from the Las Chacritas and Las Aguaditas sections during biostratigraphic studies by Serra et al. (2015) and Feltes et al. (2016) were obtained for analysis; however, the small size (< 100 μg per element) and the number of specimens available for destructive analysis limited analyses that could be completed. Sufficient conodont elements were available for samples at 57, 60, and 63 m in the Las Chacritas Formation and at 19, 27, 32, and 42 m in the Las Aguaditas Formation. For these samples approximately 1 mg of conodont elements belonging to the genera *Periodon*, *Pariostodus*, and *Protopanderodus* were added to 15 ml Teflon beakers and sonicated in 250 μl of 18 Ω ultrapure DI water for 10 minutes to remove surface contaminants and any adhering clay minerals. Conodont samples were then dissolved in 6 N HCl with 5 drops of 15 N HNO_3 to ensure complete digestion. Solutions were dried down and subsequently dissolved in 7 N HNO_3 for Sr, REE, and Nd column separation.

Where insufficient conodont elements were available, Nd and Sr were measured from carbonate of the Las Chacritas and Las Aguaditas formations. Micritic carbonate phases that show little petrographic and geochemical evidence for diagenetic recrystallization (Henderson et al., 2018) were targeted, when available, and microdrilled from polished thick sections with 0.3 or 0.5 mm tungsten carbide drill bits using a Servo tabletop drill press. Samples with elevated Sr/Ca ratios, thought to most likely preserve primary Sr-isotope signatures (Derry et al., 1994; Kaufman and Knoll, 1995; Montañez et al., 1996) were chosen for Sr- and Nd-isotope determinations. Approximately 20 mg of carbonate powder was acidified with 1 mL of 3.5 N nitric acid (HNO_3) in 15 ml Teflon

beakers and left overnight to ensure complete dissolution. Samples were then transferred into centrifuge tubes and centrifuged at 3500 RPM for 10 minutes to concentrate the insoluble fraction. Samples were then transferred into clean 15 ml Teflon tubes and a 250-µL aliquot was taken for determination of major element and rare earth element (REE) compositions. The remaining solution was dried down and subsequently dissolved in 7 N HNO_3 for Sr columns. To test for potential contributions of ^{87}Sr and ^{147}Sm from detrital clay minerals, approximately 40–80 mg of carbonate powder was acidified with 5 mL of 0.5 N acetic acid. Samples were heated for an hour to ensure complete digestion of carbonate phases and then transferred to centrifuge tubes and centrifuged at 3500 RPM for 10 minutes to concentrate insoluble components. The supernate from each sample was then transferred back into 15 mL Teflon tubes and a 250-mL aliquot was taken for determination of major-element and REE compositions. Samples were dried down and subsequently dissolved in 7 N HNO_3 for Sr, REE, and Nd columns.

3.2. Analytical chemistry and analysis

Major-element and REE concentrations were determined from aliquots of dissolved and centrifuged carbonate samples. Samples were diluted in 30 ml of 10 ppb In + 3% HNO_3 solution and analyzed on a Thermo X-series II inductively coupled plasma quadrupole mass spectrometer at the University of New Mexico Radiogenic Isotope Laboratory. Measurements were calibrated using a series of gravimetric standards, with reproducibility for all elements better than ± 5% based on replicate measurements of sample and standard solutions.

For determination of Sr- and Nd-isotope values, the soluble fraction of the initial carbonate dissolution was re-dissolved in 3 mL of 7 N HNO_3 and spiked with a calibrated $^{147}Sm/^{150}Sm$ solution for determination of $^{147}Sm/^{144}Nd$. Sample solutions were then added to 250 μL and 200 μL cation exchange columns filled with Sr-spec and Tru-spec resin, cleaned, and conditioned with 1 N HNO_3. Column treatment and cation exchange followed a modified procedure from Asmerom (1999). Columns were then separated, and 3 mL of 7 N HNO_3 and 2 mL of 1 N HNO_3 were added, respectively, to the Sr and REE columns. Columns were then eluted with 0.1% HNO_3 and samples were collected in Teflon beakers and dried down. Strontium samples were brought up again in 7 N HNO_3 and re-run through Sr columns to further Ca^{2+} removal. REE fractions were dissolved in 200 μL of 0.18 N HCl and added to REE exchange columns cleaned and conditioned with 0.18 N HCl. Nd and Sm were separated from the REE fraction following a modified procedure from Asmerom (1999). The Nd and Sm fractions were collected, dried down, and dissolved in 3% HNO_3 for analysis.

Sample solutions were then analyzed with a Thermo Neptune multi-collector inductively coupled plasma mass spectrometer with a Cetac Aridus II desolvating nebulizer in the Radiogenic Isotope Laboratory at the University of New Mexico. $^{87}Sr/^{86}Sr$, $^{143}Nd/^{144}Nd$, $^{145}Nd/^{144}Nd$, $^{150}Nd/^{144}Nd$, $^{147}Sm/^{152}Sm$, and $^{149}Sm/^{152}Sm$ were directly measured with the Neptune MC-ICP-MS. By contrast, $^{147}Sm/^{144}Nd$ was not directly measured on the Neptune and was calculated based on the isotopic abundance and isotopic ratio of the $^{147}Sm/^{150}Sm$ spike and measurement of $^{147}Sm/^{152}Sm$, $^{150}Nd/^{144}Nd$ and $^{149}Sm/^{152}Sm$. Reproducibility of $^{87}Sr/^{86}Sr$ compositions was monitored through

analysis of the National Bureau of Standards Sr standard NBS-987 ($^{87}Sr/^{86}Sr$ value of 0.71025) giving a precision of 0.710234 ± 0.000002. Reproducibility of $^{143}Nd/^{144}Nd$ was measured by replicate analyses of the La Jolla Nd isotopic standard ($^{143}Nd/^{144}Nd$ = 0.511835; Pier et al., 1989) with each batch of analyses, giving a measurement of 0.511846 ± 0.000016. Initial $^{143}Nd/^{144}Nd$ and ε_{Nd} values were calculated using an approximate depositional age of 464 Ma, which represents the best inferred age based on the biostratigraphic (Albanesi and Ortega, 2016) and radiometric ages (Thompson et al., 2012) in the Precordillera. Nd-isotope compositions are reported relative to the chondritic uniform reservoir (CHUR) in standard epsilon notation (ε_{Nd}).

4. Results and evaluation of potential diagenesis

4.1. Isotopic and elemental analysis

Carbon and oxygen isotope compositions as well as major- and trace-element compositions of carbonate phases from the Las Chacritas and Las Aguaditas formations are reported in Henderson et al. (2018) and summarized in Tables 1 and 2. Micritic carbonate phases of the Las Chacritas and Las Aguaditas formations show no discrete trends between $\delta^{13}C$ and $\delta^{18}O$ compositions indicative of resetting from interaction of carbonate minerals with diagenetic fluids. Clear late-stage diagenetic components, such as void and vein filling cements, extend over a much larger range than primary carbonate phases, which fall generally between –4‰ and –6‰ in line with other well-preserved early Paleozoic marine carbonate rocks (Henderson et al., 2018). There are also no clear relationships between Sr, Mn, or Fe concentrations between primary carbonate phases and later diagenetic phases, which supports the interpretation of only minimal isotopic

exchange during diagenesis. Rb concentration within samples in this study, generally > 1.5 ppm, suggest corrections to the measured $^{87}Sr/^{86}Sr$ values may be greater than the analytical uncertainty of Sr-measurement ($^{87}Sr/^{86}Sr \pm 0.000002$; Montanez et al., 1996). Combined, the isotopic and elemental data from these carbonate phases suggests deposition and early diagenetic stabilization of carbonate minerals in the Las Chacritas and Las Aguaditas formations in sub-oxic to anoxic marine fluids or pore waters (Henderson et al., 2018).

4.2. REE analysis

Rare earth element concentrations for the Las Chacritas and Las Aguaditas formations are provided in Table 3. Post Archean Average Shale (PAAS) normalized REE patterns of the Las Chacritas and Las Aguaditas formations show depletion of the light REE (LREE) fraction compared to the heavy REE (HREE) fraction (Appendix 2, Figs. 8 and 9). These REE patterns are consistent with the REE patterns of modern seawater (Zhao and Zheng, 2014) and those inferred for ancient carbonate rocks (Webb and Kamber, 2000; Kamber and Webb, 2001). Although changes in the concentrations of individual REE are observed, no systematic change in normalized REE patterns is observed that would indicate a change in provenance material that would explain Sr- or Nd-isotope compositions is observed in REE patterns through either the Las Chacritas or Las Aguaditas formations.

4.3. Strontium isotopes

Strontium isotope measurements of the Las Chacritas and Las Aguaditas formations are provided in tables 4, 5, and 6. Differences are observed in the strontium

isotope composition as measured in conodont apatite, and in carbonate samples that underwent either nitric or acetic acid digestion (Tables 3 and 4). Measured $^{87}Sr/^{86}Sr$ values of carbonate treated with nitric acid are more radiogenic than those carbonate samples treated with acetic acid, suggesting increased potential for liberated ^{87}Sr from Rb^{+} sites in detrital components. A cross-plot of Rb concentrations vs. $^{87}Sr/^{86}Sr$ values (Fig. 4) shows that samples treated with nitric acid have higher Rb concentrations that adversely affect calculated initial $^{87}Sr/^{86}Sr$ values. Therefore, we consider the $^{87}Sr/^{86}Sr$ values of samples dissolved in acetic acid to better represent seawater compositions, and have included only these, and conodont-derived samples, in figures 5 and 6. In the Las Chacritas Formation, average $^{87}Sr/^{86}Sr$ compositions in the *Y. crassus* Zone of 0.709015 ± 0.000182 (n = 7) decline to around 0.708987 ± 0.000109 (n = 7) in the *E. pseudoplanus* Zone and to 0.708802 ± 0.000154 (n = 5) in the *E. suecicus* Zone. In the Las Aguaditas Formation, average $^{87}Sr/^{86}Sr$ compositions in the *Y. crassus* Zone of 0.708968 ± 0.000035 (n = 5) decline to 0.708819 ± 0.000172 (n = 11) in the *E. pseudoplanus/D. tablepointensis* Zone. Sandbian $^{87}Sr/^{86}Sr$ values from the *P. anserinus* zone average 0.708628 ± 0.000118 (n = 4). Conodont apatite from the top of the *E. pseudoplanus* and *E. suecicus* Zones in the Las Chacritas Formation have $^{87}Sr/^{86}Sr$ values between 0.708673 and 0.708781, which are less radiogenic than coeval carbonate $^{87}Sr/^{86}Sr$ values (Fig. 5). In the Las Aguaditas Formation, conodont apatite $^{87}Sr/^{86}Sr$ values are less radiogenic than coeval carbonate $^{87}Sr/^{86}Sr$ values (Fig. 6). The differences observed in Sr-isotope compositions between coeval conodont apatite and carbonate are consistent with typical marine Sr-isotope preservation (Saltzman et al., 2014; Edwards et al., 2015).

4.4. Neodymium isotopes

Neodymium isotope measurements, calculated $^{143}Nd/^{144}Nd$, and ε_{Nd} values are provided in tables 5 and 6. Only one conodont sample contained sufficient Nd to determine an isotopic composition, sample LAF33; however, sample LAF33 (ε_{Nd} −7.1) is in line with ε_{Nd} values from carbonate in the Las Aguaditas Formation indicating that our carbonate ε_{Nd} values likely reflect incorporation of Nd-isotope signatures during sea-floor stabilization. Average ε_{Nd} values in the *Y. crassus* Zone increase from −7.6 ± 0.8 (n = 6) to an average of −4.3 ± 1.6 (n = 4) in the *E. pseudoplanus* Zone and −6.9 in the *E. suecicus* Zone; however, there is a lot of variability in ε_{Nd} through the MDICE interval of the Las Chacritas Formation. In the deeper water Las Aguaditas Formation, average ε_{Nd} values of −7.5 ± 1.4 (n = 5) in the *Y. crassus* Zone are similar to those observed in the *E. pseudoplanus/D. tablepointensis* Zone of −7.1 ± 0.9 (n = 9). Sandbian ε_{Nd} values in both the Las Chacritas and Las Aguaditas formations are similar with averages of −5.3 ± 1.0 (n = 4) and −5.9 ± 0.6 (n = 4), respectively.

5. Discussion

5.1. Ordovician paleoceanographic change

5.1.1. Isotopic signatures of icehouse-greenhouse ocean states

Large scale changes in the carbon isotope composition of marine carbonate through the Phanerozoic have been interpreted to reflect changes in climate states (Saltzman, 2005). In this scenario, greenhouse climate conditions in the Early Paleozoic are characterized by stratified oceans with anoxic-euxinic deep waters, nitrogen limitation in surface waters, and reduced organic productivity, resulting in relative stasis of carbon isotope compositions. During icehouse periods, enhanced ocean circulation and

mixing between surface and deep-water result in upwelling of nutrient rich deep water, high productivity in surface oceans, and increased burial of organic carbon. Global cooling in the early Paleozoic suggests that Ordovician oceans reached near modern equatorial sea-surface temperatures in the Darriwilian (Trotter et al., 2008). However, this transition to cooler ocean temperatures substantially precedes the transition to icehouse states as marked by the +4‰ Chatfieldian $\delta^{13}C$ excursion in the Late Ordovician (Sandbian; Saltzman and Young, 2005), and instead coincides with the globally recognized Middle Darriwilian isotope carbon excursion (MDICE) in Darriwilian (Ainsaar et al., 2004; Meidla et al., 2004). If proposed climatic transitions are accompanied by changes in ocean circulation, the time interval prior to the main transition to icehouse conditions—where global sea surface temperatures had dropped, but where ocean circulation changes have not yet been identified in the carbon isotope record—should record evidence of greenhouse ocean states (i.e. stratified ocean conditions). In this case, isotopic change associated with the MDICE may record evidence of disruption of a marine chemocline associated with the initiation of ocean circulation changes.

5.1.2. Darriwilian carbon isotope change

The globally recognized MDICE is identified as an approximately +1‰ excursion in China (Schmitz et al., 2010; Zhang et al., 2010; Kah et al., 2016), +1.5‰ in Baltoscandia (Ainsaar et al., 2004; Meidla et al., 2004; Ainsaar et al., 2007; Kaljo et al., 2007; Ainsaar et al., 2010; Calner et al., 2014) and Newfoundland (Thompson and Kah, 2012; Thompson et al., 2012), +2‰ in the Precordillera of Argentina (Buggisch et al.,

2003; Albanesi et al., 2013; Henderson et al., 2018), +2.5‰ in Nevada, USA (Young et al., 2016), and +4‰ in Maryland, USA (Leslie et al., 2011). Generally, the MDICE is characterized by a positive shift in C-isotope compositions of carbonate from around −2‰ during the Dapingian to values > +1‰ by the Middle Darriwilian. Previous work has noted that the initiation of the MDICE coincides with sea-surface temperatures reaching their lowest point in the Ordovician (Trotter et al., 2008), and have linked the MDICE excursion with invigorated circulation within a stratified greenhouse ocean (Thompson and Kah, 2012). In this scenario, intensified ocean circulation would provide a mechanism for nutrient-rich, oxygen depleted deep-waters to be delivered and mixed with surface waters (Van Cappellen and Ingall, 1994; Pope and Steffen, 2003; Servais et al., 2014). The resulting increase in bioavailable nutrients in surface waters would drive increased organic productivity leading to enhanced organic carbon burial and enrichment of ^{13}C in surface water environments.

The studies noted above infer the presence of stratified marine conditions from changes in the isotopic composition of shallow water facies. Recent work from the Precordillera, in which isotopic compositions were evaluated from coeval shallow and deep-water facies, provide further evidence of the existence of stratified ocean conditions in Darriwilian greenhouse times. Biostratigraphic analysis of the Las Chacritas and Las Aguaditas formations indicate that the MDICE interval (*E. pseudoplanus* Zone and *Histiodella kristinae* Subzone of the *E. suecicus* Zone) is present in both the Las Chacritas and Las Aguaditas formations (Serra et al., 2015; Feltes et al., 2016). In these successions, shallow water strata of the Las Chacritas Formation record the MDICE as a

+ 2‰ shift in carbon isotope compositions, while a − 1.5‰ shift is observed in biostratigraphically coeval strata of the Las Aguaditas Formation (Henderson et al., 2018). Such an abrupt divergence in carbon isotope compositions of these formations is interpreted to reflect deposition from geochemically distinct parts of the water column, above and below the marine chemocline, during the MDICE interval (Henderson et al., 2018). Deposition above, or below, the marine chemocline is supported by the isotopic composition of organic carbon, which abruptly drops from approximately – 26‰ to values around – 30‰ in the Las Aguaditas Formation prior to the onset of the MDICE in the Precordillera (Henderson et al., 2018). This shift is associated with deepening of facies in the Precordillera and is interpreted to reflect the presence of heterotrophic reworking of organic carbon in the water column or in the shallow substrate beneath the chemocline.

5.1.3. Darriwilian sulfur isotope change

Potential for climate driven changes in ocean circulation and subsequent mixing and ventilation of deep-water environments has also been inferred from the S-isotope record of Ordovician carbonate rocks (Thompson and Kah, 2012; Marenco et al., 2013; Kah et al., 2016). In this scenario, sluggish ocean circulation in greenhouse times would have resulted in strengthening of the chemocline, and expansion of anoxic deep-water environments. Redox-stratified ocean waters would then result in a sulfur isotope system driven by interaction between distinct sulfate and sulfide reservoirs (Kah et al., 2016). Oxidation of the deep-water sulfide reservoir is characteristic of the Hirnantian icehouse

(Yan et al., 2009; Jones and Fike, 2013; Zhou et al., 2015), but evidence for initiation of ocean circulation may lie in the Darriwilian.

A dramatic change in the isotopic composition of marine sulfate is recorded in Early Darriwilian strata in Argentina and Newfoundland as a 10‰ drop in the isotopic composition of CAS (Thompson and Kah, 2012). In this same interval, the isotopic composition of marine sulfide (recorded as $\delta^{34}S_{PY}$) is heavy and variable with $\Delta^{34}S$ ($\delta^{34}S_{CAS} - \delta_{34}S_{PY}$) values rapidly declining by 15‰ in the Darriwilian in an interval marked by the deposition of "superheavy" pyrite, where the sulfur isotope composition of sedimentary pyrite is consistently enriched relative to that of CAS (Thompson and Kah, 2012; Kah et al., 2016). These isotopic changes are used to infer disruption of stratified, euxinic marine conditions in the Middle Ordovician as increased ocean circulation drove at least local ventilation and oxygenation of an anoxic deep-water sulfide reservoir (Thompson and Kah, 2012; Kah et al., 2016; Young et al., 2016).

5.2. Strontium isotopes and understanding ocean stratification

As discussed above, environmental changes resulting from global cooling in the Darriwilian appear to denote the initial transition between greenhouse and icehouse climate states in the Ordovician. Greenhouse conditions of the early Ordovician are marked by a persistent marine chemocline that separates oxygen rich surface waters and anoxic deep waters (Thompson and Kah, 2012; Saltzman et al., 2015; Kah et al., 2016; Young et al., 2016; Edwards et al., 2018; Henderson et al., 2018). Cooling of sea-surface temperatures in the Darriwilian is then inferred to have driven enhanced vertical ocean circulation, leading to the initial destabilization of the chemocline, followed by a

transition to a much more active circulation and increased ventilation of deep water by the Late Ordovician (Sandbian; Young et al., 2016). Current evidence for stratification and mixing, however, is based in the redox chemistry of the Ordovician oceans and cannot distinguish whether ocean stratification was purely dynamic (i.e. stratification in terms of oxygen, driven by organic productivity and microbially mediated redox transformations; Küspert et al., 1982) or physical stratification (i.e. salinity stratification; Railsback et al. 1990).

Interestingly, the largest shift in the isotopic composition of marine strontium in the early Paleozoic coincides with these biogeochemical changes in the Darriwilian, with $^{87}Sr/^{86}Sr$ values falling from near 0.7090 to around 0.7078 (Fig. 1; Veizer, 1989; Gao et al., 1996; Denison et al., 1998; Qing et al., 1998; Ebneth et al., 2001; Shields et al., 2003; Young et al., 2009; Saltzman et al., 2014; Edwards et al., 2015). The $^{87}Sr/^{86}Sr$ ratio of the ocean reflects the relative changes in chemical weathering of crustal components and input to the ocean via riverine, diagenetic, and hydrothermal fluids (Banner, 2004). The isotopic composition of strontium delivered to the ocean by rivers has an average value of 0.712, which reflects a significant radiogenic contribution from old continental crust (Edmond, 1992). Younger, mantle derived basalts in sea-floor basalts and volcanic island arcs, have $^{87}Sr/^{86}Sr$ values near 0.702 (Dasch et al., 1973). Oceanic flux models show that riverine input from the continents is the dominant control on the $^{87}Sr/^{86}Sr$ value of the ocean, which is 3x the contribution of Sr to the ocean than hydrothermal alteration or diagenesis of the seafloor (Palmer and Edmond, 1989). Traditionally, the shift in $^{87}Sr/^{86}Sr$ has been explained by decreases in continental weathering with waning of Pan-African

orogenesis in the Cambrian (Richter et al., 1992; Montañez et al., 1996; Qing et al., 1998) and increased sea-level that reduced continental areas exposed to weathering (Qing et al., 1998). Other studies invoke elevated hydrothermal exchange associated with increased sea-floor spreading (Shields et al., 2003) or increased weathering of volcanic arc terranes (Ronov, 1980; Young et al., 2009).

The rapidity of Sr-isotope change in the Ordovician (~ 4–6 x 10^6 years; Shields et al., 2003) is similar to the oceanic residence time of strontium in modern seawater (~ 5 x 10^6 years; Taylor and McLennan, 1985) requiring a rate of decline in $^{87}Sr/^{86}Sr$ compositions through the Darriwilian–Sandbian interval of ~5–10 x 10^{-5} per m.y. (Shields et al., 2003; Young et al., 2009). Modeling efforts to explain the $^{87}Sr/^{86}Sr$ decline invoke increased weathering of volcanic arc terranes (e.g. a 25-fold increase in weathering of young volcanic arcs; Young et al., 2009); however, these models fail to reconcile the effects of enhanced basalt weathering on global CO_2 budgets (Berner, 2006, 2009) and the apparent decline in sea-surface temperatures through the Middle Ordovician (Trotter et al., 2008; Quinton et al., 2015). An alternative explanation for the dramatic Sr-isotope change observed in the Darriwilian–Sandbian may lay with physical mixing of ocean waters with different strontium isotope compositions, resulting from sluggish ocean circulation in the Early Ordovician (Railsback et al., 1990). Because homogeneity of marine Sr is driven by the mixing rate of the ocean, which would have been reduced during times of ocean stratification (Railsback et al., 1990; Broecker, 1999), persistent physical stratification of the oceans prior to a Middle Ordovician ventilation event may have resulted in the development of water masses with distinct Sr-isotope compositions.

Rapid mixing and ventilation of a deep-ocean stratified water body, as suggested by the marine S-isotope record (Thompson and Kah, 2012; Kah et al., 2016), could therefore play a role in the rapid decline in $^{87}Sr/^{86}Sr$ values observed in the Middle-Late Darriwilian. In this scenario, saline shelf waters dominated by radiogenic, craton-derived Sr would be displaced by hydrothermally derived less-radiogenic Sr waters during with enhanced ocean mixing.

5.2.1. Strontium isotopes in the Precordillera

Middle Ordovician strata of the Precordillera were deposited in greenhouse conditions, characterized by the presence of a strong chemocline (Thompson and Kah, 2012; Henderson et al., 2018), just prior to the rapid shift in strontium isotope compositions that is recorded globally. The $^{87}Sr/^{86}Sr$ values determined for the Las Chacritas and Las Aguaditas formations (Figs. 4 and 5) are broadly consistent with observed seawater Sr-isotope compositions in the Early to Middle Darriwilian with values around 0.7090 (Fig. 1). Strontium isotope compositions from carbonate of the Las Chacritas Formation are variable around 0.709015 ± 0.000182 (n = 7) in the *Y. crassus* Zone and 0.708987 ± 0.000109 (n = 7) in the *E. pseudoplanus* Zone before decreasing to 0.708802 ± 0.000154 (n = 5) in the *E. suecicus* Zone. The transition from less-radiogenic Sr (~0.7089) to values >0.7090 in the *E. pseudoplanu*s zone coincides with a shoaling of carbonate facies, which may indicate a facies dependent gradient of Sr-isotope compositions in the stratified Ordovician ocean. As carbonate facies of the Las Chacritas Formation begin to deepen again, reflected by increased interbedded shales in the *E. suecicus* Zone, the $^{87}Sr/^{86}Sr$ composition of carbonate decreases from more radiogenic

values around 0.7091 to values around 0.7086. Sandbian strata of the middle member of the Las Aguaditas Formation, which unconformably overlies the Las Chacritas Formation, have Sr-isotope compositions around 0.708908 ± 0.000130 (n = 4); however, two these samples have high Rb concentrations (> 2.3 ppm) suggesting potential detrital contamination of the Sr-isotope signature in these Sandbian samples.

Strontium isotope compositions of the Las Chacritas (Fig. 5) and Las Aguaditas (Fig. 6) formations appear to have fundamentally different behavior in the Precordillera during the MDICE interval. Carbonate $^{87}Sr/^{86}Sr$ from the Las Aguaditas Formation are less variable than in the shallow-water Las Chacritas Formation and show a step-wise decrease at the onset of the MDICE interval with values decreasing from around 0.7090 to 0.7088 (Fig. 5). In the Las Aguaditas Formation, $^{87}Sr/^{86}Sr$ values decrease from 0.708968 ± 0.000035 (n = 5) in the *Y. crassus* Zone to 0.708819 ± 0.000172 (n = 11) in the *E. pseudoplanus* Zone (Fig. 6). Sr-isotope compositions remain similar in the in the Sandbian *P. anserinus* Zone of the Las Aguaditas Formation.

The geochemical behavior recorded in Darriwilian strata from the Precordillera suggests a geochemical decoupling between shallow- and deep-water that could, in part, be explained in terms of physical stratification of the Ordovician ocean. Such heterogeneity in marine Sr-isotope compositions has been invoked to explain short term changes in $^{87}Sr/^{86}Sr$ compositions during greenhouse conditions in the Permian (Gruszczynski et al., 1992) and during Cretaceous ocean anoxic events (OAE2; Frijia and Parente, 2008). In the Darriwilian, tectonic induced subsidence in the Precordillera is driving a shift in depositional facies of the Las Chacritas and Las Aguaditas formations.

The step-wise decline in $^{87}Sr/^{86}Sr$ in the Las Aguaditas Formation is consistent with $\delta^{13}C_{org}$ evidence suggesting the locus of deposition shifted from at or above the chemocline to below the chemocline just prior to the MDICE (Henderson et al., 2018). The shallower water facies of the Las Chacritas Formation is characterized by variable strontium isotope compositions through the MDICE interval suggesting fluctuations in the position of the chemocline and a drop in Sr-isotope values in the *E. suecicus* Zone, which is consistent with a shift of the Las Chacritas Formation to below the chemocline in the latest Middle Darriwilian (Henderson et al., 2018). Such observations are consistent with the hypothesized gradient in $^{87}Sr/^{86}Sr$ between shallow and deeper waters. In this scenario, more radiogenic Sr (> 0.7090) reflects the average isotopic composition of the shallow ocean along the Gondwana margin in the Darriwilian. Volcanic activity along the Gondwanan margin could also contribute to less-radiogenic Sr values (Young et al., 2009); however, with reduced mixing between shallow and deep waters associated with greenhouse conditions in the Early-Middle Ordovician this non-radiogenic Sr-would be expected in shallow-waters and not in the deeper waters. Therefore, deeper-waters appear to be more influenced by non-radiogenic Sr-isotope compositions, consistent with weathering or hydrothermal alteration of young oceanic crust.

5.2.2. Neodymium isotopes in the Precordillera

A further test of the possibility of physically distinct shallow and deeper water in the Precordillera is provided by neodymium isotope compositions. Like strontium, the Nd-isotope composition of ocean waters result from the relative input from weathering of old and young crust; however, unlike strontium, Nd has a short residence time in

seawater (~400–600 years; Taylor and McLennan, 1985), which results in the formation of oceanographic reservoirs—driven, in part, by ocean circulation patterns—with distinct neodymium isotope compositions (ε_{Nd}; Piepgras and Wasserburg, 1980; Keto and Jacobsen, 1987; Stille, 1992; Holmden et al., 1998; MacLeod et al., 2008). The isotopic characteristics of these water masses is then imparted to marine carbonate rocks and preserved ε_{Nd} values can be used to trace mixing of water masses driven by changes in sea-level and ocean circulation (Fanton et al., 2002; Dopieralska et al., 2006; MacLeod et al., 2011; Theiling et al., 2012; Holmden et al., 2013). In this context, we evaluate the extent to which Nd-isotope compositions of carbonate in the Precordillera may reflect decoupling between shallow- and deep-waters in the Darriwilian.

Neodymium isotope compositions from the Precordillera range between −14.72 and −2.97 for the Las Chacritas Formation (Table 3; Fig. 4) and from −9.27 and −4.9 in the Las Aguaditas Formation (Table 4; Fig. 5). ε_{Nd} values of both the Las Chacritas and Las Aguaditas formations fall between −8 and −6 in strata deposited prior to the onset of the MDICE (Figs. 4 and 5). ε_{Nd} in the *Y. crassus* Zone of the Las Chacritas Formation are around −8 and appear to rapidly shift to values around −4 and as low as −3 at the initiation of the MDICE interval in the *E. pseudoplanus* Zone (Fig. 4). One sample, with an ε_{Nd} value of −14.71, has a $^{143}Nd/^{144}Nd$ ratio of 0.511661, well below the average ratio of 0.512125 ± 0.000089 (n = 15) and is not considered further. ε_{Nd} values in the *P. anserinus* Zone of the Las Chacritas Formation range from −6.7 to −4.1. In the deeper-water strata of the Las Aguaditas Formation, ε_{Nd} values generally vary between −9.3 and −5.1 in the *Y. crassus* Zone (Fig. 5). However, unlike in the shallower water facies of the

Las Chacritas Formation, ε_{Nd} values in the Las Aguaditas Formation do not change from those observed in strata deposited prior to the MDICE event (Fig. 5), ranging from −8.6 to −5.9 in the *E. pseudoplanus/D. tablepointensis* Zone. Values are slightly lower in the Sandbian *P. anserinus* Zone of the Las Aguaditas Formation. This variability of ε_{Nd} values of the shallower-water Las Chacritas Formation (between −8 and −3; Fig. 4), even as deeper water deposits of the Las Aguaditas Formation remain invariant, suggest geochemical decoupling between shallow- and deeper-water environments.

Previous work on Nd-isotope signatures from Late Ordovician carbonate strata from the epeiric sea of Laurentia show substantial changes associated with eustatic sea-level fluctuations (Fanton et al., 2002; Holmden et al., 2013). These studies document an increase in ε_{Nd} values (more radiogenic) associated with increasing sea-level and infer a greater influence of Panthalassa seawater ε_{Nd} (values ~ −4.0) and reduced influence of the continental weathering flux (~ −8.5) off the Taconic highlands along an east-west gradient in paleo-seawater ε_{Nd} (Grandjean et al., 1987; Holmden et al., 1998). If marine transgression drives ε_{Nd} values to more radiogenic values of the Iapetus ocean margin rather than continentally derived signatures (~ −10 to −6; Wright et al. 2002), as observed in the late Ordovician of Laurentia (Holmden et al., 2013), then increasing water depth in the Las Chacritas Formation during the Darriwilian could explain the ε_{Nd} values around −3. However, sea-level driven changes are inconsistent with ε_{Nd} values of the deeper-water Las Aguaditas Formation (−8 to −6), which retains inferred continental Nd-isotope signatures (Gleason et al., 2007) and are, therefore, unlikely to explain ε_{Nd} values of the Las Chacritas Formation.

ε_{Nd} values from the Precordillera (−5.9) and along the northeastern margin of Gondwana in the Ordovician (−5.5) are interpreted as a mixture of older stable Gondwanan cratonic rock and juvenile arc terranes off the Gondwanan margin (Astini et al., 1995; Wright et al., 2002). Carbonaceous black shales the Gualcamayo Formation at the Cerro La Chilca section, which correlates with the carbonate deposits in this study (cf. Serra et al., 2017), have ε_{Nd} values that range from −9.6 to −4.5 and average −7.5 (Gleason et al., 2007). At Cerro La Chilca, the Gualcamayo Formation diachronously overlies Upper Dapingian strata of the San Juan Formation (~469 Ma; Thompson et al., 2012) and, in places, the Gualcamayo interfingers with the siliciclastic rich facies of the Las Aguaditas Formation in northern San Juan Province (Keller, 1999). These ε_{Nd} values are consistent with those observed in the Las Chacritas and Las Aguaditas formations in this study and reflect a basinal average for the Precordillera.

Alternatively, the greater proportion of interbedded calcareous shales, similar to the basinal shales of the Gualcamayo Formation ($\varepsilon_{Nd} \sim -7.5$; Gleason et al., 2007), suggest the potential for seawater signatures to be overwhelmed by the detrital clay fraction or potentially penecontemporaneous to early-diagenetic exchange of Nd and Sm between carbonate and clay-minerals (Azmy et al., 2011; Zhao and Zheng, 2014). However, it is unclear whether the ε_{Nd} values for the Gualcamayo reflect the composition of seawater or terrigenous sediments. Therefore, neodymium isotope values from the Gualcamayo Formation ($\varepsilon_{Nd} \sim -7$; Gleason et al., 2007) provide a baseline for isotopic change in the Middle Ordovician of the Precordillera as they reflect the long-term average of ε_{Nd} from the accretionary margin of Gondwana in the Middle Ordovician.

If the long-term average of ε_{Nd} off the Gondwanan margin explains Nd-isotope compositions in the lower part of the Las Chacritas Formation and throughout the Las Aguaditas Formation, then the increased volatility and more radiogenic Nd-isotope compositions during the MDICE interval may reflect mixing with Nd from volcanic arc terranes along the Gondwanan margin, or changes in weathering sources. In this first scenario, weathering of volcanic arc terranes and mixing of shallow ocean waters across the Precordillera terrane (Fig. 7) could deliver more radiogenic ε_{Nd} to the Las Chacritas Formation. This is consistent with arc-derived igneous terranes preserved in northern Argentina with ε_{Nd} values around –3 (Pankhurst et al., 1998; Bock et al., 2000; Dahlquist et al., 2013; Martina et al., 2014). In a second scenario, volcanic activity and weathering of large volcanic rocks associated with volcanism and formation of the Famatina volcanic province in Argentina in the late Dapingian–early Darriwilian (Pankhurst et al., 1998; Fanning et al., 2004; Thompson et al., 2012). Volcanic arc terranes along the Ordovician margin of Gondwana are poorly documented; however, mafic rocks from Complejo Igneo Pocitos, the northernmost extension of the Famatina arc terrane, has more mantle derived Nd-isotope signatures with ε_{Nd} values of +0.8 to +0.7 and +2.2 to +2.7 (Thorsten Kleine et al., 2004) as well as meta-igneous rocks from the Rio Bonete region (northwest extent of the Precordillera), which range from −3.83 to +1.10 (Martina et al., 2014). Pillow lavas in the Puna have ε_{Nd} values of +3.6 and other igneous rocks in the Southern Puna Range include gabbroic rocks of the Pocitos/Tolillar region in southern Sierra de Calalaste of −0.1 to +6.9 (Bock et al., 2000). Also, in the Southern Puna Range, the Arenig Diablo Formation has ε_{Nd} values of −3 to −1 interpreted as arc rocks formed

along the Gondwanan margin (Zimmermann and Bahlburg, 2003). Furthermore, ε_{Nd} values Famatinian arc derived granites emplaced in the Ordovician have ε_{Nd} values of −6 to −3 (Pankhurst et al., 1998; Dahlquist et al., 2013). Weathering of these isotopically distinct sources in the Darriwilian may explain the variability in ε_{Nd} values observed in the shallow-water Las Chacritas Formation.

In a final scenario, variability in the shallow-water signature of the Las Chacritas Formation may reflect changes in surface runoff in the Middle–Late Darriwilian between the Gondwanan arc-derived ε_{Nd} isotopic signatures and older cratonic rocks. Although localized changes in precipitation rates and changes weathering rates in the past can be difficult to assess (Theiling et al., 2012), orogenic activity along the Gondwanan margin in the Middle–Late Ordovician can result in dramatic changes in uplift and erosion of source rocks with different ε_{Nd} compositions. Sedimentary rocks of the Negro Pienado and Achavil formations in the Famatina fold and thrust belt that accreted to Gondwana prior to the Precordillera, have ε_{Nd} values of −8.55 and −6.98 and −9.83 and −8.65, respectively, that reflect mixed Paleoproterozoic and younger sources (Collo et al., 2009). The highest ε_{Nd} values observed in the Las Chacritas Formation (−3.0) are consistent with mafic rocks in arc derived igneous terranes in northern Argentina (~ +2 to –2; Pankhurst et al., 1998; Bock et al., 2000; Dahlquist et al., 2013; Martina et al., 2014) and may reflect transient input of surficial runoff from Gondwana or Peri-gondwanan arc terranes that contributes to the geochemical composition of shallow-water environments. Reduced mixing between shallow and deep-water in the Precordillera during the Middle

Ordovician would result in the observed patterns of geochemical decoupling observed in the Nd-isotope record of the las Chacritas and Las Aguaditas formations.

6. Conclusions

Geochemical differences are observed in both the biogeochemical (C- and S-isotope) and physiochemical (Nd- and Sr-isotope) compositions of the Las Chacritas and Las Aguaditas formations. The biogeochemical records of these coeval shallow and deeper-water facies suggest ventilation of deep-water into shallow-water environments at the initiation of the MDICE and the continued presence of a strong chemocline into the Darriwilian. The observed differences in the Nd-isotope composition identified between facies are inconsistent with simple mixing of deep-marine waters with distinct $^{87}Sr/^{86}Sr$ and ε_{Nd} compositions into shallow-water environments. Instead, ε_{Nd} compositions of the Las Chacritas Formation appear decoupled from those of the deeper-water Las Aguaditas Formation, which retains a basinal ε_{Nd} signature (around −7). Variation in the ε_{Nd} composition of the Las Chacritas Formation during the MDICE interval suggests potential mixing between compositionally distinct regions sources from Gondwana or volcanic arc terranes. Thus, tectonically driven changes in source material to the Precordillera in the Middle Ordovician appear to drown out any oceanographic signatures in the ε_{Nd} record of sediments from the Precordillera. However, there does appear to be a marine influence in the ε_{Nd} and $^{87}Sr/^{86}Sr$ values of the shallower water environments in the Precordillera. Observed Nd-isotope compositions are best explained by changes in weathering of source terranes with more radiogenic ε_{Nd} compositions that drive changes in shallow water compositions, but Nd-isotope compositions in the strongly stratified

deeper water reflect the long-term average of the Gondwanan margin. The observed Sr-isotope signatures from the Las Chacritas and Las Aguaditas formations match the globally observed trend for the Middle Ordovician and suggest that the pattern of $^{87}S/^{86}Sr$ change may be driven, in-part, by oceanographic processes. Future studies with coupled strontium and neodymium isotope on strata spanning the Late-Darriwilian to Sandbian interval may better resolve potential oceanographic controls on the dramatic Sr-isotope change observed.

Acknowledgments

Funding for this project was provided by the New Directions grant from the American Chemical Society Petroleum Research Fund (54354-ND2 to Kah), along with student grants from Sigma Xi, the Geological Society of America, and SEPM (to Henderson).

References

Ainsaar, L., Kaljo, D., Martma, T., Meidla, T., Männik, P., Nõlvak, J., Tinn, O., 2010. Middle and Upper Ordovician carbon isotope chemostratigraphy in Baltoscandia: A correlation standard and clues to environmental history. Palaeogeography, Palaeoclimatology, Palaeoecology 294, 189-201. http://dx.doi.org/10.1016/j.palaeo.2010.01.003

Ainsaar, L., Meidla, T., Tinn, O., 2004. Middle and Upper Ordovician stable isotope stratigraphy across the facies belts in the East Baltic, in: Hints, O., Ainsaar, L. (Eds.), 8th Meeting on the Working Group on the Ordovician Geology of Baltoscandia. Tartu University Press, Tallinn and Tartu, Estonia, pp. 11-12.

Ainsaar, L., Meidla, T., Tinn, O., Martma, T., Dronov, A., 2007. Darriwilian (Middle Ordovician) carbon isotope stratigraphy in Baltoscandia. Acta Paleontologica Sinica 46, 1-8.

Albanesi, G.L., Bergström, S.M., Schmitz, B., Serra, F., Feltes, N.A., Voldman, G.G., Ortega, G., 2013. Darriwilian (Middle Ordovician) $\delta^{13}C_{carb}$ chemostratigraphy in the Precordillera of Argentina: Documentation of the middle Darriwilian Isotope Carbon Excursion (MDICE) and its use for intercontinental correlation. Palaeogeography, Palaeoclimatology, Palaeoecology 389, 48-63. http://dx.doi.org/10.1016/j.palaeo.2013.02.028

Albanesi, G.L., Ortega, G., 2016. Conodont and Graptolite Biostratigraphy of the Ordovician System of Argentina, in: Michael, M. (Ed.), Stratigraphy & Timescales. Academic Press, pp. 61-121. http://dx.doi.org/10.1016/bs.sats.2016.10.002

Allmendinger, R.W., Figueroa, D., Snyder, D., Beer, J., Mpodozis, C., Isacks, B.L., 1990. Foreland shortening and crustal balancing in the Andes at 30˚S latitude. Tectonics 9, 789-809. http://dx.doi.org/10.1029/TC009i004p00789

Allmendinger, R.W., Judge, P.A., 2014. The Argentine Precordillera: A foreland thrust belt proximal to the subducted plate. Geosphere 10, 1203-1218. http://dx.doi.org/10.1130/ges01062.1

Asmerom, Y., 1999. Th–U fractionation and mantle structure. Earth and Planetary Science Letters 166, 163-175. http://dx.doi.org/10.1016/S0012-821X(99)00008-4

Astini, R.A., 1994. Analisis sequencial y paleoambientes de las pelitas negras (aloformaction Gualcamayo) que suprayacen a las sucesiones carbonatica eo-Ordovicicas en la Precordillera Argentina. Revista de la Asociacion Geologica Argentina 49, 71-84.

Astini, R.A., 1995. Sedimentologia de la Formacion Las Aguaditas (talud carbonatico) y evolucion de la cuenca precordillera durante el Ordovicico medio. Revista de la Asociacion Geologica Argentina 50, 143-164.

Astini, R.A., Benedetto, J.L., Vaccari, N.E., 1995. The early Paleozoic evolution of the Argentine Precordillera as a Laurentian rifted, drifted, and collided terrane: A

geodynamic model. Geological Society of America Bulletin 107, 253-273. https://doi.org/10.1130/0016-7606(1995)107%3C0253:TEPEOT%3E2.3.CO;2

Azmy, K., Brand, U., Sylvester, P., Gleeson, S.A., Logan, A., Bitner, M.A., 2011. Biogenic and abiogenic low-Mg calcite (bLMC and aLMC): Evaluation of seawater-REE composition, water masses and carbonate diagenesis. Chemical Geology 280, 180-190. https://doi.org/10.1016/j.chemgeo.2010.11.007

Banner, J.L., 2004. Radiogenic isotopes: systematics and applications to earth surface processes and chemical stratigraphy. Earth-Science Reviews 65, 141-194. http://dx.doi.org/10.1016/S0012-8252(03)00086-2

Benedetto, J.L., 2004. The allochthony of the Argentine Precordillera ten years later (1993-2003): A new paleobiogeographic test of the microcontinental model. Gondwana Research 7, 1027-1039. http://dx.doi.org/10.1016/s1342-937x(05)71082-0

Benedetto, J.L., Vaccari, N.E., Waisfeld, B.G., Sánchez, T.M., Foglia, R.D., 2009. Cambrian and Ordovician biogeography of the South American margin of Gondwana and accreted terranes. Early Palaeozoic Peri-Gondwana Terranes: New Insights from Tectonics and Biogeography 325, 201-232. http://dx.doi.org/10.1144/sp325.11

Bergström, S.M., Chen, X.U., Gutiérrez-Marco, J.C., Dronov, A., 2009. The new chronostratigraphic classification of the Ordovician System and its relations to major regional series and stages and to $\delta^{13}C$ chemostratigraphy. Lethaia 42, 97-107. http://dx.doi.org/10.1111/j.1502-3931.2008.00136.x

Berner, R.A., 2006. GEOCARBSULF: A combined model for Phanerozoic atmospheric O_2 and CO_2. Geochimica et Cosmochimica Acta 70, 5653-5664. http://dx.doi.org/10.1016/j.gca.2005.11.032

Berner, R.A., 2009. Phanerozoic atmospheric oxygen: New results using the GEOCARBSULF model. American Journal of Science 309, 603-606. 10.2475/07.2009.03

Bock, B., Bahlburg, H., Wörner, G., Zimmermann, U., 2000. Tracing Crustal Evolution in the Southern Central Andes from Late Precambrian to Permian with Geochemical and Nd and Pb Isotope Data. The Journal of Geology 108, 515-535. 10.1086/314422

Broecker, W.S., 1999. What if the conveyor were to shut down? Reflections on a possible outcome of the great global experiment. GSA Today 9, 1-7.

Buggisch, W., Keller, M., Lehnert, O., 2003. Carbon isotope record of Late Cambrian to Early Ordovician carbonates of the Argentine Precordillera. Palaeogeography, Palaeoclimatology, Palaeoecology 195, 357-373. http://dx.doi.org/10.1016/S0031-0182(03)00365-1

Burke, W.H., Denison, R.E., Hetherington, E.A., Koepnick, R.B., Nelson, H.F., Otto, J.B., 1982. Variation of seawater $^{87}Sr/^{86}Sr$ throughout Phanerozoic time. Geology 10, 516-519. 10.1130/0091-7613(1982)10<516:vosstp>2.0.co;2

Calner, M., Lehnert, O., Wu, R., Dahlqvist, P., Joachimski, M.M., 2014. $\delta^{13}C$ chemostratigraphy in the Lower–Middle Ordovician succession of Öland (Sweden) and the global significance of the MDICE. GFF 136, 48-54. http://dx.doi.org/10.1080/11035897.2014.901409

Cañas, F.L., 2003. Selected sections of Lower to Middle Ordovician carbonate sedimentation of the Argentine Precordillera: The La Silla and San Juan formations at Cerros La Silla and Niquivil. INSUEGO, Miscelanea 8.

Carrera, M.G., 1997. Análisis paleoecológico de la fauna de poríferos del Llanvirniano tardío de la Precordillera Argentina. Ameghiniana 34, 309-316.

Carrera, M.G., Astini, R.A., 1998. Valoracion de las restriciones ambientales durante la transicion Argenigiano-Llanvirniano, Ordovícico de la Precordillera Argentina. Revista de la Asociación Geológica Argentina 53, 41-56.

Collo, G., Astini, R.A., Cawood, P.A., Buchan, C., Pimentel, M., 2009. U–Pb detrital zircon ages and Sm–Nd isotopic features in low-grade metasedimentary rocks of the Famatina belt: implications for late Neoproterozoic–early Palaeozoic evolution of the proto-Andean margin of Gondwana. Journal of the Geological Society 166, 303-319. 10.1144/0016-76492008-051

Dahlquist, J.A., Pankhurst, R.J., Gaschnig, R.M., Rapela, C.W., Casquet, C., Alasino, P.H., Galindo, C., Baldo, E.G., 2013. Hf and Nd isotopes in Early Ordovician to Early Carboniferous granites as monitors of crustal growth in the Proto-Andean margin of Gondwana. Gondwana Research 23, 1617-1630. https://doi.org/10.1016/j.gr.2012.08.013

Dasch, J.E., Hedge, C.E., Dymond, J., 1973. Effect of sea water interaction on strontium isotope composition of deep-sea basalts. Earth and Planetary Science Letters 19, 177-183. https://doi.org/10.1016/0012-821X(73)90112-X

Denison, R.E., Koepnick, R.B., Burke, W.H., Hetherington, E.A., 1998. Construction of the Cambrian and Ordovician seawater $^{87}Sr/^{86}Sr$ curve. Chemical Geology 152, 325-340. http://dx.doi.org/10.1016/S0009-2541(98)00119-3

Derry, L.A., Brasier, M.D., Corfield, R.M., Rozanov, A.Y., Zhuravlev, A.Y., 1994. Sr and C isotopes in Lower Cambrian carbonates from the Siberian craton: A paleoenvironmental record during the 'Cambrian explosion'. Earth and Planetary Science Letters 128, 671-681. http://dx.doi.org/10.1016/0012-821X(94)90178-3

Dopieralska, J., Belka, Z., Haack, U., 2006. Geochemical decoupling of water masses in the Variscan oceanic system during Late Devonian times. Palaeogeography, Palaeoclimatology, Palaeoecology 240, 108-119. http://dx.doi.org/10.1016/j.palaeo.2006.03.056

Ebneth, S., Shields, G.A., Veizer, J., Miller, J.F., Shergold, J.H., 2001. High-resolution strontium isotope stratigraphy across the Cambrian-Ordovician transition. Geochimica Et Cosmochimica Acta 65, 2273-2292. 10.1016/s0016-7037(01)00580-4

Edmond, J.M., 1992. Himalayan Tectonics, Weathering Processes, and the Strontium Isotope Record in Marine Limestones. Science 258, 1594-1597. 10.2307/2882056

Edwards, C.T., Fike, D.A., Saltzman, M.R., Lu, W., Lu, Z., 2018. Evidence for local and global redox conditions at an Early Ordovician (Tremadocian) mass extinction. Earth and Planetary Science Letters 481, 125-135. https://doi.org/10.1016/j.epsl.2017.10.002

Edwards, C.T., Saltzman, M.R., Leslie, S.A., Bergström, S.M., Sedlacek, A.R.C., Howard, A., Bauer, J.A., Sweet, W.C., Young, S.A., 2015. Strontium isotope ($^{87}Sr/^{86}Sr$) stratigraphy of Ordovician bulk carbonate: Implications for preservation of primary seawater values. GSA Bulletin 127, 1275-1289. 10.1130/b31149.1

Epstein, A.G., Epstein, J.B., Harris, L.D., Geological, S., 1977. Conodont color alteration - an index to organic metamorphism : experimental and field studies showing the application of conodont color alteration to geothermometry, metamorphism, and structural geology and for assessing hydrocarbon potential. U.S. Govt. Print. Off., Washington.

Fanning, C.M., Pankhurst, R.J., Rapela, C.W., Baldo, E.G., Casquet, C., Galindo, C., 2004. K-bentonites in the Argentine Precordillera contemporaneous with rhyolite volcanism in the Famatinian Arc. Journal of the Geological Society 161, 747-756. http://dx.doi.org/10.1144/0016-764903-130

Fanton, K.C., Holmden, C., Nowlan, G.S., Haidl, F.M., 2002. $^{143}Nd/^{144}Nd$ and Sm/Nd stratigraphy of Upper Ordovician epeiric sea carbonates. Geochimica et Cosmochimica Acta 66, 241-255. http://dx.doi.org/10.1016/S0016-7037(01)00773-6

Feltes, N., Albanesi, G.L., Bergstrom, S.M., 2016. Conodont biostratigraphy and global correlation of the middle Darriwilian-lower Sandbian (Ordovician) Las Aguaditas Formation, Precordillera of San Juan, Argentina. Andean Geology 43, 60-85. http://dx.doi.org/10.5027/andgeoV43n1-a04

Feltes, N.A., 2017. Fauna de conodontes y graptolitos de la Formación Las Aguaditas (Ordovícico) en el cordón de Los Blanquitos, Precordillera Central de San Juan, Argentina Universidad Nacional de Córdoba, Unpublished Dissertation, p. 453.

Frijia, G., Parente, M., 2008. Strontium isotope stratigraphy in the upper Cenomanian shallow-water carbonates of the southern Apennines: Short-term perturbations of marine $^{87}Sr/^{86}Sr$ during the oceanic anoxic event 2. Palaeogeography, Palaeoclimatology, Palaeoecology 261, 15-29. http://dx.doi.org/10.1016/j.palaeo.2008.01.003

Gao, G., Dworkin, S.I., Land, L.S., Elmore, R.D., 1996. Geochemistry of Late Ordovician Viola Limestone, Oklahoma: Implications for Marine Carbonate Mineralogy and Isotopic Compositions. The Journal of Geology 104, 359-367. 10.2307/30068198

Gleason, J.D., Finney, S.C., Peralta, S.H., Gehrels, G.E., Marsaglia, K.M., 2007. Zircon and whole-rock Nd-Pb isotopic provenance of Middle and Upper Ordovician siliciclastic rocks, Argentine Precordillera. Sedimentology 54, 107-136. 10.1111/j.1365-3091.2006.00820.x

Grandjean, P., Cappetta, H., Michard, A., Albare`de, F., 1987. The assessment of REE patterns and $^{143}Nd/^{144}Nd$ ratios in fish remains. Earth and Planetary Science Letters 84, 181-196. http://dx.doi.org/10.1016/0012-821X(87)90084-7

Gruszczynski, M., Hoffman, A., Malkowski, K., Veizer, J., 1992. Seawater strontium isotopic perturbation at the Permian-Triassic boundary, West Spitsbergen, and its implications for the interpretation of strontium isotopic data. Geology 20, 779-782. 10.1130/0091-7613(1992)020<0779:ssipat>2.3.co;2

Henderson, M.A., Gomez, F.J., Szynkiewicz, A., Feltes, N.A., Serra, F., Albanesi, G.L., Kah, L.C., *in prep*. Sulfur cycling in the Darriwilian (Middle Ordovician) of Argentina: Implications for ocean circulation and the redox evolution of the Ordovician ocean.

Henderson, M.A., Serra, F., Feltes, N.A., Albanesi, G.L., Kah, L.C., 2018. Paired isotope records of carbonate and organic matter from the Middle Ordovician of Argentina: Intrabasinal variation and effects of the marine chemocline. Palaeogeography, Palaeoclimatology, Palaeoecology 490, 107-130. https://doi.org/10.1016/j.palaeo.2017.10.018

Heredia, S., Beresi, M., Peralta, S., 2005. Darriwilian conodont biostratigraphy of the Las Chacritas Formation, Central Precordillera (San Juan Province, Argentina). Geologica Acta 3, 385-394.

Heredia, S., Mestre, A., 2011. Middle Darriwilian conodont biostratigraphy in the Argentine Precordillrea, in: Gutiérrez-Marco, J.C., Rábano, I., García-Bellido, D. (Eds.), Ordovician of the world. Instituto Geológico y Minero de Espana, Madrid, Spain.

Heredia, S., Mestre, A., Soria, T., Kaufmann, C., 2017. The Ordovician genus *Pygodus* (conodont) in the Cuyania Terrane, Argentina. Geological Magazine 154, 1105-1116. 10.1017/s0016756816000728

Holmden, C., Creaser, R.A., Muehlenbachs, K., Bergstrom, S.M., Leslie, S.A., 1996. Isotopic and elemental systematics of Sr and Nd in 454 Ma biogenic apatites: implications for paleoseawater studies. Earth and Planetary Science Letters 142, 425-437. http://dx.doi.org/10.1016/0012-821X(96)00119-7

Holmden, C., Creaser, R.A., Muehlenbachs, K., Leslie, S.A., Bergström, S.M., 1998. Isotopic evidence for geochemical decoupling between ancient epeiric seas and

bordering oceans: Implications for secular curves. Geology 26, 567-570. http://dx.doi.org/10.1130/0091-7613(1998)026<0567:iefgdb>2.3.co;2

Holmden, C., Mitchell, C.E., LaPorte, D.F., Patterson, W.P., Melchin, M.J., Finney, S.C., 2013. Nd isotope records of late Ordovician sea-level change—Implications for glaciation frequency and global stratigraphic correlation. Palaeogeography, Palaeoclimatology, Palaeoecology 386, 131-144. http://dx.doi.org/10.1016/j.palaeo.2013.05.014

Huff, W., Davis, D., Bergström, S., Krekeler, M., Kolata, D., Cingolani, C., 1997. A biostratigraphically well-constrained K-bentonite U-Pb zircon age of the lowermost Darriwilian Stage (Middle Ordovician) from the Argentine Precordillera. Episodes 20, 29-33. https://doi.org/10.1144/0016-764903-130

Huff, W.D., Bergström, S.M., Kolata, D.R., Cingolani, C., Davis, D.W., 1995. Middle Ordovician K-bentonites discovered in the Precordillera of Argentina: Geochemical and paleogeographical implications, in: Cooper, J.D., Droser, M.L., Finney, S.C. (Eds.), Ordovician oddesy: short papers for the seventh international symposium on the Ordovician system. SEPM, Las Vegas, Nevada, pp. 343-349.

Huff, W.D., Bergström, S.M., Kolata, D.R., Cingolani, C.A., Astini, R.A., 1998. Ordovician K-bentonites in the Argentine Precordillera: relations to Gondwana margin evolution. Geological Society, London, Special Publications 142, 107-126. 10.1144/gsl.sp.1998.142.01.06

Jones, D.S., Fike, D.A., 2013. Dynamic sulfur and carbon cycling through the end-Ordovician extinction revealed by paired sulfate–pyrite $\delta^{34}S$. Earth and Planetary Science Letters 363, 144-155. http://dx.doi.org/10.1016/j.epsl.2012.12.015

Kah, L.C., Thompson, C.K., Henderson, M.A., Zhan, R., 2016. Behavior of marine sulfur in the Ordovician. Palaeogeography, Palaeoclimatology, Palaeoecology 458, 133-153. http://dx.doi.org/10.1016/j.palaeo.2015.12.028

Kaljo, D., Martma, T., Saadre, T., 2007. Post-Hunnebergian Ordovician carbon isotope trend in Baltoscandia, its environmental implications and some similarities with that of Nevada. Palaeogeography, Palaeoclimatology, Palaeoecology 245, 138-155. http://dx.doi.org/10.1016/j.palaeo.2006.02.020

Kamber, B.S., Webb, G.E., 2001. The geochemistry of late archean microbial carbonate: Implications for ocean chemistry and continental erosion history. Geochimica et Cosmochimica Acta 65, 2509-2525.

Kaufman, A.J., Knoll, A.H., 1995. Neoproterozoic variations in the C-isotopic composition of seawater: stratigraphic and biogeochemical implications. Precambrian Research 73, 27-49. http://dx.doi.org/10.1016/0301-9268(94)00070-8

Keller, M., 1999. Argentine Precordillera: Sedimentary and plate tectonic history of a Laurentian crustal fragment in South America. Geological Society of America Special Paper 341. https://dx.doi.org/10.1130/0-8137-2341-8.1

Keller, M., Eberlein, S., Lehnert, O., 1993. Sedimentology of middle ordovician carbonates in the Argentine precordillera: evidence of regional relative sea-level changes. Geol Rundsch 82, 362-377. http://dx.doi.org/10.1007/BF00191838

Keto, L.S., Jacobsen, S.B., 1987. Nd and Sr isotopic variations of Early Paleozoic oceans. Earth and Planetary Science Letters 84, 27-41. http://dx.doi.org/10.1016/0012-821X(87)90173-7

Küspert, W., 1982. Environmental Changes During Oil Shale Deposition as Deduced from Stable Isotope Ratios, in: Einsele, G., Seilacher, A. (Eds.), Cyclic and Event Stratification. Springer Berlin Heidelberg, Berlin, Heidelberg, pp. 482-501. 10.1007/978-3-642-75829-4_36

Leslie, S.A., Saltzman, M.R., Bergström, S.M., Repetski, J.E., Howard, A., Seward, A.M., 2011. Conodont biostratigraphy and stable isotope stratigraphy across the Ordovician Knox/Beekmantown unconformity in the central Appalachians, in: Gutiérrez-Alonso, G., Diego, G.B. (Eds.), Ordovician of the World. Publicaciones del Instituto Geológico y Minero de España.

MacLeod, K.G., Isaza Londono, C., Martin, E.E., Jimenez Berrocoso, A., Basak, C., 2011. Changes in North Atlantic circulation at the end of the Cretaceous greenhouse interval. Nature Geosci 4, 779-782. http://www.nature.com/ngeo/journal/v4/n11/abs/ngeo1284.html#supplementary-information

MacLeod, K.G., Martin, E.E., Blair, S.W., 2008. Nd isotopic excursion across Cretaceous ocean anoxic event 2 (Cenomanian-Turonian) in the tropical North Atlantic. Geology 36, 811-814. 10.1130/g24999a.1

Marenco, P.J., Marenco, K.N., Lubitz, R.L., Niu, D., 2013. Contrasting long-term global and short-term local redox proxies during the Great Ordovician Biodiversification Event: A case study from Fossil Mountain, Utah, USA. Palaeogeography, Palaeoclimatology, Palaeoecology 377, 45-51. http://dx.doi.org/10.1016/j.palaeo.2013.03.007

Martin, E.E., MacLeod, K.G., Jiménez Berrocoso, A., Bourbon, E., 2012. Water mass circulation on Demerara Rise during the Late Cretaceous based on Nd isotopes. Earth and Planetary Science Letters 327–328, 111-120. http://dx.doi.org/10.1016/j.epsl.2012.01.037

Martina, F., Astini, R.A., Pimentel, M.M., 2014. Sr–Nd isotope data of basement rocks from the northernmost argentine Precordillera and its implications for the early Paleozoic evolution of SW Gondwana margin. Journal of South American Earth Sciences 56, 20-29. https://doi.org/10.1016/j.jsames.2014.08.006

McArthur, J.M., 1994. Recent trends in strontium isotope stratigraphy. Terra Nova 6, 331-358. 10.1111/j.1365-3121.1994.tb00507.x

Meidla, T., Backman, L., Dronov, A., Holmer, L., Sturesson, U., 2004. Middle-Upper Ordovician carbon isotope record from Västergötland (Sweden) and East Baltic,

in: Hints, O., Ainsaar, L. (Eds.), 8th Meeting on the Working Group on the Ordovician Geology of Baltoscandia. Tartu University Press, Tallinn and Tartu, Estonia, pp. 67-68.

Mestre, A., Heredia, S., 2013. Biostratigraphic significance of Darriwilian conodonts from Sierra de La Trampa (Central Precordillera, San Juan, Argentina). Geosciences Journal 17, 43-53. 10.1007/s12303-013-0006-2

Montañez, I.P., Banner, J.L., Osleger, D.A., Borg, L.E., Bosserman, P.J., 1996. Integrated Sr isotope variations and sea-level history of Middle to Upper Cambrian platform carbonates: Implications for the evolution of Cambrian seawater $^{87}Sr/^{86}Sr$. Geology 24, 917-920. 10.1130/0091-7613(1996)024<0917:isivas>2.3.co;2

Palmer, M.R., Edmond, J.M., 1989. The strontium isotope budget of the modern ocean. Earth and Planetary Science Letters 92, 11-26. http://dx.doi.org/10.1016/0012-821X(89)90017-4

Pankhurst, R.J., Rapela, C.W., Fanning, C.M., 2000. Age and origin of coeval TTG, I- and S-type granites in the Famatinian belt of NW Argentina. Geological Society of America Special Papers 350, 151-168. http://dx.doi.org/10.1130/0-8137-2350-7.151

Pankhurst, R.J., Rapela, C.W., Saavedra, J., Baldo, E., Dahlquist, J., Pascua, I., Fanning, C.M., 1998. The Famatinian magmatic arc in the central Sierras Pampeanas: an Early to Mid-Ordovician continental arc on the Gondwana margin. Geological Society, London, Special Publications 142, 343-367. 10.1144/gsl.Sp.1998.142.01.17

Peralta, S.H., Heredia, S., Beresi, M.S., 1999. Upper Arenigian-lower Llanvirnian sequence of the Las Chacritas river, Central Precordillera, San Juan Province, Argentina. Acta Universitatis Carolinae Geologica 43, 123-126.

Piepgras, D.J., Wasserburg, G.J., 1980. Neodymium isotopic variations in seawater. Earth and Planetary Science Letters 50, 128-138. http://dx.doi.org/10.1016/0012-821X(80)90124-7

Piepgras, D.J., Wasserburg, G.J., Dasch, E.J., 1979. The isotopic composition of Nd in different ocean masses. Earth and Planetary Science Letters 45, 223-236. http://dx.doi.org/10.1016/0012-821X(79)90125-0

Pier, J.G., Podosek, F.A., Luhr, J.F., Brannon, J.C., Aranda-Gomez, J.J., 1989. Spinel-lherzolite-bearing quaternary volcanic centers in San Luis Potosí, Mexico: 2. Sr and Nd Isotopic Systematics. Journal of Geophysical Research: Solid Earth 94, 7941-7951. http://dx.doi.org/10.1029/JB094iB06p07941

Pope, M.C., Steffen, J.B., 2003. Widespread, prolonged late Middle to Late Ordovician upwelling in North America: A proxy record of glaciation? Geology 31, 63-66. http://dx.doi.org/10.1130/0091-7613(2003)031<0063:wplmtl>2.0.co;2

Qing, H., Barnes, C.R., Buhl, D., Veizer, J., 1998. The strontium isotopic composition of Ordovician and Silurian brachiopods and conodonts: relationships to geological

events and implications for coeval seawater. Geochimica et Cosmochimica Acta 62, 1721-1733. http://dx.doi.org/10.1016/S0016-7037(98)00104-5

Quinton, P.C., Percival, I.G., Zhen, Y.Y., MacLeod, K.G., 2015. Factors influencing conodont apatite δ18O variability in the Ordovician: a case study from New South Wales, Australia. Stratigraphy 12, 265-274.

Railsback, L.B., Ackerly, S.C., Anderson, T.F., Cisneti, J.L., 1990. Palaeontological and isotope evidence for warm saline deep waters in Ordovician oceans. Nature 343, 156-159. http://dx.doi.org/10.1038/343156a0

Ramos, V.A., Jordan, T.E., Allmendinger, R.W., Mpodozis, C., Kay, S.M., Cortes, J.M., Palma, M., 1986. Paleozoic terranes of the Central Argentine-Chilean Andes. Tectonics 5, 855-880. http://dx.doi.org/10.1029/TC005i006p00855

Richter, F.M., Rowley, D.B., DePaolo, D.J., 1992. Sr isotope evolution of seawater: the role of tectonics. Earth and Planetary Science Letters 109, 11-23. http://dx.doi.org/10.1016/0012-821X(92)90070-C

Ronov, A.B., 1980. Quantitative analysis of Phanerozoic sedimentation. Sedimentary Geology 25, 311-325.

Saltzman, M.R., 2005. Phosphorus, nitrogen, and the redox evolution of the Paleozoic oceans. Geology 33, 573-576. http://dx.doi.org/10.1130/g21535.1

Saltzman, M.R., Edwards, C.T., Adrain, J.M., Westrop, S.R., 2015. Persistent oceanic anoxia and elevated extinction rates separate the Cambrian and Ordovician radiations. Geology 43, 807-810. 10.1130/g36814.1

Saltzman, M.R., Edwards, C.T., Leslie, S.A., Dwyer, G.S., Bauer, J.A., Repetski, J.E., Harris, A.G., Bergström, S.M., 2014. Calibration of a conodont apatite-based Ordovician $^{87}Sr/^{86}Sr$ curve to biostratigraphy and geochronology: Implications for stratigraphic resolution. Geological Society of America Bulletin. 10.1130/b31038.1

Saltzman, M.R., Young, S.A., 2005. Long-lived glaciation in the Late Ordovician? Isotopic and sequence-stratigraphic evidence from western Laurentia. Geology 33, 109-112. http://dx.doi.org/10.1130/g21219.1

Schmitz, B., Bergström, S.M., Xiaofeng, W., 2010. The middle Darriwilian (Ordovician) δ13C excursion (MDICE) discovered in the Yangtze Platform succession in China: implications of its first recorded occurrences outside Baltoscandia. Journal of the Geological Society 167, 249-259. http://dx.doi.org/10.1144/0016-76492009-080

Serra, F., Albanesi, G.L., Ortega, G., Bergstrom, S.M., 2015. Biostratigraphy and palaeoecology of Middle–Late Ordovician conodont and graptolite faunas of the Las Chacritas River section, Precordillera of San Juan, Argentina. Geological Magazine 152, 813-829. http://dx.doi.org/10.1017/S0016756814000752

Serra, F., Feltes, N.A., Ortega, G., Albanesi, G.L., 2017. Lower middle Darriwilian (Ordovician) graptolites and index conodonts from the Central Precordillera of San Juan Province, Argentina. Geological Journal. 10.1002/gj.3043

Servais, T., Danelian, T., Harper, D.A.T., Munnecke, A., 2014. Possible oceanic circulation patterns, surface water currents and upwelling zones in the Early Palaeozoic. Gff 136, 229-233. http://dx.doi.org/10.1080/11035897.2013.876659

Shaw, H.F., Wasserburg, G.J., 1985. Sm-Nd in marine carbonates and phosphates: Implications for Nd isotopes in seawater and crustal ages. Geochimica et Cosmochimica Acta 49, 503-518. http://dx.doi.org/10.1016/0016-7037(85)90042-0

Shields, G.A., Carden, G.A.F., Veizer, J., Meidla, T., Rong, J.-Y., Li, R.-Y., 2003. Sr, C, and O isotope geochemistry of Ordovician brachiopods: a major isotopic event around the Middle-Late Ordovician transition. Geochimica et Cosmochimica Acta 67, 2005-2025. http://dx.doi.org/10.1016/S0016-7037(02)01116-X

Stille, P., 1992. Nd-Sr isotope evidence for dramatic changes of paleocurrents in the Atlantic Ocean during the past 80 m.y. Geology 20, 387-390. 10.1130/0091-7613(1992)020<0387:nsiefd>2.3.co;2

Taylor, S.R., McLennan, S.M., 1985. The Continental Crust: Its Composition and Evolution. Blackwell, Oxford.

Theiling, B.P., Elrick, M., Asmerom, Y., 2012. Increased continental weathering flux during orbital-scale sea-level highstands: Evidence from Nd and O isotope trends in Middle Pennsylvanian cyclic carbonates. Palaeogeography, Palaeoclimatology, Palaeoecology 342, 17-26. http://dx.doi.org/10.1016/j.palaeo.2012.04.017

Thomas, W.A., 2011. The Iapetan rifted margin of southern Laurentia. Geosphere 7, 97-120. http://dx.doi.org/10.1130/ges00574.1

Thomas, W.A., Astini, R.A., 1996. The Argentine Precordillera: A traveler from the Ouachita embayment of North American Laurentia. Science 273, 752-757. http://dx.doi.org/10.1126/science.273.5276.752

Thomas, W.A., Astini, R.A., 1999. Simple-shear conjugate rift margins of the Argentine Precordillera and the Ouachita embayment of Laurentia. Geological Society of America Bulletin 111, 1069-1079. 10.1130/0016-7606(1999)111<1069:sscrmo>2.3.co;2

Thomas, W.A., Astini, R.A., Bayona, G., 2002. Ordovician collision of the Argentine Precordillera with Gondwana, independent of Laurentian Taconic orogeny. Tectonophysics 345, 131-152. http://dx.doi.org/10.1016/S0040-1951(01)00210-4

Thomas, W.A., Astini, R.A., Denison, R.E., 2001. Strontium isotopes, age, and tectonic setting of Cambrian salinas along the rift and transform margins of the Argentine Precordillera and southern Laurentia. Journal of Geology 109, 231-246. http://dx.doi.org/10.1086/319241

Thomas, W.A., Astini, R.A., Mueller, P.A., McClelland, W.C., 2015. Detrital-zircon geochronology and provenance of the Ocloyic synorogenic clastic wedge, and Ordovician accretion of the Argentine Precordillera terrane. Geosphere 11, 1749-1769. 10.1130/ges01212.1

Thompson, C.K., Kah, L.C., 2012. Sulfur isotope evidence for widespread euxinia and a fluctuating oxycline in Early to Middle Ordovician greenhouse oceans. Palaeogeography, Palaeoclimatology, Palaeoecology 313-314, 189-214. http://dx.doi.org/10.1016/j.palaeo.2011.10.020

Thompson, C.K., Kah, L.C., Astini, R., Bowring, S.A., Buchwaldt, R., 2012. Bentonite geochronology, marine geochemistry, and the Great Ordovician Biodiversification Event (GOBE). Palaeogeography, Palaeoclimatology, Palaeoecology 321–322, 88-101. http://dx.doi.org/10.1016/j.palaeo.2012.01.022

Thorsten Kleine, Klaus Mezger, Udo Zimmermann, Carsten Münker, Heinrich Bahlburg, 2004. Crustal Evolution along the Early Ordovician Proto-Andean Margin of Gondwana: Trace Element and Isotope Evidence from the Complejo Igneo Pocitos (Northwest Argentina). The Journal of Geology 112, 503-520. 10.1086/422663

Trotter, J.A., Williams, I.S., Barnes, C.R., Lécuyer, C., Nicoll, R.S., 2008. Did Cooling Oceans Trigger Ordovician Biodiversification? Evidence from Conodont Thermometry. Science 321, 550-554. http://dx.doi.org/10.1126/science.1155814

Van Cappellen, P., Ingall, E.D., 1994. Benthic phosphorus regeneration, net primary production, and ocean anoxia: A model of the coupled marine biogeochemical cycles of carbon and phosphorus. Paleoceanography 9, 677-692. http://dx.doi.org/10.1029/94PA01455

Veizer, J., 1989. Strontium isotopes in seawater through time. Annual Review of Earth and Planetary Sciences 17, 141-167. 10.1146/annurev.ea.17.050189.001041

Veizer, J., Compston, W., 1974. $^{87}Sr/^{86}Sr$ composition of seawater during the Phanerozoic. Geochimica et Cosmochimica Acta 38, 1461-1484. http://dx.doi.org/10.1016/0016-7037(74)90099-4

Webb, G.E., Kamber, B.S., 2000. Rare earth elements in Holocene reefal microbialites: A new shallow seawater proxy 64, 1557-1565.

Wright, C.A., Barnes, C.R., Jacobsen, S.B., 2002. Neodymium isotopic composition of Ordovician conodonts as a seawater proxy: Testing paleogeography. Geochemistry, Geophysics, Geosystems 3, n/a-n/a. 10.1029/2001GC000195

Wright, J., Seymour, R.S., Shaw, H.F., 1984. REE and Nd isotopes in conodont apatite: Variations with geological age and depositional environment. Geological Society of America Special Papers 196, 325-340. 10.1130/SPE196-p325

Yan, D., Chen, D., Wang, Q., Wang, J., Wang, Z., 2009. Carbon and sulfur isotopic anomalies across the Ordovician–Silurian boundary on the Yangtze Platform,

South China. Palaeogeography, Palaeoclimatology, Palaeoecology 274, 32-39. http://dx.doi.org/10.1016/j.palaeo.2008.12.016

Young, S.A., Gill, B.C., Edwards, C.T., Saltzman, M.R., Leslie, S.A., 2016. Middle–Late Ordovician (Darriwilian–Sandbian) decoupling of global sulfur and carbon cycles: Isotopic evidence from eastern and southern Laurentia. Palaeogeography, Palaeoclimatology, Palaeoecology 458, 118-132. http://dx.doi.org/10.1016/j.palaeo.2015.09.040

Young, S.A., Saltzman, M.R., Foland, K.A., Linder, J.S., Kump, L.R., 2009. A major drop in seawater $^{87}Sr/^{86}Sr$ during the Middle Ordovician (Darriwilian): Links to volcanism and climate? Geology 37, 951-954. 10.1130/g30152a.1

Zapata, T.R., Allmendinger, R.W., 1996. Thrust-front zone of the Precordillera, Argentina: A thick-skinned triangle zone. Aapg Bulletin-American Association of Petroleum Geologists 80, 359-381.

Zhang, T., Shen, Y., Algeo, T.J., 2010. High-resolution carbon isotopic records from the Ordovician of South China: Links to climatic cooling and the Great Ordovician Biodiversification Event (GOBE). Palaeogeography, Palaeoclimatology, Palaeoecology 289, 102-112. http://dx.doi.org/10.1016/j.palaeo.2010.02.020

Zhao, M.-Y., Zheng, Y.-F., 2014. Marine carbonate records of terrigenous input into Paleotethyan seawater: Geochemical constraints from Carboniferous limestones. Geochimica et Cosmochimica Acta 141, 508-531. https://doi.org/10.1016/j.gca.2014.07.001

Zhou, L., Algeo, T.J., Shen, J., Hu, Z., Gong, H., Xie, S., Huang, J., Gao, S., 2015. Changes in marine productivity and redox conditions during the Late Ordovician Hirnantian glaciation. Palaeogeography, Palaeoclimatology, Palaeoecology 420, 223-234. http://dx.doi.org/10.1016/j.palaeo.2014.12.012

Zimmermann, U., Bahlburg, H., 2003. Provenance analysis and tectonic setting of the Ordovician clastic deposits in the southern Puna Basin, NW Argentina. Sedimentology 50, 1079-1104. 10.1046/j.1365-3091.2003.00595.x

Appendix 1

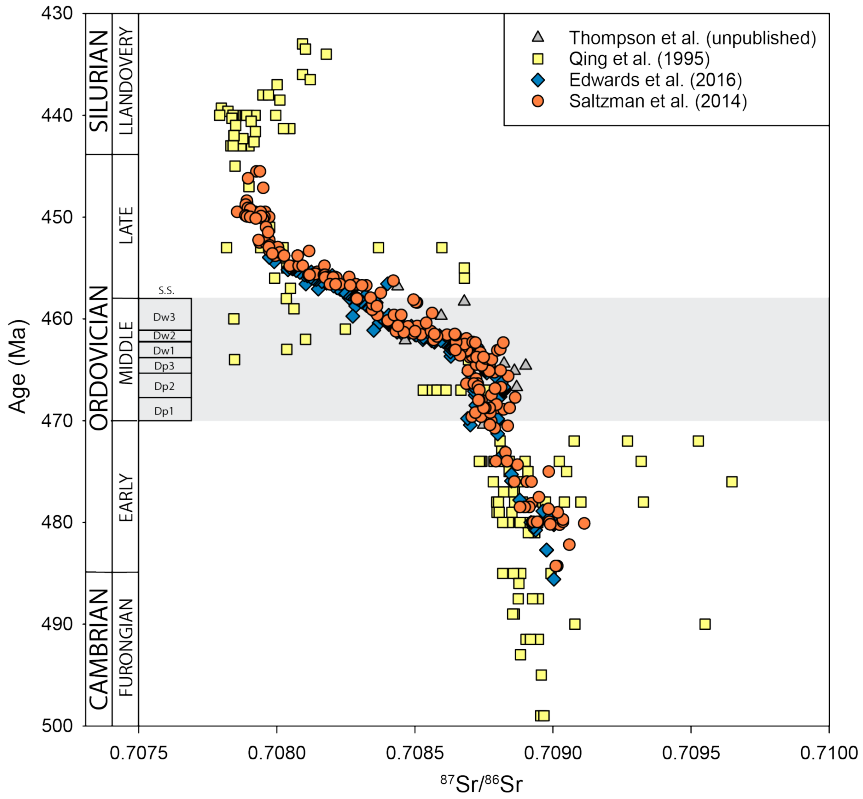

Figure 3.1: Strontium isotope curve for the early Paleozoic showing the large drop in $^{87}Sr/^{86}Sr$ values in the Darriwilian-Sandbian interval (Middle Ordovician highlighted in gray). Data plotted in yellow squares and orange circles from Qing et al. (1995) and Saltzman et al. (2014), respectively, from conodont elements. Sr-isotope measurements from fine-grained carbonate mud plotted in blue diamonds and gray triangles from Edwards et al. (2015) and unpublished data from Thompson et al., respectively. Stage slices of the Middle Ordovician interval from Bergström et al. (2009).

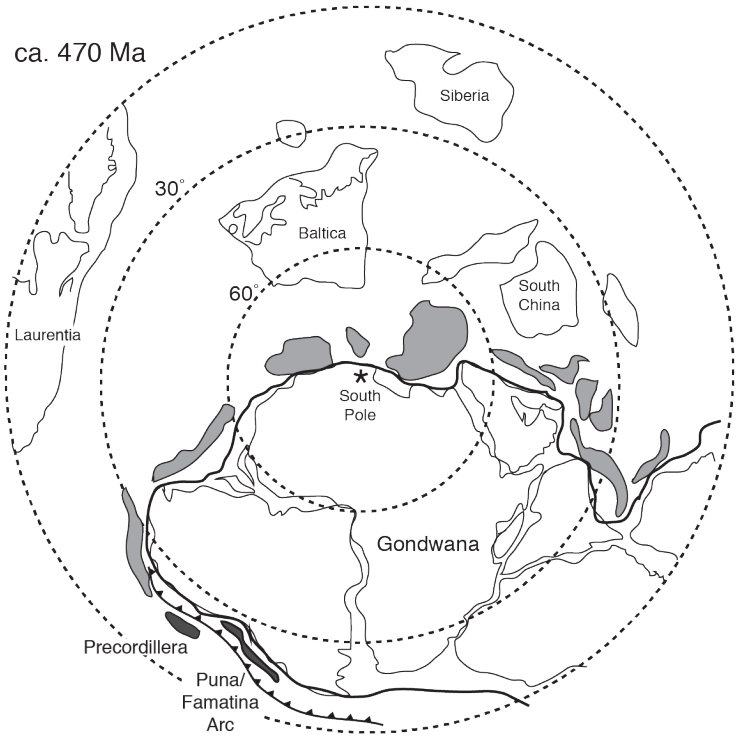

Figure 3.2: Paleogeographic reconstruction of the Middle Ordovician after Cocks and Torsvik (2002) and Astini et al. (2007). Major landmasses are depicted in white with Perigondwanan terranes in gray. The Precordilleran terrane and the Puna/Famatina Arc are shown in dark gray. Famatina Arc volcanism is the source of Middle Ordovician bentonite deposits identified in late Dapingian/early Darriwilian strata throughout the Precordillera (Fanning et al., 2004).

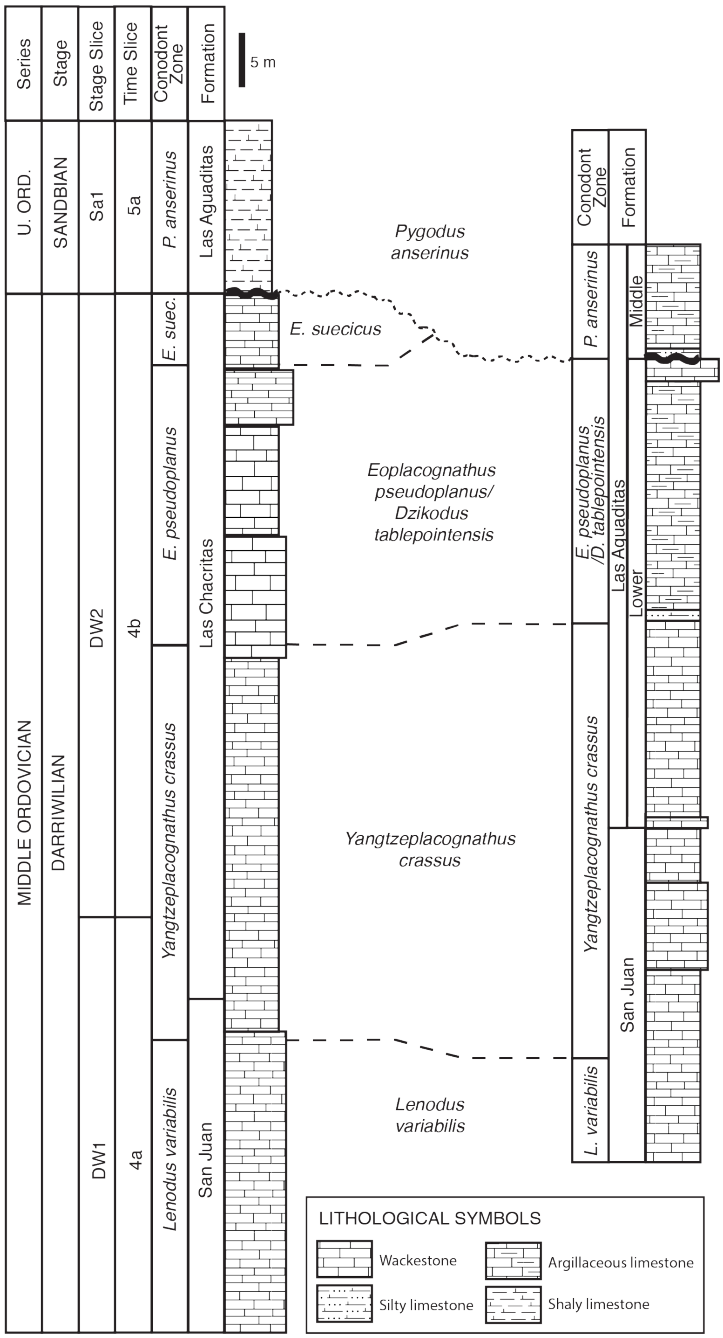

Figure 3.3: Stratigraphic correlation of the Las Chacritas River and Las Aguaditas Creek sections based on conodont biostratigraphic analysis of Serra et al., (2015) and Feltes et al., (2016). Upper Darriwilian strata (Dw3) of the upper *E. suecicus* and *P. serra* conodont Zones in the Las Chacritas Formation and the *E. suecicus* and *P. serra* Zones in the Las Aguaditas Formation have been removed during development of a regional unconformity and are overlain by Sandbian (Sa1) strata of the middle member of the Las Aguaditas Formation.

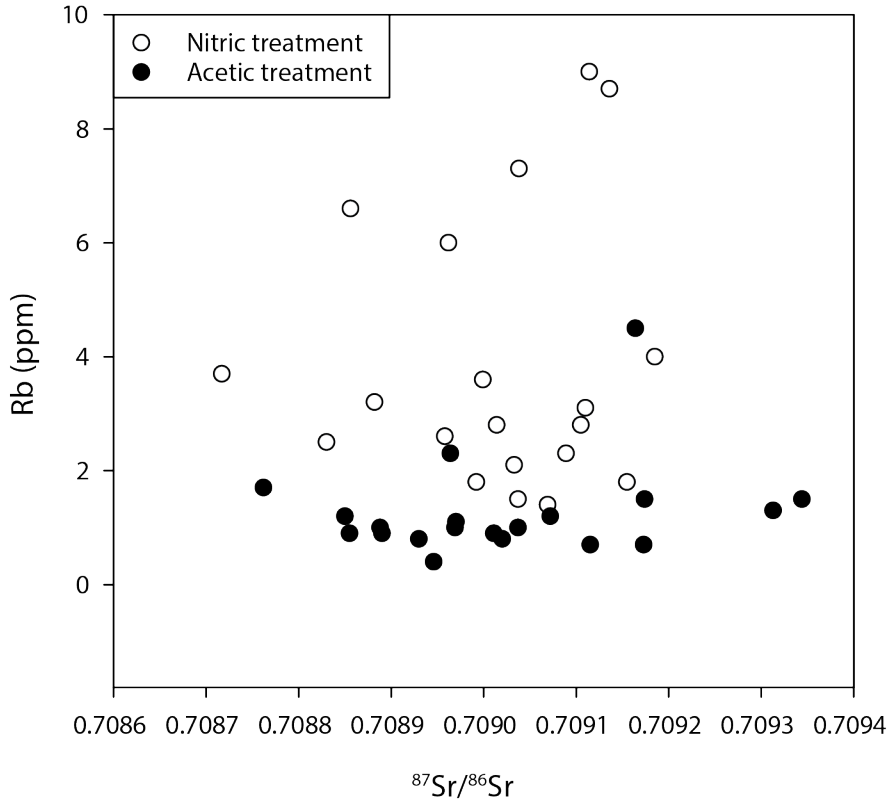

Figure 3.4: Cross-plot of Rb concentration versus Sr-isotope measurement from samples treated with nitric acid and acetic acid from the Las Chacritas Formation. Generally, samples treated with nitric acid have higher Rb concentrations than samples treated with acetic acid, suggesting potential liberation of detrital Rb that adversely affects calculated initial $^{87}Sr/^{86}Sr$ compositions. Therefore, we consider the samples treated with nitric acid to better represent seawater compositions.

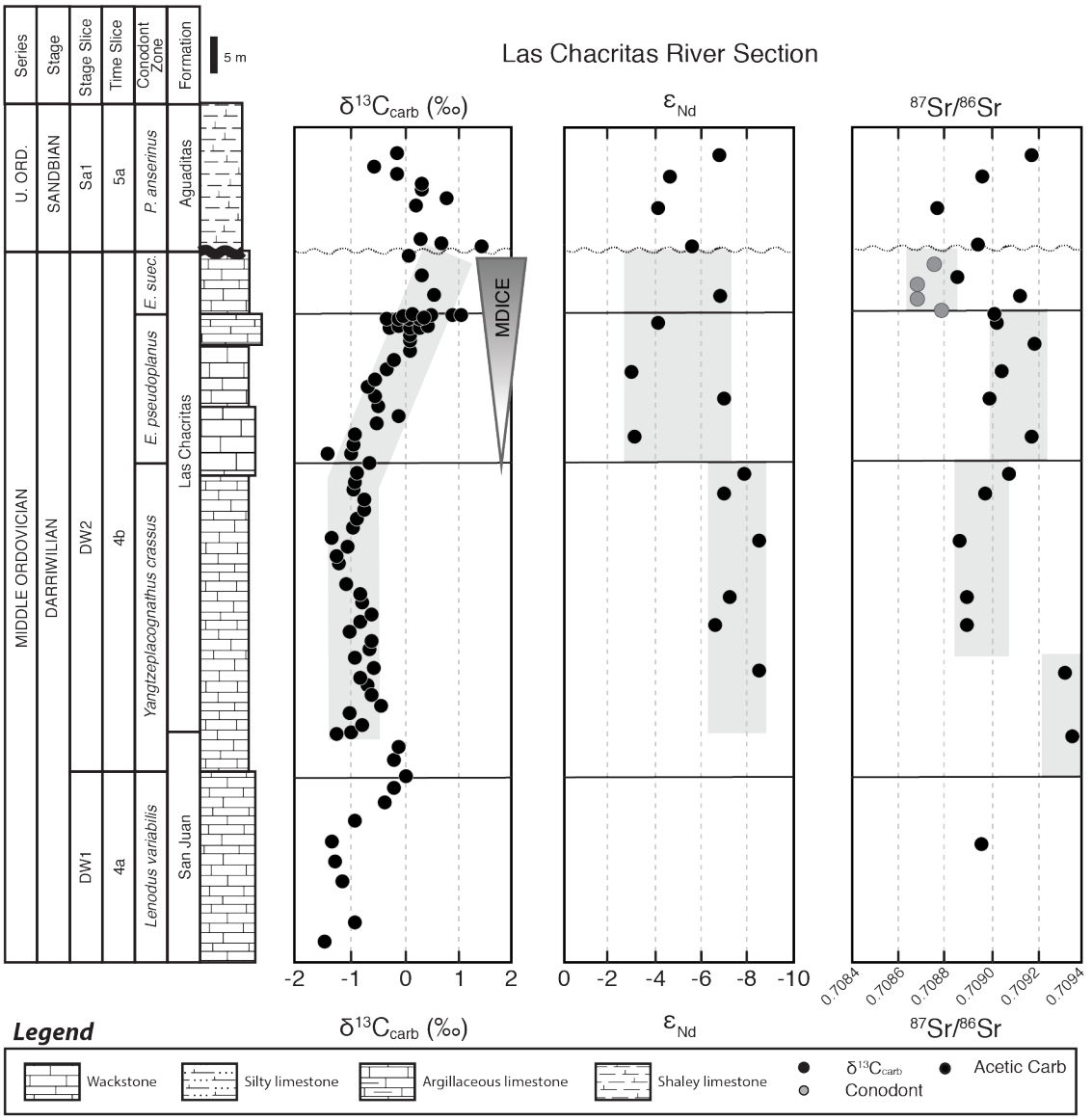

Figure 3.5: Chemostratigraphic profiles of the Las Chacritas Formation. The $\delta^{13}C_{carb}$ profile from Henderson et al. (2018) shows values around −1‰ through the *Y. crassus* Zone and the positive ~2‰ expression of the MDICE through the *E. pseudoplanus* and *E. suecicus* zones. Neodymium isotope compositions of the Las Chacritas Formation show an increase in variability from ε_{Nd} values around −6 to −8 to ε_{Nd} values as low as −3. The $^{87}Sr/^{86}Sr$ values of the Las Aguaditas Formation show average compositions declining from around 0.7090 in the Y. crassus Zone to values around 0.7089 in the *E. pseudoplanus* Zone and to values near 0.7088 in the *E. suecicus* Zone. Variability in $^{87}Sr/^{86}Sr$ within individual conodont zones appears strongly correlated with water depth.

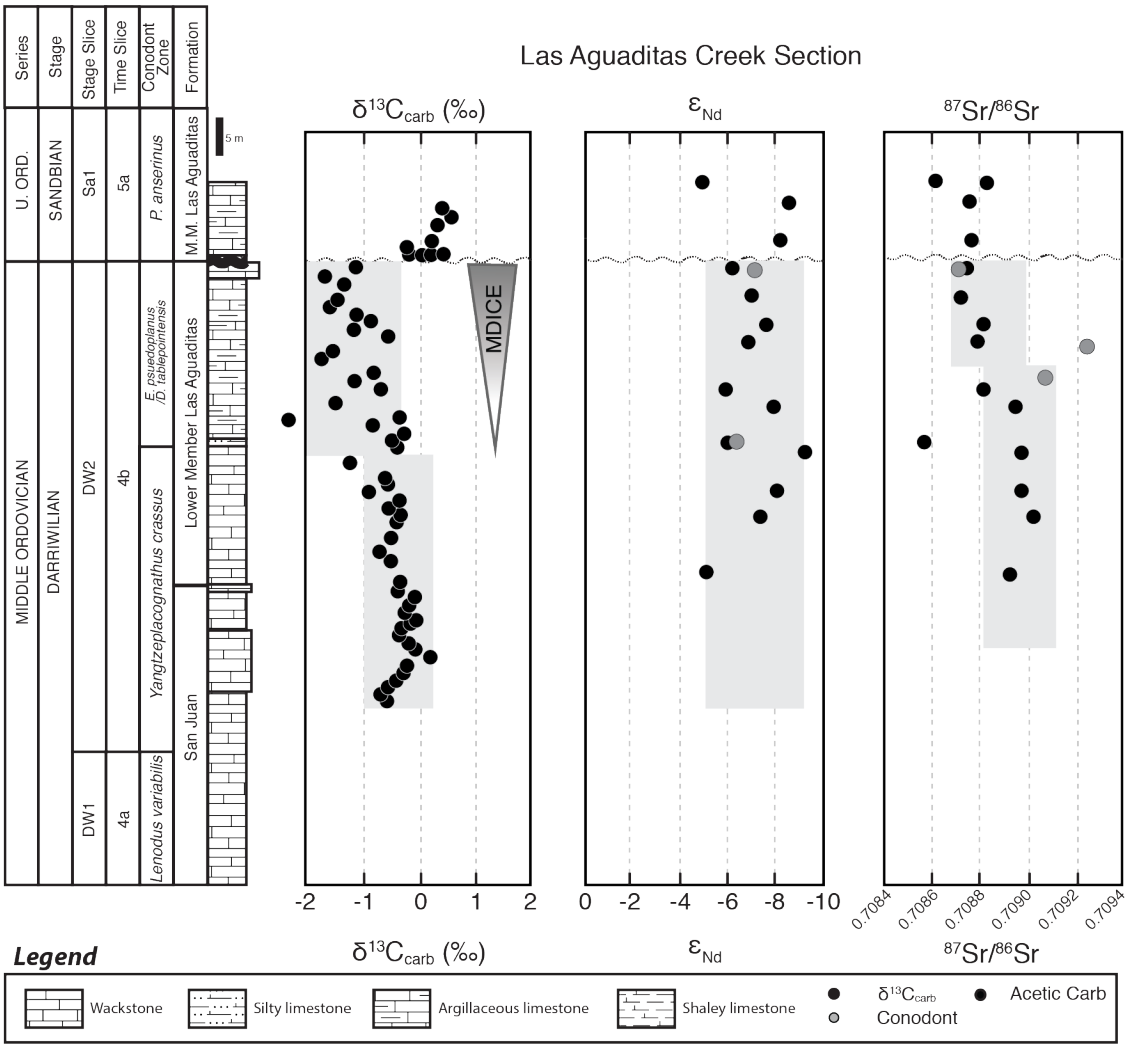

Figure 3.6: Chemostratigraphic profiles of the Las Aguaditas Formation. The abrupt decline in $\delta^{13}C_{carb}$ values from around −0.5‰ in the Y. crassus Zone to values around −1.5‰ in the *E. pseudoplanus/D. tablepointensis* Zone is interpreted to reflect migration of the Las Aguaditas Formation below the marine chemocline at the onset of the MDICE (Henderson et al., 2018). Neodymium isotope compositions in the *Y. crassus* Zone have ε_{Nd} values between −6 and −8 and no change in ε_{Nd} is observed in the *E. pseudoplanus/D. tablepointensis* Zone. The $^{87}Sr/^{86}Sr$ values of the Las Aguaditas Formation show the general trend for the Middle Ordovician, with values declining from around 0.7090 to values around 0.7088.

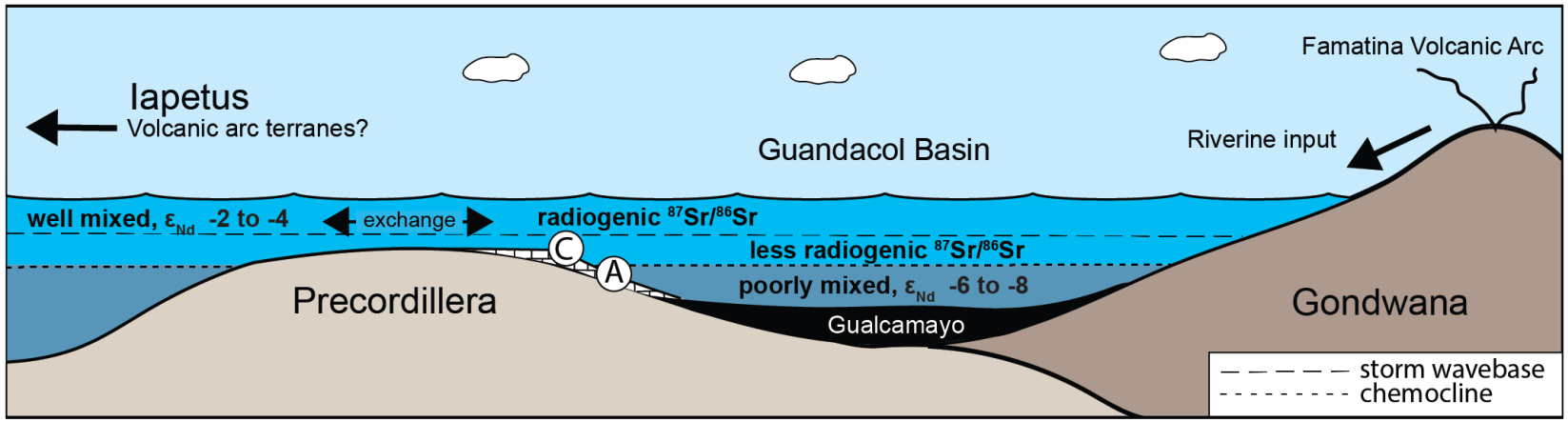

Figure 3.7: Schematic diagram of the marine shelf of the Precordillera during deposition of the Las Chacritas and Las Aguaditas formations. Geochemical decoupling between shallow- and deep-waters best explains the observed behavior of both ε_{Nd} and $^{87}Sr/^{86}Sr$ compositions. Radiogenic isotope variation can be explained by (1) exchange of Iapetan ocean waters across the Precordillera terrane, (2) volcanic activity and weathering of the Famatina volcanic province, or (3) changes in weathering changes in surface runoff between Gondwanan arc-derived terranes and older cratonic rocks.

Table 3.1: Range of isotopic and elemental concentrations of samples from the Las Chacritas River section

Sample	Height	Lithology	Conodont Zone	$\delta^{13}C$ ‰	$\delta^{18}O$	Al (ppm)	Fe	Mn	Rb	Sr	Rb/Sr	Sm/Nd
C14-2	-25	Wackestone	*L. variabilis*	-0.61	-5.5	250	1636	514	0.7	445	0.0015	0.21
C14-6	-14	Wackestone	*L. variabilis*	-0.29	-5.61	277	1127	462	0.4	414	0.0009	0.22
C14-14	0	Mudstone	*Y. crassus*	-0.25	-5.77	649	1108	512	1.5	387	0.0040	0.25
C14-22	9	Mudstone	*Y. crassus*	-0.69	-6.15	288	191	235	1.3	416	0.0031	0.23
C14-27	15	Mudstone	*Y. crassus*	-0.54	-5.83	257	924	250	0.9	695	0.0012	0.22
C14-30	19	Mudstone	*Y. crassus*	-0.57	-5.7	387	1231	315	1.0	940	0.0011	0.23
C14-36	26	Mudstone	*Y. crassus*	-0.45	-5.79	269	804	380	0.9	879	0.0010	0.23
C14-41	32	Mudstone	*Y. crassus*	-1.52	-5.85	413	1313	517	1.1	609	0.0017	0.23
C14-43	35	Wackestone	*Y. crassus*	-0.71	-5.51	599	1183	305	1.2	390	0.0030	0.22
C14-47	40	Wackestone	*E. pseudoplanus*	-1.56	-5.98	679	1267	463	1.5	442	0.0034	0.22
C14-51	45	Mudstone	*E. pseudoplanus*	-1.14	-5.74	350	1238	707	1.0	478	0.0020	0.21
C14-54	48	Mudstone	*E. pseudoplanus*	-0.32	-5.78	391	1687	636	1.0	390	0.0026	0.22
C14-57	52	Mudstone	*E. pseudoplanus*	-2.09	-6.38	223	1039	473	0.7	364	0.0019	0.20
C14-59	55	Packstone	*E. pseudoplanus*	0.01	-5.99	312	1365	530	0.8	395	0.0021	0.24
C14-60	56	Packstone	*E. pseudoplanus*	0.11	-5.72	270	1430	572	0.9	481	0.0019	0.20
C14-62	58	Mudstone	*E. suecicus*	0.039	-7.13	265	869	309	0.7	445	0.0015	0.22
C14-68	65	Silty mudstone	*P. anserinus*	0.29	-6.94	267	1371	214	0.8	721	0.0011	0.21
C14-70	70	Silty mudstone	*P. anserinus*	0.56	-6.76	848	4369	382	1.7	786	0.0022	0.20
C14-74	74	Silty mudstone	*P. anserinus*	-0.14	-7.03	1049	2725	352	2.3	794	0.0028	0.19
C14-77	77	Silty mudstone	*P. anserinus*	0.13	-6.73	1233	1507	849	4.5	1094	0.0041	0.21

*Height relative to the contact between the San Juan and Las Chacritas formations

Table 3.2: Range of isotopic and elemental concentrations of samples from the Las Aguaditas Creek section

Sample	Height	Lithology	Conodont Zone	$\delta^{13}C$ ‰	$\delta^{18}O$	Al (ppm)	Fe	Mn	Rb	Sr	Rb/Sr	Sm/Nd
A14-11	-6	Wackestone	*Y. crassus*	-0.28	-5.23	183	5701	4921	0.9	1531	0.0006	0.21
A14-15	-2	Wackestone	*Y. crassus*	-0.13	-5.37	196	4428	2847	0.7	768	0.0009	0.22
A14-21	4	Wackestone	*Y. crassus*	-0.69	-5.32	281	1241	1519	1.6	881	0.0018	0.26
A14-25	8	Mudstone	*Y. crassus*	-0.41	-4.69	325	1305	405	1.6	957	0.0017	0.30
A14-29	12	Mudstone	*Y. crassus*	-0.95	-4.95	192	2364	415	1.1	741	0.0015	0.29
A14-33	16	Mudstone	*Y. crassus*	-1.28	-5.36	798	2047	324	2.1	791	0.0027	0.27
A14-36	19	Mudstone	*E. pseudoplanus/ D. tablepointensis*	-0.45	-4.85	358	1367	346	1.1	757	0.0015	0.25
A14-41	24	Mudstone	*E. pseudoplanus/ D. tablepointensis*	-1.52	-5.32	132	1721	432	0.8	1855	0.0004	0.22
A14-43	26	Mudstone	*E. pseudoplanus/ D. tablepointensis*	-0.71	-5.29	424	1231	227	1.3	1248	0.0010	0.22
A14-47	30	Mudstone	*E. pseudoplanus/ D. tablepointensis*	-1.75	-5.15	164	292	399	1.0	1762	0.0006	0.24
A14-51	34	Mudstone	*E. pseudoplanus/ D. tablepointensis*	-1.2	-4.83	133	1521	571	0.5	1351	0.0004	0.19

Table 3.2 continued.

Sample	Height	Lithology	Conodont Zone	$\delta^{13}C$ ‰	$\delta^{18}O$	Al (ppm)	Fe	Mn	Rb	Sr	Rb/Sr	Sm/Nd
A14-58	41	Mudstone	*E. pseudoplanus/ D. tablepointensis*	-1.69	-4.68	156	249	392	1.1	770	0.0014	0.23
A14-65	43	Mudstone	*P. anserinus*	0.42	-4.07	109	2237	808	0.5	691	0.0007	0.21
A14-61	44	Packstone	*P. anserinus*	0.11	-4.28	38	3754	570	0.2	714	0.0003	0.22
A14-67	46	Silty mudstone	*P. anserinus*	0.24	-4.51	468	2651	237	1.8	1629	0.0011	0.21
A14-69	48	Silty mudstone	*P. anserinus*	0.33	-4.15	448	2342	257	1.3	1852	0.0007	0.21
A14-73	52	Silty mudstone	*P. anserinus*	--	--	316	1314	122	0.8	1068	0.0008	0.21
A14-76	55	Silty mudstone	*P. anserinus*	--	--	352	1597	122	1.0	1466	0.0007	0.22

*Height relative to the contact between the San Juan and Las Aguaditas formations

Table 3.3: REE compositions of the Las Chacritas and Las Aguaditas formations

Sample	Height	Conodont Zone	La (ppm)	Ce	Pr	Nd	Sm	Eu	Gd	Tb	Dy	Ho	Er	Tm	Yb	Lu
C14-2	-25	*L. variabilis*	3.628	6.078	0.708	2.901	0.604	0.123	0.719	0.117	0.713	0.146	0.460	0.056	0.398	0.053
C14-6	-14	*L. variabilis*	6.336	12.440	1.516	6.363	1.379	0.235	1.494	0.230	1.338	0.271	0.819	0.102	0.702	0.098
C14-14	0	*Y. crassus*	5.721	12.030	1.429	5.907	1.475	0.386	1.899	0.367	2.453	0.539	1.743	0.265	1.949	0.292
C14-22	9	*Y. crassus*	4.814	12.330	1.598	6.897	1.601	0.353	1.810	0.298	1.693	0.322	0.882	0.101	0.655	0.083
C14-27	15	*Y. crassus*	3.941	8.393	1.082	4.635	1.033	0.218	1.135	0.180	1.029	0.197	0.581	0.065	0.443	0.055
C14-30	19	*Y. crassus*	4.529	10.210	1.350	5.918	1.352	0.292	1.484	0.236	1.342	0.254	0.710	0.080	0.543	0.069
C14-36	26	*Y. crassus*	4.011	7.467	0.940	4.070	0.921	0.198	1.022	0.162	0.948	0.189	0.565	0.065	0.451	0.060
C14-41	32	*Y. crassus*	6.627	13.220	1.626	6.955	1.598	0.297	1.847	0.304	1.858	0.383	1.162	0.154	1.057	0.145
C14-43	35	*Y. crassus*	5.194	11.050	1.338	5.472	1.191	0.226	1.308	0.216	1.297	0.259	0.788	0.099	0.698	0.090
C14-47	40	*E. pseudoplanus*	8.392	18.660	2.431	10.370	2.317	0.453	2.440	0.395	2.287	0.445	1.284	0.162	1.070	0.143
C14-51	45	*E. pseudoplanus*	7.145	13.330	1.597	6.672	1.418	0.294	1.631	0.256	1.515	0.304	0.910	0.116	0.783	0.106
C14-54	48	*E. pseudoplanus*	10.490	21.460	2.450	10.030	2.207	0.548	2.457	0.400	2.404	0.486	1.473	0.198	1.370	0.189
C14-57	52	*E. pseudoplanus*	4.757	9.773	1.055	4.161	0.842	0.175	0.918	0.148	0.880	0.174	0.549	0.071	0.534	0.069
C14-59	55	*E. pseudoplanus*	4.569	7.949	0.906	4.004	0.947	0.222	0.982	0.159	0.898	0.176	0.532	0.067	0.504	0.066
C14-60	56	*E. pseudoplanus*	4.031	6.392	0.665	2.750	0.556	0.150	0.636	0.104	0.642	0.139	0.460	0.061	0.488	0.068
C14-62	58	*E. suecicus*	4.081	7.069	0.873	3.582	0.787	0.190	0.855	0.140	0.821	0.164	0.482	0.059	0.398	0.053

Table 3.3. continued.

Sample	Height	Conodont Zone	La (ppm)	Ce	Pr	Nd	Sm	Eu	Gd	Tb	Dy	Ho	Er	Tm	Yb	Lu
C14-68	65	*P. anserinus*	4.717	7.836	0.926	3.939	0.808	0.186	0.957	0.147	0.866	0.174	0.527	0.059	0.419	0.049
C14-70	70	*P. anserinus*	7.277	14.640	1.776	7.224	1.442	0.334	1.499	0.233	1.308	0.256	0.760	0.090	0.622	0.078
C14-74	74	*P. anserinus*	11.000	21.110	2.488	9.919	1.895	0.406	2.090	0.328	1.983	0.407	1.211	0.159	1.054	0.142
C14-77	77	*P. anserinus*	22.060	43.900	5.248	21.910	4.568	0.940	4.849	0.777	4.491	0.901	2.597	0.344	2.242	0.301
A14-11	-6	*Y. crassus*	13.64	25.78	2.972	12.3	2.542	0.538	2.742	0.443	2.64	0.542	1.655	0.226	1.589	0.225
A14-15	-2	*Y. crassus*	6.482	10.23	1.257	5.289	1.149	0.258	1.307	0.214	1.317	0.278	0.886	0.127	0.951	0.142
A14-21	4	*Y. crassus*	8.341	17.05	2.095	10.14	2.684	0.811	2.826	0.459	2.652	0.514	1.461	0.186	1.234	0.17
A14-25	8	*Y. crassus*	5.976	11.92	1.571	8.179	2.428	0.495	2.41	0.39	2.204	0.431	1.236	0.155	1.055	0.146
A14-29	12	*Y. crassus*	5.091	11.47	1.615	8.62	2.517	0.519	2.41	0.391	2.205	0.428	1.216	0.151	1.025	0.14
A14-33	16	*Y. crassus*	8.044	15.08	2.005	9.988	2.717	0.533	2.655	0.44	2.578	0.51	1.49	0.196	1.35	0.187
A14-36	19	*E. pseudoplanus/ D. tablepointensis*	4.495	9.067	1.06	4.506	1.145	0.204	1.095	0.169	0.854	0.16	0.444	0.059	0.384	0.056

Table 3.3. continued

Sample	Height	Conodont Zone	La (ppm)	Ce	Pr	Nd	Sm	Eu	Gd	Tb	Dy	Ho	Er	Tm	Yb	Lu
A14-41	24	*E. pseudoplanus/ D. tablepointensis*	5.557	12.16	1.604	7.03	1.528	0.33	1.649	0.259	1.486	0.294	0.873	0.11	0.729	0.097
A14-43	26	*E. pseudoplanus /D. tablepointensis*	3.142	6.253	0.73	3.134	0.691	0.195	0.773	0.124	0.727	0.144	0.433	0.051	0.366	0.045
A14-47	30	*E. pseudoplanus/ D. tablepointensis*	11.94	26.45	3.444	15.48	3.658	0.635	3.767	0.621	3.653	0.719	2.074	0.268	1.721	0.237
A14-51	34	*E. pseudoplanus/ D. tablepointensis*	20.75	36.89	4.065	15.95	3.094	0.555	3.52	0.532	3.193	0.678	2.117	0.292	2.082	0.315
A14-54	37	*E. pseudoplanus/ D. tablepointensis*	10.11	18.54	2.24	10.02	2.307	0.46	2.429	0.383	2.199	0.437	1.274	0.159	1.063	0.142
A14-58	41	*E. pseudoplanus/ D. tablepointensis*	4.225	8.143	1.077	4.864	1.117	0.254	1.241	0.191	1.083	0.211	0.614	0.07	0.479	0.063
A14-65	43	*P. anserinus*	5.707	10.29	0.975	3.902	0.801	0.17	0.907	0.147	0.865	0.174	0.555	0.073	0.57	0.075
A14-61	44	*P. anserinus*	3.556	6.791	0.737	3.16	0.689	0.148	0.764	0.122	0.695	0.135	0.399	0.045	0.342	0.04
A14-67	46	*P. anserinus*	6.097	13.76	1.646	6.955	1.457	0.301	1.558	0.248	1.438	0.29	0.875	0.109	0.751	0.097
A14-69	48	*P. anserinus*	5.93	12.79	1.54	6.553	1.35	0.276	1.463	0.231	1.354	0.274	0.833	0.105	0.721	0.096
A14-73	52	*P. anserinus*	3.82	8.708	1.103	4.79	0.985	0.198	1.054	0.167	0.979	0.192	0.588	0.069	0.487	0.061
A14-76	55	*P. anserinus*	4.936	12.01	1.494	6.498	1.421	0.256	1.455	0.235	1.369	0.275	0.836	0.106	0.721	0.093

*Height relative to the contact between the San Juan and Las Chacritas/Las Aguaditas formations

Table 3.4: Measured [Rb], [Sr], and $^{87}Sr/^{86}Sr$ compositions of samples from nitric acid treatment of the Las Chacritas Formation

Sample	Height	Lithology	Conodont Zone	Treatment	Rb (ppm)	Sr (ppm)	Rb/Sr	$^{87}Sr/^{86}Sr$ (measured)	$^{87}Sr/^{86}Sr$ (initial)
C14-53	47	Mudstone	*E. pseudoplanus*	Nitric	4.0	465	0.0085	0.709185	0.709027
C14-54	48	Mudstone	*E. pseudoplanus*	Nitric	2.3	340	0.0067	0.709089	0.708965
C14-55	50	Mudstone	*E. pseudoplanus*	Nitric	3.1	375	0.0083	0.709110	0.708955
C14-56	51	Mudstone	*E. pseudoplanus*	Nitric	2.8	423	0.0066	0.709014	0.708891
C14-57	52	Mudstone	*E. pseudoplanus*	Nitric	2.8	422	0.0067	0.709105	0.708981
C14-58	53	Mudstone	*E. pseudoplanus*	Nitric	1.8	459	0.0040	0.708992	0.708917
C14-59	55	Packstone	*E. pseudoplanus*	Nitric	1.5	450	0.0034	0.709037	0.708974
C14-60	56	Packstone	*E. pseudoplanus*	Nitric	2.1	502	0.0042	0.709033	0.708955
C14-62	58	Mudstone	*E. suecicus*	Nitric	1.8	504	0.0036	0.709155	0.709088
C14-64	61	Mudstone	*E. suecicus*	Nitric	3.2	838	0.0038	0.708882	0.708811
C14-65	62	Mudstone	*E. suecicus*	Nitric	2.5	1387	0.0018	0.708830	0.708797
C14-66	63	Mudstone	*E. suecicus*	Nitric	3.6	834	0.0044	0.708999	0.708918
C14-67	65	Silty mudstone	*P. anserinus*	Nitric	1.4	616	0.0023	0.709069	0.709026
C14-68	65	Silty mudstone	*P. anserinus*	Nitric	2.6	903	0.0029	0.708958	0.708905
C14-69	66	Silty mudstone	*P. anserinus*	Nitric	7.3	730	0.0099	0.709038	0.708853
C14-70	70	Silty mudstone	*P. anserinus*	Nitric	6.6	737	0.0089	0.708856	0.708689
C14-71	71	Silty mudstone	*P. anserinus*	Nitric	3.7	858	0.0043	0.708717	0.708636

Table 3.4. continued.

Sample	Height	Lithology	Conodont Zone	Treatment	Rb (ppm)	Sr (ppm)	Rb/Sr	$^{87}Sr/^{86}Sr$ (measured)	$^{87}Sr/^{86}Sr$ (initial)
C14-72	72	Silty mudstone	*P. anserinus*	Nitric	8.7	522	0.0166	0.709136	0.708827
C14-73	73	Silty mudstone	*P. anserinus*	Nitric	6.0	935	0.0064	0.708962	0.708843
C14-74	74	Silty mudstone	*P. anserinus*	Nitric	9.0	771	0.0117	0.709114	0.708897

*Height relative to the contact between the San Juan and Las Chacritas formations

Table 3.5: Measured $^{87}Sr/^{86}Sr$, $^{143}Nd/^{144}Nd$, $^{147}Sm/^{144}Nd$, and ε_{Nd} of the Las Chacritas Formation

Sample	Height	Lithology	Conodont Zone	Treatment	$^{87}Sr/^{86}Sr$ (measured)	$^{87}Sr/^{86}Sr$ (initial)	$^{143}Nd/^{144}Nd$ (measured)	$^{147}Sm/^{144}Nd$ (measured)	$^{143}Nd/^{144}Nd$ (initial)	ε_{Nd}
C14-6	-14	Wackestone	*L. variabilis*	Acetic	0.708946	0.708929	--	--	--	--
C14-14	0	Mudstone	*Y. crassus*	Acetic	0.709344	0.709270	--	--	--	--
C14-22	9	Mudstone	*Y. crassus*	Acetic	0.709313	0.709307	0.512020	0.136227	0.511607	-8.5
C14-27	15	Mudstone	*Y. crassus*	Acetic	0.708890	0.708867	0.512117	0.135694	0.511706	-6.6
C14-30	19	Mudstone	*Y. crassus*	Acetic	0.708888	0.708868	0.512082	0.136494	0.511669	-7.3
C14-36	26	Mudstone	*Y. crassus*	Acetic	0.708855	0.708835	0.512015	0.135821	0.511604	-8.6
C14-41	32	Mudstone	*Y. crassus*	Acetic	0.708970	0.708937	0.512102	0.137586	0.511684	-7.0
C14-43	35	Wackestone	*Y. crassus*	Acetic	0.709072	0.709016	0.512037	0.130536	0.511641	-7.8
C14-47	40	Wackestone	*E. pseudoplanus*	Acetic	0.709174	0.709110	0.512270	0.128024	0.511882	-3.1
C14-51	45	Mudstone	*E. pseudoplanus*	Acetic	0.708969	0.708932	0.512071	0.128791	0.511681	-7.0
C14-54	48	Mudstone	*E. pseudoplanus*	Acetic	0.709037	0.708989	0.512289	0.131826	0.511889	-3.0
C14-57	52	Mudstone	*E. pseudoplanus*	Acetic	0.709173	0.709138	--	--	--	--
C14-59	55	Packstone	*E. pseudoplanus*	Acetic	0.709020	0.708981	0.512255	0.140061	0.511830	-4.1
C14-60	56	Packstone	*E. pseudoplanus*	Acetic	0.709011	0.708976	--	--	--	--
LCF17	56	Conodont	*E. pseudoplanus*	HCl	0.708781	0.708781	--	--	--	--
C14-64	61	Mudstone	*E. suecicus*	Acetic	0.708850	0.708829	--	--	--	--
C14-62	58	Mudstone	*E. suecicus*	Acetic	0.709115	0.709087	0.512079	0.128783	0.511689	-6.9
LCF18	58	Conodont	*E. suecicus*	HCl	0.708673	0.708673	--	--	--	--

Table 3.5. continued.

Sample	Height	Lithology	Conodont Zone	Treatment	$^{87}Sr/^{86}Sr$ (measured)	$^{87}Sr/^{86}Sr$ (initial)	$^{143}Nd/^{144}Nd$ (measured)	$^{147}Sm/^{144}Nd$ (measured)	$^{143}Nd/^{144}Nd$ (initial)	ε_{Nd}
LCF19	60	Conodont	*E. suecicus*	HCl	0.708674	0.708674	--	--	--	--
LCF20	63	Conodont	*E. suecicus*	HCl	0.708747	0.708747	--	--	--	--
C14-68	65	Silty mudstone	*P. anserinus*	Acetic	0.708930	0.708910	0.512128	0.123723	0.511753	-5.6
C14-70	70	Silty mudstone	*P. anserinus*	Acetic	0.708762	0.708722	0.512189	0.118725	0.511829	-4.1
C14-74	74	Silty mudstone	*P. anserinus*	Acetic	0.708964	0.708911	0.512149	0.115013	0.511800	-4.7
C14-77	77	Silty mudstone	*P. anserinus*	Acetic	0.709164	0.709089	0.512071	0.123359	0.511698	-6.7

*Height relative to the contact between the San Juan and Las Chacritas formations

Table 3.6: Measured $^{87}Sr/^{86}Sr$, $^{143}Nd/^{144}Nd$, $^{147}Sm/^{144}Nd$, and ε_{Nd} of the Las Aguaditas Formation

Sample	Height	Lithology	Conodont Zone	Treatment	$^{87}Sr/^{86}Sr$ (measured)	$^{87}Sr/^{86}Sr$ (initial)	$^{143}Nd/^{144}Nd$ (measured)	$^{147}Sm/^{144}Nd$ (measured)	$^{143}Nd/^{144}Nd$ (initial)	ε_{Nd}
A14-15	-2	Wackestone	*Y. crassus*	Acetic	0.708937	0.708921	0.512181	0.132341	0.511780	-5.1
A14-21	4	Wackestone	*Y. crassus*	Acetic	0.709060	0.709026	0.512153	0.161082	0.511664	-7.4
A14-25	8	Mudstone	*Y. crassus*	Acetic	0.709007	0.708976	0.512171	0.178439	0.511630	-8.0
A14-29	12	Mudstone	*Y. crassus*	Acetic	0.709000	0.708972	0.512100	0.175939	0.511567	-9.3
A14-33	16	Mudstone	*Y. crassus*	Acetic	0.708995	0.708944	0.512136	0.164781	0.511637	-7.9
LAF22	19	Conodont	*E. pseudoplanus/ D. tablepointensis*	HCl	--	--	0.512131	0.137489	0.511715	-6.4
A14-36	19	Mudstone	*E. pseudoplanus/ D. tablepointensis*	Acetic	0.708836	0.708808	0.512198	0.151539	0.511738	-5.9
A14-41	24	Mudstone	*E. pseudoplanus/ D. tablepointensis*	Acetic	0.708797	0.708789	0.512085	0.130901	0.511688	-6.9
A14-43	26	Mudstone	*E. pseudoplanus/ D. tablepointensis*	Acetic	0.708833	0.708813	0.512055	0.132484	0.511653	-7.6
LAF27	27	Conodont	*E. pseudoplanus/ D. tablepointensis*	HCl	0.709072	0.709072	--	--	--	--
A14-47	30	Mudstone	*E. pseudoplanus/ D. tablepointensis*	Acetic	0.708723	0.708712	0.512115	0.142778	0.511682	-7.0

Table 3.6. continued.

Sample	Height	Lithology	Conodont Zone	Treatment	$^{87}Sr/^{86}Sr$ (measured)	$^{87}Sr/^{86}Sr$ (initial)	$^{143}Nd/^{144}Nd$ (measured)	$^{147}Sm/^{144}Nd$ (measured)	$^{143}Nd/^{144}Nd$ (initial)	ε_{Nd}
LAF29	32	Conodont	*E. pseudoplanus/ D. tablepointensis*	HCl	0.709245	0.709245	--	--	--	--
A14-51	34	Mudstone	*E. pseudoplanus/ D. tablepointensis*	Acetic	0.708750	0.708743	0.512076	0.115724	0.511725	-6.2
A14-54	37	Mudstone	*E. pseudoplanus/ D. tablepointensis*	Acetic	0.708781	0.708757	0.512039	0.136967	0.511624	-8.2
A14-58	41	Mudstone	*E. pseudoplanus/ D. tablepointensis*	Acetic	0.708781	0.708755	0.512016	0.137110	0.511601	-8.6
LAF33	42	Conodont	*E. pseudoplanus/ D. tablepointensis*	HCl	0.708707	0.708707	0.512118	0.145949	0.511676	-7.1
A14-61	44	Packstone	*E. pseudoplanus/ D. tablepointensis*	Acetic	0.708617	0.708611	--	--	--	--
A14-65	43	Silty mudstone	*P. anserinus*	Acetic	0.708841	0.708828	0.512171	0.125619	0.511790	-4.9
A14-67	46	Silty mudstone	*P. anserinus*	Acetic	0.708614	0.708594	0.512123	0.132026	0.511723	-6.2

Table 3.6. continued.

Sample	Height	Lithology	Conodont Zone	Treatment	$^{87}Sr/^{86}Sr$ (measured)	$^{87}Sr/^{86}Sr$ (initial)	$^{143}Nd/^{144}Nd$ (measured)	$^{147}Sm/^{144}Nd$ (measured)	$^{143}Nd/^{144}Nd$ (initial)	ε_{Nd}
A14-69	48	Silty mudstone	*P. anserinus*	Acetic	0.708538	0.708525	0.512094	0.125357	0.511714	-6.4
A14-76	55	Silty mudstone	*P. anserinus*	Acetic	0.708578	0.708564	0.512125	0.129053	0.511734	-6.0

*Height relative to the contact between the San Juan and Las Aguaditas formations

Appendix 2

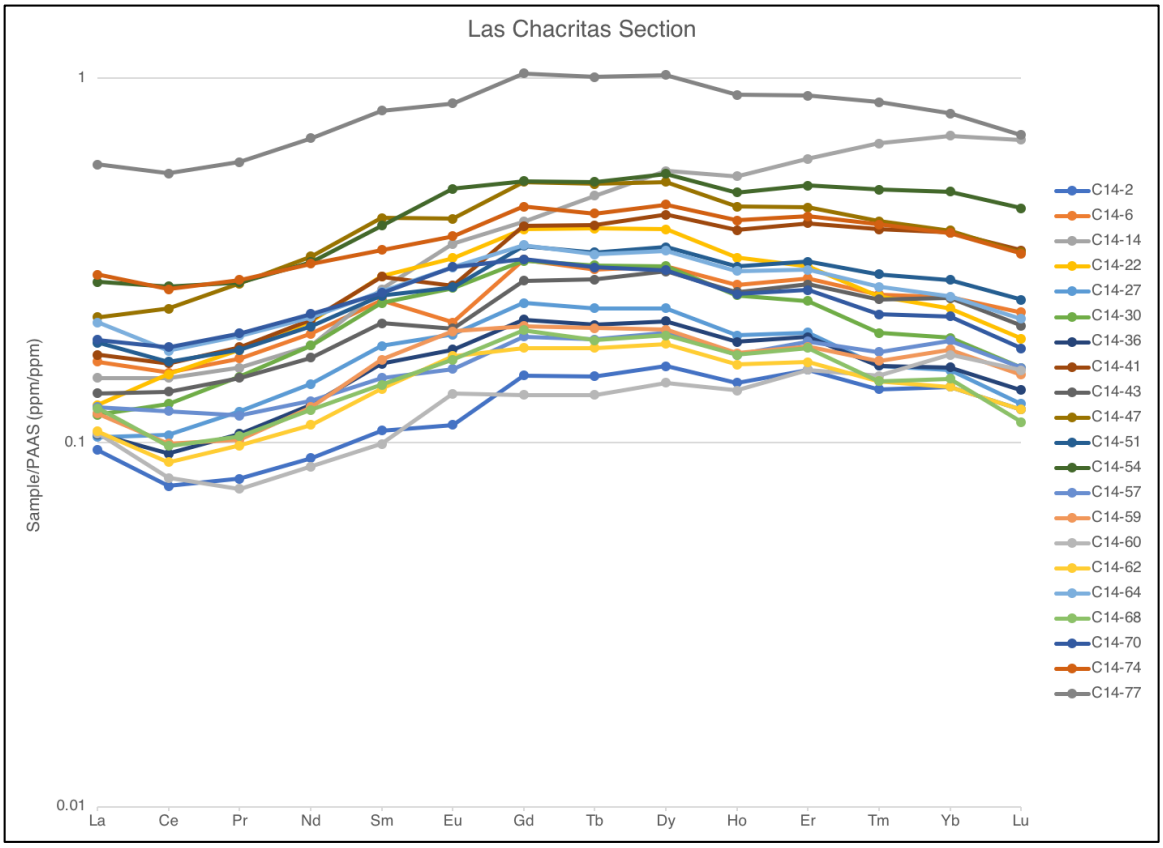

Figure 3.8: Rare earth element (REE) patterns of the Las Chacritas Formation. REE concentrations were normalized to Post Archean Average Shale (PAAS; Condie, 1993). Samples from the Las Chacritas Formation generally have depleted light REE fraction when compared to the heavy REE fraction. No systematic changes in REE patterns are observed with stratigraphic height.

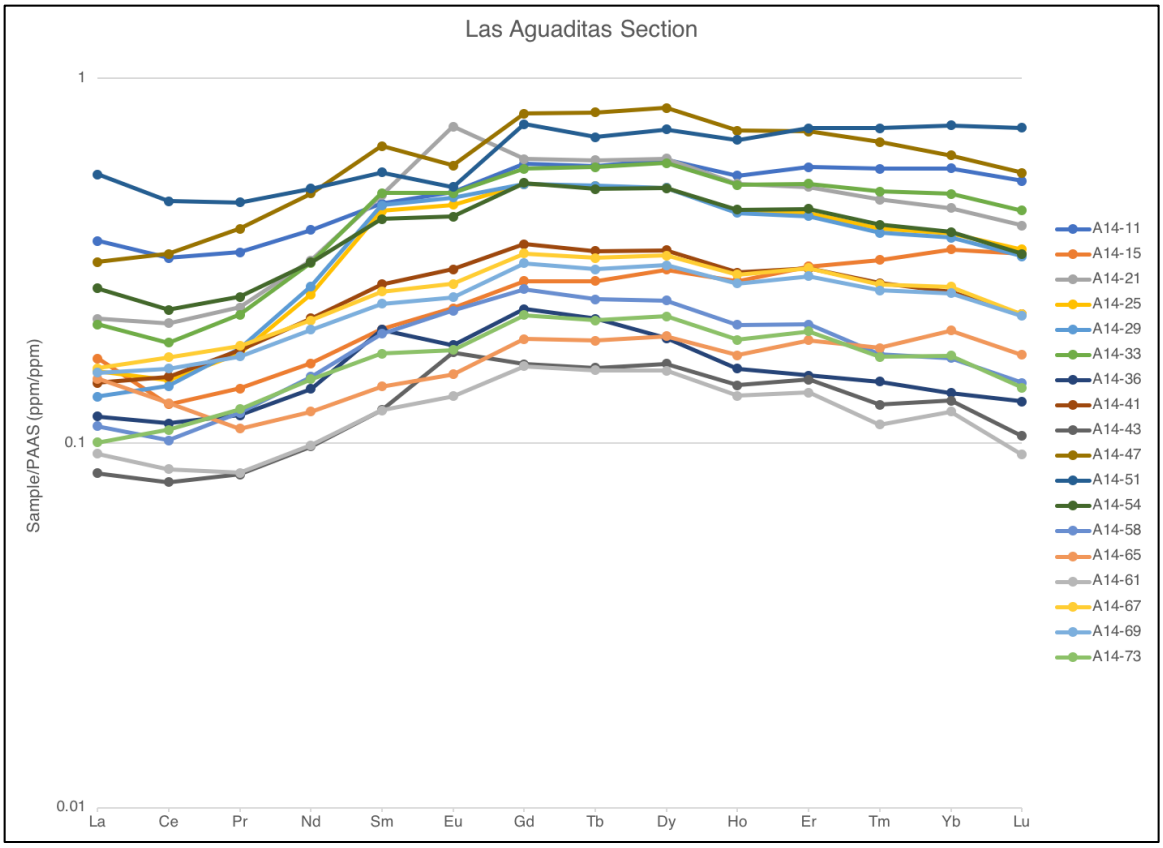

Figure 3.9: Rare earth element (REE) patterns of the Las Aguaditas Formation. REE concentrations were normalized to Post Archean Average Shale (PAAS; Condie, 1993). Samples from the Las Aguaditas Formation generally have depleted light REE fraction when compared to the heavy REE fraction. No systematic changes in REE patterns are observed with stratigraphic height; however, some samples do also show depletion in the HREE fraction, though not as extreme as that observed for the LREE fraction.

Summary

Greenhouse climate conditions of the Early Ordovician resulted in a decrease in the mixing rate of the ocean and the development of stratified ocean conditions. Global cooling through the Middle Ordovician would have led to invigorated ocean circulation, mixing of shallow- and deep-waters, and disruption of stratified ocean conditions. Geochemical evidence of such mixing is found in the biogeochemical records of carbon and sulfur, which suggest dramatic changes in ocean nutrient budgets, plausibly linked with changing ocean circulation patterns, upwelling of nutrient-rich deep water, and ventilation of the deep-ocean in the Middle Ordovician. These biogeochemical records coincide with the largest shift in the isotopic composition of marine strontium, which records values rapidly falling from more radiogenic isotopic compositions near 0.7090 to less-radiogenic values near 0.7078 in approximately 4–6 million years. However, the magnitude of Sr-isotope change over this time interval is difficult to explain with traditional weathering flux models and may include a previously unexplored oceanographic component. The purpose of this study was to explore the geochemical records of carbon, sulfur, strontium, and neodymium in coeval shallow and deeper-water depositional environments from the Argentine Precordillera to evaluate whether stratified ocean conditions were simply maintained by redox gradients in the water column or if physical separation of water masses may have driven, at least in part, the observed geochemical changes in the Middle Ordovician.

Geochemical decoupling between shallow- and deeper-water facies was observed in each isotope system investigated in this study. Middle Darriwilian limestone from the Las Chacritas Formation preserve a 2‰ positive shift in the isotopic composition of

marine carbonate and is recognized as the MDICE in the Precordillera. By contrast, coeval limestones from the deeper-water Las Aguaditas Formation have $\delta^{13}C_{carb}$ values that decline approximately 1.5‰ through the MDICE interval and represents the first known divergence from the global pattern of the MDICE. There are also small, but distinct, changes in the organic carbon records between the Las Chacritas and Las Aguaditas formations. Combined the $\delta^{13}C_{carb}$ and $\delta^{13}C_{org}$ values through the MDICE interval suggest deposition of the Las Chacritas Formation above the marine oxycline and the Las Aguaditas Formation below the oxycline. Such heterogeneity is consistent with a growing consensus for detailed environmental and diagenetic discrimination in the paleoceanography community.

Environmental differences are also observed in the sulfur isotope record of carbonate associated sulfate (CAS) and pyrite in the Middle Ordovician of the Precordillera. $\delta^{34}S_{CAS}$ values of the Las Chacritas Formation (~ +25‰) are similar to previously determined values from shallow water Darriwilian carbonate worldwide. In the deeper-water Las Aguaditas and Gualcamayo formations (deposited at and below the chemocline, respectively) $\delta^{34}S_{CAS}$ values are much lighter between 0‰ and +10‰. A similar trend is observed for the sulfur isotope composition of pyrite where shallow water $\delta^{34}S_{PY}$ is highly variable and reflects pyrite formation in sedimentary pore fluids and deeper-water environments have $\delta^{34}S_{PY}$ values around −10‰. These differences are consistent with a dual-reservoir model for sulfur cycling in the Middle Ordovician, where the isotopic composition of both CAS and pyrite is controlled by the relative fluxes of

sulfur between an oxidized (shallow-water) reservoir and a reduced (deep-water) reservoir.

Decoupling of shallow and deeper waters is also identified in the isotopic records of strontium and neodymium. Such differences are expected if physical decoupling occurs between shallow- and deep-waters occurs in the Early-Middle Ordovician greenhouse. Facies dependent strontium variation observed in both the Las Chacritas and Las Aguaditas formations may indicate the presence of a gradient in strontium isotope compositions, where shallow waters are dominated by radiogenic Sr input from the weathering of the continents and deeper-water is influenced by less-radiogenic Sr from weathering of the seafloor. Neodymium, which has a much shorter residence time than Sr and has been used to delineate mixing of distinct water masses was used to evaluate the potential for a gradient in Sr-isotope compositions to contribute to the large change in $^{87}Sr/^{86}Sr$ in the Middle Ordovician. ε_{Nd} values from the Las Chacritas and Las Aguaditas formations show differences between facies through the MDICE interval; however, these differences do not reflect simple mixing of shallow- and deep-water masses. The deeper-water deposits of the Las Aguaditas Formation reflect the long-term Nd-isotope composition from Gondwana (ε_{Nd} values ~ 6–8), whereas the shallower water record from the Las Chacritas Formation likely reflects contributions from Iapetan volcanic arc terranes, the Famatina volcanic arc terrane, or changes in local input of weathering of accreted terranes along the Gondwanan margin (ε_{Nd} values between ~ 3 and 8).

The Middle Ordovician strata explored in this dissertation show strong spatial heterogeneity in the isotopic proxy records among depositional environments. Strong

gradients observed in the isotopic composition of carbon, sulfur, strontium, and neodymium suggest stratified ocean conditions remained in the Precordillera through the Middle Darriwilian. The depth dependent differences observed in the Sr- and Nd-isotope records from the Precordillera suggest that physical separation of shallow- and deep-water contributed to ocean stratification in the Middle Ordovician. Such physical separation of water masses may have led to the development of distinct Sr-isotope compositions between shallow- and deep-water and mixing of these waters could contribute to the rapid change in $^{87}Sr/^{86}Sr$ observed in the Darriwilian. Although Sr-isotope compositions in the Precordillera follow the globally recognized pattern in the earliest Middle Darriwilian, recent biostratigraphic revisions for the Las Chacritas and Las Aguaditas formations indicate the upper Middle Darriwilian and Upper Darriwilian strata of these formations are missing. Future paleoceanographic studies on the Sr-isotope change through the Darriwilian-Sandbian interval should involve Nd-isotope determinations to evaluate potential changes and mixing of water masses with distinct isotope compositions. Paleoceanographic reconstructions are complex and require careful examination of basins that preserve coeval depositional environments to evaluate proxy records of paleoenvironmental change.

Vita

Miles Anthony Henderson was born and raised a Georgia boy. He grew up outdoors and was heavily involved in the Boy Scouts of America, where he earned his Eagle Scout Award in 2006. He finished high school at North Gwinnett High School in Suwanee, GA while participating as a dual enrollment student at Georgia Perimeter College. After high school, he continued taking courses at Georgia Perimeter College where he took a geology course to round out his schedule one semester. After the first few weeks of historical geology, he changed majors from biology and earned an associate degree in Geology in 2005 and went on to complete a bachelor's degree in geology at the University of Georgia in 2008. His interests in paleontology and environmental evolution were fueled by Dr. Sally Walker and encouraged to pursue a master's degree at the University of Tennessee under the supervision of Dr. Linda Kah. During his master's research, Miles married Viktoria Rundman in June 2009 and completed his investigation into the biogenicity of *Grypania spiralis* in July 2010. After three years working as a Project Geologist for Sierra Piedmont, Inc. he returned to the University of Tennessee in the Fall of 2013 for his doctoral work with Dr. Linda Kah. During his doctoral work at the University of Tennessee he traveled to Argentina three times, mentored undergraduate student research, welcomed his first child, Kora Grace in February 2016, and worked as a visiting researcher at the Historical Geobiology Laboratory at Stanford University and the Radiogenic Isotope Laboratory at the University of New Mexico. Miles is looking for a position that will allow him to continue paleoceanographic investigations and share his love of sedimentary geology with students in the classroom.